UNIVERSITY OF CALIFORNIA
RIVERSIDE

Graphene-based Material Systems for Nanoelectronics and Energy Storage Devices

A Dissertation submitted in partial satisfaction
of the requirements for the degree of

Doctor of Philosophy

in

Chemistry

by

Shirui Guo

March 2013

Dissertation Committee:

Dr. Mihri Ozkan, Co-Chairperson
Dr. Cengiz Ozkan, Co-Chairperson
Dr. Richard Hooley
Dr. Ming Lee Tang

This Dissertation of Shirui Guo is approved:

Committee Co-Chairperson

Committee Co-Chairperson

University of California, Riverside

Acknowledgements

Dream big, and believe in your dreams, for without dreams there is no hope, and without hope life is a world of emptiness. After years of study and research, I found without supports of many people dreams will always be dream.

I have been very fortunate with my supervisors, Professor Mihri & Cengiz Ozkan. I would like to express my heartiest gratitude and deep appreciation to my advisor Professor Mihri Ozkan. She is a great mentor, her charming personality, broad knowledge and supportive leadership nurturing me growing up towards my career goal. Her endless patience and strong support helped me overcome many crisis situations in both my scientific research and daily life. I would like to give my sincere appreciation to my research co-advisor Professor Cengiz Ozkan. His insightful and knowledgeable guidance made my graduate period more productive. Without their hard work and endless efforts, I couldn't finish the dissertation.

I am also thankful to my committee members Professor Richard Hooley and Professor Ming Lee Tang for their help and valuable comments on my dissertation. My thanks also go to Professor Christopher J. Bardeen and Professor Guy Bertrand for their valuable comments on my qualifying exam.

I am greatly indebted to many past and current members in Ozkan group for providing rich working experiences, intellectual stimulation and friendship: Dr. Alfredo Martinez-Morales, Dr. Emre Yengel, Dr. Hayri Engin Akin, Dr. Miroslav Penchev, Dr.

Jian Lin, Dr. Maziar Ghazinejad, Dr. Jiebin Zhong, Dr. Ali Guvenc, Dr. Jennifer Reiber Kyle, Dr. Xiaoye Jing, Wei Wang, Hamed Hosseini Bay, Isaac Ruiz, Aaron George, Zach Favors, Zafer Mutlu, Dennis Pleskot, Jeffrey Bell.

I would like to take this opportunity to thank Dr. Xiangdong Qin and Prof. Francisco Zaera for their great help in the collaboration of tuning electronic transport of graphene devices project at UCR. My thanks also go to Prof. Valentine Vullev and Dr. Duoduo Bao for their help in the graphene photovoltaics devices project. I thank Dr. Krassimir N. Bozhilov and Stephen McDaniel for their kind assistance in using facilities in CFAMM at UCR. I also want to thank the staff Mark Heiden, Dexter Humphrey, Dong Yan in CNSE at UCR for assisting cleanroom training and facility usage. I would like to thank Professor Yadong Yin and Professor Pingyun Feng for their encouraging and motivating to pursue my academic career goal. My thanks also go to my friends Dr. Qiao Zhang, Dr.Tao Wu, Dr. Fan Zuo, Dr. Xiang Zhao and Dr. Rui Liu for their valuable help.

Most importantly, none of this would have been possible without the love and patience of my family. I would like to express my heart-felt gratitude to my parents Fanyou Guo and Aizhen Li, my parents-in-law Xuecun Zhu and Dongyue Zhang, my wife Jianxin Zhu for everything they have done for me.

Finally, I would like to take the opportunity to thank all persons who have ever helped me before.

Dedication

To my wife Jianxin and my little princess Angela

ABSTRACT OF THE DISSERTATION

Graphene-based Material Systems for Nanoelectronics and Energy Storage Devices

by

Shirui Guo

Doctor of Philosophy, Graduate Program in Chemistry
University of California, Riverside, March 2013
Dr. Mihri Ozkan, Co-Chairperson
Dr. Cengiz Ozkan, Co-Chairperson

Graphene is an allotrope of carbon in two-dimensional crystal form that has extraordinary electrical and optical properties. In this dissertation, we present the use of graphene in applications for chemical sensors, photovoltaics and supercapacitors.

Firstly, carrier transport properties of single layer graphene films grown via chemical vapor deposition technique are tuned with functionalized molecules, polymers and inorganic nanoparticles. For example, cylindrical microdomains of polystyrene-4-polyvinylpyridine (PS-P4VP) block-copolymers (BCP) on graphene film provide spatial doping effects due to two distinct functional groups. Further, preferred interactions between CF_x or fluorine radicals and BCP micro domains on graphene introduce localized doping of graphene film leading to controlling of Dirac point shift. Interaction between graphene and inorganic nanoparticles is studied by using CdSe quantum dots as a model system. Femtosecond time-resolved spectroscopy allowes us to demonstrate for the first time fast interfacial charge transfer for such systems in the picosecond and in the hundreds of femtosecond time domains, which also demonstrates high potential for photoelectrochemical cell.

Secondly, graphene field effect transistors (GFET) as single strand DNA sensors are fabricated and detection limit as low as 3×10^{-9} M is demonstrated. Assembled BCP film on GFET sensor improved the sensor's stability and selectivity. The orientation and periodicity of the resulting cylindrical microdomains of BCP can facilitate the selective sensing property. With protective layer of BCP, sensor's stability under ambient atmosphere is improved up to 4 months.

Thirdly, two different types of carbon nanotubes (CNT)/graphene hybrids are synthesized and used in fabrication of supercapacitors. The first type hybrid is graphene and vertically aligned carbon nanotubes which is successfully grown via one step chemical vapor deposition method. Our custom seamless growth method for such hybrids provides an attractive pathway for the fabrication of novel 3-Dimensional hybrid nanostructures. The second type hybrid is graphene oxide (GO) and SWCNT composite ink (GO-SWCNT ink). SWCNTs are dispersed using a GO aqueous solution (2mg/ml) with sonication support to achieve a SWCNT concentration of 12mg/ml, the highest reported value so far without surfactant assistance. Paper based electrodes for supercapacitors are fabricated using GO-SWCNT composite ink via dip casting method. By employing different concentrations of SWCNT inside the ink, supercapacitors demonstrated different capacitance values. The highest value of specific capacitance reaches up to 295 F/g at a current density of 0.5A/g with a GO/SWCNT weight ratio of 1:5. The cycling stability for the GO-SWCNT paper electrode supercapacitors indicates capacitance retention of 85% over 60,000 cycles.

Finally, engineered interactions between nanomaterials, polymers, molecules and graphene/carbon nanotube can lead to the development of new types of devices for myriad applications.

Table of Contents

List of Tables

List of Figures

Figure 2.2 (a) Another graphene field effect transistor I_{ds}-V_g curve. (b) typical source-drain current vs. source-drain voltage (I_{ds}-V_{ds}) curves at different gate voltages.

Figure 2.3 Source-drain current vs. gate voltage (I_{ds}-V_g) curves of control sample: GFET in air for 5 min and GFET covered with BCP.

Figure 2.4 (a) I_{ds}-V_g curves for a typical pristine graphene and for BCP-covered GFET devices after drying in air, (b) Typical source-drain current vs. gate voltage (I_{ds}-V_g) curve of GFET covered with BCP and 5 days in vacuum desiccator change. (c) Typical I_{ds}-V_g curves for GFET devices: pristine graphene, graphene doped with polystyrene (PS), polyvinylpyrrolidone (PVP), and BCP covered graphene with high vacuum annealing at 50^{o}C for 12 hrs. The test was carried out by putting one drop of PS or PVP solution on GFET devices. PS and PVP solution were prepared with trichloroethylene and anhydrous ethanol respectively. (d) Normalized source-drain conductance vs. gate voltage (G_{ds}-V_g) curves for a graphene devices: pristine graphene, PS covered graphene, PVP covered graphene and BCP covered graphene. The source-drain bias for these measurements was 100 mV.

Figure 2.5 (a) Source-drain current vs. gate voltage (I_{ds}-V_g) curves from samples obtained after different plasma exposure times. The exposure time was accumulated. (b) Normalized source-drain conductance vs. normalized gate voltage (G_{ds}-V_g) curves from graphene device after different plasma exposure times.

QD-Py/graphene film (λ_{ex} = 488 nm with10-nm bandwidth; and λ_{em} = 624 nm with 40-nm bandwidth).

Figure 2.13 Absorption and emission properties of films of Py- and ODA-coated QDs: (a) dissolved in toluene; and (b, c) deposited on bare glass (QD-ODA and QD-Py) or on graphene-coated glass (QD-Py/graphene). (a) Comparison between the normalized steady-state absorption and emission spectra of QD-ODA and QD-Py suspended in toluene (λ_{ex} = 420 nm). (b) Steady-state absorption and emission spectra of QD-Py films and of single-layer graphene. The absorption spectra of the solid films were obtained from reflectance measurements using an integrating sphere, and the emission spectra were recorded using a small-angle setup (for the main panel, λ_{ex} = 420 nm; and for the inset, λ_{ex} = 600 nm). For improved visualization, the emission spectra of graphene and of QD-Py/graphene were scaled up by a factor of 50 The dotted blue line corresponds to the solution QD-Py emission spectrum (a). (a, b) For estimation of the QD band gaps, the zero-to-zero energy was calculated from the crossing points of the normalized steady-state absorption and emission spectra.

Figure 2.14 Transient absorption (TA) dynamics of QD films deposited on glass with no graphene. (a) TA spectra of a QD-ODA film recorded at different times after the excitation. (b) TA spectra of a QD-Py film in comparison with its reflectance, R, from which the ground-state absorbance was determined ($A_{400\ nm}$ = 0.10). The weak negative signal at ~650 nm was ascribed to the

stimulated emission (SE). (c) Comparison between an early-time TA features and the second derivative of the ground-state absorption of a QD-Py film, with the corresponding assignments of the absorption, A_i, and bleaching, B_i, bands. (d) Comparison between B_1-normalized TA spectra of QD-ODA and QD-Py films. (e, f) TA kinetic curves of QD films recorded at three spectral regions. For ease of comparison, the curves were plotted against different ΔA ordinates, normalizing the initial bleach minima. At 625 nm, biexponential data fits of the bleach recovery yielded: for QD-ODA $\tau_1 = 250\pm20$ ps ($\alpha_1 = -0.45$), $\tau_2 = 1.9\pm0.7$ ns ($\alpha_2 = -0.32$), and an offset $\alpha_\infty = -0.22$; for QD-Py $\tau_1 = 260\pm50$ ps ($\alpha_1 = -0.34$), $\tau_2 = 1.6\pm0.6$ ns ($\alpha_2 = -0.43$), and an offset $\alpha_\infty = -0.23$. ($\lambda_{pump} = 400$ nm, 1.5 μJ per pulse, 38-fs pulse width of the fundamental at 800 nm.)

Figure 2.15 Transient absorption (TA) dynamics of QD-Py films deposited on single-sheet graphene on glass substrates. (a) TA spectra of monolayers of pyridine-coated QDs deposited on graphene recorded at different times after the excitation. For improved signal-to-noise ratios, the samples were composed of stacks of three cover slips, with single-side deposited QD-Py/graphene monolayers (ground-state sample absorption at the excitation wavelength: $A_{400\ nm} = 0.11$). (b) Comparison between the kinetics, recorded at the B_1 and B_4 bands, of pyridine-coated QDs deposited on graphene and on bare glass. For visualization of the sub-picosecond dynamics, the early time-scale (i.e., for $t \leq 2$ ps) was extended. For the graphene samples multiexponential data

fits of the bleach recovery yielded: at 625 nm, τ_1 = 19±3 ps (α_1 = –0.49), τ_2 = 270±50 ps (α_2 = –0.42), and an offset α_∞ = –0.09; and at 515 nm, τ_1 = 260±60 fs (α_1 = –0.44), τ_2 = 3.9±1.2 ps (α_2 = –0.23), τ_3 = 60±11 ps (α_3 = –0.27), and α_∞ = –0.06 (λ_{pump} = 400 nm, 1.5 μJ per pulse, 38-fs pulse width of the fundamental at 800 nm.)

Figure 2.16 Current-voltage (*I-V*) characteristics of field-effect transistor FET devices comprising QD-Py/graphene films under illumination (λ = 365 nm, 0.2 W cm^{-2}) and under dark conditions. (a) Representative drain-source current-voltage lines for a FET device with the illumination on and off (V_{gs} = 0 V). (b) Representative *I-V* curves showing the dependence of the drain-source current, I_{ds}, on the gate voltage, V_{gs}, with the illumination on and off (V_{ds} = 0.1 V). **(c)** Photoinduced changes in the drain-source current of a FET device (V_{ds} = 0.1 V; V_{gs} = 0 V). The illumination on/off cycle involved turning the light on for 30 s, and keeping it off for 4 to 8 minute. The time constant of the current increase upon turning the illumination on was 4.3±1.6 s; and the time constant of current decrease upon turning the illumination off was 140±30 s.

Figure 2.17 Fast short circuit photocurrent (I_{sc}) photo-response of QD/graphene/ITO devices under white light illumination in photoelectrochemical cell. The inset shows an enlarged view for a small portion of the photocurrent response curve. Input light power is 30 mW/cm^2.

Figure 2.18 I-V characteristics of PEC with linear sweep voltammograms measured in three-electrode mode under white light (a) and 365nm UV (b) illumination.

Figure 3.7 (a) Resistance change of five devices after incubation in TE buffer for 8h. (b) Resistance of graphene device. R-graphene: resistance of graphene; R-graphene-buffer: Resistance of graphene device after 8 h incubation in TE buffer.

Figure 3.8 (a) Photo image of copper foil after graphene growth, (b) photo image of as-fabricated graphene field effect transistor with wire-bonding on chip-carrier, (c) Raman spectra of single-layer graphene, (d) photo image of 2 inches square of single-layer graphene on glass.

Figure 3.9 (a) AFM image of PS-P4VP block copolymer height profile (b) The surface profilometer height profile and optical image (inset) of the step-removed polymer film, the dashed line shows the scan axis along which the height profile has been measured.

Figure 3.10 Typical I_{ds}-V_g curve of BCP/graphene NaF sensor. The drain-source voltage was 100mV.

Figure 3.11 Typical Ids-Vg curve of BCP/graphene FET sensor stability test (a) time study and (b) reversibility study. The initial device was exposed to 0.5M NaF solution for 20 seconds, then measurements were conducted with different time. All of the test were conducted in air, V_{ds}=100mV.

Figure 3.12 pH detection with BCP protected GFET robust sensor: (a) typical Typical Ids-Vg curve with different pH solution; (b) linear fitting of Dirac point and pH. Buffer used here are 0.1M Tris-HCl solutions.

Figure 4.16 (a) CV curves of supercapacitor based on PGN films. The weight of one PGN film is around 200 μg/cm^2. Electrolyte: 6 M KOH aqueous. (b) Specific capacitance and energy density vs. scan rates.

List of Schemes

vertically grown carbon nanotubes as pillars and large-area graphene plane as a floor.

Chapter 1

Overview of Graphene Electronic and Energy Storage Devices

1.1 History of Graphene

The first use of graphite can be traced back to the 4th millennium B.C. when Mariţa culture applied it as a ceramic paint to decorate pottery in southeastern Europe.[1] The band theory of graphite has been studied from 1947 when P. R. Wallace used the tight binding approximation method, which assumes conduction only happens in one layer which is graphene layer.[2] Graphene, a two-dimensional (2D) monolayer of carbon atoms tightly packed into a honeycomb lattice, is basic building block for graphite and other graphitic materials of all dimentions (Figure 1.1).[3] While in Landau and Peierls argued that strictly 2D crystals were thermodynamically unstable and could not exist,[4-5] 2D graphene oxide sheets actually have been synthesized by Benjamin C. Brodie in 1859[6] and further modified by Hummers and Offeman in 1957.[7] However, until 2004, the first experimental discovery of graphene was reported by A. K. Geim and K. S. Novoselov.[8]

Many remarkable properties of graphene make it a rising star for researches and applications in various areas. Ballistic transport of electrons along the atomically thin layer, along with mobilities exceeding 15 000 cm^2 $V^{-1}s^{-1}$ and an ambipolar field effect make graphene a particularly good candidate for the next generation of semiconductor devices.[9-10] Apart from the extremely high carrier mobility, graphene absorbs only 2% of incoming light, independent of wavelength across the visible spectrum.[11] These

properties make graphene an excellent candidate for photovoltaic devices.[12-15] Transparent conducting films have been made from graphene for displays,[16] touch-screens and solar cells.[17-21] High strength and flexibility of graphene enable bendable devices which is useful in electromechanical systems.[22] The large and planar surface area of a single sheet and low electrical noise of graphene field effect ransistors make possible their use in optoelectronic and sensor applications.[23-29] A cutoff frequency of 100 gigahertz for a gate length of 240 nanometers graphene field effect transistors has been achieved, which is higher than state-of-the-art silicon transistors of the same gate length enabling application for digital data transmission.[30] The vast possibilities of graphene and the rapid advancements in research are propelling this new material towards novel achievements that are already beginning to influence industry.[31]

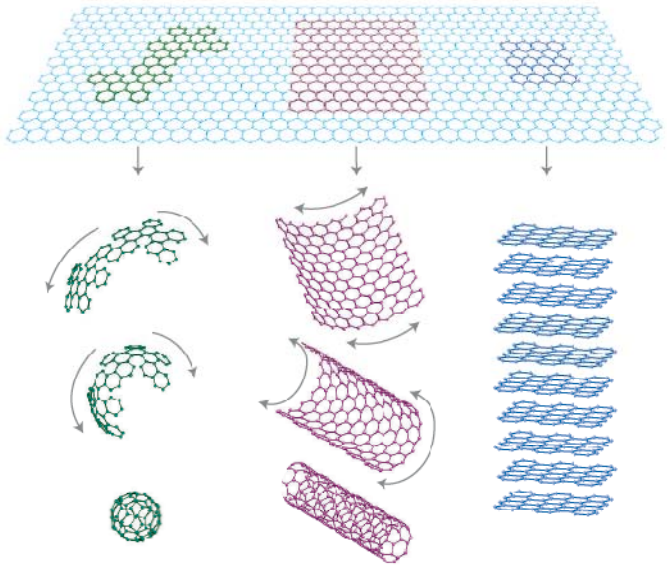

Figure 1.1 Graphene: building block for all other carbon allotropes. It can be rolled into (a) 0D buckyballs, (b) 1D CNT and stacked to form (c) 3D graphite.[3]

1.2 Graphene based Electronics

1.2.1 Synthesis of Graphene

For mass production of electronic devices, large scale synthesis of high quality graphene is necessary. Currently, there are two major approaches to achieve large scale, high quality as well as low cost production of graphene.

1.2.1.1 Chemical Vapor Deposition

In 1961, few layer graphene has been grown by pyrolyze pure carbon suboxide (C_3O_2) at 713^oC with electrolytic nickel and copper foils and reagent grade platinum foils.[32]The diffraction patterns of the obtained carbon film indicate the presence of crystalline carbon which are graphene layers. In 1969, Robertson reported synthesis of graphite/few layer graphene by decomposing methane over nickel.[33] Different transition metals require different decomposing temperatures. Pd, Ru, Ir, Ni and Cu have been utilized for growing graphite materials. However, due to the limitation of characterization techniques, graphene layers were not thoroughly characterized until 2004 when the first experimental discovery of graphene was reported by A. K. Geim and K. S. Novoselov.[8]

In 2006, Somani et al. utilized nickel sheets to grow few layer graphene, and the number of layers was estimated to be 35 layers with high resolution transmission electron microscopy.[34] This approach opened venues for graphene synthesis, although several issues like thickness control and uniformity had to be solved. Then nanometer thick (1-2 nm) graphene films grown on nickel foil (hundred micrometer) were achieved by several groups through the CVD approach.[35] The diffusion and segregation of carbon impurities

from the bulk to the surface during the annealing and cooling stages induces the formation of graphite on nickel. At the same time graphene has been grown with various catalysts including Ru,[36] Ir,[37] Co,[38-39] Re,[40] Pt,[38,41] Pd,[38] Cu,[42] Fe.[39,43-44] Revisiting the formation mechanism of the carbon layer on different transition metals provides chances to produce high quality graphene. The carbon solubility in the metal and the growth conditions determine the deposition mechanism which ultimately also defines the morphology and thickness of the graphene films. Among all of the transition metals, copper foil is of particular interest for growing single layer graphene. The phase diagram of Ni and C reveals that the solubility of carbon in nickel at high temperature (above 800 ^{o}C) forms a solid solution and lowering the temperature decreases the solubility, allowing carbon to diffuse out of Ni (Figure 1.2a).

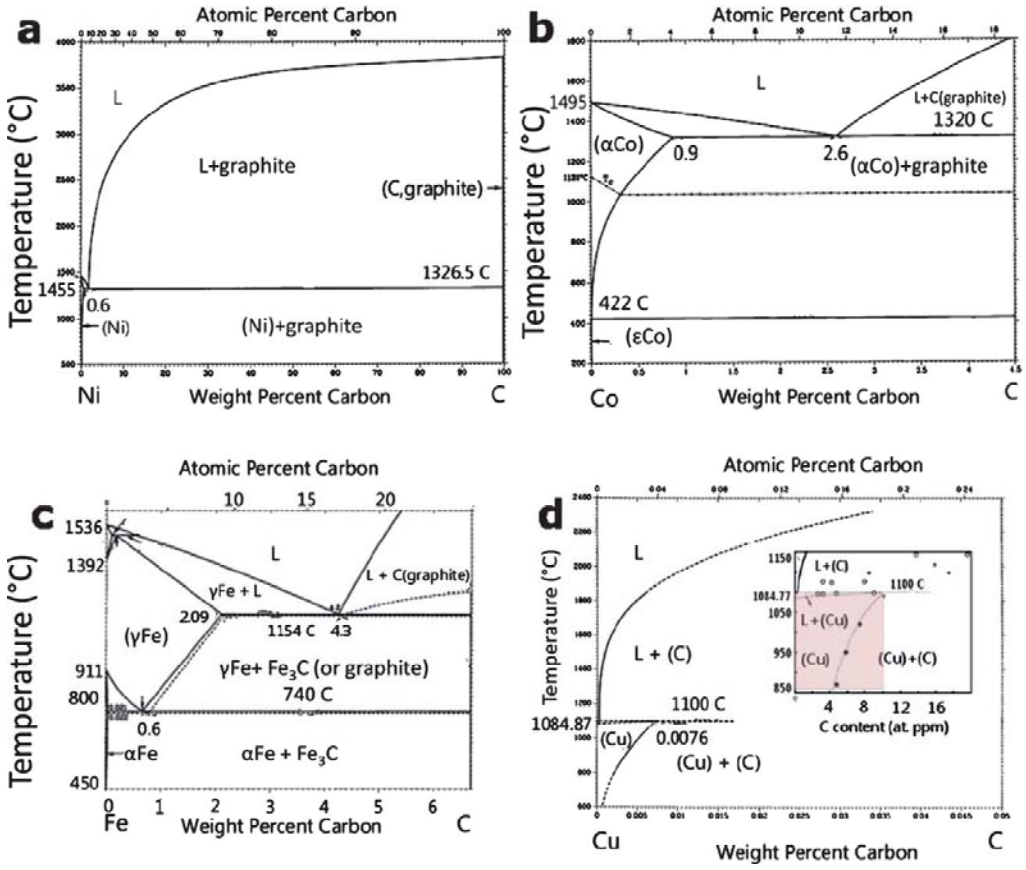

Figure 1.2 Binary phase diagrams of transition metals and carbon: (a) Ni–C; (b) Co–C; (c) Fe–C; (d) Cu–C. The low carbon solubility in Cu, of 0.008 weight % at 1084°C as reported is highlighted in the inset of panel (d) for the temperature and composition of interest for graphene growth.[45]

It is well known from metallurgical studies that the formation of metastable Ni_3C phase promotes the precipitation of carbon out of Ni. Carbon preferentially precipitates out at the grain boundaries of polycrystalline Ni substrates so that the thickness of the graphite at the grain boundaries is substantially larger than within the grains. Thus, the number of graphene layers shows significant difference along the surface of Ni. By additional etching of the as-grown graphene films with H_2 at 1000°C, single layer graphene was obtained on Ni foil.[39] Co and Fe show similar catalytic behavior as can be concluded from the phase diagrams (Figure 1.2 b, c). In contrast, copper does not form

any carbide phases (Figure 1.2 d), which makes it a good candidate for perfect graphene single layer growth.[42] From the atomic orbital point of view, we can also get the same conclusion. Carbon forms on the metal surface through forming intermediates or solid solutions with metal. The bond strength between metal and carbon highly depends on the d orbital structure of metal atoms. Fe has asymmetrical distribution of electrons in the d-shell {[Ar]$3d^6 4s^2$}, leading to mutual repulsion which may explain its higher affinity towards carbon with respect to Co {[Ar]$3d^7 4s^2$}, Ni {[Ar]$3d^8 4s^2$}and Cu where the 3d shell is progressively filled, suggesting less reactive configurations. Copper has a filled 3d-electron shell {[Ar]$3d^{10} 4s^1$}, the most stable configuration (along with the half filling $3d^5$) because the electron distribution is symmetrical which minimizes reciprocal repulsions. As a result, Cu can form only weak bonds with carbon via charge transfer from the p electrons in the sp^2 hybridized carbon to the empty 4s states of copper. [45] The $3d^7$ and $3d^8$ orbitals of Co and Ni are between the most unstable electronic configuration (Fe) and the most stable one(Cu).

With the privileges of copper foil, large scale production of high quality graphene has been achieved. Sukang Bae et. al reported roll-to-roll synthesis of 30-inch graphene films for transparent electrodes (Figure 1.3).[16] Mobility of CVD graphene varies from 300 to 5000 $cm^2\ V^{-1}s^{-1}$, which is much lower than pristine graphene obtained by micromechanical exfoliation of highly oriented pyrolytic graphite. The major hurdle is graphene domain boundaries where carbon-carbon could not form perfect sp^2-sp^2 bonds resulting in degradation of electronic properties. Large area single graphene crystals are feasible for high quality device fabrication and they have been grown with copper as the

catalyst. Qinkai Yu et. al. devised an approach using pre-patterned growth graphene seeds to control graphene nucleation, opening a route towards scalable fabrication of single-crystal graphene devices without grain boundaries (Figure 1.4 a).[46] Very recently, Zheng Yan et. al. reported 4.5mm^2 of one single graphene crystal grown on copper foil. The study shows that extensive annealing time and electrochemical polishing improve the quality of copper foil. The optimized methane/hydrogen ratio introduces less active sites for single-crystal graphene leading to large area growth (Figure 1.4 b).[47]

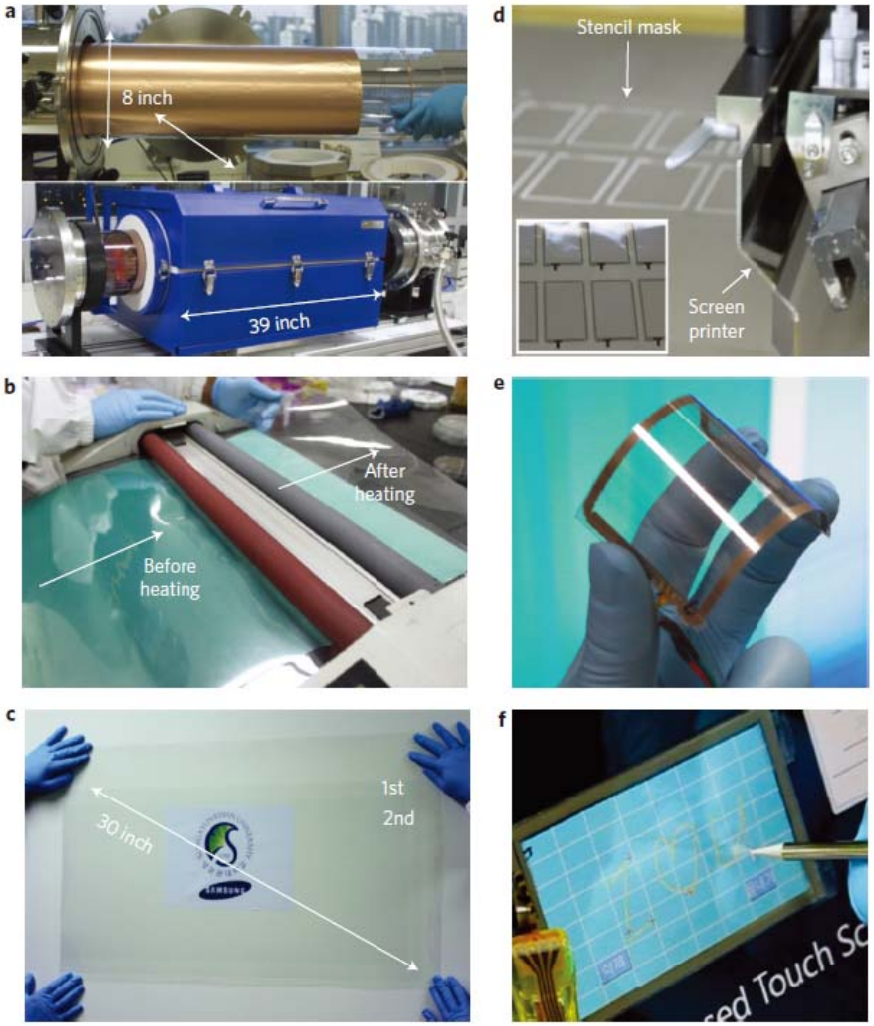

Figure 1.3 Photographs of the roll-based production of graphene films. (a) Copper foil wrapping around a 7.5-inch quartz tube to be inserted into an 8-inch quartz reactor. The lower image shows the stage in which the copper foil reacts with CH_4 and H_2 gases at high temperatures. (b) Roll-to-roll transfer of graphene films from a thermal release tape to a PET film at 120 ^oC. (c) A transparent ultralarge-area graphene film transferred on a 35-inch PET sheet. (d) Screen printing process of silver paste electrodes on graphene/PET film. The inset shows 3.1-inch graphene/PET panels patterned with silver electrodes before assembly. (e) An assembled graphene/PET touch panel showing outstanding flexibility. (f) A graphene-based touch-screen panel connected to a computer with control software.[16]

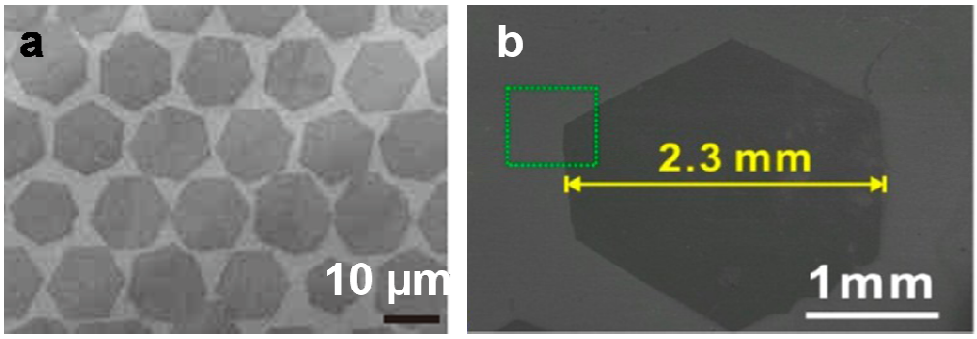

Figure 1.4 (a). SEM image of a typical graphene grain array grown from an array of seed crystals, with a relatively short growth time (15 min).[46] (b). Synthesis of large-size (~2.3 mm) single-crystal graphene monolayer domains using the CP-CVD system. Typical SEM image of as-produced graphene domains on Cu.[47]

Growth of graphene with CVD is straightforward. As illustrated in Figure 1.5, hydrogen and methane flow through MFC under certain a flow rate with optimized ratio. Decomposition of methane will happen when it flows over the copper surface at 1000^{o}C. By lowering the temperature, carbon atoms will diffuse and form graphene crystals. Typically, the copper foil is etched with acetic acid at 35^{o}C for 10min to remove any CuO. After washing the foil completely with deionized (D.I.) water, the copper foil samples are then heated up to 1000^{o}C in a 2 Torr Ar/H_2 (200:200 sccm) atmosphere and annealed for 30 minutes. The growth is conducted at 20 Torr following exposure to methane (100sccm) mixed with 20 sccm H_2 flowing at 1000^{o}C for 20 minutes. The

temperature is then reduced to 25°C at a cooling rate of 20 °C/min, during which the graphene film is formed on the copper surface. After coating with PMMA layer of copper foil. The residual copper foil underneath is then etched in $FeCl_3$ aqueous solution (0.5M) and rinsed thoroughly with HCl (3%) and D.I. water, respectively. The graphene film is finally transferred onto a Si substrate covered with 300nm thermally grown oxide for further characterization.

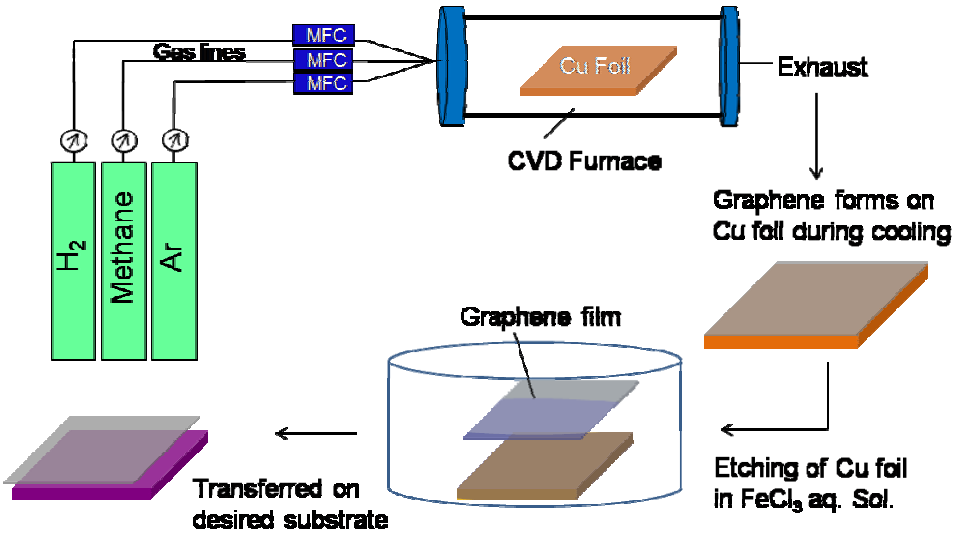

Figure 1.5 Schematic illustration of CVD synthesis of single layer graphene with copper foil. Transfer of single layer graphene consists of coating PMMA layer, etching bottom catalyst layer, rinsing graphene layer and transfer to desired substrates.

1.2.1.2 Chemical Exfoliation

Graphene produced from chemical exfoliation of graphite is also attractive compared with CVD graphene. With such an approach, large quantity and facile fabrication without high temperature processing could be realized in any chemistry lab. The obtained graphene sheets could be chemically functionalized, dispersed in polymer matrices, and deoxygenated to yield novel composites, making it a good candidate for

various applications.[48] Also, a graphene film or composite could be easily prepared according to figure 1.6.

Synthesis of graphite oxide (GO) can be achieved by placing graphite in one or more concentrated acids in the presence of an oxidizing agent. In 1859, the first graphene oxide was obtained by Brodie who utilized potassium chlorate and nitric acid to treated graphite repeatedly.[6] In 1959, Hummers and Offeman demonstrated a less hazardous and more efficient method for graphite oxidation, which involves a mixture of sodium nitrate, potassium permanganate, and concentrated sulfuric acid.[7] The method was later modified and utilized to produce high quality graphene oxide and reduced graphene oxide sheets.[49-52]

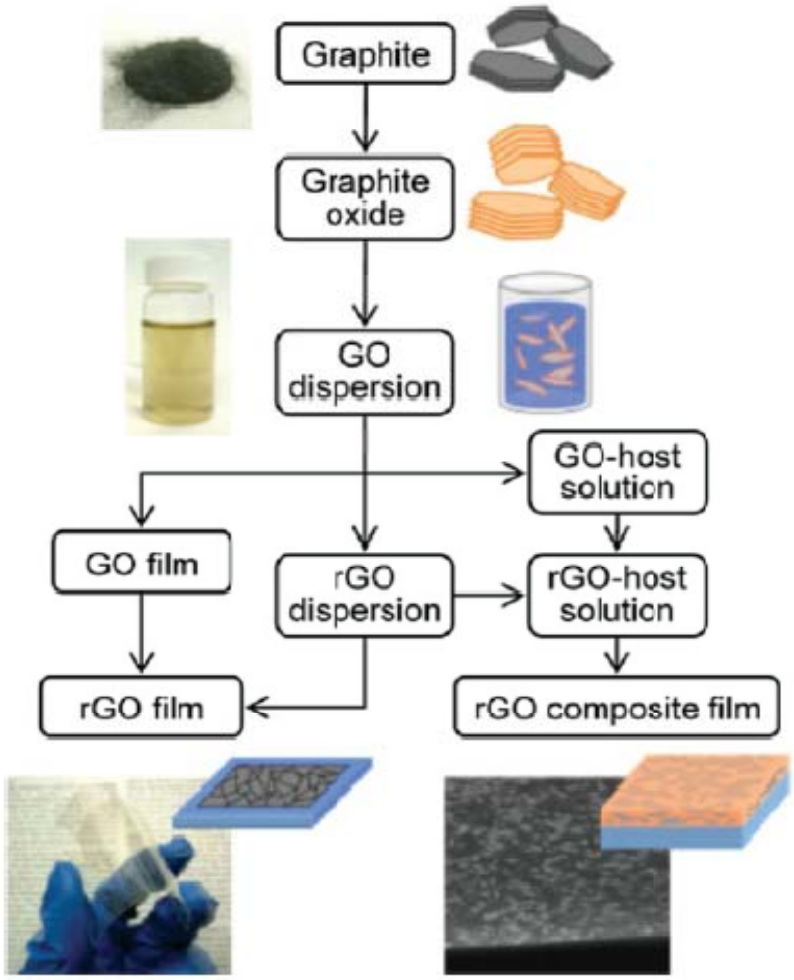

Figure 1.6 Process scheme for fabricating rGO-based thin films. The schematic illustrations show the structure of the material at each stage of the process. The gray and the orange sheets represent non-oxidized and oxidized graphene sheets, respectively.[20]

Single layer graphene oxide sheets produced from approaches mentioned above are rich in different functional groups, leading it to be a good candidate for further functionalization. The dominant chemical structures present on the surface of GO are tertiary alcohols and ethers with very low quantities of carboxylic acid at the periphery of the GO (Figure 1.7).[53]

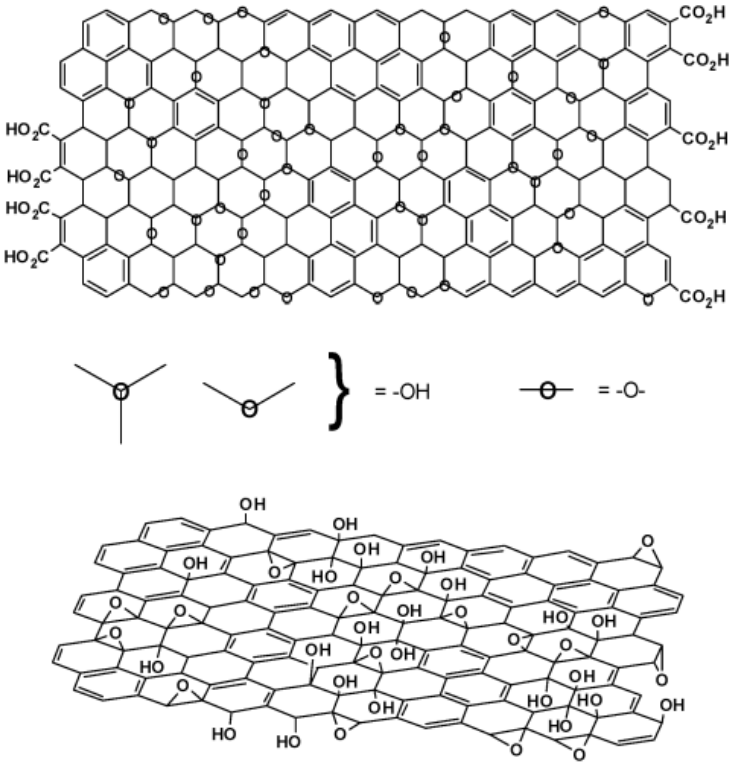

Figure 1.7 Variations of the Lerf-Klinowski model indicating ambiguity regarding the presence or absence of carboxylic acids on the periphery of the basal plane of the graphitic platelets of GO.[53]

Different approaches have been devised to obtain graphene sheets by reducing GO sheets, including thermal reduction (approximately 30% of the mass of the GO is lost during the reduction process, leaving behind vacancies and topological defects throughout the plane of the reduced graphene oxide platelet),[54] chemical reduction (N_2H_4,[55] $NaBH_4$,[56-57]) and photoreduction.[58] Among all of these methods, N_2H_4 has been deemed as the most efficient yet most toxic one. By combining $NaBH_4$ reducing and thermal annealing approaches, high quality graphene has been obtained with impurities in the final product consisting of sulfur and nitrogen and measuring less than 0.5 wt% of the

overall weight. This method is particularly effective in the restoration of the pi-conjugated structure, and leads to highly soluble and conductive graphene materials.[57]

1.2.1.3 Other Methods

The first visible graphene single layer was obtained by micromechanical exfoliation of Highly Ordered Pyrolytic Graphite in 2004 when the Nobel laureates, Geim and Novoselov used Scotch tape to peel graphene layers and to transfer them onto Si/SiO_2 substrates.[8] Later on, epitaxial graphene was obtained by thermal decomposition of SiC at 1000-1500 ^{o}C. [59]

1.2.2 Electronic Structure of Graphene

In graphene structure, each carbon atom is bonded to three other carbon atoms according to a sp^2 hybridization. The hexagonal network of carbon atoms are connected by a strong covalent sp^2-sp^2 σ-σ in-plane bonding. Due to an additional $2p_z$ orbital π-π bonding which is oriented perpendicularly to the atomic plane, the delocalized electrons appear. They are responsible for electrical conductivity of graphite which is highly anisotropic.[35] The unit cell of graphene contains 2 equivalent atoms with nearest distance of 1.42 Å (Figure 1.8 a). This crystal structure results in the touching between bonding (π) and anti-bonding (π^*) orbitals at each energy valleys K and K' when considering that hopping only occurs between the nearest neighbor atomic sites.[60] The valence and conduction bands touch at the Brillouin zone corners thus making graphene a zero-bandgap semiconductor. The carriers' speed, called as Fermi velocity, is as high as 10^6 m/s (~ 1/300 c , where c is velocity of light), and thus the electrical transport properties

of graphene are remarkably ascribed to such photon-like relativistic Dirac fermions. Particularly, the gapless graphene displays an ambipolar electric field effect with ballistic properties presenting extremely high mobility at room temperature as observed experimentally.[61-62] Furthermore, graphene can be doped by electrons or holes with tunable charge concentration, and the maximum can exceed ~ 10^{13} cm^2.[63]

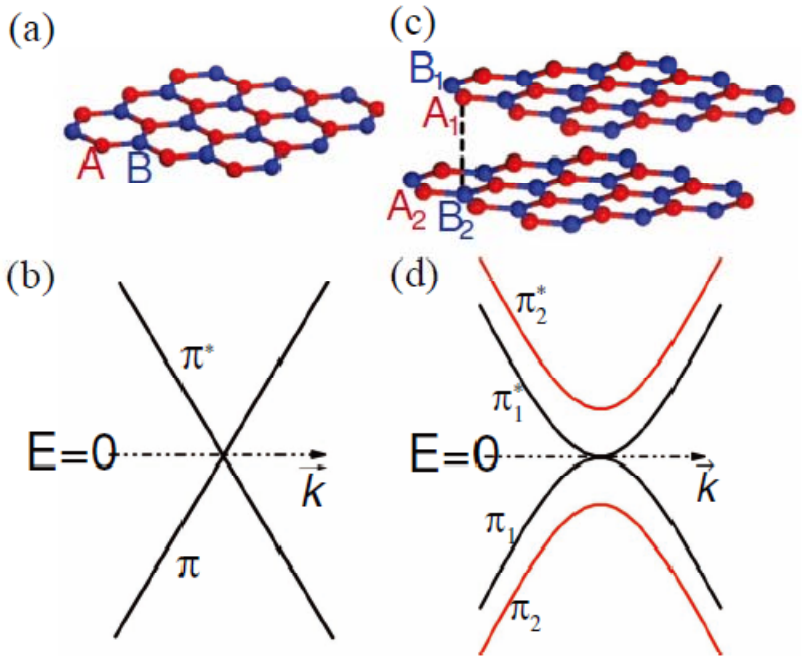

Figure 1.8 Crystal structures of graphene single layer (a) and AB-stacked bilayer (c). The unit cell of single layer graphene and bilayer graphene consist of 2 and 4 atoms in each unit cell, respectively. The hopping between nearest neighbor atom sites A and B resulting in the linear dispersive electronic band structure (b). The interlayer coupling for bilayer graphene cannot be ignored as the hopping between A 1 and B 2 affected the electronic band structure and resulting two parabolic electronic bands (d).[60]

1.2.3 Chemical Functionalization

The tuning of the graphene's Fermi level is an important factor in determining the successful operation of the electronic devices (diodes, field effect transistors, light

emitting diodes, solar cells, etc.) Tailoring the electronic properties of graphene thus is essential for broadening its applications. Chemical doping or charge transfer doping are very important to achieve the Fermi level tuning goals. p-Type doping drives the Dirac points of graphene above the Fermi level, and n-type doping drives the Dirac points below the Fermi level. Or we can say n-type or p-type doping cause a shift of the Fermi level in the graphene from the Dirac point into the conduction band or valence band. Many approaches have been applied for such purpose including molecules, nanoparticles and polymers.

Depends on the presence of electron donating or electron withdrawing functional groups, n-type or p-type doping effect could be achieved through a molecule doping approach. The presence of positive or negative charges on surface of nanoparticles could also be utilized to achieve n-type or p-type doping through a charge transfer mechanism.

Molecules	Molecular structure or functional groups (monomer)	Doping effect (*n*-type or *p*-type)
p-Toluenesulfonic acid	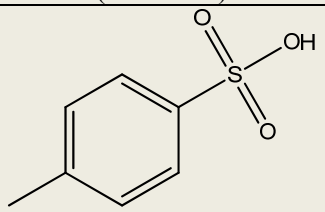	n-type [64]
tetrafluoro-tetracyanoquinodimethane (F4-TCNQ)	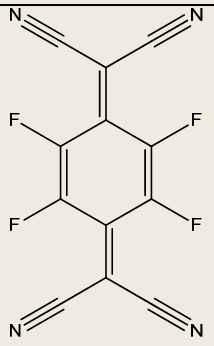	p-type [65]

4-bromobenzenediazonium tetrafluoroborate	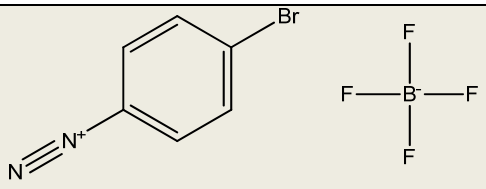	p-type[66]
poly(ethylene imine)		n-type[66]
1,5-naphthalenediamine	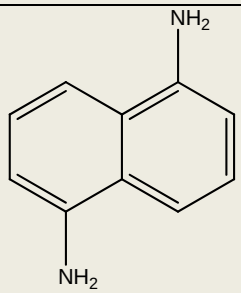	n-type[67]
9,10-dimethylanthracene	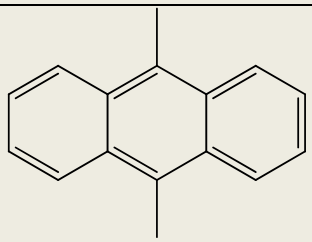	n-type[67]
9,10-dibromoanthracene	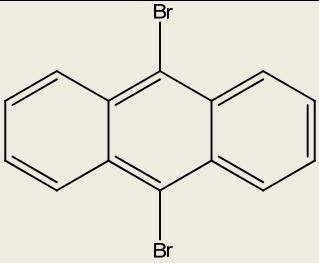	p-type[67]

tetrasodium 1,3,6,8-pyrenetetrasulfonic acid	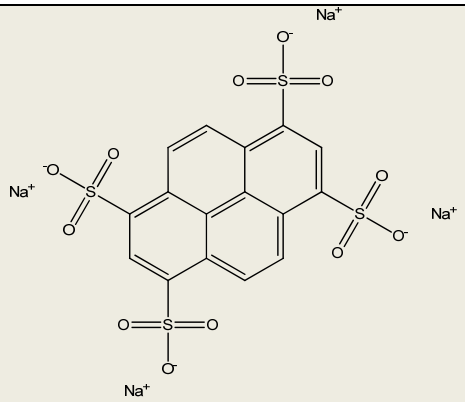	p-type[67]
water	H_2O	p-type[8]
ammonia	NH_3	n-type[62,68]
nitrogen dioxide	NO_2	p-type[62]
sulfur dioxide	SO_2	p-type[69]
benzoyl peroxide	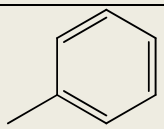	n-type[70]
tetracyanoethylene (TCNE)	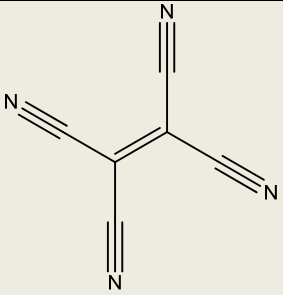	p-type[71]
(tridecafluoro-1,1,2,2-tetrahydrooctyl)trichlorosilane	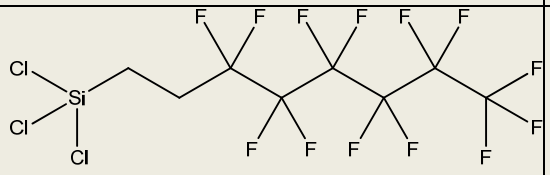	p-type[72]
ethanol	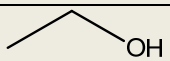	n-type[8]

nitrophenyl diazonium tetrafluoroborate	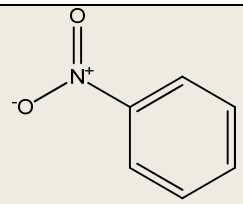	n-type[73]
azidotrimethyltin	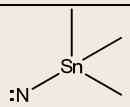	n-type[74]
2,4,6-Tris(dimethylamino)-1,3,5-Triazine	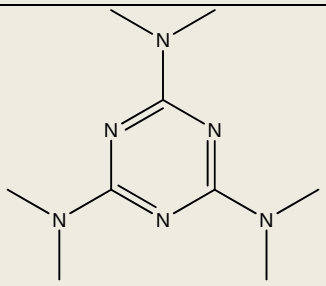	n-type[75]
p-tert-Butylcalix[4]arene	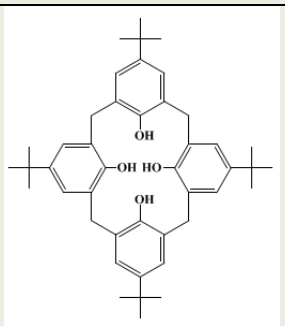	p-type[76]
4-amino-2,2,6,6-tetramethyl-1-piperidinyloxy (4-amino-TEMPO	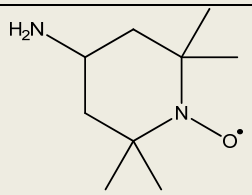	n-type[77]
CF_4	CF	p-type[10]
aminopropyltriethoxysilane	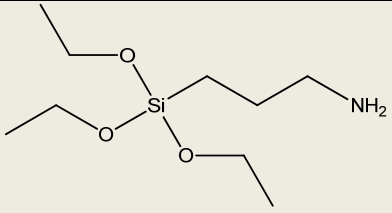	n-type[78]

hexamethyldisilazane	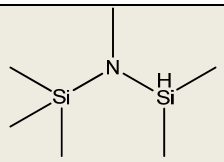	neither n-type or p-type[79-80]
hydrogen silasesquioxane (HSQ)	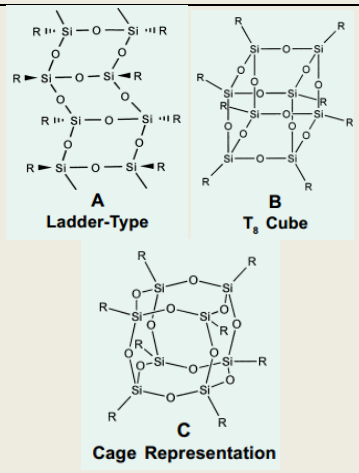	n-type[81]
Pyrene-1-sulfonic acid	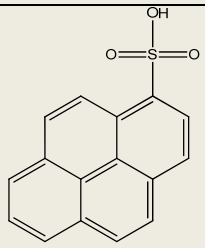	n-type[82]
3,4,9,10-perylenetetracarboxylic diimide	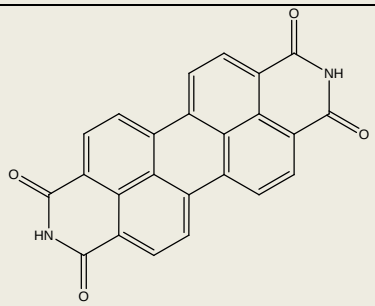	p-type[82]
1-aminopyrene	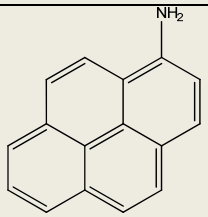	n-type[83]

1-nitropyrene	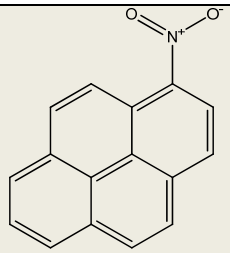	p-type[83]
1-pyrenecarboxylic acid	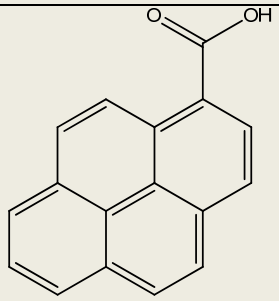	p-type[83]
1-pyrenesulfonic acid	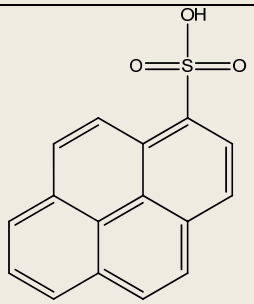	p-type[83]
poly(styrene-b-4-vinylpyridine)	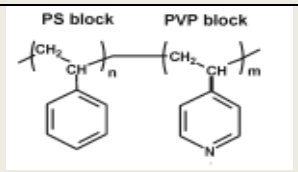	p or n type[10]
TiO_2 nanoparticles	Graphene oxide and TiO_2	Electron transfer from TiO_2 to graphene[84]
TiO_2 thin film	CVD graphene	n-type[85]
Fe_3O_4, TiO_2, CdSe nanoparticles	Ligands: trioctylphosphine oxide, oleic acid	n-type[86]
potassium	K	n-type[87]
phosphorus	P	n-type[88]
silver	Ag	n-type[89]

gold	Au	p-type[90-91]
copper	Cu	n-type[89]
bismuth	Bi	n-type[91]
antimony	Sb	n-type[91]
nitrogen	N	n-type[88]

Table 1.1 Summary of doping effects with molecules, polymers, elements and nanoparticles tuning electronic structure of graphene.

For n-type (p-type) doping the electrons have to be released into (extracted out of) the graphene layer. All of the examples (molecules, polymers, nanoparticles, elements) shown above demonstrate such ability to tune the electronic structure of graphene. However, this is still ambiguous for certain functional groups which need to be further studied. For example, with the same functional group, *p*-toluenesulfonic acid shows n-type doping while 1-pyrenesulfonic acid shows p-type doping. Note that even elements in the same group may display different doping effects to graphene devices (Ag and Au).[89] This is related to the nature of elements' electron negativity. The higher the electron negativity the higher the tendency for the element acts as an electron withdrawing property indicating p-type doping effect. Also, there is still a need to precisely manipulate the electronic structure with one or more molecules.

1.2.4 Graphene Field Effect Transistor Sensor

The unique property of graphene enables extraordinary graphene field effect transistor for a new generation of electronic devices. Graphene instead of conventional semiconductors serves as the channel which will facilitate functionalization of the

channel with various molecules, elements, and polymers providing more chances for sensor device applications. The 2D nature of graphene allows total exposure of all of its surface carbon atoms to the adsorbed molecules, providing the high surface area, and it is inherently a low-noise material due to the quality of its crystal lattice, which leads to screen charge fluctuations more than one dimensional systems such as carbon nanotubes. Considering different various gases demonstrate different doping effect (table 1.1), graphene field effect transistors should be applied effortlessly.

The theoretical surface area could be calculated from the following process using one hexagon unit cell (Figure 1.9):

The surface area of one hexagon is:

$$s = 3d_{C-C}^2 \frac{\sqrt{3}}{2} = 5.246\times10^{-20}\ m^2 \quad (1)$$

s corresponds to two carbon atoms whose weight is taking into account the atomic weight of carbon (M_C = 12.01 g/mol) and the Avogadro number (N_A= 6.023×10^{23} mol^{-1})

$$W_C = 2\ M_C / N_A = 3.988 \times 10^{-23}\ g \quad (2)$$

Combining (1) and (2) gives the specific surface area of one side of a graphene sheet ($S_{graphene}$):

$S_{graphene} = s/W_C$ = 1315 m^2/g. Thus, considering double sides of a graphene sheet, the specific surface area should be 2630 m^2/g which further demonstrates the potential application for graphene field effect transistors as sensor devices.

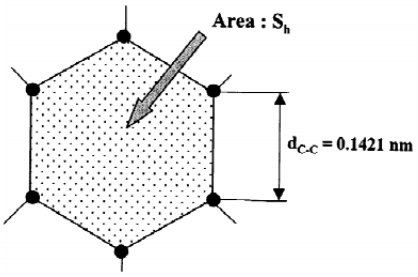

Figure 1.9 Schematic representation of the arrangement of carbon atoms within the graphene layer.[92]

1.2.4.1 Graphene Field Effect Transistor Gas Sensor

The report of individual molecule detection with graphene[62] intrigues the graphene field effect transistor sensor development. Working principles of most GFET sensors are based on electrical conductance change with exposure of gases. For example, figure 1.10 shows the device fabricated with GO film for HCN detection. Doping effects as well as charge transfer enable GFET detection of various molecules. Graphene synthesized from reducing graphene oxide, exfoliating HOPG, growing with CVD and thermal reduction from SiC have been utilized for such applications. As it is summarized in table 1.2, various detection limits have been achieved.

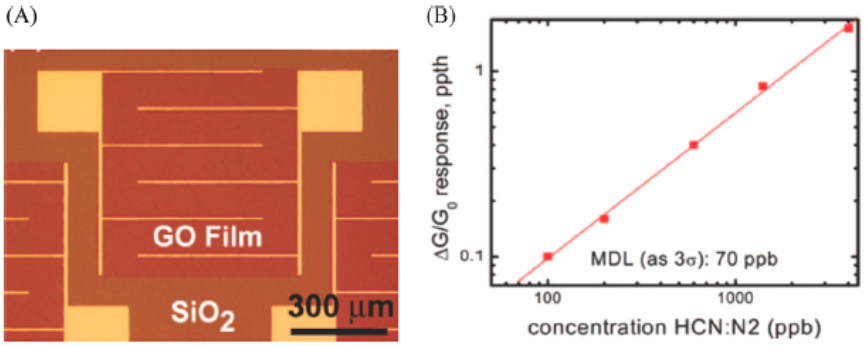

Figure 1.10 (A) Optical image of electrically isolated GO device with interdigitated metal contacts. (B) Response of an rGO sensor to different concentrations of hydrogen cyanide (HCN) as a chemical-warfare agent.[93]

Sensor material	Gases or vapor detected	Detection limit	Year
mechanically exfoliated graphene, shaped by lithography; measurements made with and without PMMA resist	H_2O, NH_3, nonanal, octanoic acid, trimethylamine	depended on vapor and presence of photoresist: e.g., 5 ppm for nonanal with resist; >30 ppm without	2009[94]
hydrazine-reduced graphene oxide with variable levels of reduction	NO_2, NH_3, dinitrotoluene (DNT)	<5 ppm NO_2 and NH_3; 28 ppb DNT	2009[95]
graphene oxide reduced chemically or thermally or by both approaches	H_2O	<0.1 Torr of H_2O vapor	2008[96]
low-temperature thermally reduced graphene oxide	NO_2	~2 ppm	2009[97-98]
nanoscale flakes of abraded graphite	NO_2	<60 ppb	2007[99]
hydrazine-reduced graphene oxide with variable levels of reduction	HCN, chloroethylethyl sulfide (CEES), dimethylmethylphosphonate (DMMP), DNT	70 ppb HCN; 0.5 ppb CEES; 5 ppb DMMP; 0.1 ppb DNT	2008[93]
mechanically exfoliated graphene, shaped by lithography	NO_2, H_2O, I_2, NH_3, CO, ethanol	~1 ppb	2007[62]
CVD graphene, Pt	H_2	25ppm	2010[100]
Epitaxial graphene, Pt	H_2	1%	2011[101]
CVD graphene	NH_3	30mTorr	2011[102]

Table 1.2 Graphene field effect transistors for various gas sensors.

Despite the advancements shown above, there are still several challenges that need to be overcome. (1) Selectivity. Graphene is exquisitely sensitive to the chemical environment and hence is easily affected by a range of different gas species and mixtures

(table 1.1). Therefore, specific identification of gas components is challenging. For example, exposure to either NO_2 or O_2 causes a similar increase in graphene conductance. Moreover it is impossible to detect a single gas from the gas mixture. For example, a mixture that contains p-type doping molecules such as NO_2 and n-type doping molecules such as NH_3 may not create any net change in the graphene's conductivity. Future research needs to focus on functionalizing the graphene with capture agents that will enable the specific binding of target gases to the graphene surface. (2) Reversibility. The thermal energy at room temperature is typically not enough to overcome the activation energy needed for molecular desorption for gases such as NO_2 and NH_3 on graphene surfaces. Typically it needs high temperature, UV, or vacuum for gas desorption to clean the graphene surface and expel the chemisorbed molecules. Such treatments usually result in an irreversible reaction between molecules and graphene devices. Still, innovative approaches to functionalize graphene surfaces are needed to control the binding energy of target molecules to the graphene surface. (3) Stability. Practical usage of sensors requires high stability regardless of changing environmental conditions such as moisture, temperature, residual charge build-up, or contamination. This creates additional difficulties for reliable and repeatable sensing. (4) Cost. To be competitive with commercial sensors, graphene-based devices must be mass producible at low cost. Therefore top-down methods such as exfoliation of GO could be used to mass produce graphene nanosheets at low cost. Moreover large scale synthesis with CVD could substantially lower the cost of graphene-based chemical sensors.

1.2.4.2 Graphene Field Effect Transistor Biosensor

Label-free biosensors with high miniaturization and integration have attracted intense research interest since they could potentially make advanced low cost molecular diagnostics routinely available. Given the high sensitivity nature of graphene and various functionalizations with ease, graphene field effect transistors have high potential for such applications. Many factors have demonstrated the lab-on-chip realization with graphene, such as the wafer scale synthesis, high quality with single layer or double layer control and thousands of circuits' production in one batch of photolithography.

For biosensors, ionic screening of the charged impurities on graphene plays an important role. NaF has been systematically studied as an example. Counterions (Na^+) in the solution could accumulate on the graphene surface to neutralize the impurity charges underneath the graphene which result in orders of magnitude increase of mobility and decrease of minimum conductivity.[24] Such effect could be utilized to monitor ionic concentration change during biological interactions.

Theoretically, ions may be specifically bound at the inner Helmhotz plane at the graphene/electrolyte interface during charging process. The ideally polarizable graphene/electrolyte interface allows the capacitive charging of the surface by H_3O^+ or OH^-, which plays a similar role as the gate potential in changing the Fermi level.[103] Many reports on GFET pH sensors are based on such mechanism.[103-107]

Another interesting mechanism is called the gating effect. Positive or negative charged biomolecules will act as gating modulators which will drive the Fermi level in the graphene from the Dirac point into the conduction band or valence band. DNA gating

effects have been well studied through Raman and theoretical modeling.[108] With such an effect single strand DNA could be identified with the low detection limit 3nM.[109]

With all of these mechanisms, GFET has been utilized for detecting various biological materials, such as DNA,[109-113] cells,[114] bacterium,[110] proteins.[110] Incorporation of nanoparticles or functionalization of graphene with polymers and selective functional groups will definitely improve its sensitivity and selectivity.

1.3 Energy Storage Devices: Supercapacitor

Electrochemical capacitors, also called supercapacitors, store energy using either ion adsorption (electrochemical double layer capacitors) or fast surface redox reactions (pseudo-capacitors). They can complement or replace batteries in electrical energy storage and harvesting applications, when high power delivery or uptake is needed. Supercapacitors (SC) are a promising high performance energy storage system due to their rapid charge and discharge rate, long operational cycle life and reliable performance at extreme temperatures. Their high power density and excellent cycling lifetime make supercapacitors suitable for a wide variety of applications like electric or hybrid electric vehicles.[115-116] Typically, for conventional electrochemical double layer capacitors (EDLCs), pristine or activated types of carbon materials have been widely used due to their unique combination of good chemical and physical properties like high conductivity, large surface area, good corrosion resistance and electrochemical stability, excellent temperature stability, processability and compatibility in composite materials and relatively low cost. Electrochemical capacitors currently fill the gap between batteries

and conventional solid state and electrolytic capacitors (Figure 1.11).[115] They store hundreds or thousands of times more charge (tens to hundreds of farads per gram) than the latter, because of a much larger surface area (1,000–2,000 $m^2 g^{-1}$) available for charge storage in EDLC. However, they have a lower energy density than batteries, and this limits the optimal discharge time to less than a minute. Intensive researches have been conducted on 0D carbon capsules, 1D carbon nanotubes/fibers (CNTs/CNFs), 2D graphene, 3D carbon hybrid nanostructure like CNT-graphene networks by chemical vapor deposition and solution processing of graphene-CNT hybrid materials.[117-124] Besides 2D graphene sheets, an innovative free-standing 3D graphene/ultrathin graphite foam structure has been demonstrated recently to have a lot of superior properties for 3D seamless interconnects and flexible networks.[125-128] Meanwhile, to improve the energy density and capacitance pseudo-capacitive materials are applied to introduce the fast surface redox reactions, which increase the capacitance and energy density. Various nanostructured redox-active materials such as RuO_2,[129] MnO_2,[116,130-132] NiO,[133] V_2O_5,[134] etc. as electrodes have been demonstrated to boost the specific capacitance to show a high energy density with a compromise in cycling stability and power density.

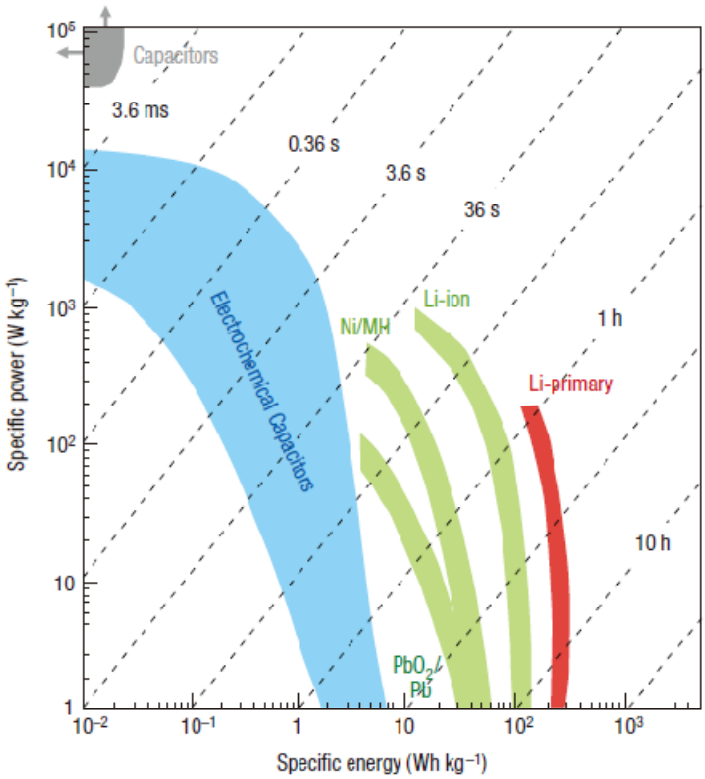

Figure 1.11 Specific power against specific energy, also called a Ragone plot, for various electrical energy storage devices. If a supercapacitor is used in an electric vehicle, the specific power shows how fast one can go, and the specific energy shows how far one can go on a single charge. Times shown are the time constants of the devices, obtained by dividing the energy density by the power.[115]

1.3.1 Graphene/Carbon Nanotube Hybrid

Theoretical studies[135-136] have indicated that 3D pillared architectures, consisting of parallel graphene layers supported by vertically aligned carbon nanotubes (VACNTs) in between, possess desirable out-of-plane transport and mechanical properties while maintaining the excellent properties of their building blocks (Figure 1.12). Monte Carlo simulations revealed that this novel material doped with lithium cations can reach hydrogen storage capacity of 41g L-1, which would meet the D.O.E's volumetric target

for mobile applications under ambient conditions. And this demonstrates the astonishing large surface area of the new material.

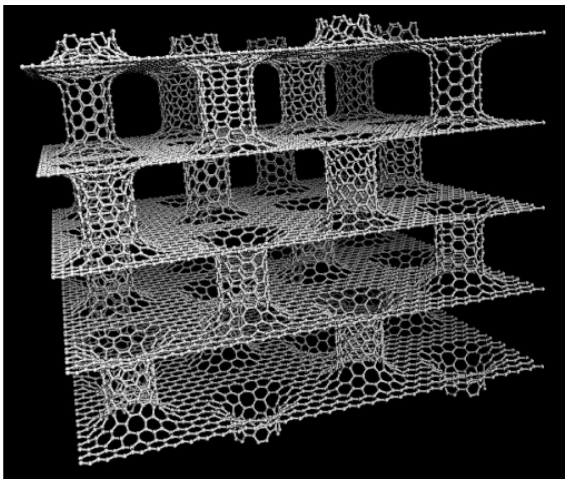

Figure 1.12 Pillared graphene. A novel 3-D network nanostructure proposed for enhanced hydrogen storage.[136]

Densely grown vertical carbon nanotube arrays possess many appealing properties useful for applications ranging from electronics to energy storage devices. Several advantages will enable the novel material to be a good candidate for energy storage devices. First, the small CNT diameter (less than 20nm) allows for better accommodation of the large volume changes without the initiation of fracture that can occur in bulk or micron-sized materials. This is consistent with previous studies that have suggested a materials-dependent terminal particle size below which particles do not fracture further. Second, each CNT is electrically connected to the metallic current collector so that all the CNTs contribute to the capacity. Third, the CNTs have direct 1D electronic pathways allowing for efficient charge transport. In electrode microstructures based on particles, electronic charge carriers must move through small interparticle contact areas. In addition, as every CNT is connected to the current-carrying electrode,

the need for binders or conducting additives, which add extra weight, is eliminated. Furthermore, our grown CNT/graphene structure could be completed in one step which facilitates its wide application on industry scale.

1.3.2 Pseudocapacitor

The specific pseudo-capacitance exceeds that of carbon materials using double layer charge storage. During the charge-discharge process, multiple electrons are involved in the reaction which increases the specific capacitance. High capacitance has been achieved for VN (1200 Fg^{-1}),[137] RuO_2 (1300 Fg^{-1}),[138] MnO_2 (2530 Fg^{-1}),[139] V_2O_5 (440 Fg^{-1}),[140] $Ni(OH)_2$ (3152 Fg^{-1}).[141] The amorphous surface of the oxide materials exposes multivalence elements providing higher capacitance.[142] Also, by coating RuO2 nanoparicles with a conductive polymer the conductance was enhanced leading to higher specific capacitance.[138] Thus the design of specific surface functionalization to improve interfacial exchange could be a generic approach to other pseudo-redox materials.

Several factors limited the application of pseudo capacitors. (1) Because redox reactions are used, pseudocapacitors suffer from a lack of stability during cycling. (2) The device usually possesses a small operating voltage window with inorganic electrolyte. As a consequence, the energy density is pretty low for such material system. To solve these problems, a hybrid material system is introduced (Figure 1.13). Synthesis of carbon materials/oxide materials could be realized through two main approaches: (1) solution in-situ reaction of oxide precursors with carbon materials; (2) deposition of oxide materials on the surface of confined shape carbon materials such as carbon nanotubes, activated carbon spheres and carbon nanofibers.

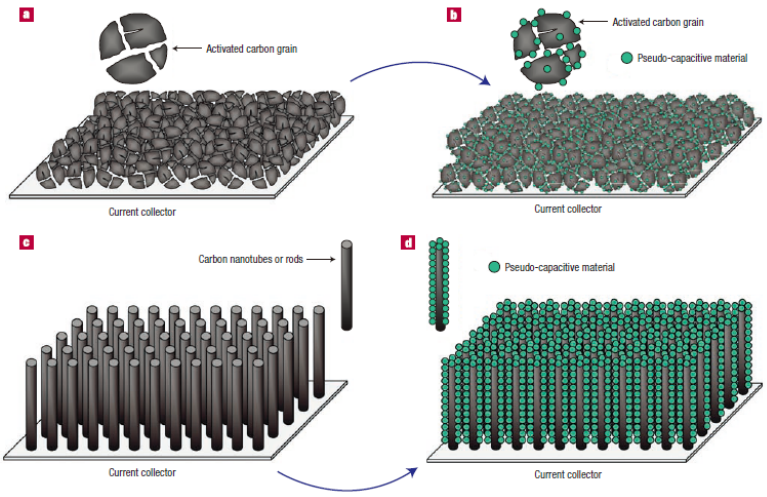

Figure 1.13 Possible strategies to improve both energy and power densities for electrochemical capacitors. (a) Decorating activated carbon grains (b) with pseudo-capacitive materials. (c) Achieving conformal deposit of pseudo-capacitive materials (d) onto highly ordered high-surface-area carbon nanotubes.[115]

For example, nanoscale MnO_2 incorporated into CNTs yielded significant capacitance enhancement, with a MnO_2-normalized capacitance up to 579 F g^{-1}.[143] A free standing film fabricated by mixing V_2O_5 nanowires and carbon nanotubes produce 42.9 F g^{-1} even at a high discharge current density of 10 A g^{-1}.[144] Core/shell structure of CNTs and MnO_2 nanowires creates to a dual storage mechanism of EDLC and pseudocapacitance leading to a maximum specific capacitance of 68 F/g, and an energy density of 4.5 Wh kg^{-1}.[145]

1.4 Contribution from This Dissertation

Graphene has attracted a lot of attention due to its remarkable intrinsic electronic properties. The ballistic transport of electrons, along with mobilities exceeding 20 000 $cm^2/V{\cdot}s$ and an ambipolar field effect, make graphene a promising candidate for the next

generation of semiconductor devices. In this dissertation, we discuss approaches of taking advantage of the limitations of graphene for sensor device applications. Also, high performance of supercapacitors and photovoltaic devices were realized by taking advantage of the superior properties of graphene. Furthermore, future advances of interesting topics have been presented. These topics might bring new discoveries or improvement for graphene/carbon nanotube based electronics and energy storage devices.

In chapter 2, it is shown that charge carrier transport in graphene can be tuned between hole and electron conduction by shifting the Fermi level with functionalized molecules, polymers and nanoparticles. Assembling cylindrical microdomains of polystyrene-4-polyvinylpyridine (PS-P4VP) block copolymers as protective layers on GFETs is a methodology to tune the electron and hole conduction of graphene. Spatially controlled fluorine doping provides a general route to refined tuning of the electronic properties of BCPs coated GFETs. Later, we incorporate monolayer pyridine functionalized CdSe nanoparticles onto single layer graphene via π-π interaction bewteen pyridine and graphene. Illumination of the quantum dots led to injection of n-carriers in the graphene phase. Transient absorption spectra provide evidence for photoinduced hole-shift from the CdSe to the pyridine ligands, thereby polarizing the surface of the quantum dots favoring the simultaneous electron transfer from the CdSe to the graphene phase. Photoresponse of the as-fabricated graphene field effect transistor demonstrates high possibility for using such a device as a photoswitch. Moreover, photoelectrochemical studies show high IPCE of 3% for monolayer CdSe quantum dots on single layer graphene.

In chapter 3, synthesis of large area, up to 4 square inches single layer graphene allows us to fabricate numerous sensors in one batch. Non-covalent functionalization of the graphene layer with 1-pyrenebutanoic acid succinimidyl ester ensures high conductivity and sensitivity of the FET device. The employed device reaches a detection limit as low as 3×10^{-9} M. Furthermore, a highly stable graphene field effect transistor (GFET) sensor for chemical sensing has been achieved by functionalization with BCP. The unique properties of block copolymers offer high stability and possible selective sensing property. The orientation and periodicity of the resulting BCP array of cylindrical microdomains facilitate the selective sensing property. With functionalization the sensor could be stable for more than 4 months under ambient atmosphere. Further pH measurement studies demonstrate the high sensitivity and practical usage for such a robust sensor.

In chapter 4, two types of carbon nanotube/graphene composite/hybrid are successfully synthesized and applied for supercapacitors. The first type consists of a graphene/vertically aligned carbon nanotube hybrid which is successfully grown with one step chemical vapor deposition method. Detailed characterizations including TEM, Raman, SEM elucidate the cohesive structure and seamless contact between the graphene floor and the CNTs in the hybrid structure. Our fabrication approach provides an attractive pathway for the fabrication of novel 3-D hybrid nanostructures, and efficient device integration. The second type is graphene oxide (GO) and single walled carbon nanotube (SWCNT) composite ink (GO-SWCNT ink). Atomic force microscopy (AFM) and scanning electron microscopy (SEM) studies demonstrate the obtained graphene

oxide (GO) flakes are single layer with size distribution from 100nm-20um. SWCNTs are dispersed using a GO aqueous solution (2mg/ml) with sonication support to achieve a SWCNT concentration of 12mg/ml, the highest reported value so far without surfactant assistance. Raman spectroscopy studies indicate that the FWHM of the G band increases with the mixing of SWCNT and GO indicating electronic structure changes via π-π interactions of GO sheets and SWCNTs. Paper based electrodes were conveniently fabricated with such GO-SWCNT composite ink via a dip casting method. By employing different concentrations of SWCNT in the ink, the paper electrodes provide different capacitance values. The highest value of specific capacitance reaches 295 F/g at a current density of 0.5A/g with a GO/SWCNT weight ratio of 1:5. The cycling stability for the GO-SWCNT paper electrode supercapacitors indicates capacitance retention of 85% over 60000 cycles.

1.5 References

(1) John. Boardman,"*The Neolithic-Eneolithic Period"* ***The Cambridge ancient history***, *3*, part1, 31-33.

(2) P. R. Wallace,"*The Band Theory of Graphite"* ***Physical Review*** *1947*, *71*, 476.

(3) A. K. Geim, K. S. Novoselov,"*The rise of graphene"* ***Nature Materials*** *2007*, *6*, 183.

(4) Re Peierls,"*Quelques propriétés typiques des corps solides"* ***Ann. Inst. Henri Poincare*** *1935*, *5*, 177.

(5) Ld Landau,"*Zur theorie der phasenumwandlungen II. Phys"* ***Z. Sowjetunion*** *1937*, *11*, 26.

(6) B.C. Brodie,"*On the atomic weight of graphite"* ***Philosophical Transactions of the Royal Society of London*** *1859*, *149*, 249.

(7) W. S. Hummers Jr, R. E. Offeman,"*Preparation of graphitic oxide"* ***Journal of the American Chemical Society*** *1958*, *80*, 1339.

(8) K. S. Novoselov, A. K. Geim, S. V. Morozov, D. Jiang, Y. Zhang, S. V. Dubonos, I. V. Grigorieva, A. A. Firsov,"*Electric field effect in atomically thin carbon films"* ***Science*** *2004*, *306*, 666.

(9) M. J. Allen, V. C. Tung, L. Gomez, Z. Xu, L. M. Chen, K. S. Nelson, C. W. Zhou, R. B. Kaner, Y. Yang,"*Soft Transfer Printing of Chemically Converted Graphene"* ***Advanced Materials*** *2009*, *21*, 2098.

(10) Shirui Guo, Maziar Ghazinejad, Xiangdong Qin, Huaxing Sun, Wei Wang, Francisco Zaera, Cengiz S. Ozkan, Mihrimah Ozkan,"*Tuning of Electron*

Transport in Graphene based Field Effect Devices using Block Co-Polymers" ***Small*** *2012*, *8*, 1073.

(11) Z. Y. Chen, S. Berciaud, C. Nuckolls, T. F. Heinz, L. E. Brus,"*Energy Transfer from Individual Semiconductor Nanocrystals to Graphene"* ***Acs Nano*** *2010*, *4*, 2964.

(12) L. M. Dai,"*Layered Graphene/Quantum Dots: Nanoassemblies for Highly Efficient Solar Cells"* ***Chemsuschem*** *2010*, *3*, 797.

(13) N. L. Yang, J. Zhai, D. Wang, Y. S. Chen, L. Jiang,"*Two-Dimensional Graphene Bridges Enhanced Photoinduced Charge Transport in Dye-Sensitized Solar Cells"* ***Acs Nano*** *2010*, *4*, 887.

(14) C. X. Guo, H. B. Yang, Z. M. Sheng, Z. S. Lu, Q. L. Song, C. M. Li,"*Layered Graphene/Quantum Dots for Photovoltaic Devices"* ***Angewandte Chemie-International Edition*** *2010*, *49*, 3014.

(15) H. X. Chang, X. J. Lv, H. Zhang, J. H. Li,"*Quantum dots sensitized graphene: In situ growth and application in photoelectrochemical cells"* ***Electrochemistry Communications*** *2010*, *12*, 483.

(16) S. Bae, H. Kim, Y. Lee, X. F. Xu, J. S. Park, Y. Zheng, J. Balakrishnan, T. Lei, H. R. Kim, Y. I. Song, Y. J. Kim, K. S. Kim, B. Ozyilmaz, J. H. Ahn, B. H. Hong, S. Iijima,"*Roll-to-roll production of 30-inch graphene films for transparent electrodes"* ***Nature Nanotechnology*** *2010*, *5*, 574.

(17) J. K. Wassei, R. B. Kaner,"*Graphene, a promising transparent conductor"* ***Materials Today*** *2010*, *13*, 52.

(18) V. C. Tung, L. M. Chen, M. J. Allen, J. K. Wassei, K. Nelson, R. B. Kaner, Y. Yang,"*Low-Temperature Solution Processing of Graphene-Carbon Nanotube Hybrid Materials for High-Performance Transparent Conductors"* ***Nano Letters*** *2009*, *9*, 1949.

(19) S. S. Li, K. H. Tu, C. C. Lin, C. W. Chen, M. Chhowalla,"*Solution-Processable Graphene Oxide as an Efficient Hole Transport Layer in Polymer Solar Cells"* ***Acs Nano*** *2010*, *4*, 3169.

(20) G. Eda, M. Chhowalla,"*Chemically Derived Graphene Oxide: Towards Large-Area Thin-Film Electronics and Optoelectronics"* ***Advanced Materials*** *2010*, *22*, 2392.

(21) S. De, P. J. King, M. Lotya, A. O'neill, E. M. Doherty, Y. Hernandez, G. S. Duesberg, J. N. Coleman,"*Flexible, Transparent, Conducting Films of Randomly Stacked Graphene from Surfactant-Stabilized, Oxide-Free Graphene Dispersions"* ***Small*** *2010*, *6*, 458.

(22) H. Chen, M. B. Muller, K. J. Gilmore, G. G. Wallace, D. Li,"*Mechanically strong, electrically conductive, and biocompatible graphene paper"* ***Advanced Materials*** *2008*, *20*, 3557.

(23) Limei Zhu, Liqiang Luo, Zhenxin Wang,"*DNA electrochemical biosensor based on thionine-graphene nanocomposite"* ***Biosensors and Bioelectronics*** *2012*, *35*, 507.

(24) F. Chen, J. L. Xia, N. J. Tao,"*Ionic Screening of Charged-Impurity Scattering in Graphene"* ***Nano Letters*** *2009*, *9*, 1621.

(25) Y. Y. Shao, J. Wang, H. Wu, J. Liu, I. A. Aksay, Y. H. Lin,"*Graphene Based Electrochemical Sensors and Biosensors: A Review"* ***Electroanalysis*** *2010*, *22*, 1027.

(26) Shi-Rui Guo, Jian Lin, Miroslav Penchev, Emre Yengel, Maziar Ghazinejad, Cengiz S. Ozkan, Mihrimah Ozkan,"*Label free DNA detection using large area graphene based field effect transistor biosensors"* ***J. Nanosci. Nanotechnol.*** *2011*, *11*, 5258.

(27) G. X. Zhu, Y. J. Liu, Z. Xu, T. A. Jiang, C. Zhang, X. Li, G. Qi,"*Flexible Magnetic Nanoparticles-Reduced Graphene Oxide Composite Membranes Formed by Self-Assembly in Solution"* ***Chemphyschem*** *2010*, *11*, 2432.

(28) Cui-Ling Zhang, Yun-Xia Yuan, Shi-Ming Zhang, Yu-Hui Wang, Zhi-Hong Liu,"*Biosensing Platform Based on Fluorescence Resonance Energy Transfer from Upconverting Nanocrystals to Graphene Oxide"* ***Angewante Chemie International Edition*** *2011*, *50*, 6851.

(29) Ying Wang, Zhaohui Li, Jun Wang, Jinghong Li, Yuehe Lin,"*Graphene and graphene oxide: biofunctionalization and applications in biotechnology"* ***Trends Biotechnol.*** *2011*, *29*, 205.

(30) Y. M. Lin, C. Dimitrakopoulos, K. A. Jenkins, D. B. Farmer, H. Y. Chiu, A. Grill, P. Avouris,"*100-GHz Transistors from Wafer-Scale Epitaxial Graphene"* ***Science*** *2010*, *327*, 662.

(31) N. O. Weiss, H. Zhou, L. Liao, Y. Liu, S. Jiang, Y. Huang, X. Duan,"*Graphene: an emerging electronic material"* ***Adv Mater*** *2012*, *24*, 5782.

(32) B. C. Banerjee, P. L. Walker, T. J. Hirt,"*Pyrolytic Carbon Formation from Carbon Suboxide"* ***Nature*** *1961*, *192*, 450.

(33) Robertso.Sd,"*Graphite Formation from Low Temperature Pyrolysis of Methane over Some Transition Metal Surfaces"* ***Nature*** *1969*, *221*, 1044.

(34) P. R. Somani, S. P. Somani, M. Umeno,"*Planer nano-graphenes from camphor by CVD"* ***Chemical Physics Letters*** *2006*, *430*, 56.

(35) A. N. Obraztsov, E. A. Obraztsova, A. V. Tyurnina, A. A. Zolotukhin,"*Chemical vapor deposition of thin graphite films of nanometer thickness"* ***Carbon*** *2007*, *45*, 2017.

(36) P. W. Sutter, J. I. Flege, E. A. Sutter,"*Epitaxial graphene on ruthenium"* ***Nature Materials*** *2008*, *7*, 406.

(37) J. Coraux, A. T. N'diaye, C. Busse, T. Michely,"*Structural coherency of graphene on Ir(111)"* ***Nano Letters*** *2008*, *8*, 565.

(38) J. C. Hamilton, J. M. Blakely,"*Carbon Segregation to Single-Crystal Surfaces of Pt,Pd and Co"* ***Surface Science*** *1980*, *91*, 199.

(39) Yagang Yao, Ching-Ping Wong,"*Monolayer graphene growth using additional etching process in atmospheric pressure chemical vapor deposition"* ***Carbon*** *2012*, *50*, 5203.

(40) A.Y. Tontegode, Ev Rut'kov,"*Intercalation by atoms of a two-dimensional graphite film on a metal"* ***Physics-Uspekhi*** *1993*, *36*, 1053.

(41) Ta Land, T. Michely, Rj Behm, Jc Hemminger, G. Comsa,"*STM investigation of single layer graphite structures produced on Pt (111) by hydrocarbon decomposition"* ***Surface Science*** *1992*, *264*, 261.

(42) X. S. Li, W. W. Cai, J. H. An, S. Kim, J. Nah, D. X. Yang, R. Piner, A. Velamakanni, I. Jung, E. Tutuc, S. K. Banerjee, L. Colombo, R. S. Ruoff,"*Large-Area Synthesis of High-Quality and Uniform Graphene Films on Copper Foils"* ***Science*** *2009*, *324*, 1312.

(43) N. A. Vinogradov, A. A. Zakharov, V. Kocevski, J. Rusz, K. A. Simonov, O. Eriksson, A. Mikkelsen, E. Lundgren, A. S. Vinogradov, N. Maartensson, A. B. Preobrajenski,"*Formation and structure of graphene waves on Fe(110)"* ***Phys. Rev. Letters*** *2012*, *109*, 026101/1.

(44) D. Kondo, K. Yagi, N. Harada, M. Sato, M. Nihei, S. Sato, N. Yokoyama, in *MRS Proceedings, Vol. 1205*, Cambridge Univ Press, **2009**.

(45) C. Mattevi, H. Kim, M. Chhowalla,"*A review of chemical vapour deposition of graphene on copper"* ***Journal of Materials Chemistry*** *2011*, *21*, 3324.

(46) Q. K. Yu, L. A. Jauregui, W. Wu, R. Colby, J. F. Tian, Z. H. Su, H. L. Cao, Z. H. Liu, D. Pandey, D. G. Wei, T. F. Chung, P. Peng, N. P. Guisinger, E. A. Stach, J. M. Bao, S. S. Pei, Y. P. Chen,"*Control and characterization of individual grains and grain boundaries in graphene grown by chemical vapour deposition"* ***Nature Materials*** *2011*, *10*, 443.

(47) J. M. Tour,"*Toward the Synthesis of Wafer-Scale Single-Crystal Graphene on Copper Foils"* ***Acs Nano*** *2012*.

(48) D. A. Dikin, S. Stankovich, E. J. Zimney, R. D. Piner, G. H. B. Dommett, G. Evmenenko, S. T. Nguyen, R. S. Ruoff,"*Preparation and characterization of graphene oxide paper"* ***Nature*** *2007*, *448*, 457.

(49) J. Y. Luo, L. J. Cote, V. C. Tung, A. T. L. Tan, P. E. Goins, J. S. Wu, J. X. Huang,"*Graphene Oxide Nanocolloids"* ***Journal of the American Chemical Society*** *2010*, *132*, 17667.

(50) Q. Yang, X. J. Pan, F. Huang, K. C. Li,"*Fabrication of High-Concentration and Stable Aqueous Suspensions of Graphene Nanosheets by Noncovalent Functionalization with Lignin and Cellulose Derivatives"* ***Journal of Physical Chemistry C*** *2010*, *114*, 3811.

(51) Y. W. Zhu, M. D. Stoller, W. W. Cai, A. Velamakanni, R. D. Piner, D. Chen, R. S. Ruoff,"*Exfoliation of Graphite Oxide in Propylene Carbonate and Thermal Reduction of the Resulting Graphene Oxide Platelets"* ***Acs Nano*** *2010*, *4*, 1227.

(52) M. D. Stoller, S. J. Park, Y. W. Zhu, J. H. An, R. S. Ruoff,"*Graphene-Based Ultracapacitors"* ***Nano Letters*** *2008*, *8*, 3498.

(53) D. R. Dreyer, S. Park, C. W. Bielawski, R. S. Ruoff,"*The chemistry of graphene oxide"* ***Chemical Society Reviews*** *2010*, *39*, 228.

(54) H. C. Schniepp, J. L. Li, M. J. Mcallister, H. Sai, M. Herrera-Alonso, D. H. Adamson, R. K. Prud'homme, R. Car, D. A. Saville, I. A. Aksay,"*Functionalized single graphene sheets derived from splitting graphite oxide"* ***Journal of Physical Chemistry B*** *2006*, *110*, 8535.

(55) S. Stankovich, D. A. Dikin, R. D. Piner, K. A. Kohlhaas, A. Kleinhammes, Y. Jia, Y. Wu, S. T. Nguyen, R. S. Ruoff,"*Synthesis of graphene-based nanosheets via chemical reduction of exfoliated graphite oxide"* ***Carbon*** *2007*, *45*, 1558.

(56) H.J. Shin, K.K. Kim, A. Benayad, S.M. Yoon, H.K. Park, I.S. Jung, M.H. Jin, H.K. Jeong, J.M. Kim, J.Y. Choi,"*Efficient reduction of graphite oxide by sodium borohydride and its effect on electrical conductance"* ***Advanced Functional Materials*** *2009*, *19*, 1987.

(57) W. Gao, L. B. Alemany, L. J. Ci, P. M. Ajayan,"*New insights into the structure and reduction of graphite oxide"* ***Nature Chemistry*** *2009*, *1*, 403.

(58) L. J. Cote, R. Cruz-Silva, J. X. Huang,"*Flash Reduction and Patterning of Graphite Oxide and Its Polymer Composite"* ***Journal of the American Chemical Society*** *2009*, *131*, 11027.

(59) C. Berger, Z. M. Song, X. B. Li, X. S. Wu, N. Brown, C. Naud, D. Mayou, T. B. Li, J. Hass, A. N. Marchenkov, E. H. Conrad, P. N. First, W. A. De Heer,"*Electronic confinement and coherence in patterned epitaxial graphene"* ***Science*** *2006*, *312*, 1191.

(60) D. Zhan, J. X. Yan, L. F. Lai, Z. H. Ni, L. Liu, Z. X. Shen,"*Engineering the Electronic Structure of Graphene"* ***Advanced Materials*** *2012*, *24*, 4055.

(61) Y. B. Zhang, Y. W. Tan, H. L. Stormer, P. Kim,"*Experimental observation of the quantum Hall effect and Berry's phase in graphene"* ***Nature*** *2005*, *438*, 201.

(62) F. Schedin, A. K. Geim, S. V. Morozov, E. W. Hill, P. Blake, M. I. Katsnelson, K. S. Novoselov,"*Detection of individual gas molecules adsorbed on graphene"* ***Nature Materials*** *2007*, *6*, 652.

(63) A. Das, S. Pisana, B. Chakraborty, S. Piscanec, S. K. Saha, U. V. Waghmare, K. S. Novoselov, H. R. Krishnamurthy, A. K. Geim, A. C. Ferrari, A. K. Sood,"*Monitoring dopants by Raman scattering in an electrochemically top-gated graphene transistor"* ***Nature Nanotechnology*** *2008*, *3*, 210.

(64) A. K. Singh, M. W. Iqbal, V. K. Singh, M. Z. Iqbal, J. H. Lee, S. H. Chun, K. Shin, J. Eom,"*Molecular n-doping of chemical vapor deposition grown graphene"* ***Journal of Materials Chemistry*** *2012*, *22*, 15168.

(65) W. Chen, S. Chen, D. C. Qi, X. Y. Gao, A. T. S. Wee,"*Surface transfer p-type doping of epitaxial graphene"* ***Journal of the American Chemical Society*** *2007*, *129*, 10418.

(66) D. B. Farmer, R. Golizadeh-Mojarad, V. Perebeinos, Y. M. Lin, G. S. Tulevski, J. C. Tsang, P. Avouris,"*Chemical Doping and Electron-Hole Conduction Asymmetry in Graphene Devices"* ***Nano Letters*** *2009*, *9*, 388.

(67) X. C. Dong, D. L. Fu, W. J. Fang, Y. M. Shi, P. Chen, L. J. Li,"*Doping Single-Layer Graphene with Aromatic Molecules"* ***Small*** *2009*, *5*, 1422.

(68) Y. C. Lin, C. Y. Lin, P. W. Chiu,"*Controllable graphene N-doping with ammonia plasma"* ***Applied Physics Letters*** *2010*, *96*.

(69) Y. J. Ren, C. F. Zhu, W. W. Cai, H. F. Li, H. X. Ji, I. Kholmanov, Y. P. Wu, R. D. Piner, R. S. Ruoff,"*Detection of sulfur dioxide gas with graphene field effect transistor"* ***Applied Physics Letters*** *2012*, *100*.

(70) H. T. Liu, S. M. Ryu, Z. Y. Chen, M. L. Steigerwald, C. Nuckolls, L. E. Brus,"*Photochemical Reactivity of Graphene"* ***Journal of the American Chemical Society*** *2009*, *131*, 17099.

(71) Y. H. Lu, W. Chen, Y. P. Feng, P. M. He,"*Tuning the Electronic Structure of Graphene by an Organic Molecule"* ***Journal of Physical Chemistry B*** *2009*, *113*, 2.

(72) B. Lee, Y. Chen, F. Duerr, D. Mastrogiovanni, E. Garfunkel, E. Y. Andrei, V. Podzorov,"*Modification of Electronic Properties of Graphene with Self-Assembled Monolayers"* ***Nano Letters*** *2010*, *10*, 2427.

(73) E. Bekyarova, M. E. Itkis, P. Ramesh, C. Berger, M. Sprinkle, W. A. De Heer, R. C. Haddon,"*Chemical Modification of Epitaxial Graphene: Spontaneous Grafting of Aryl Groups"* ***Journal of the American Chemical Society*** *2009*, *131*, 1336.

(74) J. Choi, S. N. Yang, K. J. Kim, H. Lee, S. Kim,"*Adsorption structure and doping effect of azidotrimethyltin on graphene"* ***Current Applied Physics*** *2011*, *11*, 1307.

(75) S. Park, S. Yang, H. Lim, H. Lee,"*Chemical Doping of Graphene by Altretamine(2,4,6-Tris [dimethylamino]-1,3,5-Triazine)"* ***Bulletin of the Korean Chemical Society*** *2011*, *32*, 2199.

(76) S. Park, S. Yang, K. J. Kim, K. No, H. Lee,"*p-Type Doping of Epitaxial Graphene by p-tert-Butylcalix[4]arene"* ***Bulletin of the Korean Chemical Society*** *2010*, *31*, 2809.

(77) J. Choi, H. Lee, K. J. Kim, B. Kim, S. Kim,"*Chemical Doping of Epitaxial Graphene by Organic Free Radicals"* ***Journal of Physical Chemistry Letters*** *2010*, *1*, 505.

(78) J. Park, S. B. Jo, Y. J. Yu, Y. Kim, W. Yang, W. H. Lee, H. H. Kim, B. H. Hong, P. Kim, K. Cho, K. S. Kim,"*Single-Gate Bandgap Opening of Bilayer Graphene by Dual Molecular Doping"* ***Advanced Materials*** *2012*, *24*, 407.

(79) B. N. Szafranek, D. Schall, M. Otto, D. Neumaier, H. Kurz,"*High On/Off Ratios in Bilayer Graphene Field Effect Transistors Realized by Surface Dopants"* ***Nano letters*** *2011*, *11*, 2640.

(80) M. Lafkioti, B. Krauss, T. Lohmann, U. Zschieschang, H. Klauk, K. Von Klitzing, J. H. Smet,"*Graphene on a Hydrophobic Substrate: Doping Reduction and Hysteresis Suppression under Ambient Conditions"* ***Nano Letters*** *2010*, *10*, 1149.

(81) K. Brenner, R. Murali,"*Single step, complementary doping of graphene"* ***Applied Physics Letters*** *2010*, *96*.

(82) Q. Su, S. P. Pang, V. Alijani, C. Li, X. L. Feng, K. Mullen,"*Composites of Graphene with Large Aromatic Molecules"* ***Advanced Materials*** *2009*, *21*, 3191.

(83) J. Lee, E. Hwang, E. Lee, S. Seo, H. Lee,"*Tuning of n- and p-Type Reduced Graphene Oxide Transistors with the Same Molecular Backbone"* ***Chemistry-a European Journal*** *2012*, *18*, 5155.

(84) I. V. Lightcap, T. H. Kosel, P. V. Kamat,"*Anchoring Semiconductor and Metal Nanoparticles on a Two-Dimensional Catalyst Mat. Storing and Shuttling Electrons with Reduced Graphene Oxide"* ***Nano Letters*** *2010*, *10*, 577.

(85) P. H. Ho, Y. C. Yeh, D. Y. Wang, S. S. Li, H. A. Chen, Y. H. Chung, C. C. Lin, W. H. Wang, C. W. Chen,"*Self-Encapsulated Doping of n-Type Graphene Transistors with Extended Air Stability"* ***Acs Nano*** *2012*, *6*, 6215.

(86) D. Q. Wang, X. F. Liu, L. He, Y. D. Yin, D. Wu, J. Shi,"*Manipulating Graphene Mobility and Charge Neutral Point with Ligand-Bound Nanoparticles as Charge Reservoir"* ***Nano Letters*** *2010*, *10*, 4989.

(87) J. H. Chen, C. Jang, S. Adam, M. S. Fuhrer, E. D. Williams, M. Ishigami,"*Charged-impurity scattering in graphene"* ***Nature Physics*** *2008*, *4*, 377.

(88) S. Some, J. Kim, K. Lee, A. Kulkarni, Y. Yoon, S. Lee, T. Kim, H. Lee,"*Highly Air-Stable Phosphorus-Doped n-Type Graphene Field-Effect Transistors"* ***Advanced Materials*** *2012*, *24*, 5481.

(89) Y. J. Ren, S. S. Chen, W. W. Cai, Y. W. Zhu, C. F. Zhu, R. S. Ruoff,"*Controlling the electrical transport properties of graphene by in situ metal deposition"* ***Applied Physics Letters*** *2010*, *97*.

(90) R. S. Sundaram, C. Gomez-Navarro, E. J. H. Lee, M. Burghard, K. Kern,"*Noninvasive metal contacts in chemically derived graphene devices"* ***Applied Physics Letters*** *2009*, *95*, 3.

(91) I. Gierz, C. Riedl, U. Starke, C. R. Ast, K. Kern,"*Atomic Hole Doping of Graphene"* ***Nano Letters*** *2008*, *8*, 4603.

(92) A. Peigney, C. Laurent, E. Flahaut, R. R. Bacsa, A. Rousset,"*Specific surface area of carbon nanotubes and bundles of carbon nanotubes"* ***Carbon*** *2001*, *39*, 507.

(93) J. T. Robinson, F. K. Perkins, E. S. Snow, Z. Q. Wei, P. E. Sheehan,"*Reduced Graphene Oxide Molecular Sensors"* ***Nano Letters*** *2008*, *8*, 3137.

(94) Y. P. Dan, Y. Lu, N. J. Kybert, Z. T. Luo, A. T. C. Johnson,"*Intrinsic Response of Graphene Vapor Sensors"* ***Nano Letters*** *2009*, *9*, 1472.

(95) J. D. Fowler, M. J. Allen, V. C. Tung, Y. Yang, R. B. Kaner, B. H. Weiller,"*Practical Chemical Sensors from Chemically Derived Graphene"* ***Acs Nano*** *2009*, *3*, 301.

(96) I. Jung, D. Dikin, S. Park, W. Cai, S. L. Mielke, R. S. Ruoff,"*Effect of Water Vapor on Electrical Properties of Individual Reduced Graphene Oxide Sheets"* ***Journal of Physical Chemistry C*** *2008*, *112*, 20264.

(97) G. H. Lu, L. E. Ocola, J. H. Chen,"*Gas detection using low-temperature reduced graphene oxide sheets"* ***Applied Physics Letters*** *2009*, *94*.

(98) G. H. Lu, L. E. Ocola, J. H. Chen,"*Reduced graphene oxide for room-temperature gas sensors"* ***Nanotechnology*** *2009*, *20*.

(99) M. Qazi, T. Vogt, G. Koley,"*Trace gas detection using nanostructured graphite layers"* ***Applied Physics Letters*** *2007*, *91*.

(100) W. Wu, Z. H. Liu, L. A. Jauregui, Q. K. Yu, R. Pillai, H. L. Cao, J. M. Bao, Y. P. Chen, S. S. Pei,"*Wafer-scale synthesis of graphene by chemical vapor deposition*

and its application in hydrogen sensing" ***Sensors and Actuators B-Chemical*** *2010*, *150*, 296.

(101) B. H. Chu, C. F. Lo, J. Nicolosi, C. Y. Chang, V. Chen, W. Strupinski, S. J. Pearton, F. Ren,"*Hydrogen detection using platinum coated graphene grown on SiC"* ***Sensors and Actuators B-Chemical*** *2011*, *157*, 500.

(102) J. Lin, J. B. Zhong, J. R. Kyle, M. Penchev, M. Ozkan, C. S. Ozkan,"*Molecular absorption and photodesorption in pristine and functionalized large-area graphene layers"* ***Nanotechnology*** *2011*, *22*.

(103) P. K. Ang, W. Chen, A. T. S. Wee, K. P. Loh,"*Solution-Gated Epitaxial Graphene as pH Sensor"* ***Journal of the American Chemical Society*** *2008*, *130*, 14392.

(104) Yasuhide Ohno, Kenzo Maehashi, Yusuke Yamashiro, Kazuhiko Matsumoto,"*Electrolyte-Gated Graphene Field-Effect Transistors for Detecting pH and Protein Adsorption"* ***Nano letters*** *2009*, *9*, 3318.

(105) Cheng Xiang Lim, Hui Ying Hoh, Priscilla Kailian Ang, Kian Ping Loh,"*Direct Voltammetric Detection of DNA and pH Sensing on Epitaxial Graphene: An Insight into the Role of Oxygenated Defects"* ***Anal. Chem. (Washington, DC, U. S.)*** *2010*, *82*, 7387.

(106) Lulu Ren, Tianxi Liu, Juan Guo, Shuzhong Guo, Xiaoyan Wang, Weizhi Wang,"*A smart pH responsive graphene/polyacrylamide complex via noncovalent interaction"* ***Nanotechnology*** *2010*, *21*, 335701/1.

(107) N. Lei, P. Li, W. Xue, J. Xu,"*Simple graphene chemiresistors as pH sensors: fabrication and characterization"* ***Measurement Science and Technology.*** *2011*, *22*, 107002/1.

(108) J. A. Lin, D. Teweldebrhan, K. Ashraf, G. X. Liu, X. Y. Jing, Z. Yan, R. Li, M. Ozkan, R. K. Lake, A. A. Balandin, C. S. Ozkan,"*Gating of Single-Layer Graphene with Single-Stranded Deoxyribonucleic Acids"* ***Small*** *2010*, *6*, 1150.

(109) S.R. Guo, J. Lin, M. Penchev, E. Yengel, C.S. Ozkan, M. Ozkan,"*Label Free DNA Detection using Large Area Graphene Based FET Biosensors"* ***Journal of Nanoscience and Nanotechnology*** *2010*.

(110) N. Mohanty, V. Berry,"*Graphene-Based Single-Bacterium Resolution Biodevice and DNA Transistor: Interfacing Graphene Derivatives with Nanoscale and Microscale Biocomponents"* ***Nano Letters*** *2008*, *8*, 4469.

(111) X. C. Dong, Y. M. Shi, W. Huang, P. Chen, L. J. Li,"*Electrical Detection of DNA Hybridization with Single-Base Specificity Using Transistors Based on CVD-Grown Graphene Sheets"* ***Advanced Materials*** *2010*, *22*, 1649.

(112) D. Li, S. P. Song, C. H. Fan,"*Target-Responsive Structural Switching for Nucleic Acid-Based Sensors"* ***Accounts of Chemical Research*** *2010*, *43*, 631.

(113) Z. Y. Yin, Q. Y. He, X. Huang, J. Zhang, S. X. Wu, P. Chen, G. Lu, P. Chen, Q. C. Zhang, Q. Y. Yan, H. Zhang,"*Real-time DNA detection using Pt nanoparticle-decorated reduced graphene oxide field-effect transistors"* ***Nanoscale*** *2012*, *4*, 293.

(114) T. Cohen-Karni, Q. Qing, Q. Li, Y. Fang, C. M. Lieber,"*Graphene and Nanowire Transistors for Cellular Interfaces and Electrical Recording"* ***Nano Letters*** *2010*, *10*, 1098.

(115) P. Simon, Y. Gogotsi,"*Materials for electrochemical capacitors"* ***Nature Materials*** *2008*, *7*, 845.

(116) Z. S. Wu, W. Ren, D. W. Wang, F. Li, B. Liu, H. M. Cheng,"*High-energy MnO2 nanowire/graphene and graphene asymmetric electrochemical capacitors"* ***ACS nano*** *2010*, *4*, 5835.

(117) D. H. Lee, J. E. Kim, T. H. Han, J. W. Hwang, S. Jeon, S. Y. Choi, S. H. Hong, W. J. Lee, R. S. Ruoff, S. O. Kim,"*Versatile carbon hybrid films composed of vertical carbon nanotubes grown on mechanically compliant graphene films"* ***Advanced Materials*** *2010*, *22*, 1247.

(118) R. K. Paul, M. Ghazinejad, M. Penchev, J. Lin, M. Ozkan, C. S. Ozkan,"*Synthesis of a pillared graphene nanostructure: a counterpart of three-dimensional carbon architectures"* ***Small*** *2010*, *6*, 2309.

(119) V. C. Tung, L. M. Chen, M. J. Allen, J. K. Wassei, K. Nelson, R. B. Kaner, Y. Yang,"*Low-temperature solution processing of graphene-carbon nanotube hybrid materials for high-performance transparent conductors"* ***Nano Letters*** *2009*, *9*, 1949.

(120) L. Hu, J. W. Choi, Y. Yang, S. Jeong, F. La Mantia, L. F. Cui, Y. Cui,"*Highly conductive paper for energy-storage devices"* ***Proceedings of the National Academy of Sciences of the United States of America*** *2009*, *106*, 21490.

(121) S. Murali, D. R. Dreyer, P. Valle-Vigon, M. D. Stoller, Y. Zhu, C. Morales, A. B. Fuertes, C. W. Bielawski, R. S. Ruoff,"*Mesoporous carbon capsules as electrode materials in electrochemical double layer capacitors"* ***Physical chemistry chemical physics : PCCP*** *2011*, *13*, 2652.

(122) A. P. Yu, I. Roes, A. Davies, Z. W. Chen,"*Ultrathin, transparent, and flexible graphene films for supercapacitor application"* ***Applied Physics Letters*** *2010*, *96*.

(123) Y. Zhu, S. Murali, W. Cai, X. Li, J. W. Suk, J. R. Potts, R. S. Ruoff,"*Graphene and graphene oxide: synthesis, properties, and applications"* ***Advanced Materials*** *2010*, *22*, 3906.

(124) W. Wang, S. Guo, J. Zhong, J. Lin, M. Ozkan, C. Ozkan,"*Ultracapacitors Based on Graphene/MWNT Composite Films."* ***MRS Proceedings*** *2011*, *1344*, 87.

(125) F. Yavari, Z. P. Chen, A. V. Thomas, W. C. Ren, H. M. Cheng, N. Koratkar,"*High Sensitivity Gas Detection Using a Macroscopic Three-Dimensional Graphene Foam Network"* ***Scientific Reports*** *2011*, *1*.

(126) R. Deshpande, Y. T. Cheng, M. W. Verbrugge, A. Timmons,"*Diffusion Induced Stresses and Strain Energy in a Phase-Transforming Spherical Electrode Particle"* ***Journal of the Electrochemical Society*** *2011*, *158*, A718.

(127) H. X. Ji, L. L. Zhang, M. T. Pettes, H. F. Li, S. S. Chen, L. Shi, R. Piner, R. S. Ruoff,"*Ultrathin Graphite Foam: A Three-Dimensional Conductive Network for Battery Electrodes"* ***Nano Letters*** *2012*, *12*, 2446.

(128) M. T. Pettes, H. X. Ji, R. S. Ruoff, L. Shi,"*Thermal Transport in Three-Dimensional Foam Architectures of Few-Layer Graphene and Ultrathin Graphite"* ***Nano Letters*** *2012*, *12*, 2959.

(129) C. C. Hu, K. H. Chang, M. C. Lin, Y. T. Wu,"*Design and tailoring of the nanotubular arrayed architecture of hydrous RuO2 for next generation supercapacitors"* ***Nano Letters*** *2006*, *6*, 2690.

(130) P. T. Hammond, S. W. Lee, J. Kim, S. Chen, Y. Shao-Horn,"*Carbon Nanotube/Manganese Oxide Ultrathin Film Electrodes for Electrochemical Capacitors"* ***ACS nano*** *2010*, *4*, 3889.

(131) Y. Zhu, S. Murali, M. D. Stoller, K. J. Ganesh, W. Cai, P. J. Ferreira, A. Pirkle, R. M. Wallace, K. A. Cychosz, M. Thommes, D. Su, E. A. Stach, R. S. Ruoff,"*Carbon-Based Supercapacitors Produced by Activation of Graphene"* ***Science*** *2011*, *332*, 1537.

(132) X. Wang, Y. D. Li,"*Rational synthesis of alpha-MnO2 single-crystal nanorods"* ***Chemical Communications*** *2002*, 764.

(133) C.-Y. Cao, W. Guo, Z.-M. Cui, W.-G. Song, W. Cai"*Microwave-assisted gas/liquid interfacial synthesis of flowerlike NiO hollow nanosphere precursors and their application as supercapacitor electrodes"* ***Journal of Materials Chemistry*** *2011*, *21*, 3204.

(134) Z. Chen, V. Augustyn, J. Wen, Y. W. Zhang, M. Q. Shen, B. Dunn, Y. F. Lu,"*High-Performance Supercapacitors Based on Intertwined CNT/V2O5 Nanowire Nanocomposites"* ***Advanced Materials*** *2011*, *23*, 791.

(135) F. D. Novaes, R. Rurali, P. Ordejon,"*Electronic Transport between Graphene Layers Covalently Connected by Carbon Nanotubes"* ***Acs Nano*** *2010*, *4*, 7596.

(136) G. K. Dimitrakakis, E. Tylianakis, G. E. Froudakis,"*Pillared Graphene: A New 3-D Network Nanostructure for Enhanced Hydrogen Storage"* ***Nano Letters*** *2008*, *8*, 3166.

(137) D. Choi, G. E. Blomgren, P. N. Kumta,"*Fast and reversible surface redox reaction in nanocrystalline vanadium nitride supercapacitors"* ***Advanced Materials*** *2006*, *18*, 1178.

(138) W. Sugimoto, H. Iwata, Y. Yasunaga, Y. Murakami, Y. Takasu,"*Preparation of ruthenic acid nanosheets and utilization of its interlayer surface for electrochemical energy storage"* ***Angewandte Chemie-International Edition*** *2003*, *42*, 4092.

(139) M. K. Song, S. Cheng, H. Y. Chen, W. T. Qin, K. W. Nam, S. C. Xu, X. Q. Yang, A. Bongiorno, J. Lee, J. M. Bai, T. A. Tyson, J. Cho, M. L. Liu,"*Anomalous Pseudocapacitive Behavior of a Nanostructured, Mixed-Valent Manganese Oxide Film for Electrical Energy Storage (vol 12, pg 3483, 2012)"* ***Nano Letters*** *2012*, *12*, 4416.

(140) Z. Chen, Y. C. Qin, D. Weng, Q. F. Xiao, Y. T. Peng, X. L. Wang, H. X. Li, F. Wei, Y. F. Lu,"*Design and Synthesis of Hierarchical Nanowire Composites for Electrochemical Energy Storage"* ***Advanced Functional Materials*** *2009*, *19*, 3420.

(141) G. W. Yang, C. L. Xu, H. L. Li,"*Electrodeposited nickel hydroxide on nickel foam with ultrahigh capacitance"* ***Chemical Communications*** *2008*, 6537.

(142) Q. T. Qu, P. Zhang, B. Wang, Y. H. Chen, S. Tian, Y. P. Wu, R. Holze,"*Electrochemical Performance of MnO2 Nanorods in Neutral Aqueous Electrolytes as a Cathode for Asymmetric Supercapacitors"* ***Journal of Physical Chemistry C*** *2009*, *113*, 14020.

(143) Z. Fan, J. H. Chen, B. Zhang, F. Sun, B. Liu, Y. F. Kuang,"*Electrochemically induced deposition method to prepare gamma-MnO2/multi-walled carbon nanotube composites as electrode material in supercapacitors"* ***Materials Research Bulletin*** *2008*, *43*, 2085.

(144) S. D. Perera, B. Patel, N. Nijem, K. Roodenko, O. Seitz, J. P. Ferraris, Y. J. Chabal, K. J. Balkus,"*Vanadium Oxide Nanowire-Carbon Nanotube Binder-Free Flexible Electrodes for Supercapacitors"* ***Advanced Energy Materials*** *2011*, *1*, 936.

(145) A. L. M. Reddy, M. M. Shaijumon, S. R. Gowda, P. M. Ajayan,"*Multisegmented Au-MnO2/Carbon Nanotube Hybrid Coaxial Arrays for High-Power Supercapacitor Applications"* ***Journal of Physical Chemistry C*** *2010*, *114*, 658.

Chapter 2

Graphene Nanoelectronics

2.1 Tuning of Electron Transport in Graphene based Field Effect Devices Using Block Co-Polymers

2.1.1 Introduction

Graphene has attracted a lot of attention due to its remarkable intrinsic electronic properties.[1] The ballistic transport of electrons, along with mobilities exceeding 15,000 $cm^2/V{\cdot}s$ and an ambipolar field effect, make graphene a promising candidate for the next generation of semiconductor devices.[2] Charge carrier transport in graphene can be tuned between hole and electron conduction by shifting the Fermi level with an applied electrical field.[3-4] Having the ability to accurately control charge carrier transport and spatially modulate the charge carrier density will provide a significant capability for future graphene nanoelectronics. Several methods have been developed to achieve this goal, including band gap engineering by fabricating graphene nanoribbons[5-7] or nanomeshes,[8] utilizing bilayer graphene[9] to obtain a narrow band gap, and doping of graphene layers to obtain n-type or p-type materials.[10-11] Doping or chemical functionalization is another approach for modifying the electronic properties of graphene. Modulating the charge carrier densities provides a tuning of the Fermi level, hole and electron mobilities and a shift of the Dirac neutrality point. Several surface doping approaches with different materials have been utilized to modify the electronic properties of graphene, including metals (Ca, Ag, Au, Ti, Bi, K, etc.),[12-14] aromatic molecules,[15]

poly(ethylene imine),[16] non-metal elements (N, B, etc.),[17-19] semiconductors or nanoparticles,[20] and aryl groups.[21] Meanwhile, side or edge doping has been demonstrated to exert an important role in altering the bandgap of graphene nanoribbons[22] as well as in obtaining graphene field effect transistors (GFETs) with higher on/off ratios[23] and higher electron and hole mobilities.[24] In spite of all these advances, it is still a great challenge to achieve controlled tuning of the electronic properties of graphene. A better way to partially dope graphene with specific molecules using a controllable method is needed to support further developments in fabricating novel graphene nanoelectronics. In this section, we discuss the use of di-block copolymers (BCP) for this purpose.

The ability of BCPs to assemble into ordered arrays of spheres, cylinders, and lamellae structures makes them attractive templates and scaffolds for nanopatterning.[25-26] The unique structure of BCPs, with their chemical functional groups in one chain, is likely to provide a viable mechanism for tuning the electronic properties of GFETs. Moreover, the ordered structure with two distinctive functional groups provides a means to achieve partial doping in a controllable way. We will describe how the unique structure of the BCPs can provide additional benefit as protective layers for GFETs, which will be advantageous for applications in sensing.

Recently GFETs have attracted attention for potential biochemical sensing applications. Several studies have demonstrated the high sensitivity of sensors resulting from the intrinsic properties of graphene, in applications such as pH measurements,[27] DNA detection,[28-29]and gas[30-31]sensing. However, the sensitivity of GFETs has in some

cases proven to be inferior to that of other sensors, instabilities and unreliability of the device were observed in other cases, and low electrical responses for intrinsic graphene based devices were shown in certain examples.[32] It would be highly desirable to develop GFET sensors with higher sensitivity and reliability. The hexagonal domain structure of BCP provides heterogeneous nanoscale patterns for achieving spatially selective sensor architectures.

In this section we discuss a block-copolymer doping effect to graphene layers, and demonstrate control of the neutrality point shift in GFETs by fluorine doping via CF_4 plasma processing. The ordered structure of the BCP enables the tuning of electron transport in graphene layers and devices.

2.1.2 Experimental

*Materials synthesis and characterization***.** Graphene was synthesized using a copper foil as catalyst. Typically, the copper foil was cleaned with organic solvents and etched with acetic acid at 35 ^{o}C for 10 min to remove any surface oxides and other impurities. After washing it thoroughly, the copper was thermally annealed for 30 min by heating to 1,000 ^{o}C in a reducing atmosphere: Ar/H_2 (flow rates 200:200 sccm, maintaining pressure of 2 Torr). While maintaining the same temperature, the annealed copper surface was exposed to methane for 20 minutes (at 100 sccm flow rate) mixed with H_2 at pressure elevated to 20 Torr. The metal sample, with the subsequent grown graphene on its surface, was cooled down to 25^{o}C at a cooling rate of 20 ^{o}C min^{-1}. The graphene-covered surface was coated with polymethylmethacrylate (PMMA) and the copper was etched with $FeCl_3$ (0.5 M aqueous solution). The PMMA-bound graphene sheet was washed

thoroughly (with HCl (3%) and deionized water) and transferred to glass or to SiO_2-coated Si substrate. The PMMA layer was dissolved in organic solvent leaving the graphene sheet on the inorganic substrate.

Fabrication of graphene based field effect devices: CVD grown large-area graphene sheets are patterned and etched by oxygen plasma to rectangular shapes using photolithography and a Reactive Ion Etch (RIE) system. Two terminal devices with Ti/Au (2nm/80nm) electrodes (shown in the inset of Scheme 1) are then fabricated. The device is evaporated with back gate Ti/Au (2nm/100nm). The distance between the source and drain in the devices are set to 70μm, and the width of the patterned graphene layer is 50 μm.

Fabrication of PS-P4VP block copolymer: The block copolymer used in this study is Poly(styrene-b-4-vinylpyridne) (PS-b-P4VP), purchased form Polymer Source, with a molecular weight of 69kg/mol (M_n, PS = 51 kg/mol, M_n, PVP = 18 kg/mol) and a molecular weight distribution of M_w/M_n = 1.15. The block copolymers were dissolved in toluene/tetrahydrofuran at room temperature to make 0.6 wt% polymer solutions, which are subsequently spin-coated at 2200 rpm onto silicon wafers with 300nm thermally grown silicon dioxide on it. In order to develop well-defined, well-ordered cylindrical microdomains in the BCP films, appropriate volume fractions and molecular weights were selected. The choices of volume fraction and molecular weight provide control over the morphology (cylindrical in this case) and size/separation distance in the BCP microdomains. Using the above-mentioned data, BCP domains spontaneously assembled into a range of well-defined cylinders of a minor polymer block, in a matrix of major

polymer blocks. BCP cylindrical domains were then vertically aligned on the substrate by using a solvent annealing technique. This provided a very simple but robust route to generate almost defect-free microstructures over large areas in block copolymer thin films.

Characterization: Raman spectra were taken using a Renishaw micro-Raman spectrometer with a 488 nm visible laser as the excitation source. Atomic force microscopy (AFM) was conducted using a Multimode-5 Veeco instrument operated in the tapping mode using standard silicon cantilevers. The XPS data were obtained using an EA11-MCD system equipped with an Mg−Kα X-ray source (1486.6 eV) and a 100 mm concentric hemispherical electron energy analyzer.[30] All of the XPS peak positions were referenced to the graphene C 1s peak at 284.6 eV and the surface concentrations are calculated from the respective peak areas using reported atomic sensitivity factors.

Materials: Nanoparticles of CdSe, stabilized with octadecylamine, were purchased from NN-Labs, LLC (Fayetteville, AR). Although under the vendor's description, the particles (CZ620) were expected to have core/shell CdSe/ZnS architecture, TEM analysis revealed that the suspension contained mixture of about 58% CdSe nanocrystals (5.3±0.4 nm), and 40% ZnS nanocrystals (5.2±0.4 nm). About 80% of the CdSe nanocrystals were identified to have cubic sphalerite-type structure and the rest were hexagonal wurtzite-type. Most of the ZnS particles (more than 90%) exhibited wurtzite structure, and a small amount were identified as sphalerite-type. Only for a negligibly small portion of the octadecylamine-coated nanoparticles (about 1% or less) the TEM analysis provided acceptable evidence for core/shell structure (Figure 1a).

About 2% of the particles analyzed in the TEM could not be identified reliably to distinguish between wurtzite-type CdS or sphalerite-type ZnS. Emission spectroscopy, however, did not provide evidence for the presence of nanocrystals with bandgaps smaller than about 3.2 eV suggesting that CdS was not present. Varying the excitation wavelength from 600 to 380 nm for diluted suspensions and for solid samples did not cause shifts in the emission band and did not result in new characteristic emission peaks of QDs of cadmium chalcogenides, such as CdS or Cd_2SeS (Figure 2a, b). This finding indicates that most probably the crystalline nanoparticles, for which we could not be identified unambiguously in the TEM, were composed of broadband zinc chalcogenides.

For exchanging the ODA with pyridine ligands we used a coagulation-and-resuspension procedure. About 0.5 ml of 2 mg ml^{-1} of nanoparticles were precipitated with ethanol, centrifuged at 9,000 rpm for 10 min and the clear liquid decanted. Pyridine (0.2 ml) was added to the solid pellet, and the particles were resuspended by mild sonication for about 10 min. Hexane was added to precipitate the nanoparticles from the suspension, the liquid decanted after centrifugation, and the solid resuspended in fresh pyridine. The procedure was then repeated two additional times to obtain pyridine-coated nanoparticles, QD-Py, and ligand exchange was confirmed with FTIR. None of the pyridine-coated nanoparticles exhibited core/shell structure (Figure 1b).

For the preparation of the QD-Py/graphene hybrid films, diluted QD-Py suspension was dropped on graphene surfaces. After 1 min, the samples were rinsed with copious amounts of ethanol several times. This process was repeated three to five times. The stacked structures for the TA studies were assembled by placing cover glass slips

(each coated with QD-Py/graphene films on one side) on top of one other, separated with ~100-μm spacer positioned at the slip edges, fixed together with transparent tape. Thus, the QD-Py/graphene films were not in contact with the films or the bare glass surfaces on the neighboring slips.

Electron microscopy: The scanning electron microscopy (SEM) images were recorded with Leo SUPRA 55 microscope. Transmission electron microscopy (TEM) was performed with a FEI-Philips CM300 microscope, operating at 200 and 300 kV accelerating voltage, equipped with a LaB_6 electron gun, an EDAX energy-dispersive spectrometer (EDS) and Gatan MSC794 digital camera. Samples were prepared by dispersing the powder nanoparticles in distilled water through ultrasonic agitation and depositing a drop of the resulting suspension onto copper TEM grids coated with a thin amorphous carbon support film. High-resolution images were obtained by recording through-focus series of images close to Scherzer defocus for individual particles and particle aggregates. Phase identification was based on lattice spacings, measured from fast Fourier transform (FFT) of the HRTEM images of each particle (Figure 1a, b).

Fluorescence microscopy: The fluorescence images were recorded using a BD Pathway 855 HT confocal microscope, equipped with Olympus objectives (2×, NA = 0.08; and 20×, NA = 0.75), a xenon arc lamp, a 488nm (10-nm bandwidth) bandpass excitation filter, a LP dichroic mirror (495 nm cutoff wavelength), a 624 nm (40-nm bandwidth) emission bandpass filter, and a CCD camera. To image large-area samples using the 2× objective, a montage was built from individual images, each consisting of 1024×1344 pixels and representing a 3.197×4.196 mm^2 region (image pixel area = 3.122

μm^2). For higher-resolution imaging, the 20× objective was used and each pixel on the images covered an area of 312 nm^2. To correct for uneven illumination throughout the wide fields of view, each recorded image, $I(x,y)$, was divided by a background image, $I_{BG}(x,y)$, that is, an image of a uniformly fluorescent sample collected using the same optical path, normalized for the average background intensity, $\langle I_{BG} \rangle$: i.e. $I_{corrected}(x,y) = \langle I_{BG} \rangle I(x,y) / I_{BG}(x,y)$.

Cyclic voltammetry: The cyclic voltammetry (CV) measurements were conducted at ambient room temperature using a Reference 600 potentiostat-galvanostat (Gamry Instruments, Warminster, PA), equipped with a three-electrode cell. A glassy carbon electrode was employed as a working electrode. A Pt wire and saturated calomel electrode (Gamry Instruments) were used as a counter electrode and a reference electrode, respectively. Before and after the measurements, the reference electrodes were stored in saturated solution of KCl. To prevent contamination, the reference electrode was brought into contact with the sample solutions via two salt bridges. The samples of nanoparticles were suspended in anhydrous acetonitrile electrolyte solutions containing 0.1 M tetrabutylammonium hexafluorophosphate. Prior to each scan, the electrolyte suspension of nanoparticles was purged with pure argon gas, and the voltammograms were recorded at scan rate of 50 mV s^{-1}. After completing the CV measurements for each sample, ferrocene was added to the solution and its half potential was compared with the previously reported, 0.45 V vs. SCE.[91] For the QD-ODA samples, we observed: (1) a reversible wave with $E^{(1/2)}$ = –0.82 V vs. SCE; (2) an irreversible wave with an anodic peak, E_A = –1.6 V vs. SCE; and (2) an irreversible wave with a cathodic peak, E_C = 1.2 V

vs. SCE. For the QD-Py, we observed similar voltammograms with: (1) a reversible reduction wave with $E^{(1/2)} = -0.86$ V vs. SCE; (2) an irreversible reduction wave with $E_A = -1.9$ V vs. SCE; and (3) two irreversible oxidation waves with cathodic peak potentials at 1.2 and 1.9 V vs. SCE. After several oxidation scans of the pyridine-coated QDs, an additional anodic peak at –0.6 V vs. SCE appeared. Considering that the SCE potential (multiplied by the Faraday constant) is 4.68 eV under the energy of an electron at rest in vacuum,[92] and using the data for the reversible reduction waves, we estimated that the lowest energy levels of the conduction band (or of the LUMOs) of the QD-ODA and QD-Py were at –3.86 eV and –3.82 eV vs. the vacuum level.

Absorption and emission spectroscopy: Steady-state UV/visible absorption spectra were recorded using a JASCO V-670 spectrophotometer (Tokyo, Japan). For the liquid samples, we used the double-beam instrument in a transmission mode. For the solid film samples, e.g., QDs film on glass slides and QD/graphene hybrid solid samples, the absorption spectra were obtained from diffuse reflectance spectroscopy measurements using a 60 mm ψ integrating sphere equipped with an individual detector (Model ISN-723, JASCO, Japan). For baseline, a transparent glass slide as a blank was used, and under identical settings the reflection spectra of the solid samples were recorded with the film, coating the sides, facing the integrating sphere. For all samples of solid films and for the glass blank, aluminum foil as a back-reflector was placed behind the glass slides. The absorption spectrum, A vs. λ, was determined from the reflectance, R: $A(\lambda) = -(1/2)\lg(R(\lambda))$, where the division by 2 accounted for the reflector on the back of the transparent substrates.

Steady-state emission measurements were conducted using a FluoroLog-3 spectrofluorometer (Horiba-Jobin-Yvon) equipped with double-grating monochromators and a TBX single-photon-counting detector. For the liquid samples, we used right-angle settings, and for the solid-film samples, the emission was recorded at small-angle configuration.[93]

The fluorescence quantum yields, Φ_f, of the liquid sample were estimated from absorbance measured in transmission mode, and emission measured at right-angle settings, at room temperature using 10 mm optical-length quartz cuvette. For reference, we used a solution of rhodamine 6G in ethanol (Φ_{f0} = 0.94). All solution samples were purged with N_2. For the solid films, i.e., QDs on glass slides and the QD/graphene hybrid solid samples, the quantum yields were calculated from small-angle emission measurements and from the reflectance at the excitation wavelength (λ_{ex} =600 nm). For the solid glass-slide samples, a solution of the reference was placed in a 2 mm optical-length quartz cuvette, and mounted on the sample holder of the integrating sphere and on the small-angle emission setup.

Time-resolved emission measurements of the solid films were conducted in a reflection mode with a FluoroLog-3 spectrofluorometer (Horiba-Jobin-Yvon) and a NanoLED laser was used for an excitation source (λ_{ex} = 406 nm; half-height pulse width, $W_{1/2}$ = 195 ps). The intensity of the excitation light was attenuated by placing reflection neutral-density filters on the beam path. For recording the profile of the excitation pulse (i.e., the instrument response function), we used aqueous solution of bovine serum albumin as a scatterer, setting $\lambda_{em} = \lambda_{ex}$ = 406 nm. The fluorescence decays were collected

near the QD emission maxima, λ_{em} = 630 nm, and fitted to mono- and multi-exponential functions via a deconvolution algorithm. The quality of the fits was monitored by examination of the residuals. All least-squares data fits were conducted using Igor Pro, version 6 (Wavematrics, Inc.) on MacOS and Windows XP workstations. There is a key limitation in the use of emission spectroscopy for characterizing strongly quenched heterogeneous systems such as QD-Py/graphene hybrid films. For luminophores with emission quantum yields smaller than 0.01, however, ensemble-average measurements represent less than 1% of the photoinitiated events. Therefore, we resorted to TA study.

Transient absorption spectroscopy: The TA spectra were recorded in transmission mode using a Helios pump-probe spectrometer (Ultrafast Systems, LLC, Florida) equipped with a delay stage allowing maximum probe delays of 3.2 ns at 7 fs temporal step resolution, and with white-light generators providing UV/visible spectral range from 350 to 800 nm.

The laser source for the Helios was a SpitFire Pro 35F regenerative amplifier (Spectra Physics / Newport) generating 800-nm pulses (38 fs, 3.5 mJ, 55 nm bandwidth) at 1 kHz repetition rate. The amplifier was pumped with an Empower 30 Q-switched laser ran at 20 W, and a MaiTai SP oscillator provided the seed beam.

For the pump, 500 mW of the amplifier output was sent into an optical parametric amplifier, OPA-800CU (Newport), equipped with a second- and forth-harmonic generators, 2G and 4G, respectively. For the reported data, the signal was tuned between 1520 and 1,600 nm and the 4G output (380 to 400 nm) was sent to the Helios spectrometer, passed through an attenuating filter, a depolarizer, a chopper (blocking

every other pump pulse), and converged on the sample surface (about 2 mm beam diameter). The pump power was tuned between 1 and 5 μJ per pulse, which allowed for establishing the changes in the TA spectra due to the increase in the electron population in the CdSe conduction band.[94] The analysis here is based on TA data for which the pump was tuned to 400 nm with energy of 1.5 μJ per pulse.

For the probe, 10 mW of the amplifier output was reflected several meters back and forth over the table (to compensate for the pump delay in the OPA), introduced into the Helios, passed through the delay stage, the white-light generator, and focused on the sample surfaces, ensuring complete overlap by the pump beam. To obtain reasonable TA signal-to-noise ratios for the QD-Py/graphene samples, we used stacks of thin glass substrates, i.e., microscope cover slips one-sidedly coated with single-sheet graphene and QDs. Namely, we probed a stack of QD-Py/graphene monolayers separated from one another by hundreds of micrometers of dielectric, and a total optical density exceeding the ground-state absorption of the QD films with no graphene. For the samples of stacked cover slips, the recorded Raman-scattering repose of the blank samples provided the data for the chirp correction as implemented by using Surface Xplorer (Ultrafast Systems, LLC). The transient kinetics was analyzed using Surface Xplorer and Igor Pro. To exclude the spatial mismatching of the pump and probe for stacked cover slips, we aligned the pump and probe to make sure they overlapped as they enter and exit of the sample. The diameter of the pump beam is larger than the probe beam's making the overlap possible for the angle, at which the two beams cross each other in the sample.

Photoelectrical measurements: The current-voltage measurements were carried out at room temperature, using an HP 4156C semiconductor parameter analyzer. For the investigating the photoinduced effects, the graphene films on the FET devices were illuminated with an UV lamp (365 nm) and power density of 0.2 W/cm^2.

2.1.3 Results and Discussion

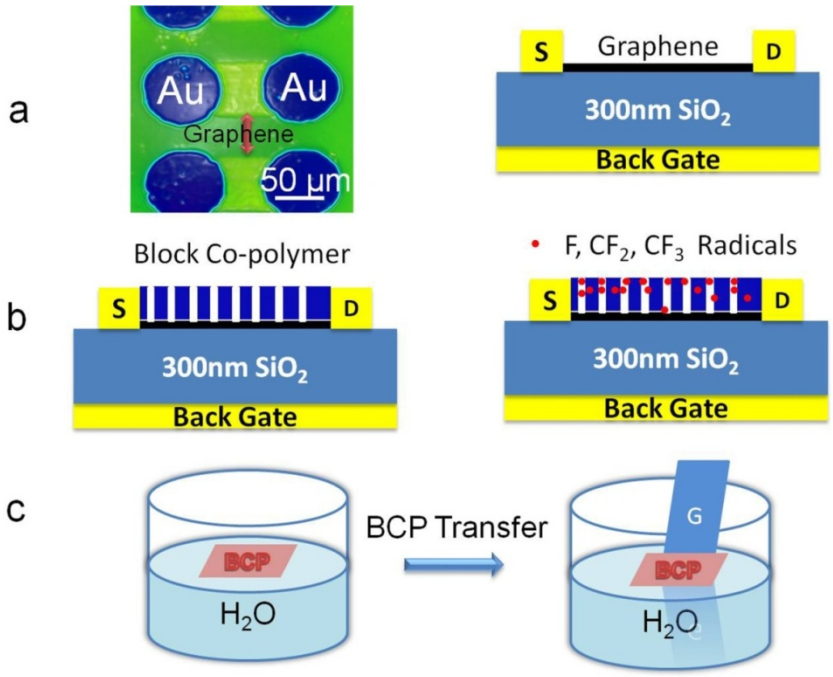

Scheme 2.1 Schematic illustration of the experimental setup. (a) fabrication of GFET samples with back-gate; the left image shows an optical microscopy picture of a typical device and BCP coating, (b) fluorine doping of BCP coated device, (c) the cartoon of transferring BCP to GFET.

Scheme 1 outlines the procedures for doping and BCP layer transfer. After device fabrication, BCP layers were transferred onto the device (scheme 2.1c). Briefly, the as-

assembled copolymer films were peeled off from the Si/SiO_2 substrate using 1wt% HF solution. The polymer film was then collected with graphene substrate and BCP microdomains were transferred onto synthesized fabricated graphene device. This technique is similar to the TEM sample preparation of metal loaded block copolymers.[33] The whole sample was then preserved under vacuum at 40 ^oC overnight so that polymer film can relax properly on the graphene. The patterned BCP was assembled according to well known protocols: typically, the Poly(styrene-b-4-vinylpyridne) (PS-b-P4VP) BCPs were dissolved in toluene/tetrahydrofuran at room temperature to make a 0.6 wt% polymer solution that was subsequently spin-coated at 2200 rpm onto a silicon wafer with 300 nm thermally grown silicon dioxide. The as-spun copolymer films were then exposed to tetrahydrofuran vapor at room temperature for 180 min using a solvent annealing technique.[33] In this process, exposure of thin films of BCP microdomains to saturated solvent vapor increased the mobility of the copolymer micelles resulting in the redistribution of those BCP microdomains.[34-36] Atomic force microscopy (AFM) images (Figure 2.1a) confirm the formation arrays of hexagonally ordered P4VP cylinders, with a typical dimater of ~ 30nm were organized after annealing. The two different functional groups, i.e. benzyl and pyridine, are expected to induce a doping effect to the GFET device. To substantiate this assumption, individual polymers (P4VP and PS) and as-formed BCP film were transferred onto GFETs as shown in scheme 1, and the current-voltage (I-V) measurements were obtained. All the I-V measurements were carried out with a HP 4155C semiconductor parameter analyzer at room temperature.

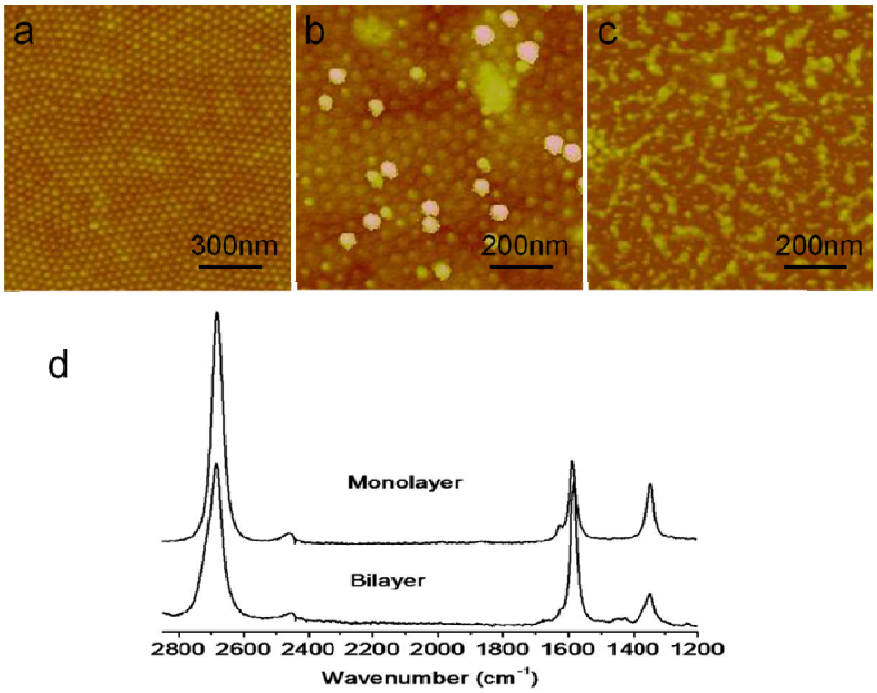

Figure 2.1 (a) AFM images of PS-P4VP block-copolymers: as assembled on Si substrates; the dark dots represent hexagonally-ordered cylindrical domains (minor component, P4VP), the bright background shows the matrix (major component, PS). (b) AFM images of the BCP after a 110s of plasma exposure. (c) AFM images of BCP after a 200s plasma exposure. (d) Raman spectra of monolayer and bilayer graphene samples.

Large-area graphene sheets were synthesized via a CVD method using copper foil as the catalyst. Raman spectra obtained from our samples indicate that the graphene sheets used here are single layer (Figure 2.1d). Figure 2a shows a typical I_{ds}-V_g curve obtained from a GFET, indicating a low defect density in the as-synthesized graphene. Average values of hole and electron mobilities were calculated as μ_{hole}= 685 $cm^2/V{\cdot}s$, and μ_e= 425 $cm^2/V{\cdot}s$ respectively. Hole and electron mobilities reach as high as 1500 $cm^2/V{\cdot}s$ and 852 $cm^2/V{\cdot}s$ respectively (Figure 2.2a), indicating the high quality of the as-grown graphene, and the Ohmic contact properties of the fabricated devices (Figure 2.2b) also attest to this fact. However, the charge carrier transport properties of graphene could

easily be changed by exposure to air even for a short time. An experiment with a control sample showed that 5 min of exposure to air shifts the neutrality point up to +7V (Figure 2.3). This phenomenon was ascribed to the doping effect of water molecules to graphene surfaces.[1] Remarkably, the neutrality point shifts to right by +20V after BCP was transferred onto the GFET (Figure 2.4).

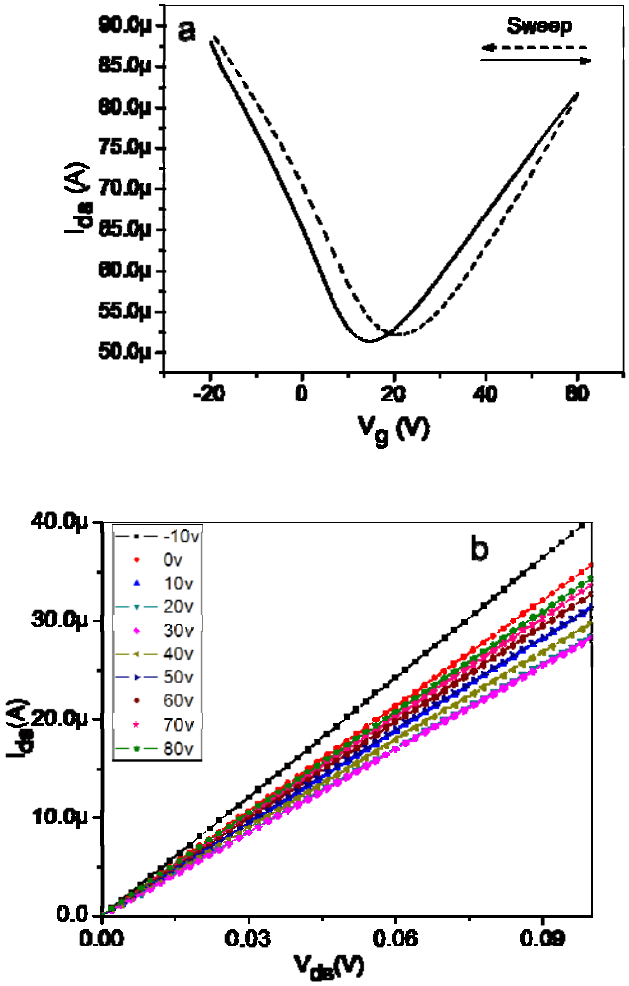

Figure 2.2 (a) Another graphene field effect transistor I_{ds}-V_g curve. (b) typical source-drain current vs. source-drain voltage (I_{ds}-V_{ds}) curves at different gate voltages.

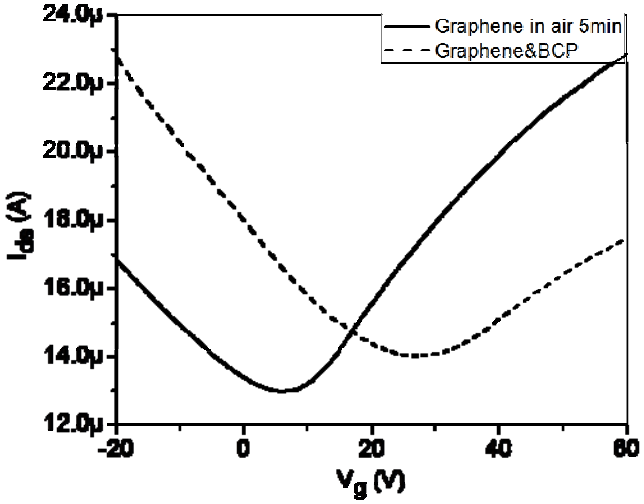

Figure 2.3 Source-drain current vs. gate voltage (I_{ds}-V_g) curves of control sample: GFET in air for 5 min and GFET covered with BCP.

After 5 days of drying in a vacum dessicator, only a tiny shift in the neutrality point was observed (Figure 2.4b). However, high vacuum annealing at 50^{o}C for 12hrs showed that neutrality point of BCP covered GFET shifted to zero which indicates that the previous results were probably caused by a small amout of water molecules trapped between BCP and graphene sheet.[37] Interestingly, the hole and electron mobilities were increased and decreased respectively. To further understand the doping role of BCP's polymer blocks, i.e. P4VP and PS, the doping effects were investigated individually for these homopolymers. Figure 2c shows the I_{ds}-V_g curves of GFET covered with P4VP and PS on the surface. It clearly demonstrates a left shift of the neutrality point after P4VP was patterned on the surface of graphene which shows a n-type doping effect. Both the electron and hole mobilities decreased for PS and PVP which may be caused by short range scattering. [16] However, having PS on the surface of graphene doesn't change the

neutrality point, indicating no doping effect via PS patterning. Furthermore, the minimum conductivity was increased for all the polymers, especially for BCP doped GFET. It has been reported that minimum conductivity generally decreases by improving the homogeneity of the samples,[38] and inhomogeneous potentials created by short-range scatterers cause suppression of conductivity for both carrier types.[16] Thus, the result demonstrates the inhomogeneity of the sample upon transferring the polymer onto the graphene surface.

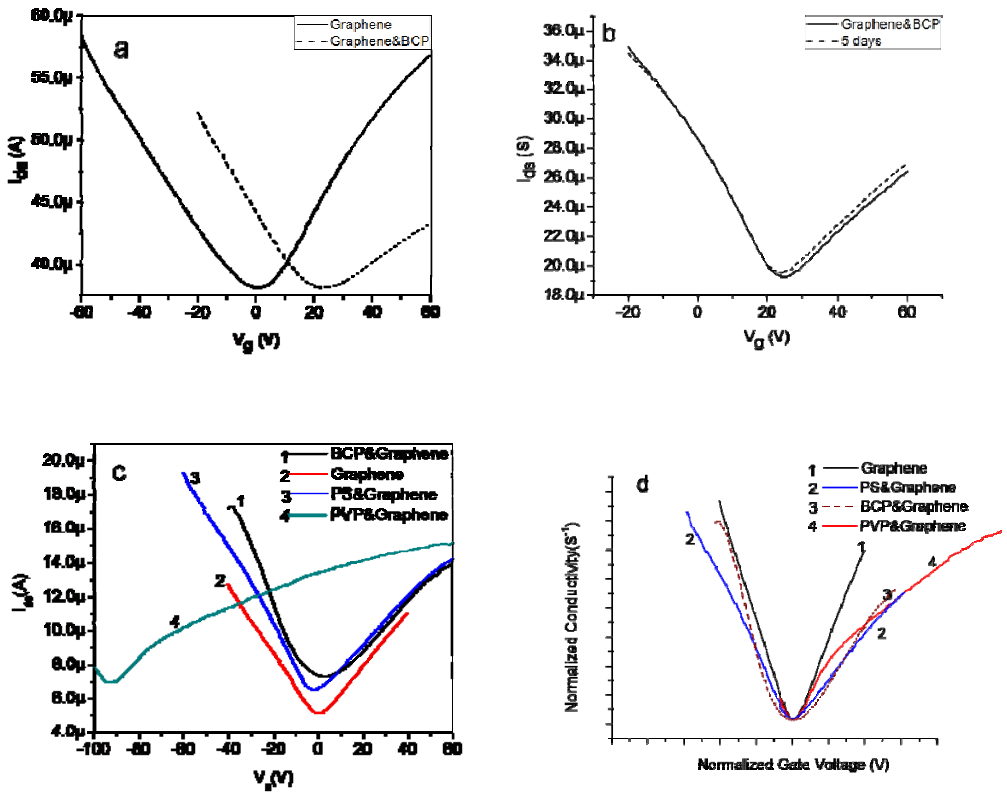

Figure 2.4 (a) I_{ds}-V_g curves for a typical pristine graphene and for BCP-covered GFET devices after drying in air, (b) Typical source-drain current vs. gate voltage (I_{ds}-V_g) curve of GFET covered with BCP and 5 days in vacuum desiccator change. (c) Typical I_{ds}-V_g curves for GFET devices: pristine graphene, graphene doped with polystyrene (PS), polyvinylpyrrolidone (PVP), and BCP covered graphene with high vacuum annealing at 50^{o}C for 12 hrs. The test was carried out by putting one drop of PS or PVP solution on GFET devices. PS and PVP solution were prepared with trichloroethylene and anhydrous ethanol respectively. (d) Normalized source-drain conductance vs. gate voltage (G_{ds}-V_g) curves for a graphene devices: pristine graphene, PS covered graphene, PVP covered graphene and BCP covered graphene. The source-drain bias for these measurements was 100 mV.

Prerviously, asymmetric electron and hole conduction branches after doping were observed for GFETs using the doping effect of poly(ethylene imine) (PEI).[16] In our case, the hole conduction was slightly increased while the electron conduction was largely supressed (Figure 2.4d), so the two branches display a different pattern compared to the

case observed with PEI doped GFETs.[16] Both PS and P4VP decreased the conductivity of electron branch caused by short range scattering (Figure 2.4d), while they acted different for hole conduction. P4VP provides a n-type doping effect while the electron conduction was suppressed indicating short range scattering, causing a decrease in electron mobility. The estimated volume ratio of P4VP/PS in the present BCP is 0.73 with varying coverage areas on the graphene surface resulting in spatially different transport properties. This result suggests a good approach to change the concentration of holes and electrons with this spatially selective doping effect. The electron and hole mobilities were calculated using the following equation:

$$\mu = [(\Delta I_{ds}/V_{ds}) \times (L/W)]/C_{ox}\Delta V_g,$$

where L and W are the channel length and width, respectively, C_{ox} is the silicon oxide gate capacitance (which is 1.08×10^{-8} F/cm^2 for a gate oxide thickness of 300 nm), and I_{ds}, V_{ds}, and V_g are the drain−source current, the drain−source voltage, and the gate voltage, respectively.

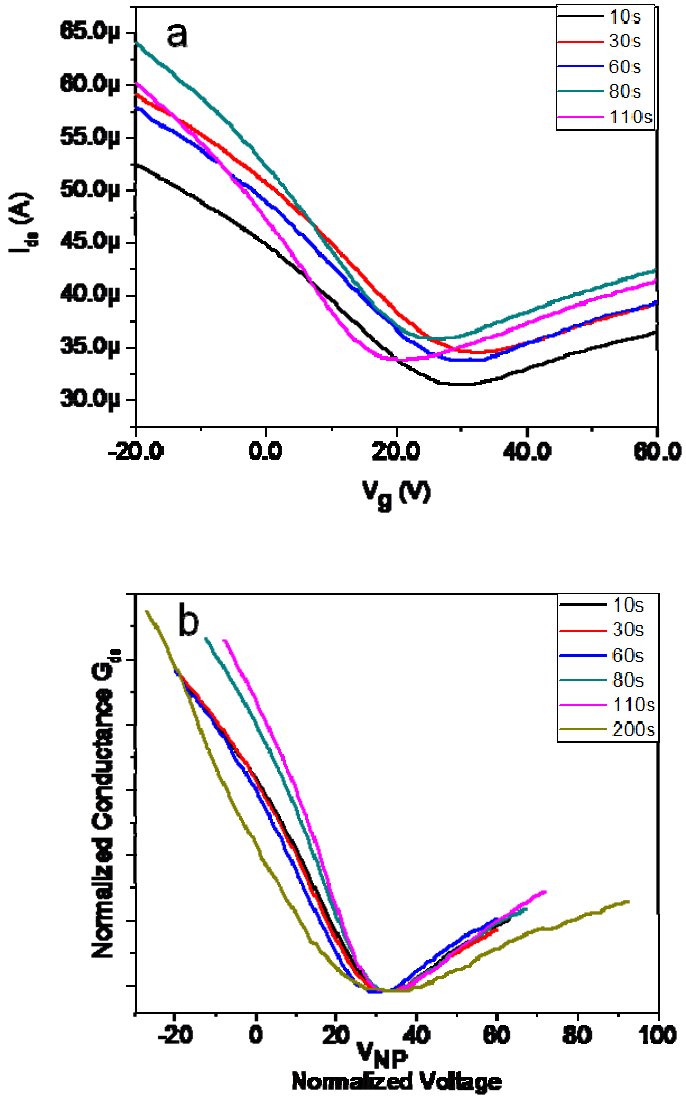

Figure 2.5 (a) Source-drain current vs. gate voltage (I_{ds}-V_g) curves from samples obtained after different plasma exposure times. The exposure time was accumulated. (b) Normalized source-drain conductance vs. normalized gate voltage (G_{ds}-V_g) curves from graphene device after different plasma exposure times.

To further control the neutrality point shift of the device, a simple fluorine doping method was implemented. Briefly, all of the BCP-covered devices were fluorinated in a reactive ion etching (RIE) machine. The plasma treatment was carried out at room

temperature with the CF_4 gas pressure fixed at 10 mTorr with different exposure times, while the CF_4 flow rate was kept constant at 50 sccm, and graphene fluorination was performed with an RF power level of 25W. It has already been shown that carbon materials can be doped with fluorine by exposure to a CF_4 plasma,[39] and fluorine doping of graphene oxide (and its subsequent substitution by an amine group) has been recently reported.[40] Also, Duan et al.[8] have reported a graphene nanomesh novel structure with BCP as the template. They demonstrated that PS and PVP have different sensitivity to treatments with O_2 plasma, enabling the nanomesh fabrication. Here we speculated that such a difference might be utilized in doping BCP-protected GFETs using a CF_4 plasma. The covalent attachment of partial fluorine groups and carbon fluoride groups to graphene could offer an opportunity for achieving some unique transport properties, and the partial doping of BCP could indirectly alter these as well. Figure 2.5a shows a shift in the neutrality point with different exposure times to CF_4 plasma. With an increase in exposure time, the neutrality point first shifted to right towards a positive value, and then shifted to left a little bit; and finally shifted to right again at longer exposure times. In this process, F, CF_2 and CF_3 radicals in the plasma play an important role in the reaction with BCP and graphene. Similar trends were observed with a total of 14 selected devices on 3 different samples (Figure 2.6). Note that different devices required varying exposure times in modulating the shift of the neutrality point, perhaps because of different coverage patterns of BCP on the devices.

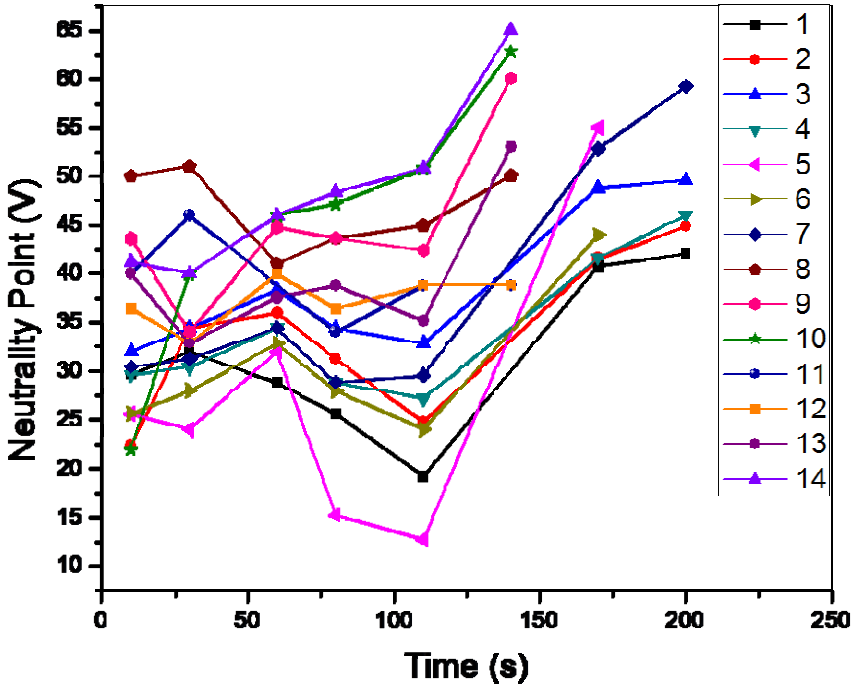

Figure 2.6 Neutrality point shift curves with different exposure times to CF_4 plasma of 14 devices. The I-V test points were 10s, 30s, 60s, 80s, 110s, 140s, 170s, 200s.

The controllable shift mechanism could be explained by further analysing the doping effect of the particular polymer. Initially, polymer chains could be destroyed by forming C-F bonds, which introduce electron acceptors thus causing a p-type doping. Chen et al.[41] reported that electron transfer from graphene to adsorbed tetrafluorotetracyanoquinodimethane ((F4-TCNQ) is responsible for the p-type doping of graphene. In our case, the chain C-F bonds formed during the plasma treatment acted in the same manner. With increasing the treatment time, the benzyl and pyridine groups react further with the CF_4 plasma, introducing more electron acceptors, and the neutrality point then shifts further to more positive values. Another possibility is that the

flurocarbon polymer may have formed on the surface of BCP which will indirectly cause p-type doping in graphene. The disappearance of these two functional groups enables restoring the pristine graphene properties, hence the subsequent reverse shift of the neutrality point is observed. Figure 2.5b shows the normalized conductance-gate voltage curves obtained for different plasma exposure times. It is observed that with increasing exposure time, the electron conduction is preserved, whereas the hole conduction is altered significantly. During the plasma reaction process, it is likely to have more dangling bonds generated in polymer chains that are producing positive/negative charges which may induce a n/p-type doping effect. Considering the complexity of the experimental system, it is very difficult to pinpoint whether positively or negatively charged molecules are produced. Together with the charged molecules and the electron accepting characteristic of the CF_x group on the device, an increase in the hole mobility was observed. When the exposure time was increased from 10s to 110s , the hole mobility increased from 440 $cm^2/V{\cdot}s$ to 724 $cm^2/V{\cdot}s$. AFM images taken after a 110s of CF_4 plasma treatment show that the domains of PS and P4VP are not clear any more. This further clarifies the reaction mechanism. Moreover, the minimum neutrality point couldn't be returned to the value of that of pristine graphene because of the doping effect of the fluorinated polymer. These results point to a general route for tuning the transport properties of polymer-coated graphene; theoretically, any kind of polymer could be doped with fluorine which will produce a polymer with fluorine groups and this could further change the transport properties of graphene layers.

When the time of exposure of our samples to the CF_4 plasma was increased to 170s, the neutality point shifted towards right significantly, presumably because of direct doping of graphene with F, CF_2 or CF_3 radicals. The BCP-ordered structures were completely removed when the time increased to 200s, but the corresponding AFM image shows that some residues still remain on the graphene surface which could display a p-type doping effect (Figure 2.1c). The loss of the protective layer should at the same time introduce more chances of F doping on the graphene and further decrease its conductivity. The need for this harsh treatment to remove the BCP demonstrates the stability of the BCP layer, which indicates that such BCP could be utilized as a protective layer for other applications, such as biochemical sensors. A control experiment was conducted by exposing the device without a BCP layer to plasma treatment for 10s, during which 60% of the devices weren't conductive anymore and those which preserved their conductivty had a high positive neutrality point value (Figure 2.7). The minimum value of conductance increased from 5×10^{-5}S to 6.8×10^{-5}S after plasma processing. This result further ractifies the significant role that BCP could play both as a protective layer and a doping layer to GFETs.

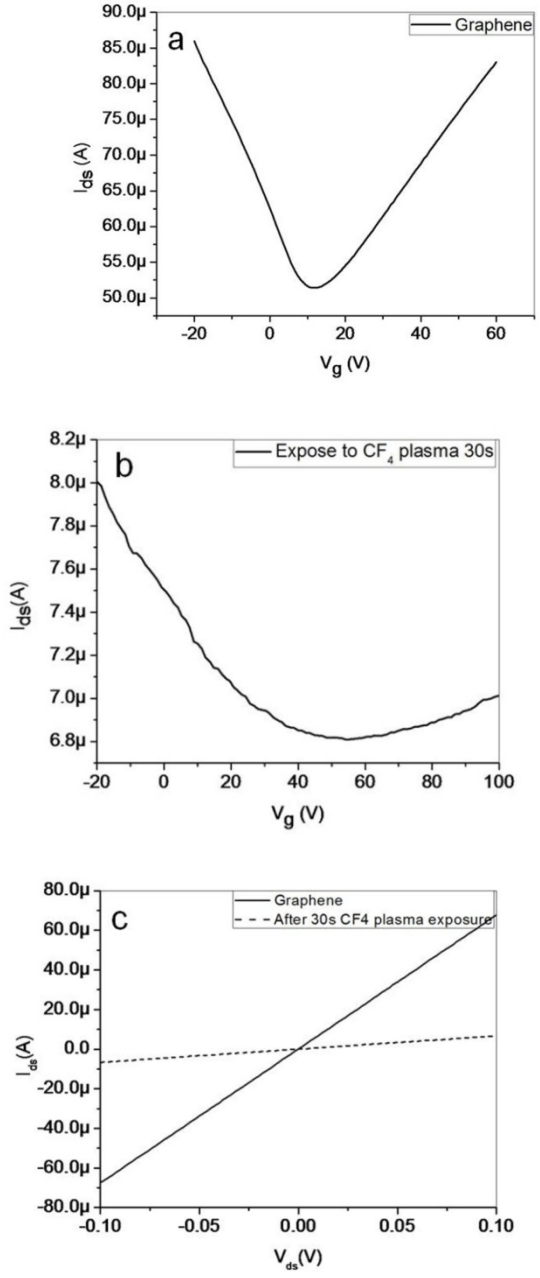

Figure 2.7 Typical source-drain current vs. gate voltage (I_{ds}-V_g) curves of control sample of pristine graphene before (a) and after 30s CF_4 plasma treatment (b), And (c) I_{ds}-V_{ds} curves of these two smaples which show the one order increase of resistivity after 30s plasma treatment.

	Peak 1	Peak 2	Peak 3	Peak 4
Position (eV)	284.6	286.3	287.9	289.3
Area (%)	68	19	7	6
Assignment	C-C	C-O	C=O	C(O)O

Table 2.1 The peak positions, peak areas, and assignments obtained from blank sample fittings.

	Peak 1	Peak 2	Peak 3	Peak 4	Peak 5	Peak 6
Position	284.6	286.3	287.9	289.3	291.1	293.2
Area (%)	51	17	12	8	8	4
Assignment	C-C	C-O	C=O or **C**-CF_3	C(O)O Or C-F	C-F_2	C-F_3

Table 2.2 The peak positions, peak areas, and assignments obtained from F-doped sample fittings.

To further examine the doping effect of fluorine to CVD grown graphene sheets, both x-ray photoelectron spectroscopy (XPS) and Raman spectroscopy data were taken for blank graphene and for graphene exposed to CF_4 plasma for 10s. The reactive ion plasma etching conditions used here were the same as in the doping experiments disscussed above. It is clear that the intensity of the D peak of fluorinated graphene is much larger than that of the G and 2D peaks (Figure 2.8).

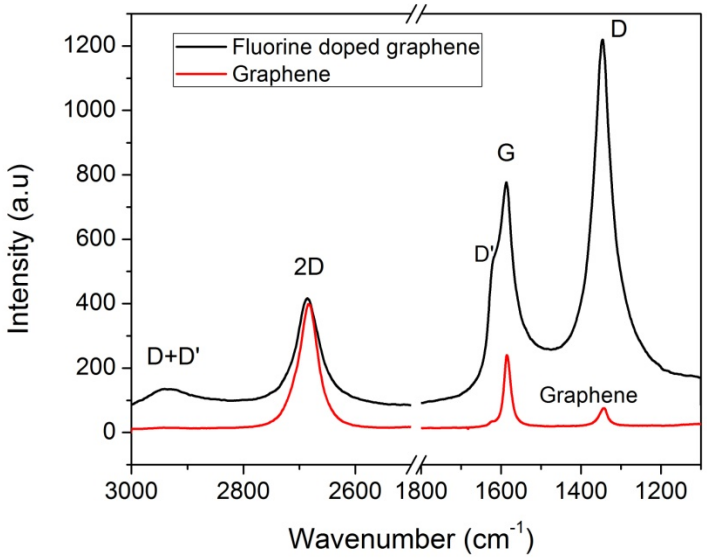

Figure 2.8 Raman spectra of graphene and fluorine doped graphene with CF4 plasma treatment for 10s.

As the D resonance requires a defect for its activation, its presence is associated with an increased degree of disorder. Several studies on carbon nanotube and carbon bulk materials showed that sp^3 bond which is produced from breaking of the sp^2 network in graphene contributes to D peak intensity increase. The XPS study further confirms the existence of significant amounts of F in the films after plasma treatment (Figure 2.9). Interestingly, the total intensity of C drops while the intensities of O and Si (from the underlying substrate) increase (Figure 2.10). This may be caused by partial removal of the graphene layer during plasma processing. Deconvolution of the C 1s peak, following a procedure similar to that reported in the literature[38,41], was carried out to better identify the carbon species present on the surface. Plots of the fittings of the C peaks are shown in Figure 2.11, and the resulting peak areas, peak positions, and assignments are listed in Tables 2.1 and 2.2. It was determined that a 10s exposure of graphene to the CF_4 plasma

results in high levels of F doping. Based on the measured area and atomic sensitivity factor of F (1s) and C(1s), the estimated F/C ratio is approximately 56%.

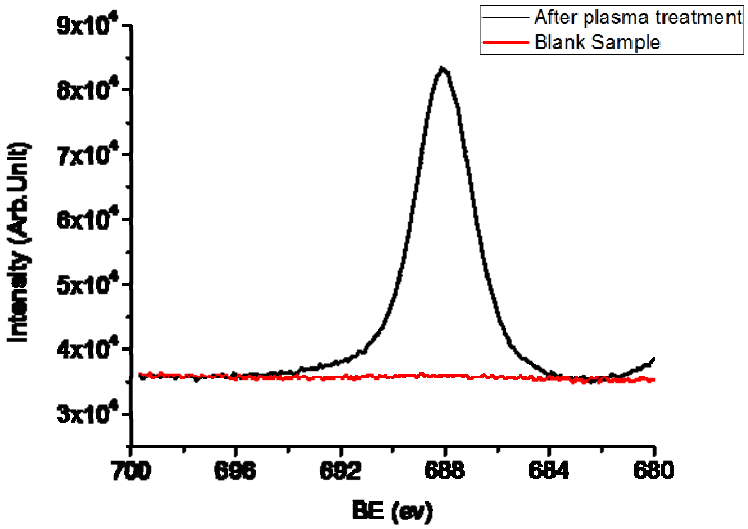

Figure 2.9 F 1s XPS spectra from a blank graphene sample (red traces) and from a sample after a CF_4 plasma treatment for 10s (black traces).

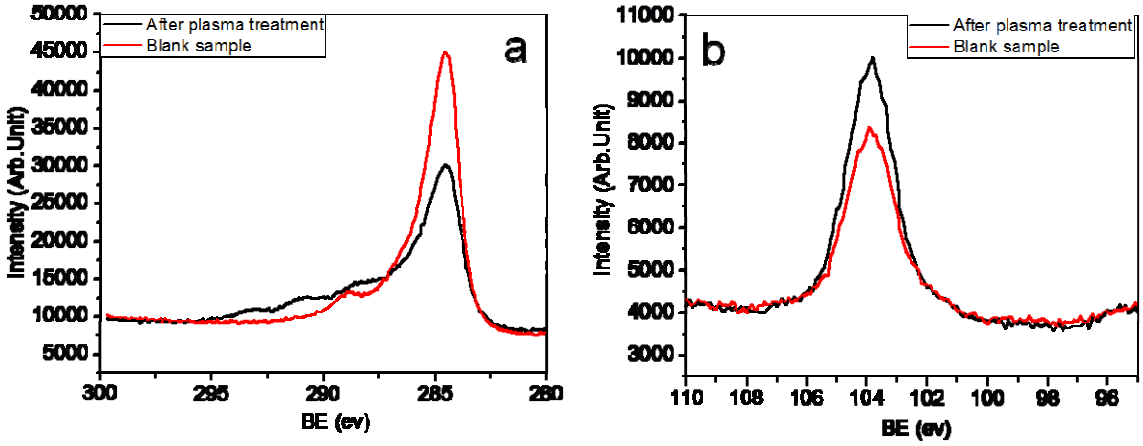

Figure 2.10. Plots the XPS spectra of (a) C 1s and (b) Si 2p.

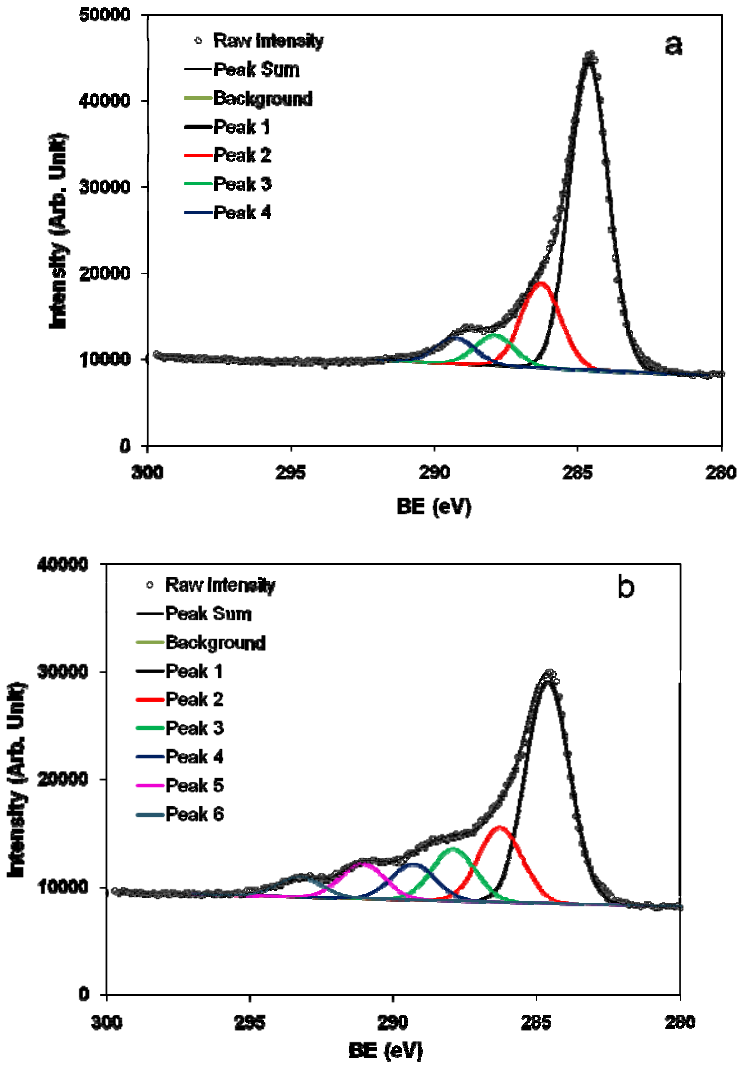

Figure 2.11 Plots of the fittings for the C is XPS peak obtained from the (a) blank and (b) 10s CF_4 plasma-exposed samples.

It has to be noted that the CF_4 plasma itself could introduce carbon atoms which indicates the probable higher ratio of doping F for graphene. These doping effects are strong enough to break the honeycomb structure of graphene, which would lead to the decrease in conductivity indicated by our electrical conductivity survey (Figure 2.7). In fact, a significant fraction of the fluorine is found in CF_3 and CF_2 moieties, proving that

there is some degree of sp^2 to sp^3 carbon hybridization conversion in the graphene upon plasma treatment. The presence of C=O bonds in the blank sample also demonstrates a p-type doping behavior of the sample, a possible reason for the positive shift of the neutrality point after the sample is exposed to air.

2.1.4 Conclusion

In conclusion, assembling cylindrical microdomains of BCPs as protective layers on GFETs is a methodology to tune the electron and hole conduction of graphene. Spatially controlled fluorine doping could provide a general route to refined tuning of the electronic properties of BCP coated GFETs. Particularly interesting is that the BCP template could produce spatially ordered, organic–inorganic and organic–bioparticle hybrid materials[26] which could be further utilized for sensing of gas or ions as permeable materials.

2.2 Photoinduced Electron Transfer between Pyridine-Coated Cadmium Selenide Quantum Dots and Single-Sheet Graphene

2.2.1 Introduction

Recent advances in photovoltaics have demonstrated that composites of graphene and quantum dots (QDs) are promising candidates for energy-conversion applications.[42-46] The ability to attain graphene sheets with relatively large areas, along with its metallic-like lateral electrical conductivity, has drawn the ever-growing interest on this carbon allotrope as the media of choice for collection and transport of photo-generated charge carriers in photovoltaic (PV) devices.[46-50]

The absorbance of single-sheet graphene, however, does not exceed ~10^{-2} in the visible region of the spectrum.[51-53] Furthermore, photoexcited graphene undergoes ultrafast relaxation to low-lying excited states (i.e., only tenths of eV above the ground state), with lifetimes of the optical phonons that barely exceed 1 ps.[54-55] These short lifetimes of graphene excited states, along with its relatively small absorptivity throughout the visible spectral region, present a principal shortcoming for the use of this carbon allotrope as a single sheet by itself for light-energy conversion applications.

In graphene-based composites, chalcogenide QDs are the principal light sensitizers because of their: (1) relatively long excited-state lifetimes; and (2) relatively large bandgaps, tunable between ~1.5 and >3 eV. In the design of PV devices, bulk-heterojunction (BHJ)[42] and tandem[46] architectures allow not only for an increase in the contact area between the graphene phase and the QD sensitizers, but also for an increase in the overall light absorptivity of the composite films.

Zero-dimensional semiconductor nanoarchitectures, such as quantum dots, with their size-tunable optical and electronic properties, provide the means for attaining widely diverse hybrid structures with solid conductors or semiconductors.[56-57] The QD unique properties, such as relatively high energy conversion efficiency (beyond the Schockley-Queisser limit),[58] photostability, and size-controllable band gaps and redox properties, make them highly desirable for light harvesting applications.[59-60]

Implementing elegant multiscale architectures in quantum-dot-sensitized PV devices has allowed for concurrent attainment of increased light absorptivity, decreased paths of exciton migration (prior to charge separation), and efficient collection of charge

carriers.[61-66] Conversely, BHJ materials provide facile means for constructing large-area PV devices that, while lacking the potential for high conversion efficiency, do not have the fabrication complexity of QD-containing structures requiring multiscale order.[67-70] In such heterophasic PV devices, one-dimensional conducting materials, i.e., quantum wires (QRs), provide pathways for long-range charge transport uninterrupted by interfaces, which is essential for increased carrier-collection efficiencies. Indeed, carbon nanotubes and other QRs have become intricate components of recently developed PV devices.[68-70]

Alternatively, two-dimensional materials, such as quantum wells (QWs), provide unique capabilities for efficient collection of photogenerated charge carriers within the same phase, spread over large working areas.[42,46,48] The two-dimensional QW morphology of graphene, along with its high electron and hole mobility,[71] has made this carbon allotrope a desirable scaffold for optoelectronic and photovoltaic applications.[72-73]

Many of the proposed QD/QW hybrid material for PV applications employ graphene oxide (GO) or reduced graphene oxide (RGO) as QW.[42-44,74-75] The dispersion of graphitic carbon into exfoliated sheets of GO offers chemical-based approaches for producing RGO sheets.[50,75] Reduction of GO sheets, however, allows only for a partial restoration of the sp^2 network.[76-78]

As an alternative, others and we have employed chemical vapor deposition (CVD) for growing films of graphene with structural and electronic properties superior to those of RGO.[79-83] Most importantly, size scalability of graphene films grown via CVD is the key advantage for meeting the requirements for fabricating large-area PV and other

optoelectronic devices: e.g., CVD allows for fabricating single-sheet graphene with areas exceeding five square inches.[79,84]

Graphene is known to quench photoluminescence (PL) of cadmium chalcogenide QDs.[85-86] Three phenomena can account for the reported emission quenching: (1) resonance energy transfer; (2) electron-exchange energy transfer; and (3) charge separation. Non-radiative dipole-dipole resonance energy transfer (i.e., via Förster mechanism) does not require electronic coupling between the materials and can be effective between the QDs and the graphene surfaces even at distances that exceed 10 nm.[87] For high-symmetry systems, however, that involve transition quadrupoles and transition octapoles (instead of transition dipoles), the distances for efficient resonance energy transfer are shortened.[88]

Alternatively, electron-exchange energy transfer (i.e., via Dexter mechanism)[88] involves simultaneous oppositely directed electron-transfer processes: i.e., from the conduction band of the photoexcited QDs to the graphene and from the graphene to the valence band of the excited QDs. Because electron-exchange energy transfer requires electronic coupling between materials, its efficiency falls off considerably for interfacial QD-graphene distances exceeding about 1 nm. Furthermore, for such Dexter-type energy transfer, the rates of the two opposing electron transfer steps should be compatible. When one of the opposing electron-transfer processes is faster than the other, however, the QD-exciton deactivation results in charge separation: i.e., either electron or hole transfer from the QDs to the graphene. This photoinduced charge separation is the key process for light

harvesting QD/QW materials, i.e., for converting absorbed light energy into free n- and p-carriers.

The balance between the three mechanisms of PL quenching in QD/graphene hybrids depends not only on the match between the electronic properties of the QDs and the graphene, but also on the media that separates the QD and the graphene. For example, coating with alkyl derivatives increases the stability and solubility of QDs. Such alkyl coatings, however, efficiently suppress charge transfer,[89] making resonance energy transfer to graphene the prevailing quenching pathway, as recently demonstrated for CdSe/ZnS QDs functionalized with trioctylphosphine oxide.[85] Alternatively, when bare CdSe/ZnS QDs were deposited on graphene, their PL quenching resulted from photoinduced charge separation.[86] Analogously to QD/QW, for QD/QR devices (i.e., devices of QDs on single-wall carbon nanotubes) stabalizing the CdSe QDs with coatings of small aromatic amines, i.e., pyridine, was essemtial for attaining photoconversion.[90]

In this section, we utilized large-area CVD-fabricated single-sheet graphene to investigate the interfacial photoinduced charge transfer between pyridine-coated CdSe QDs and the carbon allotrope. Although the Fermi level of graphene lies between the valence and the conduction band of the inorganic particles, we observed preferential directionality of the photoinduced electron transfer from CdSe phase to the carbon allotrope.

Time-resolved spectroscopy revealed three modes of photoinduced charge separation: (1) a picosecond transfer of relaxed electrons from CdSe to graphene; (2) a sub-picosecond transfer high-energy carriers to graphene; and (3) a direct excitation to

CdSe-graphene charge-transfer states. In addition, we observed evidence for pico- and subpico-second formation of pyridine radical cation, indicating hole transfer from the CdSe phase to the aromatic coating ligands. Concurrently, the photoelectric properties of the QD/QW films revealed that the light-induced processes populated the graphene phase with n-carriers, indicating for photoinduced transfer of electrons from the CdSe to the carbon allotrope. While the hole shift to the coating pyridine ligands would decrease the overall distance for electron transfer from the graphene phase, this process was less favorable than the electron transfer from the chalcogenide to the carbon allotrope. We ascribed the observed preferred directionality of photoinduced electron transfer from the QDs to the relatively large reorganization energy for injecting holes at energy levels considerably below the graphene Dirac points.

2.2.2 Results and Discussion

2.2.2.1 Hybrid Films of Quantum Dots and Graphene

A method based on CVD allowed us to synthesize single layers of graphene with areas of about 2 in^2, as we have previously reported.[82] We deposited the graphene on smooth substrates such as glass and silicon, and characterized it using Raman spectroscopy and fluorescence quenching microscopy.[83]

For a light-sensitizer of the hybrid films, we employed CdSe QDs that were coated with octadecylamine (ODA) or pyridine (Py). We used commercially available ODA-coated QD samples that were a 3:2 mixture of CdSe and ZnS crystals with an average diameter of about five nanometers as determined by transmission electron

microscopy, TEM (Figure 2.12a). Because of the bandgap difference between the two materials, we could selectively photoexcite the CdSe QDs in the visible and near UV regions without interference from the ZnS particles. Therefore, we can regard the light-absorbing material as predominantly CdSe QD photosensitizers diluted with ZnS QDs, and hence our discussion focuses on the former. Treating of QD-ODA with Py resulted in an exchange of the aliphatic with the aromatic ligands as we confirmed using infrared spectroscopy. As determined with TEM, the treatment with pyridine did not alter the inorganic components of the particles (Figure 2.12b).

Covalent grafting of graphene with functional materials requires breaking of its π-conjugation. Therefore, we resorted to non-covalent self-assembly to coat the graphene surfaces with QDs. Dropping diluted suspensions of pyridine-coated QDs on the surfaces of the carbon allotrope, followed by multiple washes, produced hybrid graphene films with organically coated inorganic nanoparticles. We observed that pyridine coatings of the QDs was essential for obtaining densely packed monolayers of QDs with minimum clumps over large areas of graphene (Figure 2.12c, d). The QD-Py nanoparticles tend to form monolayer islands with density of about 1.14 particles per 100 nm^2 calculated from SEM images (Figure 2.12d). The ODA-coated QDs did not manifest the same propensity for self-assembly in monolayers on the carbon substrate (Figure S1). Hence, the balance between the interfacial energies between the three phases, i.e., the solvent (pyridine/toluene), the graphene and the pyridine coatings, provided the optimal conditions for self-assembly of monolayers of QDs on single-sheet graphene.

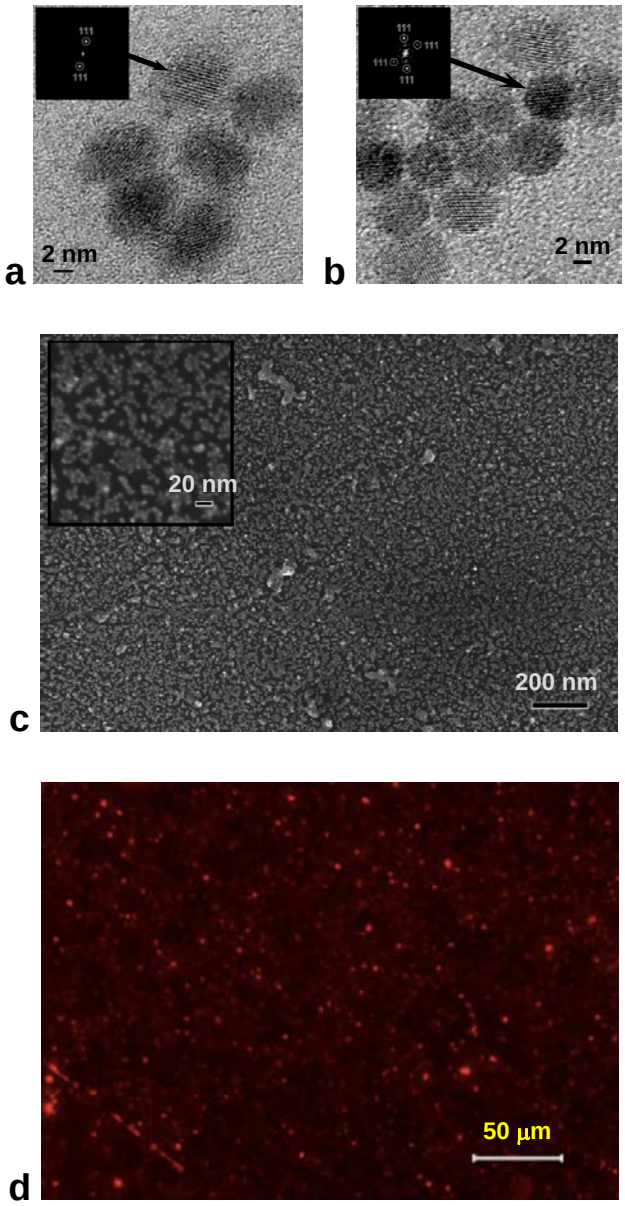

Figure 2.12 Microscopy images of quantum dots (QDs) and of QD films. (a, b) Representative transmission electron microscopy (TEM) images of (a) QD-ODA, and (b) QD-Py. Insets: FFTs of the lattice images of selected particles. The reflections were estimated to be from {111} planes of cubic CdSe, as indexed in the FFTs of the lattices. (c) Scanning electron microscopy (SEM) image of QD-Py/graphene film. Inset: SEM image of the film at higher magnification. (d) Confocal fluorescence microscopy image of QD-Py/graphene film (λ_{ex} = 488 nm with10-nm bandwidth; and λ_{em} = 624 nm with 40-nm bandwidth).

Coating of QDs with pyridine indeed enhances their adherence to carbon-based surfaces, such as highly oriented pyrolitic graphite and carbon nanotubes,[95-97] which was in agreement with our observations (Figure 2.12c, d). To drive the fomation of QD monolayers on graphene, the pyridine moieties had to provide an approach for sufficiently strong adhesion between the CdSe QDs and the carbon allotrope. With the coordination bond between pyridine and a metal ion, such as cadmium and zinc, lying on the plane of the aromatic ring, the organic ligands in the QD-Py would be oriented away from the surfaces of the inorganic nanoparticles.[98-99] Therefore, at the point of contact between a QD-Py and graphene, the pyridine aromatic rings are unlikely to orient in parallel to the surface of the carbon allotrope (without introducing significant bond tension). As a result, π-π stacking cannot account for the observed adhesion, as it has been previously suggested for adsorption of Py-coated nanoparticles to similar carbon allotropes.[49,90,95,97] Considering the structural features of the face-to-edge interactions between aromatic residues in proteins and other biomolecules,[100-102] we ascribed the observed QD-Py adhesiveness to favorable contacts between the graphene π-conjugation and the edges of the obliquely oriented pyridine ligands.

2.2.2.2 Absorption and Emission Properties of The Hybrid Films

The exchange of the aliphatic ligands, ODA, with the aromatic amine, Py, caused only about three-to-four nanometer red shifts in the QD absorption and emission spectra, corresponding to about a 10-meV decrease in the optical band gap (Figure 2.13a). When

deposited as films on glass surfaces, the pyridine-coated QDs exhibited about five-to-seven nanometer red shift and broadening of their spectral features (Figure 2.13b), which was consistent with electronic coupling between the QDs when clustered into the solid assemblies. Overall, the optical band gap of the CdSe QDs was about 2 eV, as estimated from the absorption and emission spectra analogously to estimate the zero-to-zero energy, $\mathscr{E}_{00}$, of organic chromophores (Figure 2.13a, b).

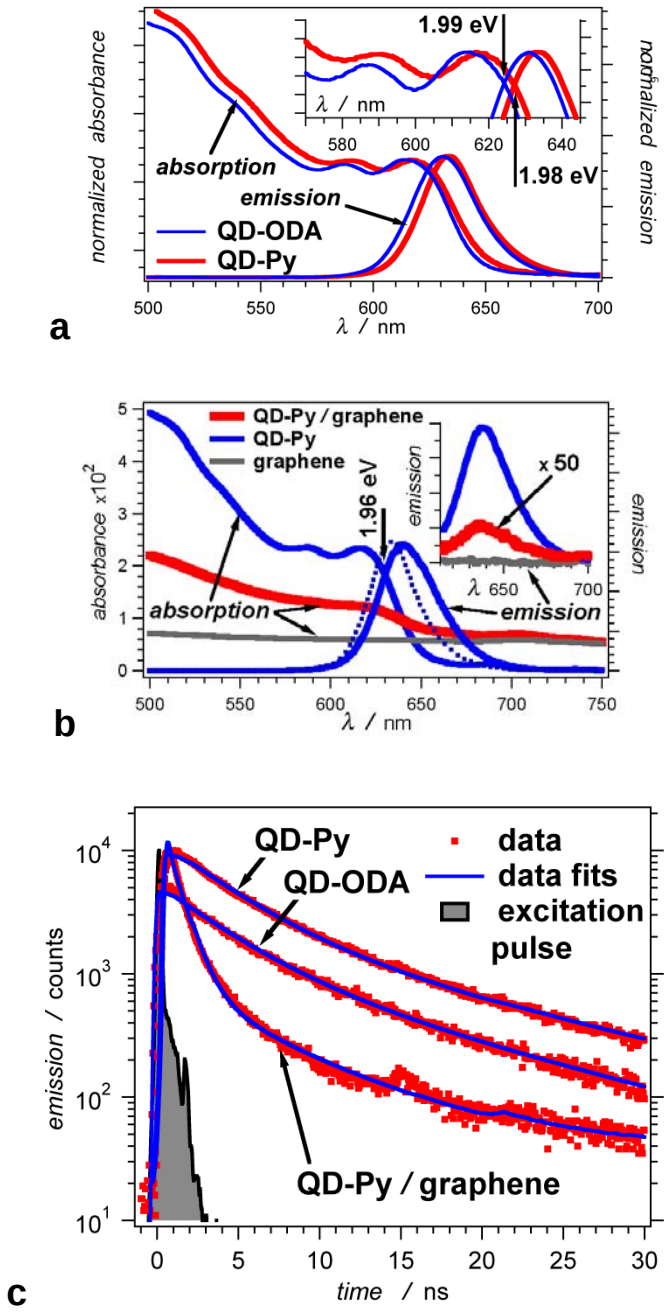

Figure 2.13 Absorption and emission properties of films of Py- and ODA-coated QDs: (a) dissolved in toluene; and (b, c) deposited on bare glass (QD-ODA and QD-Py) or on graphene-coated glass (QD-Py/graphene). (a) Comparison between the normalized steady-state absorption and emission spectra of QD-ODA and QD-Py suspended in toluene (λ_{ex} = 420 nm). (b) Steady-state absorption and emission spectra of QD-Py films and of single-layer graphene. The absorption spectra of the solid films were obtained from reflectance measurements using an integrating sphere, and the emission spectra

were recorded using a small-angle setup (for the main panel, λ_{ex} = 420 nm; and for the inset, λ_{ex} = 600 nm). For improved visualization, the emission spectra of graphene and of QD-Py/graphene were scaled up by a factor of 50 The dotted blue line corresponds to the solution QD-Py emission spectrum (a). (a, b) For estimation of the QD band gaps, the zero-to-zero energy was calculated from the crossing points of the normalized steady-state absorption and emission spectra.

Conversely, the presence of graphene had a pronounced effect on the pyridine-coated QDs (Figure 2.13b). The single-sheet graphene induced: (1) a loss of fine structure and broadening of the QD-Py absorption spectra (as apparent at the red edge); and (2) quenching of the QD emission (Figure 2.13b). The former was indicative of ground-state electronic coupling between the confined CdSe states and the graphene, i.e., coupling mediated through the pyridine layer separating the carbon substrate from the CdSe semiconductor (Scheme 2.2). The latter was indicative of efficient photoinduced processes that deactivated the CdSe excited states, i.e., processes such as charge or energy transfer occurring in time scales shorter than the lifetimes of the CdSe excited states that decay radiatively. Indeed, while the emission quantum yield, Φ, of the QD-Py films on glass was 0.028±0.003, the values of Φ for the QD-Py mono-layer on graphene ranged between about $2\times10^{-4} - 2\times10^{-3}$.

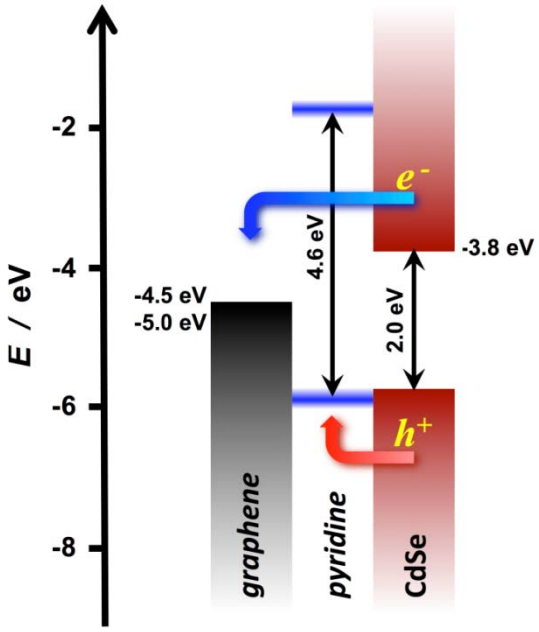

Scheme 2.2 Band diagram and charge transfer between pyridine-coated CdSe QDs and graphene.

To quantify the observed graphene-induced quenching of the QD luminescence, we resorted to time-resolved emission spectroscopy, as implemented by time-correlated single-photon counting (TCSPC). Biexponential functions provided reasonably good fits for the emission decays of the QDs deposited on glass with no graphene (Figure 2.13c).[89,103] The fits produced principal components with lifetimes ranging between 3 and 4 ns, and minor components with lifetimes longer than 10 ns (Figure 2.13c). Multiexponential functions fitting for QD-Py/graphene yielded average lifetimes smaller than about 0.5 ns (Figure 2.13c)

In the absence of graphene, the exchange of the organic ligands of the QDs had a negligible effect on the observed emission decays (Figure 2.13c): i.e., trend of slight

decrease in the lifetimes upon exchanging ODA with Py was within the experimental uncertainty. When QD-Py nanoparticles were deposited on graphene, however, their emissive states exhibited predominantly short lifetimes, i.e., in the sub-nanosecond time domain (Figure 2.13c). These findings demonstrated that coating the QDs with small aromatic ligands not only drove their self-assembly into monolayers over the graphene, but also provided considerable electronic coupling between the semiconducting chalcogenide and the carbon allotrope essential for mediating photoinduced processes responsible for the observed emission quenching.

Comparison of the emission quantum yields, Φ, obtained from different QD-Py/graphene samples (from steady-state measurements) with their emission lifetimes, τ (from TCSPC), presented a discrepancy with important implications. While the measured emission-decay lifetimes from the different QD-Py/graphene samples exhibited only about two-fold variations between the samples, the corresponding values of Φ varied about an order of magnitude, i.e., they were between ~15 and ~150 times smaller than Φ of the QD-Py films on glass. In contrast, the values of τ of the QD-Py/graphene samples were only 10 – 20 times smaller than τ of QD-Py films deposited on bare glass without graphene.

We ascribe this discrepancy to the inherent heterogeneity of the solid-film samples. While most of the QDs were deposited as monolayers on the graphene, multilayered clusters of QDs (i.e., film imperfections) were the principal source of the PL. The emission quantum yield averages the properties of all QDs deposited on the graphene. In the monolayers, all QDs were in direct contact with graphene. The

multilayers, however, contained QDs that were not in contact with graphene. Should Φ of the multilayered QDs exceed with at least two orders of magnitude Φ of the monolayered QDs, a few percent variations in the amount of clustered QDs (from a sample to sample) would alter the measured ensemble-average emission quantum yield with an order of magnitude or more, which was consistent with our observations.

Fluorescence microscopy allowed us to confirm the origin of the observed discrepancy between the trends in the values of τ and Φ for the QD-Py/graphene samples. SEM images of QD-Py/graphene samples revealed relatively dense coverage of surfaces with nanoparticles, (Figure 2.12c, d). Confocal fluorescence microscopy images of the same films showed that most of the areas covered with the QD-Py nanoparticles were dark (Figure 1d). Concurrently, the same images of the QD-Py/graphene films also showed spots with high emission intensity, which we attributed to agglomerated sites of pyridine-coated QDs on the graphene film (Figure 2.12d), i.e. sites containing QDs that lack sufficient electronic coupling with the graphene.

These results suggested that the QD-Py/graphene PL from the strongly luminescent QD clusters dominated the emission from the spectroscopy measurements (Figure 2.13b). If the mono-layered pyridine-coated QDs were not luminescent (i.e., if the τ values of the graphene-quenched PL of the QD-Py nanoparticles did not exceed a few picosecond, which is under the dynamic range of TCSPC), variations in the amount of multilayered QDs would change the PL intensity (and hence the calculated Φ), but would not alter to the same extent the rates with which these clustered QDs decay radiatively. Thus, the emission quenching rate constant of about 5×10^{9} s^{-1}, extracted from

TCSPC measurements, represented the photoinduced process mostly from the clustered QDs that were not in a direct contact with the graphene surface.

2.2.2.3 Transient-Absorption Dynamics

To overcome the limitation of emission spectroscopy and to discover the real interaction between monolayer QDs and graphene, we employed pump-probe transient-absorption spectroscopy that allowed us to monitor transitions involving the confined CdSe states regardless of their radiative characteristics.[103] Transient absorption (TA) spectra of the QD films on glass exhibited the characteristic features of transitions between confined states of cadmium chalcogenide nanocrystals (Figure 2.14).[94,104-105] Within the first few hundred femtoseconds after the excitation, the Stark effect from the photoinduced redistribution of charge carriers manifested itself in: (1) bleaching of the ground-state absorption resulting in B_i bands; and (2) shifts in the energy levels of the states associated with the optical transitions, resulting in A_i bands at the blue or red edges of the B_i bands (Figure 2.14a – c).[94] The similarity between the early-time TA spectra and the second derivative of the ground-state absorption of the CdSe QDs was in accord with the Coulombic origin of the A_i and B_i features that appeared immediately after the excitation (Figure 2.14c).[106]

The further growth of the B_1 and B_2 bands, which continued for a few picoseconds after the excitation pulse, was ascribed to the dynamics of intraband relaxation.[94] Indeed, sub-picosecond and picosecond intraband relaxation of the photoexcited CdSe QDs, leading to filling of the low-lying $1S_e$ quantum size level (QSL)

with electrons,[107] further enhances the magnitude of the B_1 and B_2 TA bands.[94] At the high-energy transitions (e.g., at 530 – 515 nm) within about 400 fs, ΔA reached its most negative values (Figure 2.14e). In comparison, the B_1 and B_2 bands manifested slower growth, exhibiting multiexponential kinetics with $\langle \tau \rangle \approx 1$ ps, to reach their most negative ΔA values at about 5 ps (Figure 2.14e). This picosecond growth of B_1 and B_2 was consistent with the filling of the low-lying QSLs in the conduction band (CB) with electrons via intraband relaxation.[94]

The recovery of the ground state absorption (i.e., the bleach recovery) manifested biexponential kinetics, which was quite similar for the QD-ODA and QD-Py films with no graphene (Figure 2.14f). For the QD-ODA and for QD-Py, the time constants, τ, of the fast components of the bleach recovery at the B_1 bands were about 250 ps, and of the slow components – close to 2 ns (Figure 2.14f). The nanosecond slow-components of the TA kinetics, however, should be viewed with caution in a somewhat qualitative manner. The upper limit of the time dynamic range of the pump-probe setup was 3.2 ns. Therefore, we cannot claim statistical significance for values of τ exceeding ~1 ns: i.e., it is challenging to claim statistical discernibility between such time constants that are relatively long for the recorded datasets, and the baseline offset, $\alpha_\infty \approx \alpha_{\text{unrecoverable TA}} + \Sigma\alpha_i \exp(-t / (\tau_i >> 1 \text{ ns}))$. Meanwhile, fitting the B_1 kinetics with triexponential functions, in which we introduced the lifetime values from the TCSPC studies (Figure 2) and kept them fixed, yielded similar time constants, τ_1, for the fast components. This latter triexponential analysis, however, required an assumption that the kinetics of the bleach recovery at 625 nm followed the kinetics of deactivation of the PL states of the CdSe.

Do pyridine ligands affect the excited-state kinetics of the QDs? The TA spectra of the QD-ODA and the QD-Py films had quite similar TA features. In the B_1 and B_2 spectral regions, they exhibited practically the same TA kinetics (Figure 2.14a, b, e, f). Conversely, a closer examination of the TA spectra at the region between 520 and 570 nm reveled that QD-Py films had consistently more positive ΔA than QD-ODA films, which persisted over tens of picoseconds (Figure 2.14d). The TA kinetic curves recorded at 570 nm further illustrate this trend (Figure 2.14e, f). Such TA feature has been previously reported for pyridine-coated CdSe QDs and was ascribed to the radical-cation transient of the ligand ($Py^{+\bullet}$).[108] Indeed, pyridine is a hole scavenger for chalcogenide QDs.[109-110] The absorption of the $Py^{+\bullet}$ transient extends from the near UV to the mid visible spectral region,[111-112] and in the TA spectra of pyridine-coated CdSe QDs, it appears as a weak broad band at wavelengths shorter than ~570 nm.[108] Our findings, therefore, suggested that QD-Py films exhibited a charge-transfer excited state, in which the holes resided on the pyridine ligands.

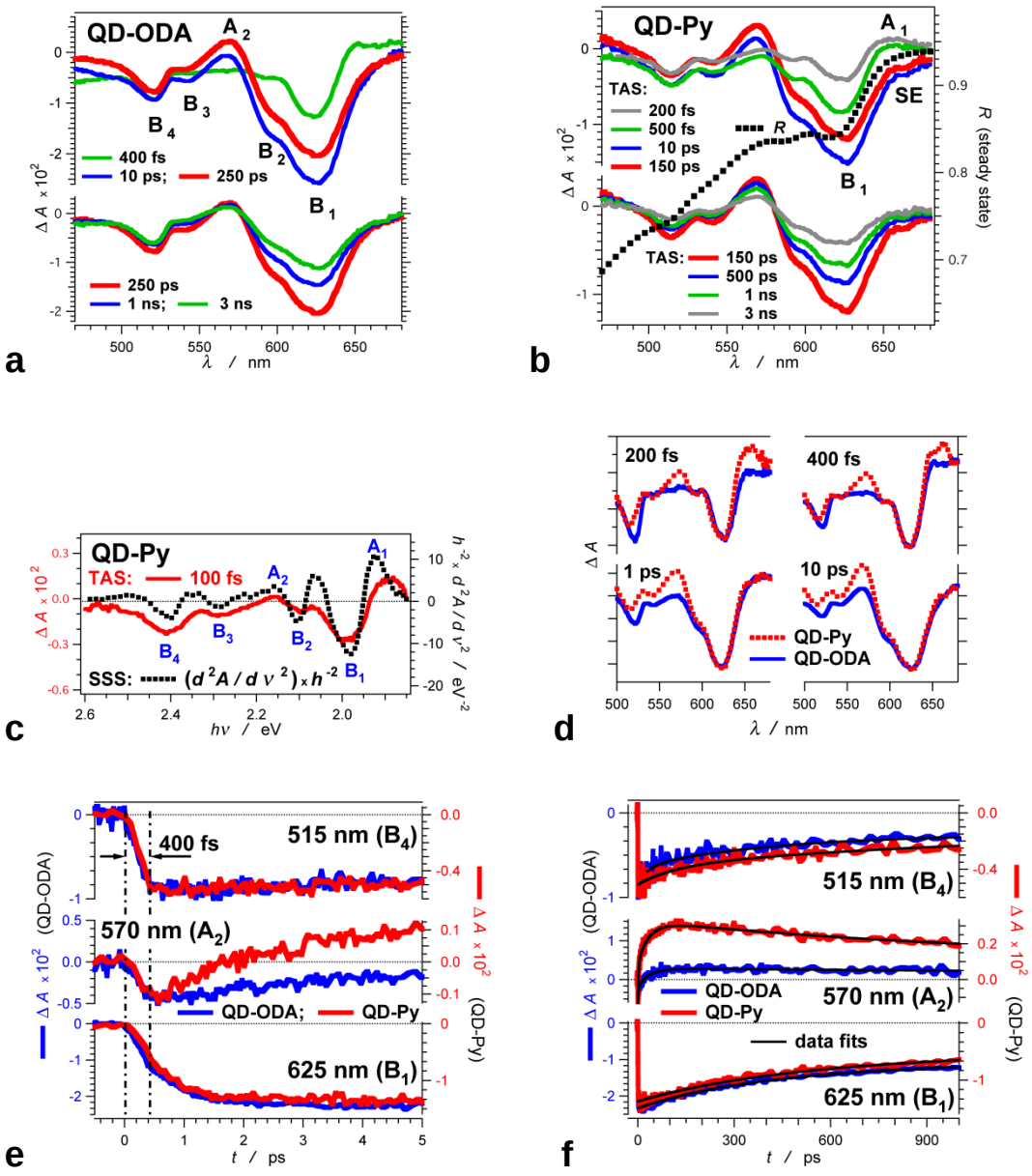

Figure 2.14 Transient absorption (TA) dynamics of QD films deposited on glass with no graphene. (a) TA spectra of a QD-ODA film recorded at different times after the excitation. (b) TA spectra of a QD-Py film in comparison with its reflectance, *R*, from which the ground-state absorbance was determined ($A_{400\ nm}$ = 0.10). The weak negative signal at ~650 nm was ascribed to the stimulated emission (SE). (c) Comparison between an early-time TA features and the second derivative of the ground-state absorption of a QD-Py film, with the corresponding assignments of the absorption, A_i, and bleaching, B_i, bands. **(d)** Comparison between B_1-normalized TA spectra of QD-ODA and QD-Py films. **(e, f)** TA kinetic curves of QD films recorded at three spectral regions. For ease of

comparison, the curves were plotted against different ΔA ordinates, normalizing the initial bleach minima. At 625 nm, biexponential data fits of the bleach recovery yielded: for QD-ODA $\tau_1 = 250\pm20$ ps ($\alpha_1 = -0.45$), $\tau_2 = 1.9\pm0.7$ ns ($\alpha_2 = -0.32$), and an offset $\alpha_\infty = -0.22$; for QD-Py $\tau_1 = 260\pm50$ ps ($\alpha_1 = -0.34$), $\tau_2 = 1.6\pm0.6$ ns ($\alpha_2 = -0.43$), and an offset $\alpha_\infty = -0.23$. (λ_{pump} = 400 nm, 1.5 μJ per pulse, 38-fs pulse width of the fundamental at 800 nm.)

Deposition of pyridine-coated QDs on single-sheet graphene dramatically changed their TA dynamics (Figure 2.15). The bleach recovery at the B_1 band had two principal components with time constants of about 20 and 300 ps (Figure 2.15b), which was consistent with previously reported rates of photoinduced electron transfer between CdSe QDs and single-wall carbon nanotubes.[113]

The TA kinetic curves for QD-Py/graphene, however, did not exhibit the picosecond features of intraband relaxation that we observed for the other QD films. For the samples without graphene the growth of the B_1 band continued a few picoseconds after the excitation (Figure 2.14e, 4b). For QD-Py/graphene films, ΔA at 625 nm grew to its minimum within about 400 fs, prior to initiating the bleach recovery (Figure 2.15b). Similarly, the bleach recovery at 515 nm for QD-Py/graphene samples exhibited considerably faster rates than the rates of the B_4 dynamics of the other QD samples (Figure 2.15b). For QD-Py/graphene, ΔA at 515 nm reached its minimum at about 300 fs, followed by bleach recovery with a sub-picosecond principal kinetic component: τ_1 = 0.26 ps with $\alpha_1 = -0.44$ (Figure 2.15b). Because the B bands are indicative of populating the low-lying QSLs in the conduction band with electrons,[94] these kinetic findings for QD-Py/graphene indicated that the photogenerated negative charge carriers were

removed from the conduction band of CdSe prior to their picosecond intraband relaxation. Namely, some of the pathways of deactivation of the confined CdSe excited states involved unrelaxed charge carriers, such as "hot" electrons.[114]

A close examination of the TA spectra of the QD-Py/graphene films revealed the lack of the "dip" at 540 – 550 nm characteristic for the B_3 band, which was especially apparent for the sub-picosecond QD-Py spectra (Figure 2.15a vs. 2.14b). While the negative ΔA values were indicative for the CdSe bleach bands in the QD-Py/graphene films, the broad TA spectral feature, between about 530 and 560 nm with slightly more positive ΔA, could be ascribed to the transients of oxidized pyridine, $Py^{+\bullet}$. The low absorptivity of the $Py^{+\bullet}$ transient in comparison with the CdSe TA B_i bands, along with the inherently small signal-to-noise ratio of the TA of monolayered QD-Py/graphene films, makes this interpretation somewhat challenging. The formation of $Py^{+\bullet}$ upon photoexcitation of pyridine-coated CdSe QDs, however, was consistent not only with the comparison between the QD-Py and QD-ODA films without graphene (Figure 3d), but also with previous reports on similar nanoparticles.[108]

Another characteristic of the TA for the QD-Py/graphene was the noticeably small ΔA values. The ground-state optical density at the excitation wavelength was similar for all samples within a factor of two. Concurrently, the ΔA values for the TA of QD-Py/graphene films were consistently about an order of magnitude smaller than the ΔA values of the QD-Py films without graphene (Figure 2.14, 2.15). This finding indicated that a part of the absorbed light energy did not generate excited states with TA features in the visible region of the spectrum. A plausible explanation could be sought in the direct

photoexcitation to charge-transfer states between the CdSe and the graphene phase. (Indeed, such relatively long-range interfacial charge separation does not have TA features detectible in the visible region of the spectrum, consistent with the electron-transfer induced TA bleach recovery.[113,115]) As we mentioned above, the broadening of the QD-Py/graphene ground-state absorption in comparison with the QD films with no graphene (Figure 2.13b), suggested for a relatively strong electronic coupling between the CdSe and the graphene that would be essential for a direct photoexcitation to states with such long-range charge-transfer character.

Control sample of ODA-coated QDs on graphene showed smaller effect on the TA dynamics (Figure S2). Most of the bleach recovery of $B_1$for QD-ODA/graphene followed a biexponential pattern with time constants of about 0.2 and 2 ns. At early times, however, a fast positive change in the ΔA contributed to about 10% of the bleach recovery for the QD-ODA/graphene TA at 625 nm, i.e., τ_1 about 13 ps with $\alpha_1 = 0.13$ (Figure 2.15b). Because this is a relatively small contribution to the TA kinstics, we cannot readily ascribe it to the intrinsic properties of the QD-ODA/graphene films. While this fast TA feature is in agreement with the rates of charge transfer between CdSe QDs and carbon allotropes,it can also be representative of a small population of QDs that have defects in their coatings at the interface with graphene: i.e., defects that provide pathways for pronouncedly efficient quenching of the states responsible for the B_1 band.

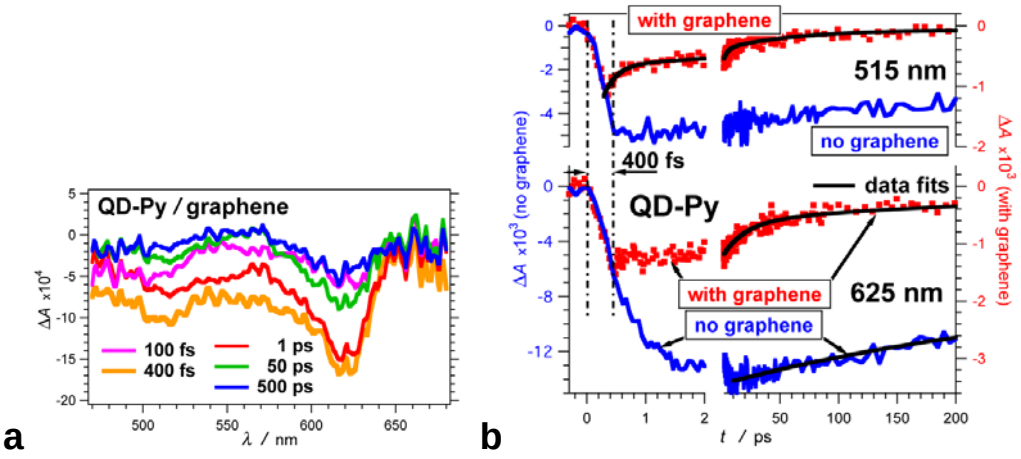

Figure 2.15 Transient absorption (TA) dynamics of QD-Py films deposited on single-sheet graphene on glass substrates. (a) TA spectra of monolayers of pyridine-coated QDs deposited on graphene recorded at different times after the excitation. For improved signal-to-noise ratios, the samples were composed of stacks of three cover slips, with single-side deposited QD-Py/graphene monolayers (ground-state sample absorption at the excitation wavelength: $A_{400\ nm} = 0.11$). (b) Comparison between the kinetics, recorded at the B_1 and B_4 bands, of pyridine-coated QDs deposited on graphene and on bare glass. For visualization of the sub-picosecond dynamics, the early time-scale (i.e., for $t \leq 2$ ps) was extended. For the graphene samples multiexponential data fits of the bleach recovery yielded: at 625 nm, $\tau_1 = 19\pm3$ ps ($\alpha_1 = -0.49$), $\tau_2 = 270\pm50$ ps ($\alpha_2 = -0.42$), and an offset $\alpha_\infty = -0.09$; and at 515 nm, $\tau_1 = 260\pm60$ fs ($\alpha_1 = -0.44$), $\tau_2 = 3.9\pm1.2$ ps ($\alpha_2 = -0.23$), $\tau_3 = 60\pm11$ ps ($\alpha_3 = -0.27$), and $\alpha_\infty = -0.06$ ($\lambda_{pump} = 400$ nm, 1.5 μJ per pulse, 38-fs pulse width of the fundamental at 800 nm.)

2.2.2.4 Photoelectric Properties of The Hybrid Films

To examine if the observed PL quenching and the accelerated bleach recovery of the Py-coated QDs deposited on graphene were a result of photoinduced electron transfer from the CdSe to the carbon allotrope, we fabricated field effect transistor (FET) devices incorporating QD-Py/graphene hybrid films (Scheme 2.3). Using CVD, we patterned single-sheet graphene on p-doped silicon wafer covered with thin insulating layer of SiO_2. Gold strips formed source and drain contacts, and the graphene with the isolated Si substrate formed the gate (Scheme 2.3).

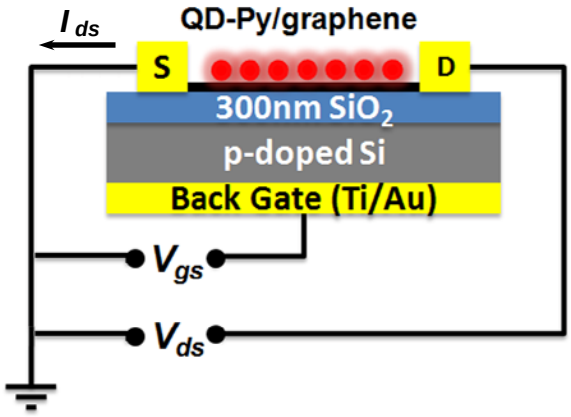

Scheme 2.3 Field effect transistor (FET) with hybrid film deposited on the insulating SiO_2 layer over the gate, and providing electrical contact between the source (S) and the drain (D).

Due to this lack of continuous network (Figure 2.12d), the QD-Py layer did not provide a direct electrical contact between the source and the drain, as evident from the lack of detectible conductivity in the FET devices that did not contain graphene. Concurrently, the carrier mobility that we estimated for single-sheet graphene from the FET devices without QDs was 1,500 $cm^2\ V^{-1}\ s^{-1}$, which was at the lower end of reported values for charge mobility in CVD-grown graphene of about 1,000 to 6,000 $cm^2\ V^{-1}\ s^{-1}$.[116-117] Since the charge mobility in the carbon allotrope was considerably higher than that of the broken QD network, we concluded that the single-sheet graphene (rather than the QD layer) was the principal carrier-transporting medium for the FET devices.

Upon illumination, the conductivity of the QD-Py/graphene hybrid films increased, as evident from the increase in the slope of the curves showing the effect of the applied drain-source voltage, V_{ds}, on the measured current, I_{ds} (Figure 2.16a). Namely, illumination of the QD-Py nanoparticles (that were the principal light absorber in the

film) increased the number of charge carriers in the graphene phase (that provided the electrical contact between the drain and the source), which was consistent with photoinduced charge transfer (i.e., transfer of electrons and/or holes) from the QDs to the carbon allotrope. In addition, the observed linearity in the current dependence on the voltage demonstrated metallic characteristics of the single-sheet graphene film.

Concurrently, the curves representing the dependence of I_{ds} on the applied gate voltage, V_{gs}, revealed n-doping of the graphene upon photoexcitation of the QDs. The illumination caused a negative shift in the Dirac point, i.e., in the minimum of I_{ds} vs. V_{gs} at constant V_{ds} (Figure 2.16b), which was indicative of n-doping of the conductive media.[12] Because the graphene, and not the QD layer, acted as a carrier channel in the FET devices, this light-induced n-doping of the conducting media was an indication of injection of electrons from the QDs into the carbon allotrope. A collection of positive charges in the QD layer, i.e., positive front gating that opposes the potential of the back gate, would also cause a negative shift in the $I_{ds}/V_{back\ gate}$ Dirac point.[118-119] Both phenomena that could lead to the observed negative shift were consistent with prevalent photoinduced electron transfer from the CdSe to the graphene phase.

The kinetics of photoswitching of the FET devices provided evidence for long-lived photoinduced charging of the QD-Py/graphene films (Figure 2.16c). Turning on the illumination of the QD films caused an increase in I_{ds}, which reached saturation within a few seconds, $\tau \approx 4$ s (Figure 2.16c). Although the rate constants of the photoinduced charge transfer exceeded 10^{10} s^{-1}, as estimated from the time-resolved spectroscopy studies, the kinetics of this I_{ds} jump represented the attainment of steady state between the

light-driven influx of n-carrier into the graphene phase, the loss of the n-carriers via back charge transfer or trapping, and the in- and out-transport of the charge carriers through the source and drain terminals. Conversely, turning off the illumination did not cause a fast drop in I_{ds}. Instead, the measured current gradually decreased with a time constant of about 140±30 s (Figure 2.16c), which was in agreement with previous reports on photoswitching mediated by hybrid materials of pyridine-coated CdSe QDs and carbon nanotubes.[90] This finding indicated that minutes after ceasing the illumination, photogenerated charge carriers still lingered in the film that was consistent with the energy-storage capabilities of graphene hybrid materials.[120-122]

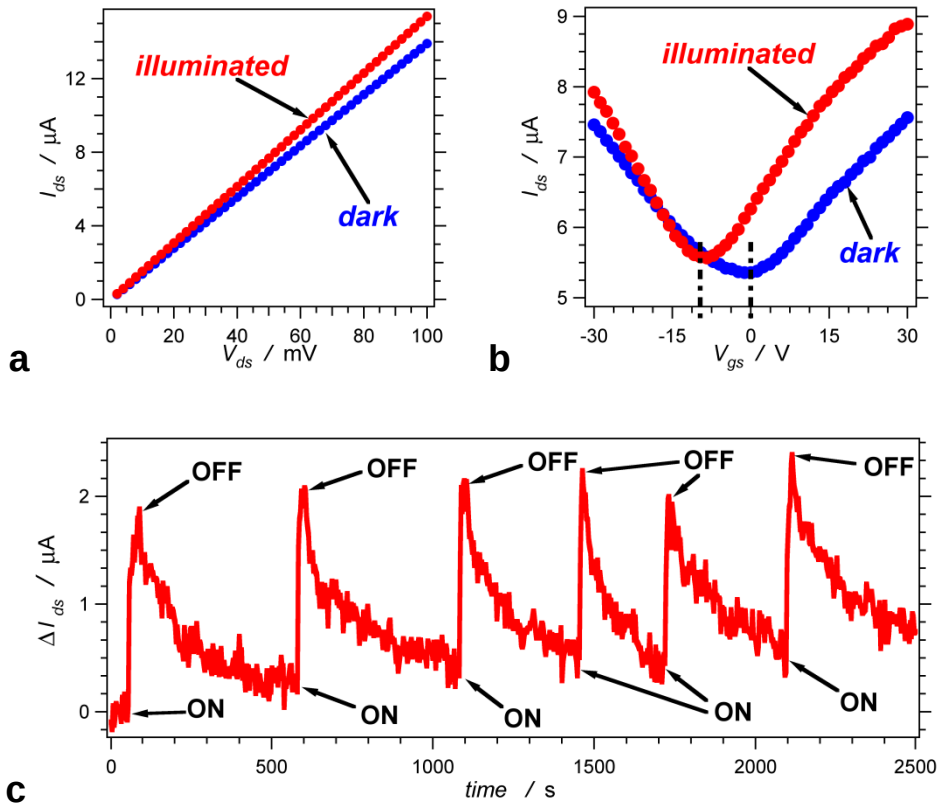

Figure 2.16 Current-voltage (*I-V*) characteristics of field-effect transistor FET devices comprising QD-Py/graphene films under illumination (λ = 365 nm, 0.2 W cm^{-2}) and under dark conditions. (a) Representative drain-source current-voltage lines for a FET device with the illumination on and off (V_{gs} = 0 V). (b) Representative *I-V* curves showing the dependence of the drain-source current, I_{ds}, on the gate voltage, V_{gs}, with the illumination on and off (V_{ds} = 0.1 V). (c) Photoinduced changes in the drain-source current of a FET device (V_{ds} = 0.1 V; V_{gs} = 0 V). The illumination on/off cycle involved turning the light on for 30 s, and keeping it off for 4 to 8 minute. The time constant of the current increase upon turning the illumination on was 4.3±1.6 s; and the time constant of current decrease upon turning the illumination off was 140±30 s.

2.2.2.5 Photoinduced Charge Transfer Between Cdse QDs and Graphene

The reported work function of graphite is 4.5–5.0 eV,[123-125] placing its Fermi level between the valence and the conduction band of the CdSe QDs (Scheme 2.2).[86] Therefore, the photoexcited QDs can act as electron donors and as electron acceptors. Concurrently, the QDs can also act as energy donors, transferring their excitons into the

graphene phase via a resonance (Förster-like) or an electron-exchange (Dexter) mechanism.[87-88] In fact, Brus *et al.* have reported efficient resonance energy transfer from CdSe QDs (λ_{em} = 655 nm) to single-sheet graphene with time constants of about 250 ps.[85] We observed similar dynamics for the deactivation of the CdSe excited state in the QD-Py/graphene films as illustrated by the principal emission decay time constant, τ_1 = 180±30 ps (Figure 2.13c), and the slow component of TA B_1 recovery, τ_2 = 270±50 ps (Figure 2.15b). Despite the similarities between our kinetic findings and the previously reported energy-transfer dynamics, we do not have evidence to prove or disprove whether this emission and TA dynamics was a result of energy-transfer processes mediated in the QD-Py/graphene films. Nevertheless, the photoinduced n-doping of the graphene (Figure 2.16b) indicated that the Py-coated CdSe QDs were preferentially electron donors.

The considerable increase in the rates of the TA bleach induced by the carbon allotrope (Figure 2.15b) was consistent with electron transfer from the CdSe to the graphene phase since the B_i bands were associated with populating with electrons of the low-lying QSLs in the chalcogenide conduction band.[113,115] Concurrently, the evidence for transients of oxidized pyridine, $Py^{+\bullet}$, suggested for oppositely directed photoinduced electron transfer, i.e., from the ligands to the vacated QSLs in the CdSe valence band. The latter process would place holes on the aromatic moieties between the chalcogenide and the carbon allotrope, considerably shortening the paths of electron transfer from the graphene to the QD-Py. Nevertheless, the photoelectrical findings indicated that the photoinduced electron transfer from the CdSe QDs to the graphene was faster than the oppositely directed charge transduction.

As previously indicated, the reorganization energy of the graphene phase provides the kinetic control responsible for the observed directionality of the photoinduced electron transfer from the QDs to the graphene.[86] Electrochemically we estimated that the lowest energy level of the conduction band of the QDs was about –3.8 eV from vacuum level, placing the valence band at about –5.8 eV. Therefore, the graphene Fermi level, which for the non-doped allotrope crosses its Dirac points, was about 0.8 to 1.3 eV above the valence band of the CdSe nanocrystals (or the highest occupied molecular orbital, HOMO, of the pyridine ligands). Electron transfer from graphene to the valence band of CdSe or to the HOMO of pyridine, thus, requires coupling with a large-momentum phonon for generating a hole significantly offset in energy from the Dirac points.[86,126] Hence, the electron transfer from graphene to the vacated HOMOs of the pyridines or QSLs in the valence band of the photoexcited CdSe requires significantly more energy dissipation than electron transfer from the conduction band of the CdSe QDs to the graphene.[86] This larger reorganization energy for the electron transfer to the photoexcited pyridine-coated CdSe makes the hole transfer from the QDs slower than the electron transfer from the QDs to the graphene, which was consistent with our observations of preferential photoinduced n-doping of the conducting media of the QD-Py/graphene films.

As previously discussed, the TA findings suggested three modes of photoinduced electron transfer from the pyridine-coated QDs to graphene: (1) a twenty-picosecond transfer of "relaxed" electrons from the lowest QSLs of the CdSe conduction band; (2) a sub-picosecond transfer of "hot" electrons, prior to their interband relaxation; and (3) a

direct photoexcitation to CdSe-graphene charge-transfer states. Meanwhile, the hole shift from the CdSe to the pyridine ligands (Figure 2.14d)[108] did not overcome the electron transfer from the QDs to the graphene. While reorganization energy would impede the hole transfer to the graphene phase, the accumulation of the holes in the pyridine ligands would polarize the surface of the QDs, i.e., generating electrets with the positive poles of their dipoles pointing to the exterior of the CdSe particles. Such polarization of the QD surfaces is still favorable for electron transfer from the CdSe phase.

2.2.2.6 Photoelectrochemical Cell

While the mono-layer QDs on graphene was achieved, the material should display good photovoltaic properties with all the advantages, such as appropriate band gap, high carrier concentration as conductor, high crystallinity and fast electron transfer.

To demonstrate the potential application of such hybrid material for solar cells, a photoelectrochemical cell (PEC) was constructed. PEC is one of the promising light harvesting devices for future energy development.[127] QD/graphene/ITO was used as a working electrode and Pt wire was used as a counter electrode. The photocurrent responses of the QD/graphene/ITO device are prompt, steady and reproducible during repeated on/off cycles of light illumination (Figure 2.17). The photo-response has similar effect with CNT/TiO_2 hybrid material.[46] 1-D characteristic of graphene endows it higher surface area which promotes a higher chance for charge transfer from 0-D materials. Compared with 2-D (CNT)/0-D (QD) hybrid structure, 1-D (graphene)/ 0-D (QD) hybrid structure facilitates faster electron transfer.[128] This fast response represents fast charge

transfer between QD and graphene which paves the way for developing a solar cell anode with higher efficiency.

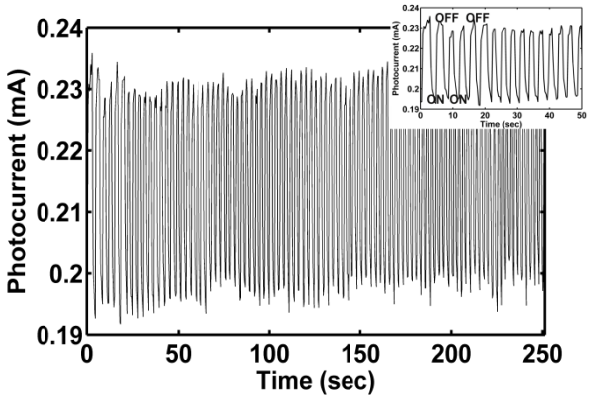

Figure 2.17 Fast short circuit photocurrent (I_{sc}) photo-response of QD/graphene/ITO devices under white light illumination in photoelectrochemical cell. The inset shows an enlarged view for a small portion of the photocurrent response curve. Input light power is 30 mW/cm^2.

Photocurrent generation curves are shown in Figure 2.18. Apparently, short circuit photocurrent density (I_{sc}) increased with light or UV illumination compared with dark condition. The I_{sc} could reach 450 μA/cm^2, which is much higher than previously reported CNT/QD hybrid material. The increase of UV illumination could reach 0.2 mA/cm^2, while it still reaches 0.12 mA/cm^2 with much lower power white light illumination. It is reported that a multilayer graphene/QD hybrid could reach higher I_{sc} due to larger electron transfer.[128] Here one layer of CVD graphene could get half of the maximum photocurrent density achieved with 8-layer reduced graphene/CdS[129] which demonstrates the better performance of current hybrid material. IPCE with UV lamp illumination is calculated as 3% which is comparable with CdS/SWCNT.[129] This relative low IPCE is reasonable for single layer hybrid. Even when the power of lamp is as low as

30mW, the I_{sc} could reach 78% of the UV illumination condition. With multilayer of QD/graphene hybrid, better transmission of light, higher IPCE is expected.

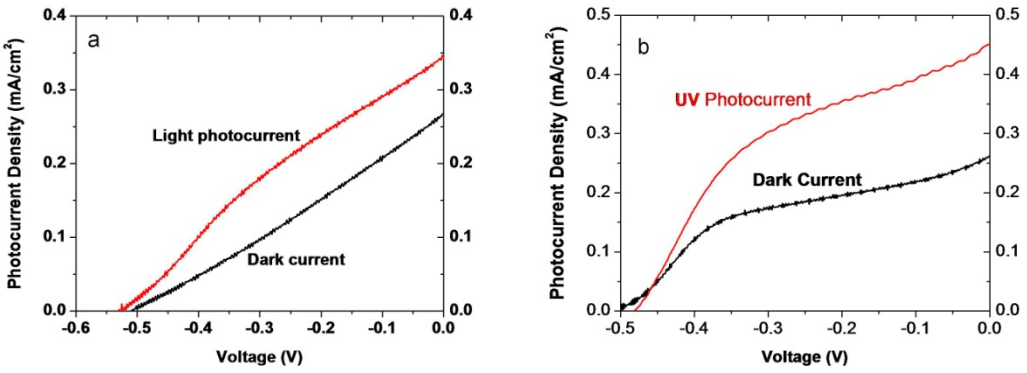

Figure 2.18 I-V characteristics of PEC with linear sweep voltammograms measured in three-electrode mode under white light (a) and 365nm UV (b) illumination. Electrolyte: 0.1M aqueous Na_2S; input light power: 30mW/cm^2 and UV power: 200mW/cm^2.

2.2.3 Conclusion

Probing the electronic transitions between quantized levels in CdSe QDs provided evidence for three modes of interfacial photoinduced electron transfer from the inorganic chalcogenide to the graphene phase. The concurrent hole transfer from the CdSe to the pyridine ligands did not provide light-induce p-doping of the graphene, indicating that positive charges remained in the organic coatings of the QDs. Analogous to proton-coupled electron transfer,[130-132] the simultaneously occurring hole shift and electron transfer may prove importance for efficient interfacial charge transduction between semiconducting and organic media, which further paves way to discover new materials for photovoltaic devices.

Quantum dots decorated graphene device exhibits excellent photo-switching property making it promising as a long wavelength sensitive photodetector. 1-D (graphene)/ 0-D (QD) hybrid structure facilitates electron transfer faster. When used as photoelectrochemical cell anode, this hybrid material displays both high photon to current conversion efficiency (IPCE) and fast photo-switch response.

2.3 Future Work

I. Universal doping of graphene with plasma.

In section 2.1, we presented controlling Dirac point shift via fluorine doping method. This work actually was finished on August 10th, 2010. At that time, this was the first original work for fluorination of graphene. Later, several reports on fluorine graphene were reported with different approaches including XeF_2, F_2. In contrast, plasma doping of graphene is simpler, less toxic and unsophisticated to be applied potentially for mass production.

(1) Fluorine graphene. (a) Mechanism study of reactive ion etching (RIE) CF_4 or CHF_3 plasma doping of graphene. Experiments should be conducted with different concentration and different fluorination time. Raman, FTIR and XPS should be applied to study the CF_x or F radicals with carbon atoms. High quality of single layer or multiple layer graphene should be used in the study. (b) Patterned fluorinated graphene for electronic devices. Metrology of graphene is an important area for systematically check the quality of graphene. Previously, with the fluorination graphene we have demonstrated the applicability of the confocal fluorescence quenching metrology method for detecting

defects of graphene. Thus the plasma doping will certainly provide more rooms for such studies including oxygen doping for defects. (c) Fluorinated nanoribbon graphene for p-type semiconductor. While nanoribbon could open bandgap of graphene, producing p or n type semiconductor is possible by functionalizing the edge of graphene nanoribbon. Since fluorine doping of graphene introduces electron withdrawing groups which will produce p-type semiconductors.

(2) Plasma doping of graphene with NH_3 or other gases. Since fluorine or hydrogen doping of graphene could be achieved with plasma, other gases could be also applied for such purpose which will introduce n-doping effect leading to n-type semiconductor. Furthermore, n-type nanoribbon could also be produced with such doping approach.

II. Semiconductor nanomaterials with graphene.

In section 2.2, QDs attached to graphene provides evidence that charge transfer could happen with such hybrid material which may leads to many potential applications.

(1) TiO_2 nanoparticles and graphene. Electron transfer from TiO_2 to graphene has been observed and applied for reducing graphene oxide. The combination provides chances for oxygen reduction reaction (ORR) or water splitting reaction.

(2) Functionalized core/shell nanoparticles and graphene. With core/shell structure, the stability is expected to improve and the combination will produce more stable devices for photodetector or photo-switch.

2.4 References

(1) K. S. Novoselov, A. K. Geim, S. V. Morozov, D. Jiang, Y. Zhang, S. V. Dubonos, I. V. Grigorieva, A. A. Firsov,"*Electric field effect in atomically thin carbon films"* ***Science*** *2004*, *306*, 666.

(2) M. J. Allen, V. C. Tung, L. Gomez, Z. Xu, L. M. Chen, K. S. Nelson, C. W. Zhou, R. B. Kaner, Y. Yang,"*Soft Transfer Printing of Chemically Converted Graphene"* ***Advanced Materials*** *2009*, *21*, 2098.

(3) E. J. H. Lee, K. Balasubramanian, R. T. Weitz, M. Burghard, K. Kern,"*Contact and edge effects in graphene devices"* ***Nature Nanotechnology*** *2008*, *3*, 486.

(4) F. Wang, Y. B. Zhang, C. S. Tian, C. Girit, A. Zettl, M. Crommie, Y. R. Shen,"*Gate-variable optical transitions in graphene"* ***Science*** *2008*, *320*, 206.

(5) X. L. Li, X. R. Wang, L. Zhang, S. W. Lee, H. J. Dai,"*Chemically derived, ultrasmooth graphene nanoribbon semiconductors"* ***Science*** *2008*, *319*, 1229.

(6) X. T. Jia, M. Hofmann, V. Meunier, B. G. Sumpter, J. Campos-Delgado, J. M. Romo-Herrera, H. B. Son, Y. P. Hsieh, A. Reina, J. Kong, M. Terrones, M. S. Dresselhaus,"*Controlled Formation of Sharp Zigzag and Armchair Edges in Graphitic Nanoribbons"* ***Science*** *2009*, *323*, 1701.

(7) L. Y. Jiao, L. Zhang, X. R. Wang, G. Diankov, H. J. Dai,"*Narrow graphene nanoribbons from carbon nanotubes"* ***Nature*** *2009*, *458*, 877.

(8) J. W. Bai, X. Zhong, S. Jiang, Y. Huang, X. F. Duan,"*Graphene nanomesh"* ***Nature Nanotechnology*** *2010*, *5*, 190.

(9) T. Ohta, A. Bostwick, T. Seyller, K. Horn, E. Rotenberg,"*Controlling the electronic structure of bilayer graphene"* ***Science*** *2006*, *313*, 951.

(10) X. R. Wang, X. L. Li, L. Zhang, Y. Yoon, P. K. Weber, H. L. Wang, J. Guo, H. J. Dai,"*N-Doping of Graphene Through Electrothermal Reactions with Ammonia"* ***Science*** *2009*, *324*, 768.

(11) S. Y. Zhou, G. H. Gweon, A. V. Fedorov, P. N. First, W. A. De Heer, D. H. Lee, F. Guinea, A. H. C. Neto, A. Lanzara,"*Substrate-induced bandgap opening in epitaxial graphene"* ***Nature Materials*** *2007*, *6*, 770.

(12) J. H. Chen, C. Jang, S. Adam, M. S. Fuhrer, E. D. Williams, M. Ishigami,"*Charged-impurity scattering in graphene"* ***Nature Physics*** *2008*, *4*, 377.

(13) H. Lee, J. Ihm, M. L. Cohen, S. G. Louie,"*Calcium-Decorated Graphene-Based Nanostructures for Hydrogen Storage"* ***Nano Letters*** *2010*, *10*, 793.

(14) I. Gierz, C. Riedl, U. Starke, C. R. Ast, K. Kern,"*Atomic Hole Doping of Graphene"* ***Nano Letters*** *2008*, *8*, 4603.

(15) X. C. Dong, D. L. Fu, W. J. Fang, Y. M. Shi, P. Chen, L. J. Li,"*Doping Single-Layer Graphene with Aromatic Molecules"* ***Small*** *2009*, *5*, 1422.

(16) D. B. Farmer, R. Golizadeh-Mojarad, V. Perebeinos, Y. M. Lin, G. S. Tulevski, J. C. Tsang, P. Avouris,"*Chemical Doping and Electron-Hole Conduction Asymmetry in Graphene Devices"* ***Nano Letters*** *2009*, *9*, 388.

(17) L. S. Panchokarla, K. S. Subrahmanyam, S. K. Saha, A. Govindaraj, H. R. Krishnamurthy, U. V. Waghmare, C. N. R. Rao,"*Synthesis, Structure, and*

Properties of Boron- and Nitrogen-Doped Graphene" ***Advanced Materials*** *2009*, *21*, 4726.

(18) S. S. Yu, W. T. Zheng, Q. Jiang,"*Electronic Properties of Nitrogen-/Boron-Doped Graphene Nanoribbons With Armchair Edges"* ***Ieee Transactions on Nanotechnology*** *2010*, *9*, 78.

(19) D. C. Wei, Y. Q. Liu, Y. Wang, H. L. Zhang, L. P. Huang, G. Yu,"*Synthesis of N-Doped Graphene by Chemical Vapor Deposition and Its Electrical Properties"* ***Nano Letters*** *2009*, *9*, 1752.

(20) I. V. Lightcap, T. H. Kosel, P. V. Kamat,"*Anchoring Semiconductor and Metal Nanoparticles on a Two-Dimensional Catalyst Mat. Storing and Shuttling Electrons with Reduced Graphene Oxide"* ***Nano Letters*** *2010*, *10*, 577.

(21) E. Bekyarova, M. E. Itkis, P. Ramesh, C. Berger, M. Sprinkle, W. A. De Heer, R. C. Haddon,"*Chemical Modification of Epitaxial Graphene: Spontaneous Grafting of Aryl Groups"* ***Journal of the American Chemical Society*** *2009*, *131*, 1336.

(22) Q. M. Yan, B. Huang, J. Yu, F. W. Zheng, J. Zang, J. Wu, B. L. Gu, F. Liu, W. H. Duan,"*Intrinsic current-voltage characteristics of graphene nanoribbon transistors and effect of edge doping"* ***Nano Letters*** *2007*, *7*, 1469.

(23) B. J. Kim, H. Jang, S. K. Lee, B. H. Hong, J. H. Ahn, J. H. Cho,"*High-Performance Flexible Graphene Field Effect Transistors with Ion Gel Gate Dielectrics"* ***Nano letters*** *2010*, *10*.

(24) C. Attaccalite, L. Wirtz, M. Lazzeri, F. Mauri, A. Rubio,"*Doped Graphene as Tunable Electron-Phonon Coupling Material"* ***Nano Letters*** *2010*, *10*, 1172.

(25) H. Otsuka, Y. Nagasaki, K. Kataoka,"*Self-assembly of poly(ethylene glycol)-based block copolymers for biomedical applications"* ***Current Opinion in Colloid & Interface Science*** *2001*, *6*, 3.

(26) Y. Lin, A. Boker, J. B. He, K. Sill, H. Q. Xiang, C. Abetz, X. F. Li, J. Wang, T. Emrick, S. Long, Q. Wang, A. Balazs, T. P. Russell,"*Self-directed self-assembly of nanoparticle/copolymer mixtures"* ***Nature*** *2005*, *434*, 55.

(27) Y. Ohno, K. Maehashi, Y. Yamashiro, K. Matsumoto,"*Electrolyte-Gated Graphene Field-Effect Transistors for Detecting pH Protein Adsorption"* ***Nano Letters*** *2009*, *9*, 3318.

(28) X. C. Dong, Y. Shi, W. Huang, P. Chen, L. J. Li,"*Electrical Detection of DNA Hybridization with Single-Base Specificity Using Transistors Based on CVD-Grown Graphene Sheets"* ***Advanced Materials*** *2010*, *22*, 1.

(29) S.R. Guo, J. Lin, M. Penchev, E. Yengel, C.S. Ozkan, M. Ozkan,"*Label Free DNA Detection using Large Area Graphene Based FET Biosensors"* ***Journal of Nanoscience and Nanotechnology*** *2010*.

(30) F. Schedin, A. K. Geim, S. V. Morozov, E. W. Hill, P. Blake, M. I. Katsnelson, K. S. Novoselov,"*Detection of individual gas molecules adsorbed on graphene"* ***Nature Materials*** *2007*, *6*, 652.

(31) V. Dua, S. P. Surwade, S. Ammu, S. R. Agnihotra, S. Jain, K. E. Roberts, S. Park, R. S. Ruoff, S. K. Manohar,"*All-Organic Vapor Sensor Using Inkjet-Printed Reduced Graphene Oxide"* ***Angewandte Chemie-International Edition*** *2010*, *49*, 2154.

(32) Y. P. Dan, Y. Lu, N. J. Kybert, Z. T. Luo, A. T. C. Johnson,"*Intrinsic Response of Graphene Vapor Sensors"* ***Nano Letters*** *2009*, *9*, 1472.

(33) S. Park, J. Y. Wang, B. Kim, T. P. Russell,"*From nanorings to nanodots by patterning with block copolymers"* ***Nano Letters*** *2008*, *8*, 1667.

(34) Y. Xuan, J. Peng, L. Cui, H. F. Wang, B. Y. Li, Y. C. Han,"*Morphology development of ultrathin symmetric diblock copolymer film via solvent vapor treatment"* ***Macromolecules*** *2004*, *37*, 7301.

(35) S. H. Kim, M. J. Misner, T. Xu, M. Kimura, T. P. Russell,"*Highly oriented and ordered arrays from block copolymers via solvent evaporation"* ***Advanced Materials*** *2004*, *16*, 226.

(36) C. Lee, S. H. Kim, T. P. Russell,"*Controlling Orientation and Functionalization in Thin Films of Block Copolymers"* ***Macromolecular Rapid Communications*** *2009*, *30*, 1674.

(37) P. L. Levesque, S. S. Sabri, C. M. Aguirre, J. Guillemette, M. Siaj, P. Desjardins, T. Szkopek, R. Martel,"*Probing Charge Transfer at Surfaces Using Graphene Transistors"* ***Nano Letters***, *11*, 132.

(38) A. K. Geim, K. S. Novoselov,"*The rise of graphene"* ***Nature Materials*** *2007*, *6*, 183.

(39) T. Shirasaki, F. Moguet, L. Lozano, A. Tressaud, G. Nanse, E. Papirer,"*Fluorination of carbon blacks: an X-ray photoelectron spectroscopy study IV. Reactivity of different carbon blacks in CF4 radiofrequency plasma"* ***Carbon*** *1999*, *37*, 1891.

(40) S. B. Bon, L. Valentini, R. Verdejo, J. L. G. Fierro, L. Peponi, M. A. Lopez-Manchado, J. M. Kenny,"*Plasma Fluorination of Chemically Derived Graphene Sheets and Subsequent Modification With Butylamine"* ***Chemistry of Materials*** *2009*, *21*, 3433.

(41) W. Chen, S. Chen, D. C. Qi, X. Y. Gao, A. T. S. Wee,"*Surface transfer p-type doping of epitaxial graphene"* ***Journal of the American Chemical Society*** *2007*, *129*, 10418.

(42) I. V. Lightcap, P. V. Kamat,"*Fortification of CdSe Quantum Dots with Graphene Oxide. Excited State Interactions and Light Energy Conversion"* ***Journal of American Chemical Society*** *2012*, *134*, 7109.

(43) Q. Li, B. Guo, J. Yu, J. Ran, B. Zhang, H. Yan, J. R. Gong,"*Highly Efficient Visible-Light-Driven Photocatalytic Hydrogen Production of CdS-Cluster-Decorated Graphene Nanosheets"* ***Journal of American Chemical Society*** *2011*, *133*, 10878.

(44) P. K. Santra, P. V. Kamat,"*Mn-Doped Quantum Dot Sensitized Solar Cells: A Strategy to Boost Efficiency over 5%"* ***Journal of American Chemical Society*** *2012*, *134*, 2508.

(45) T. Dufaux, J. Boettcher, M. Burghard, K. Kern,"*Photocurrent distribution in graphene-CdS nanowire devices"* ***Small*** *2010*, *6*, 1868.

(46) C. X. Guo, H. B. Yang, Z. M. Sheng, Z. S. Lu, Q. L. Song, C. M. Li,"*Layered Graphene/Quantum Dots for Photovoltaic Devices"* ***Angewandte Chemie-International Edition*** *2010*, *49*, 3014.

(47) H. Bi, F.-Q. Huang, J. Liang, X.-M. Xie, M.-H. Jiang,"*Transparent Conductive Graphene Films Synthesized by Ambient Pressure Chemical Vapor Deposition Used as the Front Electrode of CdTe Solar Cells"* ***Advanced Materials*** *2011*, *23*, 3202.

(48) C.-L. Hsu, C.-T. Lin, J.-H. Huang, C.-W. Chu, K.-H. Wei, L.-J. Li,"*Layer-by-Layer Graphene/TCNQ Stacked Films as Conducting Anodes for Organic Solar Cells"* ***ACS Nano*** *2012*, in press.

(49) X. Geng, L. Niu, Z. Xing, R. Song, G. Liu, M. Sun, G. Cheng, H. Zhong, Z. Liu, Z. Zhang, L. Sun, H. Xu, L. Lu, L. Liu,"*Aqueous-Processable Noncovalent Chemically Converted Graphene-Quantum Dot Composites for Flexible and Transparent Optoelectronic Films"* ***Advanced Materials*** *2010*, *22*, 638.

(50) G. Eda, M. Chhowalla,"*Chemically Derived Graphene Oxide: Towards Large-Area Thin-Film Electronics and Optoelectronics"* ***Advanced Materials*** *2010*, *22*, 2392.

(51) A. Gray, M. Balooch, S. Allegret, S. De Gendt, W.-E. Wang,"*Optical detection and characterization of graphene by broadband spectrophotometry"* ***Journal of Applied Physics*** *2008*, *104*, 053109/1.

(52) I. Jung, M. Vaupel, M. Pelton, R. Piner, D. A. Dikin, S. Stankovich, J. An, R. S. Ruoff,"*Characterization of Thermally Reduced Graphene Oxide by Imaging Ellipsometry"* ***Journal of Physical Chemistry C*** *2008*, *112*, 8499.

(53) C. Lee, J. Y. Kim, S. Bae, K. S. Kim, B. H. Hong, E. J. Choi,"*Optical response of large scale single layer graphene"* ***Applied Physics Letters*** *2011*, *98*, 071905/1.

(54) B. Gao, G. Hartland, T. Fang, M. Kelly, D. Jena, H. Xing, L. Huang,"*Studies of Intrinsic Hot Phonon Dynamics in Suspended Graphene by Transient Absorption Microscopy"* ***Nano Letters*** *2011*, *11*, 3184.

(55) L. Huang, B. Gao, G. Hartland, M. Kelly, H. Xing,"*Ultrafast relaxation of hot optical phonons in monolayer and multilayer graphene on different substrates"* ***Surf. Sci.*** *2011*, *605*, 1657.

(56) A. P. Alivisatos, I. Gur, N. A. Fromer, C. P. Chen, A. G. Kanaras,"*Hybrid solar cells with prescribed nanoscale morphologies based on hyperbranched semiconductor nanocrystals"* ***Nano Letters*** *2007*, *7*, 409.

(57) X. G. Peng,"*Band Gap and Composition Engineering on a Nanocrystal (BCEN) in Solution"* ***Accounts of Chemical Research*** *2010*, *43*, 1387.

(58) R. Loef, A. J. Houtepen, E. Talgorn, J. Schoonman, A. Goossens,"*Study of Electronic Defects in CdSe Quantum Dots and Their Involvement in Quantum Dot Solar Cells"* ***Nano Letters*** *2009*, *9*, 856.

(59) P. V. Kamat,"*Quantum Dot Solar Cells. Semiconductor Nanocrystals as Light Harvesters"* ***Journal of Physical Chemistry C*** *2008*, *112*, 18737.

(60) Prashant V. Kamat,"*Boosting the Efficiency of Quantum Dot Sensitized Solar Cells through Modulation of Interfacial Charge Transfer"* ***Accounts of Chemical Research*** *2012*, in press.

(61) Omar K. Farha, Christopher E. Wilmer, Ibrahim Eryazici, Brad G. Hauser, Philip A. Parilla, Kevin O'neill, Amy A. Sarjeant, Sonbinh T. Nguyen, Randall Q. Snurr, Joseph T. Hupp,"*Designing Higher Surface Area Metal-Organic Frameworks:*

Are Triple Bonds Better Than Phenyls?" ***Journal of American Chemical Society*** *2012*, in press.

(62) H.-J. Son, X. Wang, C. Prasittichai, N. C. Jeong, T. Aaltonen, R. G. Gordon, J. T. Hupp,"*Glass-Encapsulated Light Harvesters: More Efficient Dye-Sensitized Solar Cells by Deposition of Self-Aligned, Conformal, and Self-Limited Silica Layers"* ***Journal of American Chemical Society*** *2012*, *134*, 9537.

(63) P. Diao, Z. Liu,"*Vertically Aligned Single-Walled Carbon Nanotubes by Chemical Assembly - Methodology, Properties, and Applications"* ***Adv. Mater.*** *2010*, *22*, 1430.

(64) N. R. De Tacconi, W. Chanmanee, K. Rajeshwar, J. Rochford, E. Galoppini,"*Photoelectrochemical Behavior of Polychelate Porphyrin Chromophores and Titanium Dioxide Nanotube Arrays for Dye-Sensitized Solar Cells"* ***Journal of Physical Chemistry C*** *2009*, *113*, 2996.

(65) A. Kongkanand, K. Tvrdy, K. Takechi, M. Kuno, P. V. Kamat,"*Quantum Dot Solar Cells. Tuning Photoresponse through Size and Shape Control of CdSe-TiO2 Architecture"* ***Journal of American Chemical Society*** *2008*, *130*, 4007.

(66) T. Hasobe, S. Fukuzumi, P. V. Kamat,"*Stacked-cup carbon nanotubes for photoelectrochemical solar cells"* ***Angewante Chemie International Edition*** *2006*, *45*, 755.

(67) S. Chaudhary, H. Lu, A. M. Mueller, C. J. Bardeen, M. Ozkan,"*Hierarchical Placement and Associated Optoelectronic Impact of Carbon Nanotubes in Polymer-Fullerene Solar Cells"* ***Nano Letters*** *2007*, *7*, 1973.

(68) S. Ren, M. Bernardi, R. R. Lunt, V. Bulovic, J. C. Grossman, S. Gradecak,"*Toward Efficient Carbon Nanotube/P3HT Solar Cells: Active Layer Morphology, Electrical, and Optical Properties"* ***Nano Letters*** *2011*, *11*, 5316.

(69) Z. Y. Wang, S. N. Liu, P. Wu, C. X. Cai,"*Detection of Glucose Based on Direct Electron Transfer Reaction of Glucose Oxidase Immobilized on Highly Ordered Polyaniline Nanotubes"* ***Analytical Chemistry*** *2009*, *81*, 1638.

(70) G. M. A. Rahman, D. M. Guldi, R. Cagnoli, A. Mucci, L. Schenetti, L. Vaccari, M. Prato,"*Combining Single Wall Carbon Nanotubes and Photoactive Polymers for Photoconversion"* ***Journal of American Chemical Society*** *2005*, *127*, 10051.

(71) K. S. Novoselov, A. K. Geim, S. V. Morozov, D. Jiang, Y. Zhang, S. V. Dubonos, I. V. Grigorieva, A. A. Firsov,"*Electric field effect in atomically thin carbon films"* ***Science*** *2004*, *306*, 666.

(72) F. Bonaccorso, Z. Sun, T. Hasan, A. C. Ferrari,"*Graphene photonics and optoelectronics"* ***Nature Photonics*** *2010*, *4*, 611.

(73) X. Wan, Y. Huang, Y. Chen,"*Focusing on energy and optoelectronic applications: A journey for graphene and graphene oxide at large scale"* ***Accounts of Chemical Research*** *2012*, *45*, 598.

(74) A. N. Cao, Z. Liu, S. S. Chu, M. H. Wu, Z. M. Ye, Z. W. Cai, Y. L. Chang, S. F. Wang, Q. H. Gong, Y. F. Liu,"*A Facile One-step Method to Produce Graphene-CdS Quantum Dot Nanocomposites as Promising Optoelectronic Materials"* ***Advanced Materials*** *2010*, *22*, 103.

(75) K. P. Loh, Q. L. Bao, G. Eda, M. Chhowalla,"*Graphene oxide as a chemically tunable platform for optical applications"* ***Nature Chemistry*** *2010*, *2*, 1015.

(76) M. J. Allen, J. D. Fowler, V. C. Tung, Y. Yang, B. H. Weiller, R. B. Kaner,"*Temperature dependent Raman spectroscopy of chemically derived graphene"* ***Applied Physics Letters*** *2008*, *93*.

(77) L. J. Cote, R. Cruz-Silva, J. X. Huang,"*Flash Reduction and Patterning of Graphite Oxide and Its Polymer Composite"* ***Journal of the American Chemical Society*** *2009*, *131*, 11027.

(78) H. Yamaguchi, G. Eda, C. Mattevi, H. Kim, M. Chhowalla,"*Highly Uniform 300 mm Wafer-Scale Deposition of Single and Multilayered Chemically Derived Graphene Thin Films"* ***Acs Nano*** *2010*, *4*, 524.

(79) S. Bae, H. Kim, Y. Lee, X. F. Xu, J. S. Park, Y. Zheng, J. Balakrishnan, T. Lei, H. R. Kim, Y. I. Song, Y. J. Kim, K. S. Kim, B. Ozyilmaz, J. H. Ahn, B. H. Hong, S. Iijima,"*Roll-to-roll production of 30-inch graphene films for transparent electrodes"* ***Nature Nanotechnology*** *2010*, *5*, 574.

(80) X. M. Feng, J. Q. Hu, X. H. Chen, J. S. Xie, Y. Y. Liu,"*Synthesis and electron transfer property of sulfhydryl-containing multi-walled carbon nanotube/gold nanoparticle heterojunctions"* ***Journal of Physics D-Applied Physics*** *2009*, *42*.

(81) D. A. C. Brownson, R. V. Gorbachev, S. J. Haigh, C. E. Banks,"*CVD graphene vs. highly ordered pyrolytic graphite for use in electroanalytical sensing"* ***Analyst*** *2012*, *137*, 833.

(82) S. Guo, M. Ghazinejad, X. Qin, H. Sun, W. Wang, F. Zaera, M. Ozkan, C. S. Ozkan,"*Tuning Electron Transport in Graphene-Based Field-Effect Devices using Block Co-polymers"* ***Small*** *2012*, *8*, 1073.

(83) J. R. Kyle, A. Guvenc, W. Wang, M. Ghazinejad, J. Lin, S. Guo, C. S. Ozkan, M. Ozkan,"*Centimeter-Scale High-Resolution Metrology of Entire CVD-Grown Graphene Sheets"* ***Small*** *2011*, *7*, 2599.

(84) K. S. Kim, Y. Zhao, H. Jang, S. Y. Lee, J. M. Kim, K. S. Kim, J.-H. Ahn, P. Kim, J.-Y. Choi, B. H. Hong,"*Large-scale pattern growth of graphene films for stretchable transparent electrodes"* ***Nature*** *2009*, *457*, 706.

(85) Z. Y. Chen, S. Berciaud, C. Nuckolls, T. F. Heinz, L. E. Brus,"*Energy Transfer from Individual Semiconductor Nanocrystals to Graphene"* ***Acs Nano*** *2010*, *4*, 2964.

(86) A. V. Klekachev, M. Cantoro, M. H. Van Der Veen, A. L. Stesmans, M. M. Heyns, S. De Gendt,"*Electron accumulation in graphene by interaction with optically excited quantum dots"* ***Physica E-Low-Dimensional Systems & Nanostructures*** *2011*, *43*, 1046.

(87) T. Forster,"**Zwischenmolekulare Energiewanderung Und Fluoreszenz"* ***Annalen Der Physik*** *1948*, *2*, 55.

(88) D. L. Dexter,"*A Theory of Sensitized Luminescence in Solids"* ***Journal of Chemical Physics*** *1953*, *21*, 836.

(89) H. Lu, D. Bao, M. Penchev, M. Ghazinejad, V. I. Vullev, C. S. Ozkan, M. Ozkan,"*Pyridine-coated lead sulfide quantum dots for polymer hybrid photovoltaic devices"* ***Advanced Science Letters*** *2010*, *3*, 101.

(90) S. Jeong, H. C. Shim, S. Kim, C. S. Han,"*Efficient Electron Transfer in Functional Assemblies of Pyridine-Modified NQDs on SWCNTs"* ***ACS Nano*** *2010*, *4*, 324.

(91) D. Bao, B. Millare, W. Xia, B. G. Steyer, A. A. Gerasimenko, A. Ferreira, A. Contreras, V. I. Vullev,"*Electrochemical Oxidation of Ferrocene: A Strong Dependence on the Concentration of the Supporting Electrolyte for Nonpolar Solvents"* ***Journal of Physical Chemistry A*** *2009*, *113*, 1259.

(92) S. Trasatti,"*The Absolute Electrode Potential: an Explanatory Note (Recommendations 1986)"* ***Pure and Applied Chemistry*** *1986*, *58*, 955.

(93) J. Wan, M. S. Thomas, S. Guthrie, V. I. Vullev,"*Surface-bound proteins with preserved functionality"* ***Annual Biomedical Engineering*** *2009*, *37*, 1190.

(94) V. I. Klimov,"*Optical Nonlinearities and Ultrafast Carrier Dynamics in Semiconductor Nanocrystals"* ***The Journal of Physical Chemistry B*** *2000*, *104*, 6112.

(95) Q. W. Li, B. Q. Sun, I. A. Kinloch, D. Zhi, H. Sirringhaus, A. H. Windle,"*Enhanced self-assembly, of pyridine-capped CdSe nanocrystals on individual single-walled carbon nanotubes"* ***Chemistry of Materials*** *2006*, *18*, 164.

(96) B. H. Juarez, M. Meyns, A. Chanaewa, Y. X. Cai, C. Klinke, H. Weller,"*Carbon Supported CdSe Nanocrystals"* ***Journal of the American Chemical Society*** *2008*, *130*, 15282.

(97) C. G. Lu, A. Akey, W. Wang, I. P. Herman,"*Versatile Formation of CdSe Nanoparticle-Single Walled Carbon Nanotube Hybrid Structures"* ***Journal of the American Chemical Society*** *2009*, *131*, 3446.

(98) A. C. Carter, C. E. Bouldin, K. M. Kemner, M. I. Bell, J. C. Woicik, S. A. Majetich,"*Surface structure of cadmium selenide nanocrystallites"* ***Physical Review B*** *1997*, *55*, 13822.

(99) M. G. Berrettini, G. Braun, J. G. Hu, G. F. Strouse,"*NMR analysis of surfaces and interfaces in 2-nm CdSe"* ***Journal of the American Chemical Society*** *2004*, *126*, 7063.

(100) M. Egli, V. Tereshko, G. N. Mushudov, R. Sanishvili, X. Y. Liu, F. D. Lewis,"*Face-to-face and edge-to-face pi-pi interactions in a synthetic DNA hairpin with a stilbenediether linker"* ***Journal of the American Chemical Society*** *2003*, *125*, 10842.

(101) R. Meurisse, R. Brasseur, A. Thomas,"*Aromatic side-chain interactions in proteins. Near- and far-sequence His-X pairs"* ***Biochimica Et Biophysica Acta-Proteins and Proteomics*** *2003*, *1649*, 85.

(102) I. Ohno, M. Tomizawa, N. Miyazu, G. Kushibiki, K. Noda, Y. Hasebe, K. A. Durkin, T. Miyake, S. Kagabu,"*Structural features of phenoxycarbonylimino*

neonicotinoids acting at the insect nicotinic receptor" ***Bioorganic & Medicinal Chemistry Letters*** *2010*, *20*, 5933.

(103) J. Wan, A. Ferreira, W. Xia, C. H. Chow, K. Takechi, P. V. Kamat, G. Jones, V. I. Vullev,"*Solvent dependence of the charge-transfer properties of a quaterthiophene-anthraquinone dyad"* ***Journal of Photochemistry Photobiology, A*** *2008*, *197*, 364.

(104) A. J. Morris-Cohen, M. T. Frederick, L. C. Cass, E. A. Weiss,"*Simultaneous Determination of the Adsorption Constant and the Photoinduced Electron Transfer Rate for a Cds Quantum Dot–Viologen Complex"* ***Journal of the American Chemical Society*** *2011*, *133*, 10146.

(105) C. Burda, S. Link, M. Mohamed, M. El-Sayed,"*The relaxation pathways of CdSe nanoparticles monitored with femtosecond time-resolution from the visible to the IR: Assignment of the transient features by carrier quenching"* ***Journal of Physical Chemistry B*** *2001*, *105*, 12286.

(106) D. J. Norris, A. Sacra, C. B. Murray, M. G. Bawendi,"*Measurement of the Size-Dependent Hole Spectrum in CdSe Quantum Dots"* ***Physical Review Letters*** *1994*, *72*, 2612.

(107) A. I. Ekimov, F. Hache, M. C. Schanneklein, D. Ricard, C. Flytzanis, I. A. Kudryavtsev, T. V. Yazeva, A. V. Rodina, A. L. Efros,"*Absorption and Intensity-Dependent Photoluminescence Measurements on Cdse Quantum Dots: Assignment of the 1st Electronic-Transitions"* ***Journal of the Optical Society of America B-Optical Physics*** *1993*, *10*, 100.

(108) V. I. Klimov, A. A. Mikhailovsky, D. W. Mcbranch, C. A. Leatherdale, M. G. Bawendi,"*Mechanisms for intraband energy relaxation in semiconductor quantum dots: The role of electron-hole interactions"* ***Physical Review B*** *2000*, *61*, 13349.

(109) V. Chikan, D. F. Kelley,"*Carrier relaxation dynamics in GaSe nanoparticles"* ***Nano Letters*** *2002*, *2*, 1015.

(110) P. Guyot-Sionnest, M. Shim, C. Matranga, M. Hines,"*Intraband relaxation in CdSe quantum dots"* ***Physical Review B*** *1999*, *60*, R2181.

(111) K. Enomoto, J. A. Laverne, S. Seki, S. Tagawa,"*Formation and decay of the triplet excited state of pyridine"* ***Journal of Physical Chemistry A*** *2006*, *110*, 9874.

(112) G. R. Dey, D. B. Naik, P. Dwibedy, K. Kishore,"*Reactions of oxidizing radicals with 2- and 3-aminopyridines: a pulse radiolysis study"* ***Radiation Physics and Chemistry*** *2002*, *64*, 395.

(113) B. Farrow, P. V. Kamat,"*CdSe Quantum Dot Sensitized Solar Cells. Shuttling Electrons Through Stacked Carbon Nanocups"* ***Journal of American Chemical Society*** *2009*, *131*, 11124.

(114) A. Pandey, P. Guyot-Sionnest,"*Hot Electron Extraction From Colloidal Quantum Dots"* ***Journal of Physical Chemistry Letters*** *2010*, *1*, 45.

(115) C. Burda, T. C. Green, S. Link, M. A. El-Sayed,"*Electron shuttling across the interface of CdSe nanoparticles monitored by femtosecond laser spectroscopy"* ***Journal of Physical Chemistry B*** *1999*, *103*, 1783.

(116) G. X. Ni, Y. Zheng, S. Bae, H. R. Kim, A. Pachoud, Y. S. Kim, C. L. Tan, D. Im, J. H. Ahn, B. H. Hong, B. Ozyilmaz,"*Quasi-Periodic Nanoripples in Graphene Grown by Chemical Vapor Deposition and Its Impact on Charge Transport"* ***ACS Nano*** *2012*, *6*, 1158.

(117) J. Lee, L. Tao, Y. Hao, R. S. Ruoff, D. Akinwande,"*Embedded-gate graphene transistors for high-mobility detachable flexible nanoelectronics"* ***Applied Physics Letters*** *2012*, *100*.

(118) J. Lin, D. Teweldebrhan, K. Ashraf, G. Liu, X. Jing, Z. Yan, R. Li, M. Ozkan, R. K. Lake, A. A. Balandin, C. S. Ozkan,"*Gating of Single-Layer Graphene with Single-Stranded Deoxyribonucleic Acids"* ***Small*** *2010*, *6*, 1150.

(119) P. K. Ang, M. Jaiswal, C. H. Y. X. Lim, Y. Wang, J. Sankaran, A. Li, C. T. Lim, T. Wohland, O. Barbaros, K. P. Loh,"*A Bioelectronic Platform Using a Graphene-Lipid Bilayer Interface"* ***ACS Nano*** *2010*, *4*, 7387.

(120) J. G. Radich, P. V. Kamat,"*Origin of Reduced Graphene Oxide Enhancements in Electrochemical Energy Storage"* ***ACS Catal.*** *2012*, *2*, 807.

(121) R. K. Paul, M. Ghazinejad, M. Penchev, J. Lin, M. Ozkan, C. S. Ozkan,"*Synthesis of a Pillared Graphene Nanostructure: a Counterpart of Three-Dimensional Carbon Architectures"* ***Small*** *2010*, *6*, 2309.

(122) J. Lin, J. Zhong, D. Bao, J. Reiber-Kyle, W. Wang, V. Vullev, M. Ozkan, C. S. Ozkan,"*Supercapacitors based on pillared graphene nanostructures"* ***Journal of Nanoscience and Nanotechnology*** *2012*, *12*, 1770.

(123) J. O. Hwang, J. S. Park, D. S. Choi, J. Y. Kim, S. H. Lee, K. E. Lee, Y.-H. Kim, M. H. Song, S. Yoo, S. O. Kim,"*Workfunction-Tunable, N-Doped Reduced Graphene Transparent Electrodes for High-Performance Polymer Light-Emitting Diodes"* ***ACS Nano*** *2012*, *6*, 159.

(124) A. Misra, M. Waikar, A. Gour, H. Kalita, M. Khare, M. Aslam, A. Kottantharayil,"*Work function tuning and improved gate dielectric reliability with multilayer graphene as a gate electrode for metal oxide semiconductor field effect device applications"* ***Applied Physics Letters*** *2012*, *100*, 233506/1.

(125) Y.-J. Yu, Y. Zhao, S. Ryu, L. E. Brus, K. S. Kim, P. Kim,"*Tuning the graphene work function by electric field effect"* ***Nano Letters*** *2009*, *9*, 3430.

(126) A. H. Castro Neto, F. Guinea, N. M. R. Peres, K. S. Novoselov, A. K. Geim,"*The electronic properties of graphene"* ***Reviews of Modern Physics*** *2009*, *81*, 109.

(127) M. Gratzel,"*Photoelectrochemical cells"* ***Nature*** *2001*, *414*, 338.

(128) Y. D. Yang, L. T. Qu, L. M. Dai, T. S. Kang, M. Durstock,"*Electrophoresis coating of titanium dioxide on aligned carbon nanotubes for controlled syntheses of photoelectronic nanomaterials"* ***Advanced Materials*** *2007*, *19*, 1239.

(129) V. Huynh My Hang, J. Meyer Thomas,"*Proton-coupled electron transfer"* ***Chemical Review*** *2007*, *107*, 5004.

(130) J. M. Mayer,"*Proton-coupled electron transfer: A reaction chemist's view"* ***Annual Review Physical Chemistry*** *2004*, *55*, 363.

(131) R. I. Cukier, D. G. Nocera,"*Proton-coupled electron transfer"* ***Annual Review Physical Chemistry*** *1998*, *49*, 337.

Chapter 3

Graphene Field Effect Transistor for Biosensor and Chemical Sensor

3.1 Label Free DNA Detection using Large Area Graphene Based FET Biosensors

3.1.1 Introduction

The development of sensors capable of detecting DNA sequence variations has attracted a lot of attention in current studies. A number of different sensor configurations have been developed with impressively low detection limit and high sensitivity, such as surface plasmon resonance[1], electrochemical detection analysis[2-3], field effect transistors (FETs)[4-7], etc. Sensors based on FETs are promising to revolutionize bio-analytical research by offering the direct, real-time, highly specific, ultrasensitive, and label-free detection of the desired biomolecule[8-10]. Although there are plenty of achievements in carbon nanotube (CNT)[11-14] and nanowire based FET devices[2,8,15], there are still a lot of limitations including non-specific binding[10], instability of the device[16] and high cost that limits the future applications.

Recently graphene acting as channel material in FETs has been widely studied[18-21]. Graphene could be used to detect individual gas molecules due to high mobility and low electrical noise[22]. Graphene based FETs (GFET) exhibit their potential applications in pH sensors due to their dramatic conductance change with the electrolytic gating effect. The GFETs also have high sensitivity for biomolecule detection[23]. Most of the GFET sensors are based on graphene derived from exfoliation or chemical reduction, which has limited their wide scale application due to the high cost of manufacturing and the inability to

produce large area devices, or the low level of conductivity. As a result of these issues, CVD based graphene layers are becoming more attractive alternatives. Synthesis of large-area graphene films of the order of centimeters on copper substrates or via nickel catalyst layers using chemical vapor deposition have been reported recently[24-25]. These films can be easily transferred onto the desired substrates by a simple contact method, which provides more opportunities for extensive applications of graphene layers. In addition, many identical devices could be fabricated via conventional photolithographic patterning as opposed to electron beam lithography (EBL) which is a serial process rendering mass production impossible.

In this section, we report on large area graphene based FET biosensors for DNA detection which provide exceptional response to hybridization at ambient conditions. The low detection limit (LOD) is as low as 10^{-9} mol/L. The large surface area of the graphene layers endows the device's high sensitivity. And the low cost fabrication of the device via photolithography paves the way for future large scale applications.

3.1.2 Experimental

For the synthesis of large area graphene layers, typically a 250 nm thick Ni film is deposited on Si/SiO_2 substrates via electron beam evaporation (EBE). The Ni samples were then heated up to 900^{o}C in Ar/H_2 (600:500 sccm) atmosphere and annealed for 30 minutes in order to form a polycrystalline Ni film with large grain size[26]. After flowing methane (30sccm) mixed with Ar/H_2 at 900^{o}C under ambient pressures for 1 minute, the temperature was cooled down to 25^{o}C cooling rate 10 ^{o}C/s.[27] After that the Ni underneath was etched using a mild HCl aqueous solution (3%). The graphene film was finally

transferred onto a Si substrate with a 300nm thick thermally grown oxide for further characterization and experiments[28]. Next, the graphene layer was patterned and etched by oxygen plasma into rectangular shapes using photolithography and Reactive Ion Etching (RIE). And then the four terminal devices with Ti/Au (8nm × 80nm) electrodes (shown in the inset Figure 3a) were fabricated. Before conducting the electrical measurements, the devices were annealed under Ar/H_2 atmosphere at 400^{o}C for 1h to remove any potential contaminants such as photoresist residues on the graphene layer[29]. After that, the devices were immersed in a 2mg/ml 1-Pyrenebutanoic acid succinimidyl ester in anhydrous methanol solution for 2h to achieve the non-covalent functionalization. 1ml methanol solution was used to remove the extra PBASE on the device, which was then blow-dried with high purity nitrogen. The complementary DNA (c-DNA) hybridization process was carried out at room temperature for 4h to allow complete hybridization. Finally, the sample was rinsed with 2% SDS and DI water before electrical measurement. Several tools were used for characterization and measurements: Atomic force microscopy was conducted with (Multimode-5, Veeco) operated in the tapping mode using standard silicon cantilevers. Transmittance and UV-vis spectra were recorded with a Shimadzu UV-240 spectrophotometer at room temperature. I-V measurements were conducted at room temperature using Agilent 4155C. Raman spectra were taken using Renishaw micro-Raman spectrometer. The spectra were excited by the 488 nm visible laser. A Leica optical microscope with 50x objective was used to collect the backscattered light from the graphene samples. The spectra were recorded with the 1800 lines/mm grating.

3.1.3 Results and Discussion

Recently, Berry and co-workers [30] reported that graphene oxide (GO) modified with amine group could tether DNA strand and the hole density increased by 5.61×10^{12} cm^{-2}. However, the low conductivity of GO and non-linear I-V property may not be practical for the quantitative detection of DNA hybridization. Functionalization of the FET channel is crucial for achieving high fidelity sensing. Here, 1-pyrenebutanoic acid succinimidyl ester (PBASE) was used to functionalize the surface to keep the intrinsic high conductivity of graphene (Figure 3.1). This molecule could irreversibly attach to the side wall of carbon nanotubes via the π-π non-covalent bond interaction[31]. The absorption spectrum was taken to prove the functionalization process (Figure 3.1). The ester could easily react with primary amine groups which enable the probe DNA immobilize on graphene surface. Confocal laser scanning microscopy image was taken to prove that the probe DNA was successfully immobilized on graphene surface (Figure 1b). After incubating the probe DNA with PBASE modified graphene, it was washed with 2% SDS to get rid of the non-covalently bonded DNA. Then complementary DNA labeled with FAM was incubated with the probe DNA anchored device. Then it was washed again with 2% SDS solution before obtaining confocal scanning laser image. The green fluorescence observed in Figure 1b from FAM indicated that complementary DNA was successfully immobilized on graphene surface.

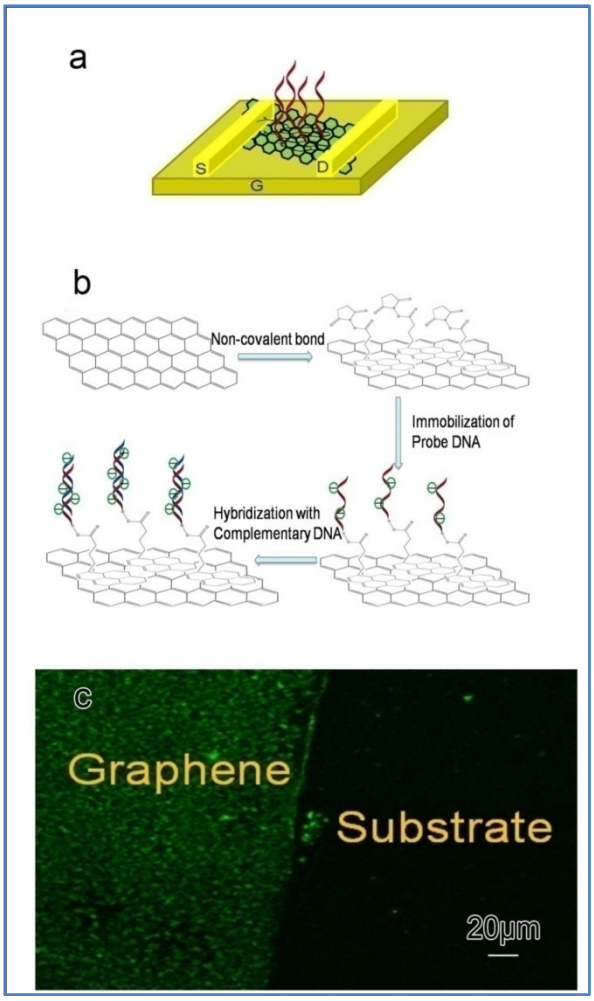

Figure 3.1 a) Schematic illustration of graphene device; b) Schematic illustration of the graphene sensor concept: modifying graphene with noncovalent bond and its binding of DNA strand. c) Confocal laser scanning microscope image of graphene after immobilization with c-DNA. The probe DNA sequence is: (5'-3')Amine-AAC-TGC-CAG-CCT-ATG-TCC-AA, complementary DNA sequence is: (5'-3')FAM-TTG-GAC-ATA-GGC-TGG-CAG-TT.

Transmittance and Raman spectroscopy were used to characterize the layers of graphene (Figure 3.2). Although the CVD grown graphene layers used in our experiment consists of a few layers with an average of 3 layers instead of a single layer, the high conductivity and large surface area ensure its high sensitivity. It can be seen from the

Figure 3.3, after functionalization with DNA, the surface of graphene becomes certain rough which further proves the successful immobilization of DNA.

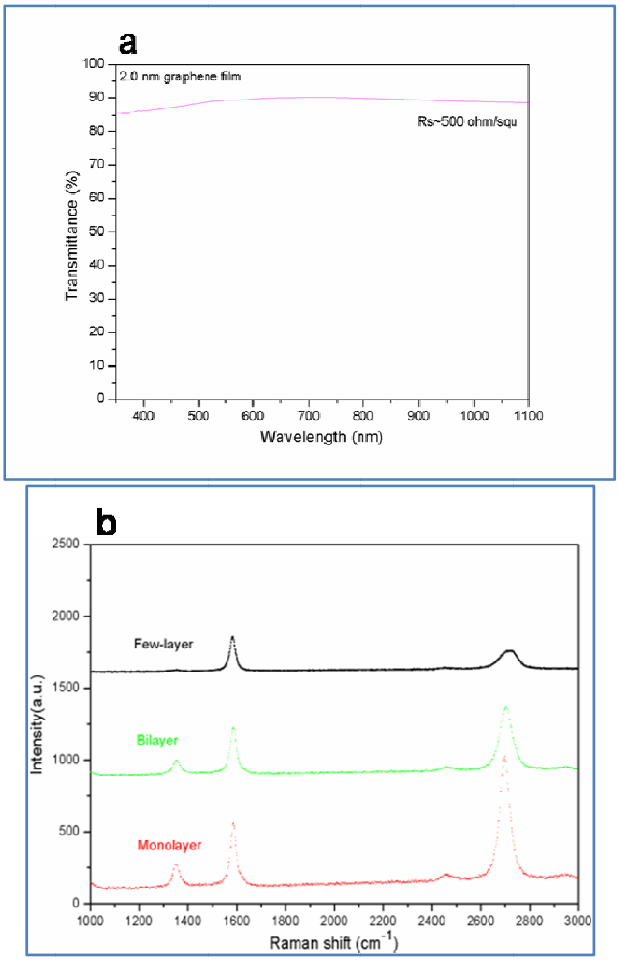

Figure 3.2 a) Transmittance of CVD graphenen film. The transmittance is 90% which prove the average layer of graphene is 3. b) Raman spectra of the synthesized CVD graphene.

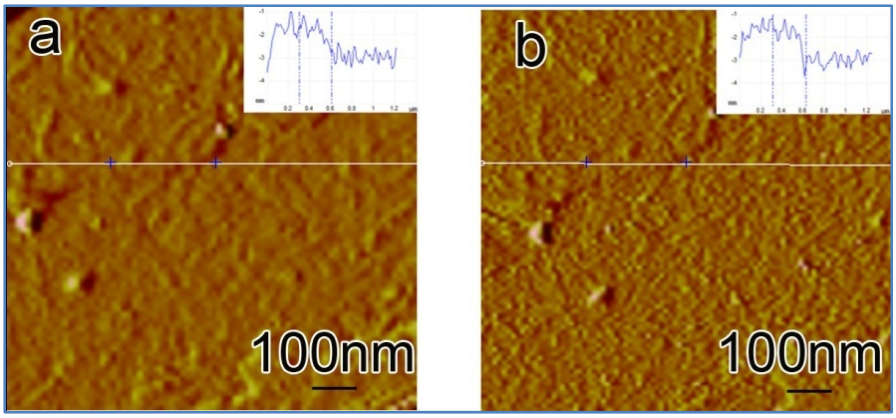

Figure 3.3 AFM images of graphene before (a) and after (c) probe DNA immobilization.

As illustrated in Figure 3.4a, typical current voltage (I-V) curves of the graphene layer were linear, suggesting the Ohmic nature of the electrical contacts. The results also rule out the existence of graphene/metal electrode contact issues (e.g. forming a Schottky barrier), which can hinder the device electrical conductivity and overall performance. Additionally, it shows higher conductivity than GO reduced graphene[30]. As calculated from the back-gate measurements by using the following equation (1), the electron and hole mobility are 290 $cm^2/V.s$ and 430 $cm^2/V.s$, respectively.

$$\mu = \left(\frac{\Delta I_{ds}}{\Delta V_{gs}} \right) / \left(\frac{C_g W V_{ds}}{L} \right) \qquad (1)$$

It can be seen from Figure 3b that the hole mobility of graphene layer kept almost constant during the whole process. Also the parallel shift of Dirac point (minimum conductance point) is noticed, which is caused by the DNA negative gating effect[32]. After functionalization of the device with PBASE, the conductivity increased by 45%. The increased hole density was calculated to be $7.45\times10^{12} cm^{-2}$ using the Drude model:

$$\Delta p = \left(R_2^{-1} - R_1^{-1} \right) / \left(\mu_p q (\frac{W}{L}) \right) \qquad (2)$$

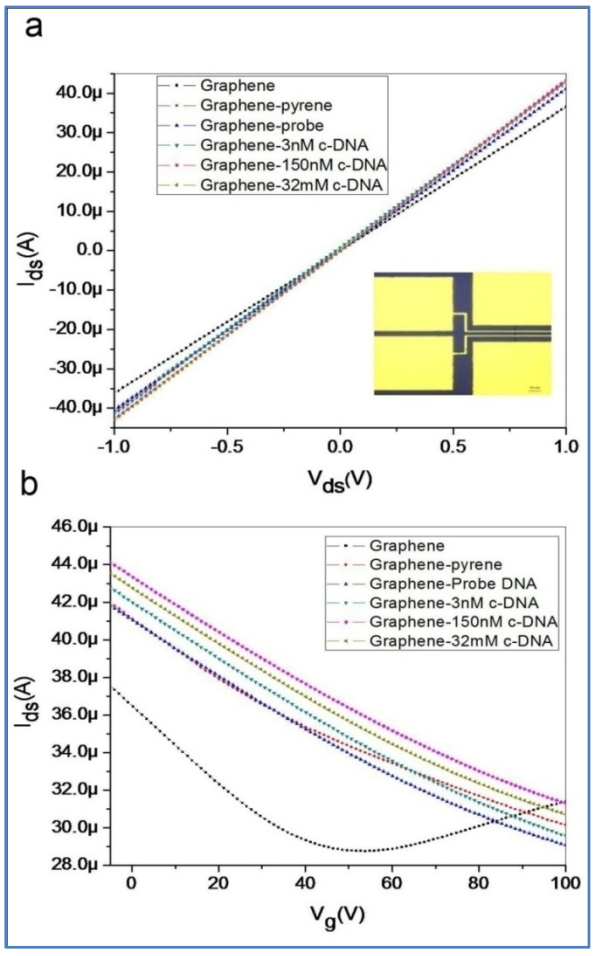

Figure 3.4 Typical I-V curve. (a) I_{ds}-V_{ds}, V_g=0, Inset: typical microscope image of the four point probe device. (b) I_{ds}-V_g, V_{ds}=1.0v. The probe DNA sequence is: (5'-3')Amine-AAC-TGC-CAG-CCT-ATG-TCC-AA, complementary DNA sequence is: (5'-3')-TTG-GAC-ATA-GGC-TGG-CAG-TT.

It has been reported that single strand DNA fragments could be used as a negative potential gating agents to increase the hole density of graphene.[32] FET sensors based on graphene layers to detect DNA hybridization have been reported very recently[33]. The non-covalent bonded DNA caused a "left" shift of the Dirac point with a decrease of the

conductivity. The shift was deemed as an electron transfer effect caused by non-electrostatic stacking interaction between DNA and graphene layer. While comparing the two contradictory results, the current results show that the negative charge effect is more pronounced than the electron transfer effect. Even in dry conditions, DNA negative charge could be detected due to the gating effect by nanowire based FET[15]. In the present model, PBASE could anchor amine terminated DNA on graphene surface without changing the high conductivity property. It also could partially avoid the non-covalent binding of DNA on graphene surface-- non-electrostatic stacking interaction. The device was washed three times with 2% SDS and twice with DI water before conducting each electrical measurement to further avoid any non-specific binding of DNA fragments. Compared with noncovalent attachment methods, the covalent anchoring of oligonucleotides on the graphene surface provided better stability and less nonspecific hybridization for DNA sensing[34].

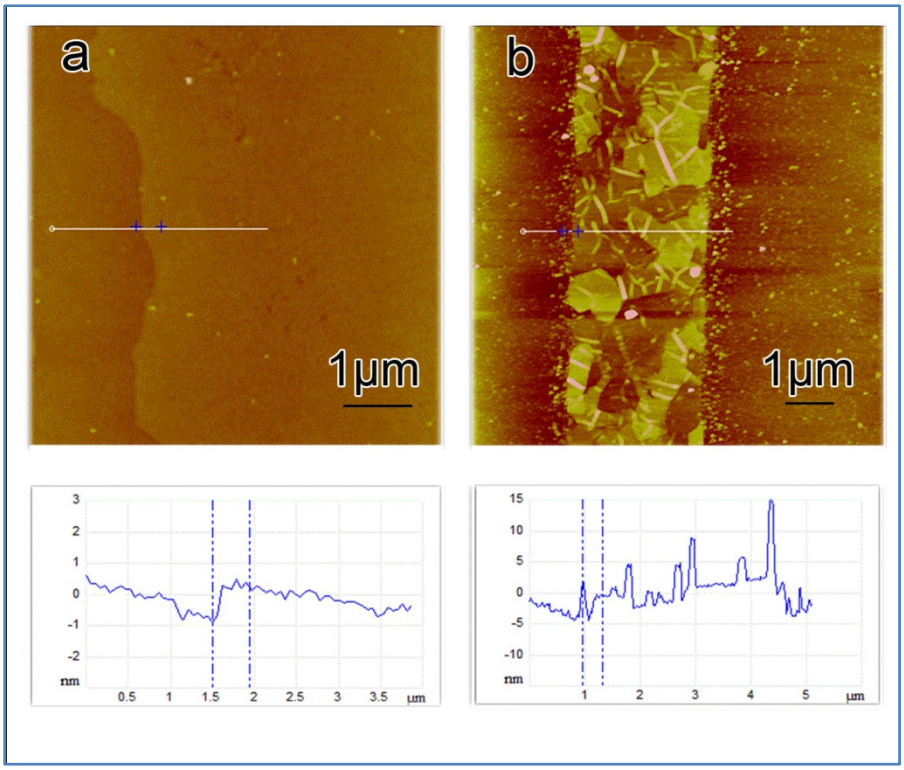

Figure 3.5 AFM images of graphene before (a) and after (b) photolithography.

Although the chemistry of functionalization step is ideal, the roughness of CVD grown graphene layer will introduce a barrier to achieve the perfect immobilization. AFM images (Figure 3.5) show the structure of a CVD grown graphene layer before and after photolithography. It is clear that some photoresist residue is on the surface of graphene layer which may cause the Dirac point of the intrinsic graphene layer shift to 40V(Figure 3.4b). Consequently, some part of graphene may have low coverage of probe DNA, which will cause low response to hybridization event.

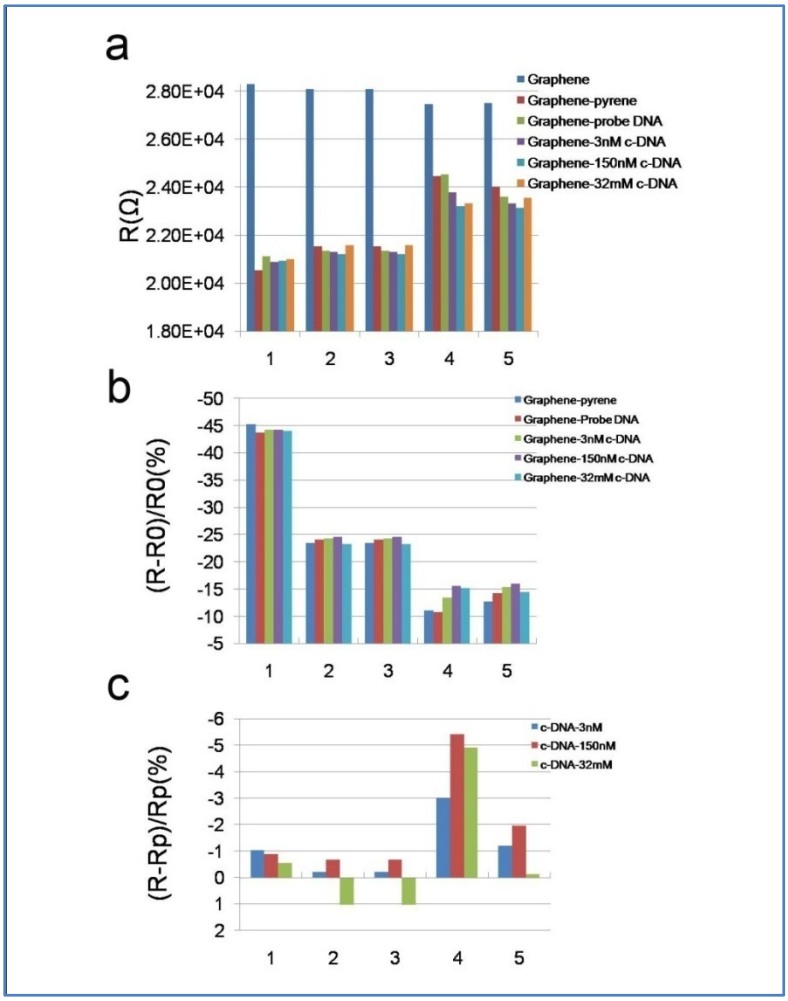

Figure 3.6 (a) Resistance of 5 devices; (b) Resistance change of five devices compare with resistance of bare graphene device; (c) Resistance change dependence on concentration of complementary DNA. Ro-resistance of graphene, Rp-resistance of graphene immobilized with probe DNA, c-DNA: complementary DNA.

As illustrated in Figure 3.6a, the resistance of the device decreased substantially after functionalization with PBASE. And with the increase of DNA concentration, the resistance further decreases. Water molecules absorbed on graphene layers will result in hole charge carriers and thus p-type GFETs will be produced[35-36]. In order to exclude the error that water molecule and other ions might bring about, control experiments were

conducted in bare buffer for 8h (Figure 3.7). The resistance increased by 30-45% after incubation which could be caused by both doping effect and contact metal work function change[37] (Figure 3.7). However, the resistance decreased by 15-45% as DNA molecules were introduced into the same buffer (Figure 3.6b). And the hybridization of the DNA probes on the surface with the complimentary DNA target further reduced the resistance by 0.5-5%. The low detection limit in the current device is nearly 3nM which is comparable to CNT-based FET devices. Hybridization of DNA to the surface-immobilized DNA probe creates a high density of negative charges on the graphene surface, providing an electrostatic gating effect, which in turn increases the hole concentration in graphene, resulting in the observed decrease in resistance. It is reported that the selective attachment of DNA molecules on various segments of the FET device affects the sensing mechanism of the carbon nanotube biosensor[37]. Compared to the control experiment, DNA molecules were attached to the graphene layer channel instead of the metal electrodes. Thus, the detection mechanism is the depletion of channel carriers instead of the Schottky barrier[38].

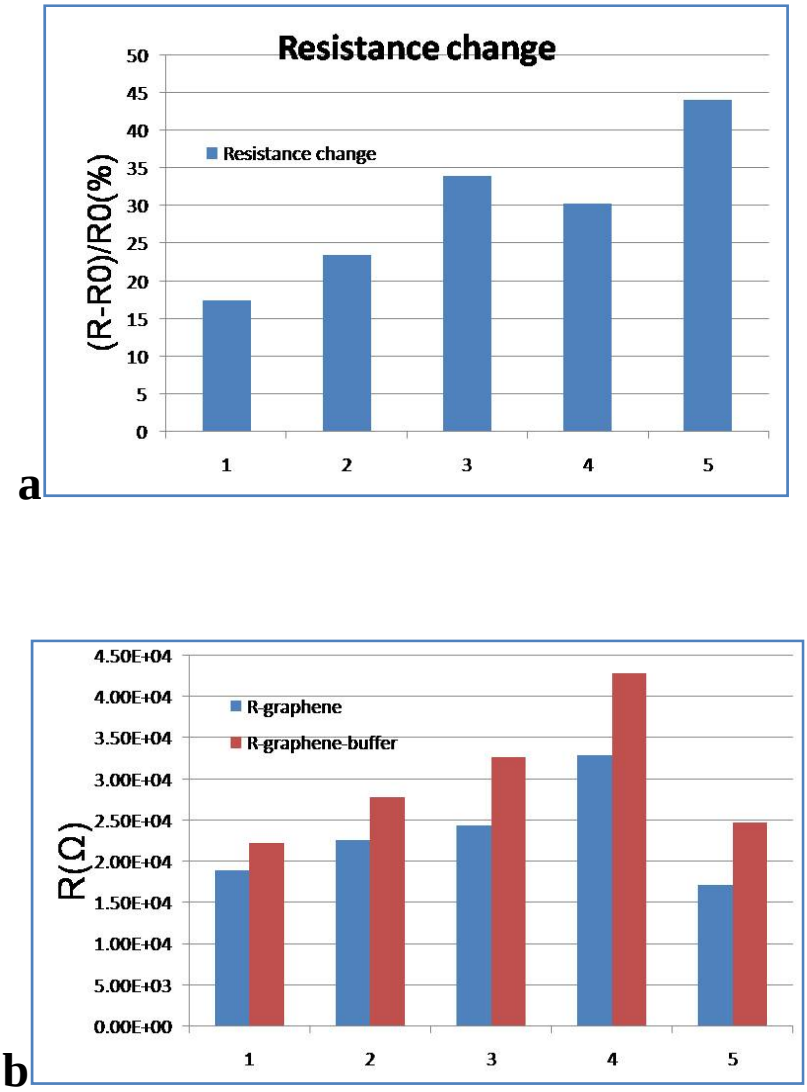

Figure 3.7 (a) Resistance change of five devices after incubation in TE buffer for 8h. (b) Resistance of graphene device. R-graphene: resistance of graphene; R-graphene-buffer: Resistance of graphene device after 8 h incubation in TE buffer.

When the concentration of c-DNA reached 32mM, the resistance increased instead of decreasing (Figure 3.6). One reason is that some probe DNA possibly attached to the surface of graphene with non-covalent bond. The non-covalent interaction is weak and such interaction could be destroyed by hybridization with c-DNA[39]. When the concentration of c-DNA increased to a certain amount, the non-specific binding of DNA

was washed away. Thus the resistance increased due to less pronounced negatively charged DNA gating effect. The other reason is the metal electrode work function was slightly changed due to long time treatment with buffer as shown by control experiment (Figure 3.7). The electrical measurement shows that the graphene based FET DNA sensor is applicable and further investigation of the device to detect mismatched DNA is being conducted.

3.1.4 Conclusion

Large area graphene based FET devices have been fabricated via photolithography. Successful modification of the device enables the device detect the DNA to the nanomolar level. The negatively charged effect of DNA molecule could be used for next generation of graphene based DNA sensor. We believe that large area graphene layers with higher quality (less photoresist residue and monolayers) will provide more sensitive DNA sensors for future real-time, label free and ultrasensitive applications. Future directions will be towards large scale applications with integrated microfluidic channels for sample preparation and delivery to achieve “lab-on-chip” goal.

3.2 Block Copolymer Graphene Field Effect Transistor Robust Chemical Sensor

3.2.1 Introduction

The large surface area and excellent electrical conductivity of graphene allow it to act as an "electron wire" for oxidation-reduction active sites.[41] Many types of electrochemical biosensors with reduced graphene oxide (RGO) have been developed due to such properties.[42] As an alternative, graphene obtained via chemical vapor deposition (CVD) with structural and electronic properties superior to those of RGO.[40,43] Most importantly, size scalability of graphene films grown via CVD is the key advantage for meeting the requirements for fabricating large-area graphene field effect transistors (GFETs): e.g., CVD allows the growth of single-layer graphene with areas exceeding 30 square inches.[43]

Recently, GFETs have been intensively researched for possible sensing applications. Many studies have been conducted showing the high sensitivity of sensors resulting from the intrinsic properties of graphene, in applications such as pH sensor,[23,44] gas sensors,[22,36] and protein sensors[30,45]. However, the sensitivity of GFETs has in some cases proven to be inferior to that of other sensors, instabilities and unreliability of the device has been seen in other cases, and low electrical responses for intrinsic graphene devices in certain examples.[46] We have reported label-free DNA sensor with GFET,[47] the device would be more stable given certain functionalization and protection of graphene. Thus, it would be highly desirable and practical to develop GFET sensors with higher sensitivities and stabilities. Meanwhile, we have studied functionalization of GFET with

block copolymers. We were motivated in this work by the fact that the hexagonal structure of block copolymer (BCP) could possibly result in heterogeneous patterns with nanoscale spacings that may offer new opportunities for achieving a selective sensing function.

Diblock copolymers can assemble into ordered periodic arrays of spherical, cylinderial, or lamellae structures, which make them very promising templates in nanoscale fabrication.[26, 27] In chapter 2, we discussed tuning of electronic transport of GFET with BCPs.[48] The structure of BCPs, with their chemical functional groups in one chain, is likely to provide a viable mechanism for tuning the electronic property of GFETs. The finding also indicates that the BCPs can provide additional contribution in the form of a protective layer for GFETs, which will be advantageous for application as sensor. In this section, we systematically investigated BCP funcationalized GFET sensor stability for solution detection. An example of NaF detection by BCP functionalized GFET sensor demonstrates its high potential for long-term use. The detection of pH values further demonstrates the practical usage for such sensor.

3.2.2 Experimental

3.2.2.1 Synthesis of Graphene

CVD graphene was synthesized according to the description in Chapter 2.

3.2.2.2 Fabrication of Graphene Based Field Effect Devices

CVD grown large-area graphene sheets were patterned and etched by oxygen plasma to rectangular shapes using photolithography and a Reactive Ion Etch (RIE)

system. Two terminal devices with Ti/Au (2nm/80nm) electrodes (shown in the inset of Scheme 1) were then fabricated. The device was evaporated with back gate Ti/Au (2nm/100nm). The distance between the source and drain in the devices were set to 70μm, and the width of the patterned graphene layer is 50 μm.

3.2.2.3 Fabrication of PS-P4VP Block Copolymer

The block copolymer used in this study is Poly(styrene-b-4-vinylpyridne) (PS-b-P4VP), purchased form Polymer Source, with a molecular weight of 69kg/mol (M_n, PS = 51 kg/mol, M_n, PVP = 18 kg/mol) and a molecular weight distribution of M_w/M_n = 1.15. The block copolymers were dissolved in toluene/tetrahydrofuran at room temperature to make 0.6 wt% polymer solutions, which were subsequently spin-coated at 2200 rpm onto silicon wafers with 300nm thermally grown silicon dioxide on it. In order to develop well-defined, well-ordered cylindrical microdomains in the BCP films, appropriate volume fractions and molecular weights were selected. The choices of volume fraction and molecular weight provided control over the morphology (cylindrical in this case) and size/separation distance in the BCP microdomains.

3.2.2.4 Characterization

Raman spectra were taken using a Renishaw micro-Raman spectrometer with a 532 nm visible laser as the excitation source. Atomic force microscopy (AFM) was conducted using a Multimode-5 Veeco instrument operated in the tapping mode using standard silicon cantilevers. Electrical measurements were conducted with semiconductor

analyzer HP4510. Electron and hole mobility can be extracted from the linear regime of the transfer characteristics using $\mu = [(\Delta I_{ds}/V_{ds}) \times (L/W)]/C_{ox}\Delta V_g$, where L (70um) and W (50um) are channel length and width, respectively, C_{ox} is silicon oxide gate capacitance (which is 1.08×10^{-8} F/cm^2 for a gate oxide thickness of 300 nm), and I_{ds}, V_{ds}, and V_g are drain−source current, drain−source voltage, and gate voltage, respectively.

3.2.3 Results and Discussion

3.2.3.1 CVD Graphene for GFET

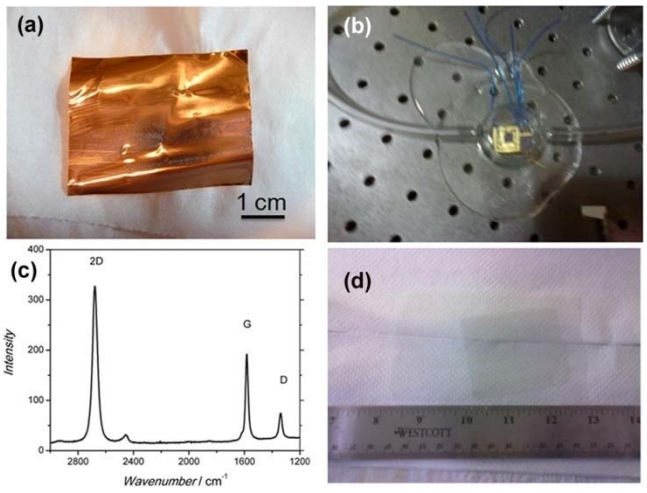

Figure 3.8 (a) Photo image of copper foil after graphene growth, (b) photo image of as-fabricated graphene field effect transistor with wire-bonding on chip-carrier, (c) Raman spectra of single-layer graphene, (d) photo image of 2 square inches of single-layer graphene on glass.

It is desirable to use large area graphene for mass production of sensors. Single layer graphene was synthesized with chemical vapor deposition by using copper foil as

catalyst. As it is shown in figure 3.8 a and d, a four inches square graphene has been successfully synthesized and transferred onto glass substrate. The large area graphene synthesis and transfer allow us to conveniently fabricate GFET. Raman spectra taken on the sample show the 2D (2628 cm^{-1}), G (1615 cm^{-1}), and D (1314 cm^{-1}) peaks. I_{2D}/I_G ratio is two indicating present sample is single layer graphene.

3.2.3.2 Block Copolymer for GFET Device Sensor

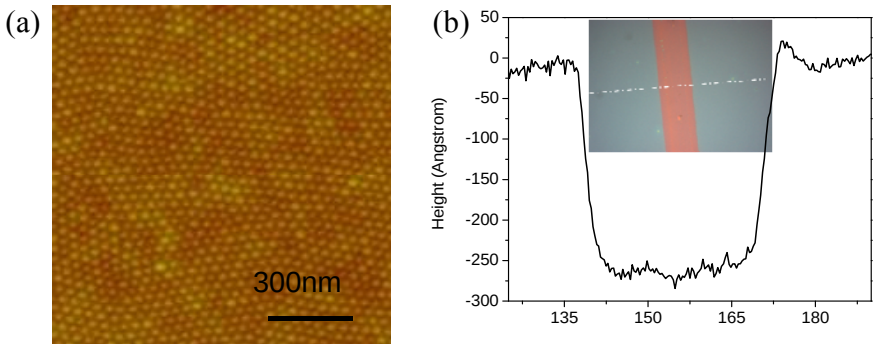

Figure 3.9 (a) AFM image of PS-P4VP block copolymer height profile (b) The surface profilometer height profile and optical image (inset) of the step-removed polymer film, the dashed line shows the scan axis along which the height profile has been measured.

The hexagonal periodical structure of BCP was well formed through self-assembly mechanism (Figure 3.9). With different weight ratio of polystyrene (PS) and poly(4-vinyl pyridine) (P4VP), cylindrical structure with different pore size could be achieved.[49-50] Each domain size used in this study is 30nm as measured with AFM (Figure 3.8a). To determine the polymer's thickness, a selected narrow section of the polymer film was removed and subsequently the sample's height profile was measured by a surface profilometer (Dektak 8 - Veeco). To guarantee the consistency, the height

profiles measured in three different linear scans and results were compared. All results agreed the thickness to be 27-30nm (Figure 3.8b).

In 1991, Sakai et. al. reported resistive-type humidity sensor using polyvinylpyridine.[51] The hydrophilic property as well as its insolubility in water enable the high sensitivity to water molecules. In 2002, Kosonen[49] reported P4VP as ionic conducting channel. Although the conductivity (10^{-7}-10^{-6} S/cm at room temperature) of P4VP is low, it still provides opportunity as ionic transport channel. Endowed with these features, i.e. hydrophilic, ionic conductivity of P4VP and periodic structure of BCP, PS-P4VP demonstrates feasibility for selective ions penetration.

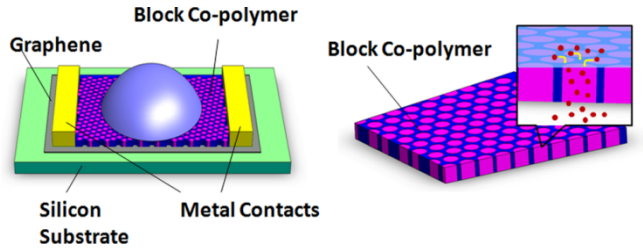

Scheme 3.1 Block copolymer protected graphene field effect transistor for solution detection. Pink part represents PVP and blue part represents PS.

Schematic illustration of the robust device shows that block copolymer serves as membrane for ions transport (scheme 3.1). It has been studied that P4VP brushes is pH-responsive and the integration of it into solid state nanochannels will produce nano-channel device. By manipulating the proton concentration in the surrounding environment, ions transport through P4VP nano-channel will be easily achieved.[52] Here, the BCP film will serve as such a role for sensor application. To fabricate the BCP

functionalized GFET, the BCP layer was transferred onto GFET using dipping-fishing method. Further relaxation in air under 40°C was necessary to remove water molecules and to provide smooth contact between graphene and BCP. Note that the transferring process may bring wrinkles which will cause water molecules captured underneath BCP.

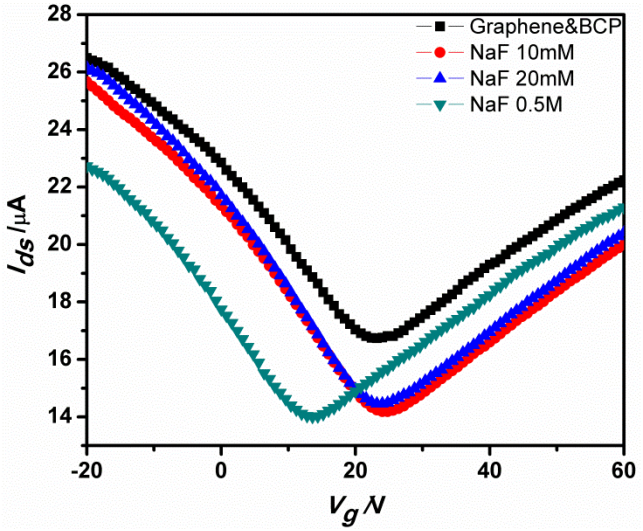

Figure 3.10 Typical I_{ds}-V_g curve of BCP/graphene NaF sensor. The drain-source voltage was 100mV.

After the protective layer was attached on to GFET, drops of different solution may be applied onto graphene. The validation of the assumption that BCP acts as a protective layer for added stability in these sensors was proven in sensing experiments using a NaF solution. It has been reported that NaF could cause a negative shift in the neutrality point of sensors due to its screen effect. Debye length is utilized to quantify the screening effect with different ionic strength of the NaF ionic solution. With Graham equation simplified for 1:1 electrolyte solution, the Debye length for 10mM, 20mM and 0.5M are 3nm, 2nm and 0.4nm respectively (equation 1).[53] The ionic conducting domain,

P4VP, facilitates F^- ions diffusion closer to graphene layer. Meanwhile the dipole-dipole interaction between F^- ions and pyridinyl groups provides stable signal for such type of sensor (Scheme 3.2).

$$\lambda = \frac{0.304}{\sqrt{[NaF]}}\,nm \qquad \text{Equation (1)}$$

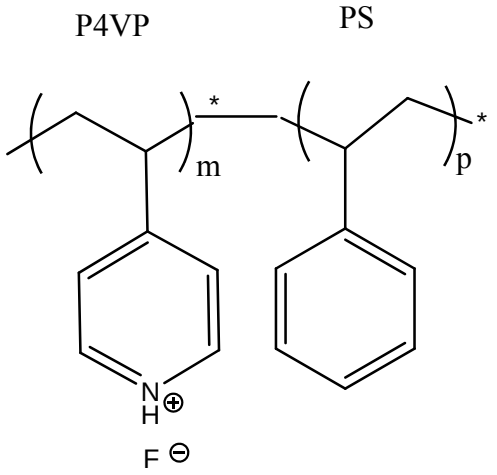

Scheme 3.2 Reaction between P4VP and F^- ion: eletrostatic interaction between pyridinyl group and fluoride ion.

Negative shift was not observed until the concentration of NaF increased to 0.5M. Two reasons may be accounted for the phenomenon. On one hand, the low ion permeability of PS because of its hydrophobic property prevents the buildup of screening charges in the thin layer of water between the block copolymer and graphene. On the other hand, the response may also attribute to the incubation time of the device. To avoid possible solution penetration underneath BCP layer, only 20 seconds incubation was applied onto the device. Kinetically, slow ionic diffusion at low concentration into P4VP channel which is 25nm long (Figure 3.9b) may prevent the buildup of impurity charge

potential adjacent to graphene. Therefore, the negative shift was not observed for 10mM solution. Nontheless, charge neutrality point decreases indicating charge carrier changes which is consistent with Chen's report.[54] This could be useful for discern the slight charge impurity change with slight concentration change. When the concentration increased to 20mM no change was observed for the charge neutrality point, suggesting no more change of carrier concentrations. This phenomenon indicates the saturation of charges or saturation of F^- ions in block copolymer (scheme 3.2).

3.2.3.3 Stability Study of BCP GFET Sensor

When the exposure concentration was increased to 0.5M, the neutrality point shifted up to -10V (Figure 3.10) indicating the effect of impurity charge potential on graphene device.

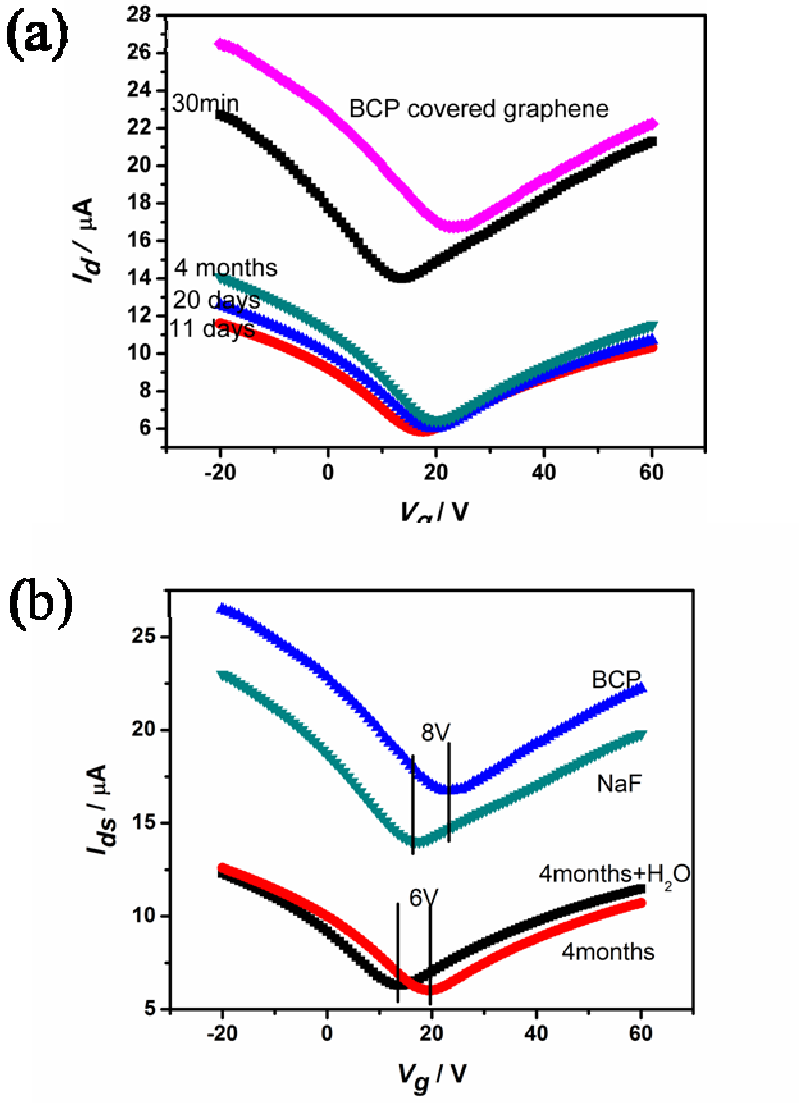

Figure 3.11 Typical Ids-Vg curve of BCP/graphene FET sensor stability test (a) time study and (b) reversibility study. The initial device was exposed to 0.5M NaF solution for 20 seconds, then measurements were conducted with different time. All of the test were conducted in air, V_{ds}=100mV.

We further investigated the durability of the device after functionalization over 4 months range (Figure 3.11). The Dirac point shifted to negative value after 30min which is the same with the result just after 20sec. exposure to 0.5M NaF solution. This indicates the saturation of P4VP channel with F^- ions. After 11 days, the Dirac point shifted to

positive. And it continued to shift to positive with the lapse of time. However, the Dirac point does not return to the initial value of BCP-graphene one indicating F^- ions exertion charge potential adjacent to graphene layer. Another important fact is that the charge neutrality point decreased after 11 days storage under ambient atmosphere. We attribute the phenomena to further migration of F^- ions within P4VP channel closer to graphene layer (scheme 3.2).

8 V Dirac point shift was observed with 0.5M NaF solution drops on the fresh-prepared device. After 4 months stored in ambient atmosphere, we placed drops of D.I. water on the same device soaked with 0.5M NaF. Surprisingly, the device still works perfect. Although the Dirac point shift of 6V is less than the fresh-prepared one, the reliability confirms the protective functionality of BCP. After F^- ions diffusing into P4VP channel, they were immobilized by interaction between pyridinyl group of P4VP and themselves. With water molecules penetrating into P4VP channel, F^- ions were released to "free motion". This process facilitates re-buildup of impurity charge adjacent to graphene. Therefore, Dirac point shift was observed again.

The interesting phenomena may provide a new sensor architecture to detect molecular changes under "dry" condition based on GFETs devices. Furthermore, the distinct surface tensions of P4VP (hydrophilic) and PS (hydrophobic) facilitates the partial and orderly absorption of water and hydrophilic charged ions. This property could be applied for the selective sensing of different gases. For example, a small amount of water could be used to disolve HCl and NH_3 vapors, which have high solubility in water, and the neutrality of the device could be changed based on the different charges. The

protective properties of the BCP would enable the sensor to be used over long periods of time.

3.2.3.4 pH Detection with BCP GFET Sensor

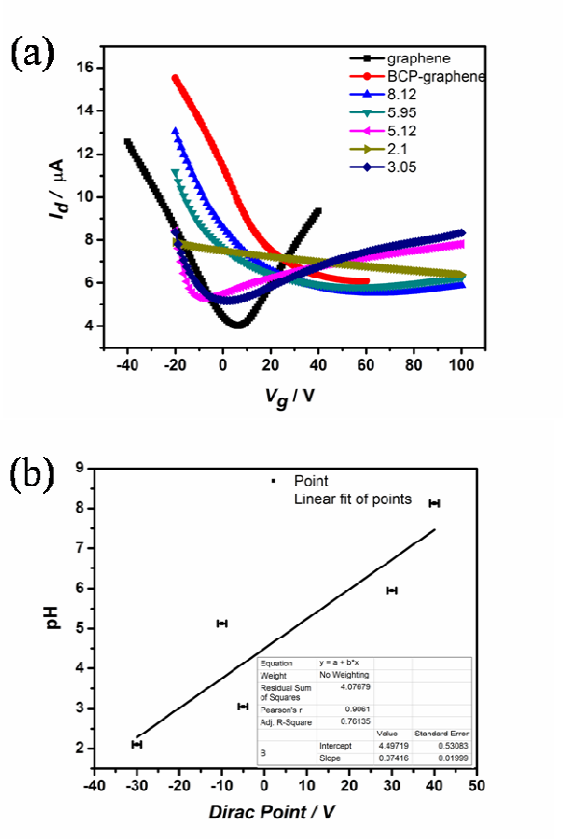

Figure 3.12 pH detection with BCP protected GFET robust sensor: (a) typical Typical Ids-Vg curve with different pH solution; (b) linear fitting of Dirac point and pH. Buffer used here are 0.1M Tris-HCl solutions.

To further confirm the robust sensor could be used for practical solution detection, pH measurements were conducted. It has been reported that GFET could be feasible as pH sensor.[23,45] Ohno et.al. applied mechanically derived graphene for such application. Eletrolyte gating effects were monitored and employed for pH sensing. In our case,

charge impurity potential buildup in the channel plays more important role. And the Dirac point is also linear fitted with pH value (Figure 3.12), which provides evidence for such application of GFET.[23] Here for our device, with decrease of pH, Dirac point shifted to more and more negative. The neutrality point coninues decreasing with decrease of pH which is different from previous pristine graphene.[23] Still this phenomena attributes to the channel length of P4VP.

3.2.4 Conclusion

The BCP-covered GFET could detect 1mM NaF solution. It was also determined that the orientation and periodicity of the resulting BCP array of cylindrical microdomains facilitate the selective sensing property. These findings pave the way for developing more durable and sensitive graphene-based sensors for chemical or biological applications under ambient conditions. This method also paves the way for developing more selective and more stable sensors out of BCP-covered GFET device to be used under ambient atmospheres. Particularly interesting is the fact that these new devices could be used for chemical sensing by incorporating charged ions or molecules into orderly pattern under "dry" conditions.

3.3 Future Work

Graphene field effect transistor biosensor.

(1) In section 3.1 we presented GFET ssDNA sensor. To improve the slectivity and sensitivity, further functionalization of graphene is needed. By introducing conductive polymers which have functional groups easier to be functionalized, the

selectivity could be enhanced. Also, other biomolecules could be easier immobilized on the surface of graphene resulting broden application of GFET sensor. The large production and minaturization of GFET devices certainly deliver opportunities for lab-on-chip applications.

(2) In section 3.2, the high stability of GFET protected by block co-polymer provides us a bright future for further application of such devices. To date, this finding is the very first findings with such stability in ambient condition. Furthermore, by changing the functional groups on block copolymer, interesting devices may be devised for tuning electron transport and furhter application for various types of sensors. For example, hydrophilic and hydrophobic part on PS-P4VP block copolymer will provide sites for electron donating or withdrawing groups interactions. Therefore, Lewis acid (accepting electron lone pairs, for example HCl) or base (donating electron lone pairs for example NH_3) of dry gases could be detected with such devices due to the slectivity of pyridine group on P4VP.

3.4 References

(1) S. P. Fang, H. J. Lee, A. W. Wark, R. M. Corn,"*Attomole microarray detection of MicroRNAs by nanoparticle-amplified SPR imaging measurements of surface polyadenylation reactions"* ***Journal of the American Chemical Society*** *2006*, *128*, 14044.

(2) J. Wang,"*Electrochemical biosensors: Towards point-of-care cancer diagnostics"* ***Biosensors & Bioelectronics*** *2006*, *21*, 1887.

(3) D. Grieshaber, R. Mackenzie, J. Voeroes, E. Riemhult,"*Electrochemical Biosensors: Sensor Principles and Architectures"* ***Sensors*** *2008*, *8*, 1440.

(4) L. Jagannathan, V. Subramanian,"*DNA detection using organic thin film transistors: Optimization of DNA immobilization and sensor sensitivity"* ***Biosensors & Bioelectronics*** *2009*, *25*, 288.

(5) E. Stern, A. Vacic, M. A. Reed,"*Semiconducting Nanowire Field-Effect Transistor Biomolecular Sensors"* ***IEEE Transactions on Electron Devices*** *2008*, *55*, 3119.

(6) A. B. Artyukhin, M. Stadermann, R. W. Friddle, P. Stroeve, O. Bakajin, A. Noy,"*Controlled electrostatic gating of carbon nanotube FET devices"* ***Nano Letters*** *2006*, *6*, 2080.

(7) R. B. M. Schasfoort, S. Schlautmann, L. Hendrikse, A. Van Den Berg,"*Field-effect flow control for microfabricated fluidic networks"* ***Science*** *1999*, *286*, 942.

(8) J. Hahm, C. M. Lieber,"*Direct ultrasensitive electrical detection of DNA and DNA sequence variations using nanowire nanosensors"* ***Nano Letters*** *2004*, *4*, 51.

(9) M. Curreli, R. Zhang, F. N. Ishikawa, H. K. Chang, R. J. Cote, C. Zhou, M. E. Thompson,"*Real-Time, Label-Free Detection of Biological Entities Using Nanowire-Based FETs"* ***Ieee Transactions on Nanotechnology*** *2008*, *7*, 651.

(10) M. T. Martinez, Y. C. Tseng, N. Ormategui, I. Loinaz, R. Eritja, J. Bokor,"*Label-Free DNA Biosensors Based on Functionalized Carbon Nanotube Field Effect Transistors"* ***Nano Letters*** *2009*, *9*, 530.

(11) X. C. Dong, C. M. Lau, A. Lohani, S. G. Mhaisalkar, J. Kasim, Z. X. Shen, X. N. Ho, J. A. Rogers, L. J. Li,"*Electrical detection of femtomolar DNA via gold-nanoparticle enhancement in carbon-nanotube-network field-effect transistors"* ***Advanced Materials*** *2008*, *20*, 2389.

(12) K. Maehashi, K. Matsumoto,"*Label-Free Electrical Detection Using Carbon Nanotube-Based Biosensors"* ***Sensors*** *2009*, *9*, 5368.

(13) J. Kang, J. Lee, T. H. Kim, J. Park, M. J. Seong, S. Hong,"*Large-scale assembly of carbon nanotube-based flexible circuits for DNA sensors"* ***Nanotechnology*** *2008*, *19*, 4.

(14) K. Balasubramanian, M. Burghard,"*Biosensors based on carbon nanotubes"* ***Analytical and Bioanalytical Chemistry*** *2006*, *385*, 452.

(15) X. Wang, C. S. Ozkan,"*Multisegment nanowire sensors for the detection of DNA molecules"* ***Nano Letters*** *2008*, *8*, 398.

(16) Y. Yamamoto, K. Maehashi, Y. Ohno, K. Matsumoto,"*Highly Sensitive Biosensors Based on High-Performance Carbon Nanotube Field-Effect Transistors"* ***Sensors and Materials*** *2009*, *21*, 351.

(17) J. H. Chen, C. Jang, S. Xiao, M. Ishigami, M. S. Fuhrer,"*Intrinsic and extrinsic performance limits of graphene devices on SiO2"* ***Nature Nanotechnology*** *2008*, *3*, 206.

(18) T. J. Echtermeyer, M. C. Lemme, M. Baus, B. N. Szafranek, A. K. Geim, H. Kurz,"*Nonvolatile switching in graphene field-effect devices"* ***Ieee Electron Device Letters*** *2008*, *29*, 952.

(19) X. Liang, Z. Fu, S. Y. Chou,"*Graphene transistors fabricated via transfer-printing in device active-areas on large wafer"* ***Nano Letters*** *2007*, *7*, 3840.

(20) Z. Chen, Y. M. Lin, M. J. Rooks, P. Avouris,"*Graphene nano-ribbon electronics"* ***Physica E: Low-dimensional Systems and Nanostructures*** *2007*, *40*, 228.

(21) X. Li, X. Wang, L. Zhang, S. Lee, H. Dai,"*Chemically derived, ultrasmooth graphene nanoribbon semiconductors"* ***Science*** *2008*, *319*, 1229.

(22) F. Schedin, A. K. Geim, S. V. Morozov, E. W. Hill, P. Blake, M. I. Katsnelson, K. S. Novoselov,"*Detection of individual gas molecules adsorbed on graphene"* ***Nature Materials*** *2007*, *6*, 652.

(23) Y. Ohno, K. Maehashi, Y. Yamashiro, K. Matsumoto,"*Electrolyte-Gated Graphene Field-Effect Transistors for Detecting pH Protein Adsorption"* ***Nano Letters*** *2009*, *9*, 3318.

(24) X. S. Li, W. W. Cai, J. H. An, S. Kim, J. Nah, D. X. Yang, R. Piner, A. Velamakanni, I. Jung, E. Tutuc, S. K. Banerjee, L. Colombo, R. S. Ruoff,"*Large-Area Synthesis of High-Quality and Uniform Graphene Films on Copper Foils"* ***Science*** *2009*, *324*, 1312.

(25) K. S. Kim, Y. Zhao, H. Jang, S. Y. Lee, J. M. Kim, K. S. Kim, J. H. Ahn, P. Kim, J. Y. Choi, B. H. Hong,"*Large-scale pattern growth of graphene films for stretchable transparent electrodes"* ***Nature*** *2009*, *457*, 706.

(26) A. Reina, X. Jia, J. Ho, D. Nezich, H. Son, V. Bulovic, M. S. Dresselhaus, J. Kong,"*Large area, few-layer graphene films on arbitrary substrates by chemical vapor deposition"* ***Nano Letters*** *2008*, *9*, 30.

(27) Q. Yu, J. Lian, S. Siriponglert, H. Li, Y. P. Chen, S. S. Pei,"*Graphene segregated on Ni surfaces and transferred to insulators"* ***Applied Physics Letters*** *2008*, *93*, 113103.

(28) A. Reina, H. Son, L. Jiao, B. Fan, M. S. Dresselhaus, Z. F. Liu, J. Kong,"*Transferring and Identification of Single-and Few-Layer Graphene on Arbitrary Substrates"* ***Journal of Physical Chemistry C*** *2008*, *112*, 17741.

(29) M. Ishigami, J. H. Chen, W. G. Cullen, M. S. Fuhrer, E. D. Williams,"*Atomic structure of graphene on SiO2"* ***Nano Letters*** *2007*, *7*, 1643.

(30) N. Mohanty, V. Berry,"*Graphene-Based Single-Bacterium Resolution Biodevice and DNA Transistor: Interfacing Graphene Derivatives with Nanoscale and Microscale Biocomponents"* ***Nano Letters*** *2008*, *8*, 4469.

(31) R. J. Chen, Y. Zhang, D. Wang, H. Dai,"*Noncovalent sidewall functionalization of single-walled carbon nanotubes for protein immobilization"* ***J. Am. Chem. Soc*** *2001*, *123*, 3838.

(32) D. Teweldebrhan, J. Lin, K. Ashraf, G. Liu, X. Jing, Z. Yan, R. Li, M. Ozkan, R. K. Lake, A. A. Balandin, C. S. Ozkan,"*Gating of Single Layer Graphene Using Single-Stranded Deoxyribonucleic Acids "* ***Small*** *2010*, *in press*.

(33) X. C. Dong, Y. Shi, W. Huang, P. Chen, L. J. Li,"*Electrical Detection of DNA Hybridization with Single-Base Specificity Using Transistors Based on CVD-Grown Graphene Sheets"* ***Advanced Materials*** *2010*, *22*, 1.

(34) Z. Li, Y. Chen, X. Li, T. I. Kamins, K. Nauka, R. S. Williams,"*Sequence-specific label-free DNA sensors based on silicon nanowires"* ***Nano Letters*** *2004*, *4*, 245.

(35) T. O. Wehling, A. I. Lichtenstein, M. I. Katsnelson,"*First-principles studies of water adsorption on graphene: The role of the substrate"* ***Applied Physics Letters*** *2008*, *93*, 202110.

(36) T. O. Wehling, K. S. Novoselov, S. V. Morozov, E. E. Vdovin, M. I. Katsnelson, A. K. Geim, A. I. Lichtenstein,"*Molecular doping of graphene"* ***Nano Letters*** *2008*, *8*, 173.

(37) R. J. Chen, H. C. Choi, S. Bangsaruntip, E. Yenilmez, X. Tang, Q. Wang, Y. L. Chang, H. Dai,"*An investigation of the mechanisms of electronic sensing of protein adsorption on carbon nanotube devices"* ***J. Am. Chem. Soc*** *2004*, *126*, 1563.

(38) B.L. Allen, P. D. Kichambare, A Star,"*Carbon Nanotube Field-Effect-Transistor-Based Biosensors"* ***Advanced Materials*** *2007*, *19*, 1439.

(39) C. H. Lu, H. H. Yang, C. L. Zhu, X. Chen, G. N. Chen,"*A Graphene Platform for Sensing Biomolecules"* ***Angewandte Chemie-International Edition*** *2009*, *48*, 4785.

(40) K. S. Novoselov, A. K. Geim, S. V. Morozov, D. Jiang, Y. Zhang, S. V. Dubonos, I. V. Grigorieva, A. A. Firsov,"*Electric field effect in atomically thin carbon films"* ***Science*** *2004*, *306*, 666.

(41) Tapas Kuila, Saswata Bose, Partha Khanra, Ananta Kumar Mishra, Nam Hoon Kim, Joong Hee Lee,"*Recent advances in graphene-based biosensors"* ***Biosensors and Bioelectronics*** *2011*, *26*, 4637.

(42) Tessy Theres Baby, S. S. Jyothirmayee Aravind, T. Arockiadoss, R. B. Rakhi, S. Ramaprabhu,"*Metal decorated graphene nanosheets as immobilization matrix for amperometric glucose biosensor"* ***Sens. Actuators, B*** *2010*, *B145*, 71.

(43) S. Bae, H. Kim, Y. Lee, X. F. Xu, J. S. Park, Y. Zheng, J. Balakrishnan, T. Lei, H. R. Kim, Y. I. Song, Y. J. Kim, K. S. Kim, B. Ozyilmaz, J. H. Ahn, B. H. Hong, S. Iijima,"*Roll-to-roll production of 30-inch graphene films for transparent electrodes"* ***Nature Nanotechnology*** *2010*, *5*, 574.

(44) P. K. Ang, W. Chen, A. T. S. Wee, K. P. Loh,"*Solution-Gated Epitaxial Graphene as pH Sensor"* ***Journal of the American Chemical Society*** *2008*, *130*, 14392.

(45) Yasuhide Ohno, Kenzo Maehashi, Kazuhiko Matsumoto,"*Chemical and biological sensing applications based on graphene field-effect transistors"* ***Biosensors and Bioelectronics*** *2010*, *26*, 1727.

(46) Y. P. Dan, Y. Lu, N. J. Kybert, Z. T. Luo, A. T. C. Johnson,"*Intrinsic Response of Graphene Vapor Sensors"* ***Nano Letters*** *2009*, *9*, 1472.

(47) S.-R. Guo, J. Lin, M. Penchev, E. Yengel, M. Ghazinejad, C. S. Ozkan, M. Ozkan,"*Label free DNA detection using large area graphene based field effect transistor biosensors"* ***J. Nanosci. Nanotechnol.*** *2011*, *11*, 5258.

(48) S. Guo, M. Ghazinejad, X. Qin, H. Sun, W. Wang, F. Zaera, C. S. Ozkan, M. Ozkan,"*Tuning of Electron Transport in Graphene based Field Effect Devices using Block Co-Polymers"* ***Small*** *2012*, *8*, 1073.

(49) H. Kosonen, S. Valkama, J. Hartikainen, H. Eerikainen, M. Torkkeli, K. Jokela, R. Serimaa, F. Sundholm, G. Ten Brinke, O. Ikkala,"*Mesomorphic structure of poly(styrene)-block-poly(4-vinylpyridine) with oligo(ethylene oxide)sulfonic acid side chains as a model for molecularly reinforced polymer electrolyte"* ***Macromolecules*** *2002*, *35*, 10149.

(50) J. Ruokolainen, M. Saariaho, O. Ikkala, G. Ten Brinke, E. L. Thomas, M. Torkkeli, R. Serimaa,"*Supramolecular routes to hierarchical structures: Comb-coil diblock copolymers organized with two length scales"* ***Macromolecules*** *1999*, *32*, 1152.

(51) Y. Sakai, Y. Sadaoka, M. Matsuguchi, Y. Kanakura, M. Tamura,"*A Humidity Sensor Using Polytetrafluoroethylene-Graft-Quaternized-Polyvinylpyridine"* ***Journal of the Electrochemical Society*** *1991*, *138*, 2474.

(52) I. Szleifer, M. Tagliazucchi, O. Azzaroni,"*Responsive Polymers End-Tethered in Solid-State Nanochannels: When Nanoconfinement Really Matters"* ***Journal of the American Chemical Society*** *2010*, *132*, 12404.

(53) P. K. Ang, M. Jaiswal, C. H. Y. X. Lim, Y. Wang, J. Sankaran, A. Li, C. T. Lim, T. Wohland, O. Barbaros, K. P. Loh,"*A Bioelectronic Platform Using a Graphene-Lipid Bilayer Interface"* ***Acs Nano*** *2010*, *4*, 7387.

(54) J. H. Chen, C. Jang, S. Adam, M. S. Fuhrer, E. D. Williams, M. Ishigami,"*Charged-impurity scattering in graphene"* ***Nature Physics*** *2008*, *4*, 377.

Chapter 4

Graphene/Carbon Nanotube Hybrid for Supercapacitors

4.1 Assembled Graphene Oxide and Single Walled Carbon Nanotube Ink for Stable Supercapacitors

4.1.1 Introduction

Carbon allotropes have been useful for many applications such as electronic devices,[1-3] sensors,[4-7] photovoltaic devices,[8-10] and energy storage devices.[11-12] Recently, supercapacitor has attracted a lot of attentions due to its high power density and long cycle lifetime compared to batteries. [11,13-14] Carbon nanotubes have been recognized as a significant material for such application due to its high surface area as well as high conductivity and stability under electrochemical conditions. There are several processing challenges limiting the use of SWCNTs for many applications: (1) low solubility or dispersion concentration in water or organic solvents; (2) aggregation without surface functionalization or surfactant assistance due to van der Waal's interaction, which reduces its surface area and further reduces the capacitance.[15-16] Therefore, it is crucial to develop an approach to overcome such processing challenges.

Many methods have been employed to disperse SWCNTs with various functionalization methods, including acid treatment,[15,17] surfactant binding,[18] non-covalent binding molecules.[19-20] While non-covalent functionalization could disperse SWCNT without introducing any surfactant or reducing its conductivity, it is still challengeable to achieve high concentration of SWCNT dispersion. Graphene oxide (GO)

has attracted a lot of attention due to the amphiphilic property. Huang[21] reported GO as a surfactant and Dai[22] applied this for carbon nanotube dispersion. Such findings indicate the powerful role that GO flakes can play in dispersing SWCNTs. Recently, it is reported that the content of carboxyl group may affect the capacitance of CNT.[23] Meanwhile varying reduction rate significantly affects the performance of reduced graphene oxide (rGO) as supercapacitor electrodes.[24] Although combining CNT and reduced graphene oxide for higher performance supercapacitor have been broadly studied,[25-29] it is very important to investigate GO–SWCNT composite system instead of rGO–SWCNT in terms of supercapacitor performance in order to achieve a lower cost fabrication approach.

One of an important aspects in fabricating energy storage devices is the current collector. Many types of current collector were utilized for carbon material based supercapacitor researches, such as Ni foam,[30-31] Ti foil,[25] stainless steel[27] and copper mesh.[24] However, these types of current collector require binder material for fabrication. Recently, paper based electrodes are attractive for supercapacitor due to its low cost, light weight, high flexibility, binder-free process and the fact that there is no need to have an extra current collector.[32-33] Hence, the development of high stability ink material is crucial for low cost and high-throughput preparation of paper based electrodes.

In this section, we describe the synthesis and application of a GO and SWCNT composite ink (GO–SWCNT ink) for fabricating electrochemically stable supercapacitors. The interaction between GO and CNT not only provides means to separate CNTs but also individual GO sheets, which increases the effective active area for electrochemical reaction. We achieved over 12 mg/ml of SWCNT dispersed in water without surfactant

assistance. The dispersion demonstrates high stability and permeability as ink material to prepare paper electrodes and it is an effective ink material for preparing paper electrodes. Paper based supercapacitor electrodes were easily fabricated with such material without other additives, binders, or additional current collectors. Our approach provides a binder free ink-printing method for large scale fabrication of electrochemical energy storage devices.

4.1.2 Experimental

4.1.2.1 Preparation of Graphene Oxide

Graphene oxide (GO) was prepared by using a modified Hummers method.[34-37] 1 g of graphite (Sigma-Aldrich) and 0.75 g of $NaNO_3$ were placed in a flask. Then, 75 mL of H_2SO_4 was added with stirring in an ice-water bath, and 4.5 g of $KMnO_4$ were slowly added over about 1 h. Stirring was continued for 2 h in the ice-water bath. Then the flask was placed in 35^{o}C oil bath for 2h. 100ml water was added into the flask which causes the temperature rising to 95^{o}C, after 1 h stirring 3 mL of H_2O_2 (30 wt % aqueous solution) was added, and the mixture was stirred for 2 h at room temperature. The mixture was washed thoroughly with deionized water through filtration, and then the GO flake was dispersed in water with mechanical agitation. The obtained GO (0.1 g) was dispersed in water (100 mL). This dispersion was sonicated for 30 min. To get pure single layer GO the following repeated method was applied. First, the obtained dispersion was sonicated another 30 min, and the dispersion was centrifuged at 1000rpm/min for 20 min to remove large particles in the solution. After several centrifugations, the upper solution was then

centrifuged at 8000rpm/min for 20 min to remove soluble impurities and small GO layers. This step was repeated several times until the upper part is clear. Then the precipitation was dispersed in D.I. water with mild sonication.

4.1.2.2 Preparation of GO/SWCNT Supercapacitor

Various amounts of SWCNT (Sigma-Aldrich 05925) were added into as-obtained GO solution with concentration of 2mg/ml. After 10-25 minutes of ultrasonication, the black ink was formed. A piece of woven paper was dipped into the solution and then dried in vacuum oven at 45 ^{o}C for 2 hours. A two-electrode measurement technique was employed for the electrochemical measurements, where two pieces of carbon-ink soaked paper were assembled into a sandwich structure with a porous membrane (Celgard 3501) separator. 6 M KOH aqueous solution was used as the electrolyte. The packaging of the supercapacitor cell was conducted at room temperature in atmosphere. The two electrodes of the packaged cell were connected to an electrochemical analyzer (Gamry Reference 600™) with an alligator clip. Cyclic voltammetry (CV), chronopotentiometry [charge-discharge (CD)] was performed to characterize the stability of the device. Cyclic voltammetry scans were performed with a voltage window of 1 volt in the range -0.5 to 0.5 V at scan rates ranging from 5mV sec^{-1} to 500 mV sec^{-1}. Potentiostatic EIS measurements were performed between 0.1Hz and 1MHz with amplitude of 10 mV.

4.1.2.3 Characterization

Atomic force microscopy was conducted with (Multimode-5, Veeco) operated in the tapping mode using standard silicon cantilevers. FTIR spectra were recorded with a

Bruker Equinox 55 with microscope and step scan (0.5 cm^{-1} resolution) at room temperature. Raman spectra were taken using a Renishaw micro-Raman spectrometer with a 532 nm visible laser as the excitation source. The SEM images were recorded with Leo SUPRA 55 microscope.

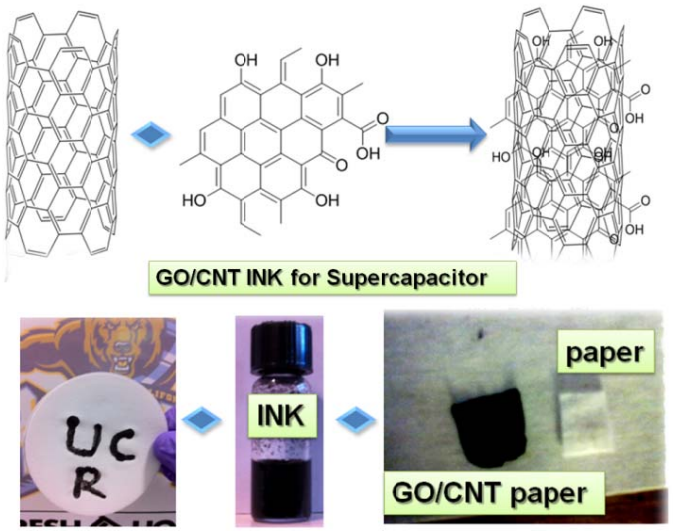

Scheme 4.1 GO-SWCNT non-covalent interactions, and preparation of supercapacitor electrodes with GO/SWCNT ink and paper.

4.1.3 Results and Discussion

With modified Hummer's method, we synthesized single layer GO. AFM images demonstrate the thickness of as-synthesized single layer GO is 0.5nm (Figure 4.1a, b). SEM images demonstrate that the size distribution of obtained GO is in the range of 100nm-20um (Figure 4.1 c, d). Raman spectra of D (1320 cm^{-1}), G (1573 cm^{-1}), and 2D (2640 cm^{-1}) bands demonstrating the characteristic peaks of GO. I_D/I_G ratios of 1:1 and 2:1 confirm double layer or single layer GO.[3] Uniform size of GO could be obtained with

various centrifuge steps. Size distribution from 200-500nm of GO was applied for dispersing SWCNT (Figure 4.2). With uniform and smaller size of GO, we expect to see a better interaction with SWCNT.

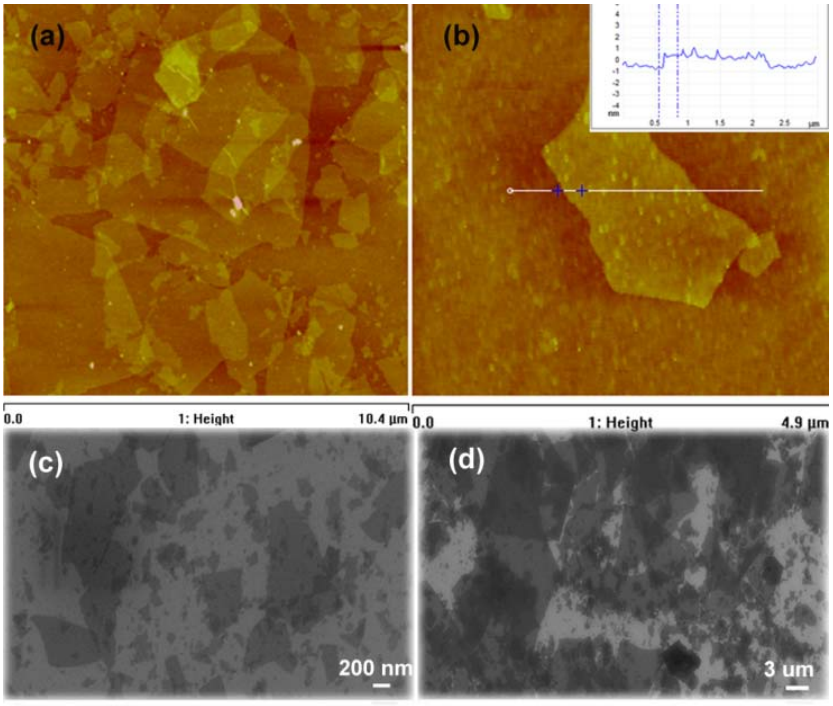

Figure 4.1 AFM and SEM images of as-synthesized GO (graphene oxide) single layer: (a,b) AFM images, inset shows a single layer of graphene oxide height profile of AFM image, (c,d) SEM images at different magnification factors.

It has been studied that the dominant chemical structures present on the surface of GO are tertiary alcohols and ethers with very low quantities of carboxylic acid at the periphery of the GO.[38] This structure feature provides fascinating properties for GO. While hydroxyl group, ketone group, ether group and carboxylic group provide chance for hydrogen bonding between GO and water molecules, the intact π bond will provide chance for π-π stacking. FTIR spectra of GO further confirms the presence of these functional groups (Figure 4.3a). Bending of C–OH groups (1378 cm^{-1}), C=O (1715 cm^{-1})

stretching vibration and the C–O, C–C stretching of epoxy groups at 1094 and 857 cm^{-1}, characterize the spectrum of air-dry GO.[22,39] Dai[22] and Li[40] have demonstrated negative charge effect of GO facilitating the dispersion of CNT with electrophoresis experiments. We tune the pH of dispersion with NaOH or/and HCl to further test the property of the dispersion. With increase of pH the dispersion becomes stable without precipitation even after one month. When the pH is 4, the dispersion is very unstable, precipitation appears 10 min after ultrasonication-assisted dispersion. However with addition of 1M NaOH the stability of the dispersion increases, which is demonstrated in Figure 4.4d. The stability of such dispersion demonstrates potential for long-term use of the solution. It is possible with the increase of OH^- concentration, carboxylic group was deprotonated resulting in more negatively charged species, which facilitates separation of SWCNT bundles.

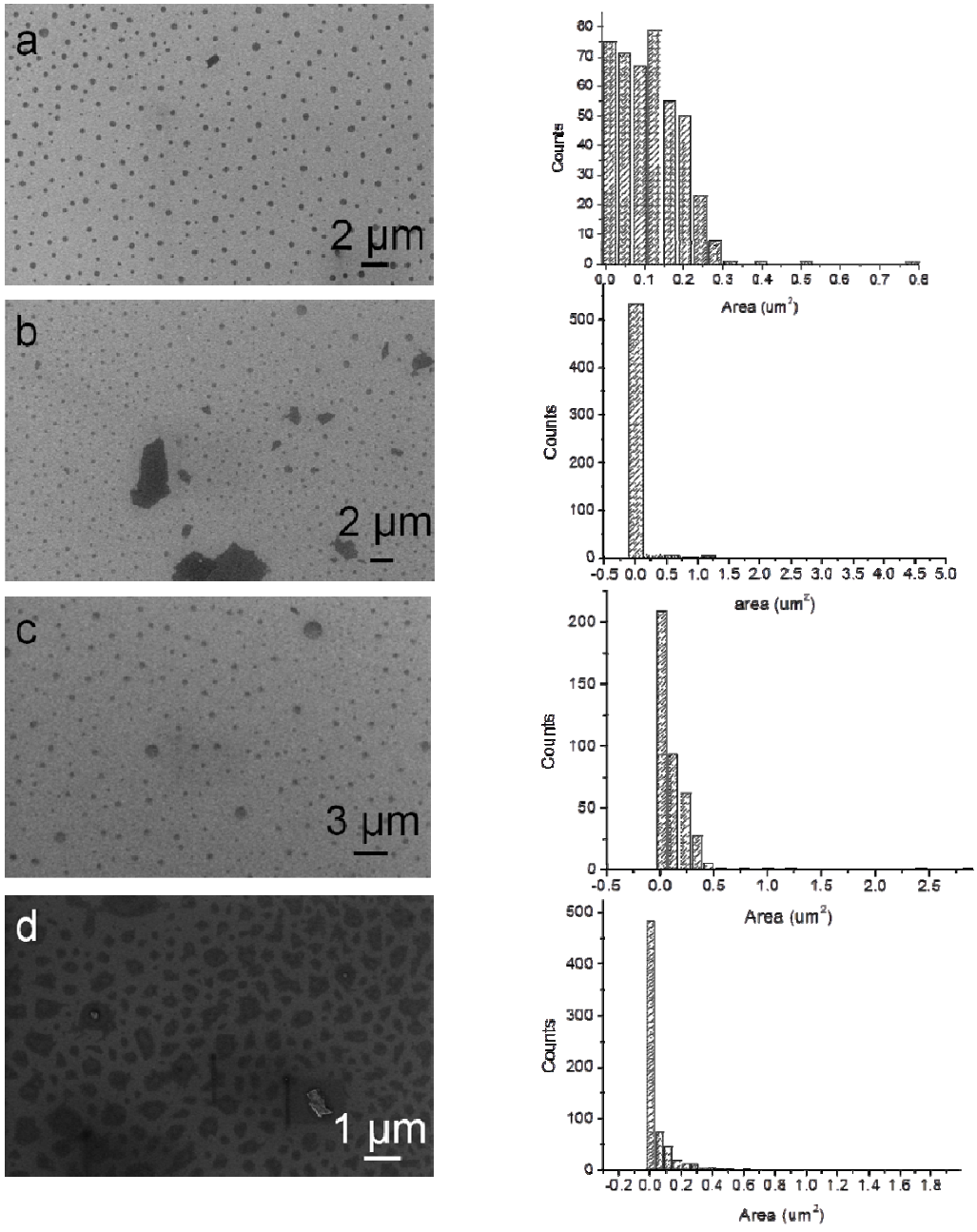

Figure 4.2 SEM images GO flakes with different size distribution.

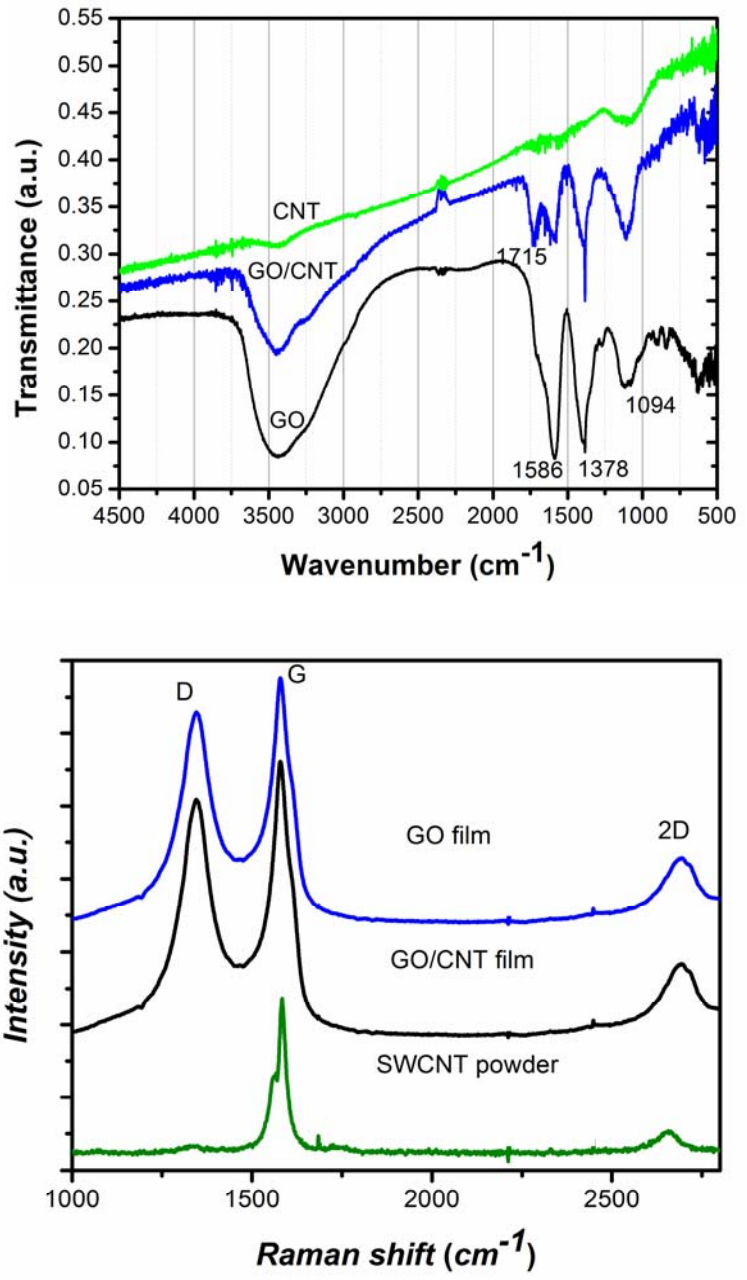

Figure 4.3 (a) FTIR and (b) Raman spectra of GO, SWCNT and GO/SWCNT composite ink. GO and GO/SWCNT are prepared by dropping a solution on glass slides followed by drying in air. SWCNT original powder is used for characterization. FTIR spectra is taken with KBr pellet.

To investigate the ability of GO to disperse SWCNT, we intentionally increase the weight ratio between SWCNT and GO. Surprisingly, 12mg/ml of SWCNT could be

achieved with 2mg/ml GO solution (Figure 4.4). To our knowledge, this is the highest concentration achieved and provides further opportunities for achieving SWCNT dispersions for a number of applications without surfactant assistance.

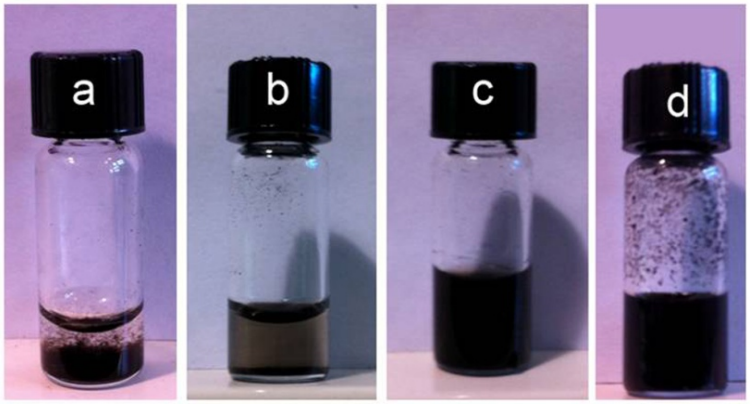

Figure 4.4 Photo images of 5mg SWCNT dispersed in 2mg/ml of GO at different pH values: (a) 4, (b) 7, (c) 9, (d) 12, and the volume difference results from the addition of NaOH. Note that black materials visible inside in (d) are residues after shaking. High concentration of SWCNT results in high viscosity. Supporting figure 2 shows the high viscosity for 10mg/ml concentration of SWCNT.

GO and SWCNTs tend to restack or form bundles due to van der Waals force. The non-covalent interaction between GO and SWCNT impacts not only on the separation of SWCNT bundles but also on the prevention of GO restacking. Figure 4.5 shows the SEM images of as-obtained material on paper. It is very clear that SWCNT were separated and embedded in GO film. Though partial restacking of GO sheets happens after mixing with the SWCNTs, they play a role in preventing further restacking which provides the chance for realizing single GO sheets (scheme 4.1). Interaction of molecules with graphene could be characterized with Raman spectra where D, G and 2D band are useful in understanding the effects of chemical interaction.[41] The full-width-at-half-maximum (FWHM) of the G band increases with the mixing of SWCNT and GO

indicating electronic structure changes with π-π interaction of GO sheets and SWCNTs (Figure 4.3b).

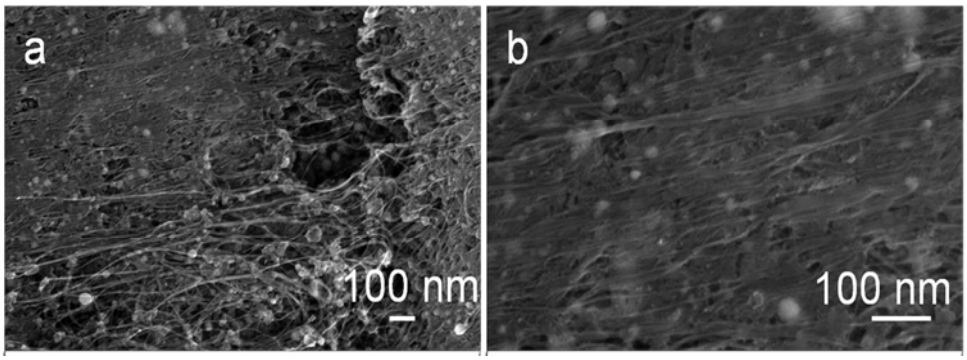

Figure 4.5 SEM images of aligned GO/SWCNT composite ink material transferred on paper.

Such a synergetic effect increases the surface area of both SWCNT and GO, which increases the active sites for electrochemistry reaction. Effort-less binding with paper of such material provides means for low cost fabrication of electrodes without any binder or additives. Hence, this composite ink material could provide tremendous opportunities for low-cost roll-to-roll fabrication of electrochemical double layer capacitors (EDLC). We further demonstrate this potential by characterizing the EDLCs based on SWCNT–GO paper electrodes.

4.1.4 Electrochemical Study

Woven paper is utilized for fabricating the paper based electrodes by dipping in the as-obtained GO-SWCNT ink for a few seconds and subsequently drying in a vacuum oven at 45^{o}C for 2 hours. The process enables a convenient and scalable way of fabricating low-cost binder-free electrode. As it is shown in scheme 1, the as-prepared material is easily patterned and attached on paper by either simply drawing or printing.

Here GO/SWCNT acts not only active material but also current collector, which offers possibility for miniature energy storage devices.[42] Cyclic voltammetry (CV) was performed to evaluate the electrochemical performance of the electrodes assembled in a symmetric two-electrode supercapacitor cell. It can be seen from Figure 4.6, with different ratio of GO/SWCNT the achieved specific capacitance is different. The specific capacitances of GO/SWCNT ratio 5:1, 1:1, 1:3, 1:5 at 5mv/s are 42.8 F/g, 24.0 F/g, 102.8 F/g, 124.2 F/g respectively. The specific capacitance C_s values are calculated from CV curves by using Eq. (1):

$$C_s = \frac{\int IdV}{m \times \Delta V \times S} \quad (1)$$

Where C_s is the specific capacitance, $\int IdV$ is the integrated area of the CV curve, m is the mass of the active materials of one electrode, ΔV is the voltage window, and S is the scan rate. With the increase of CNT the capacitance increases. The slight distortion from rectangular shape of CV curve is due to pseudocapacitance resulted from various functional groups on graphene oxide.[22]

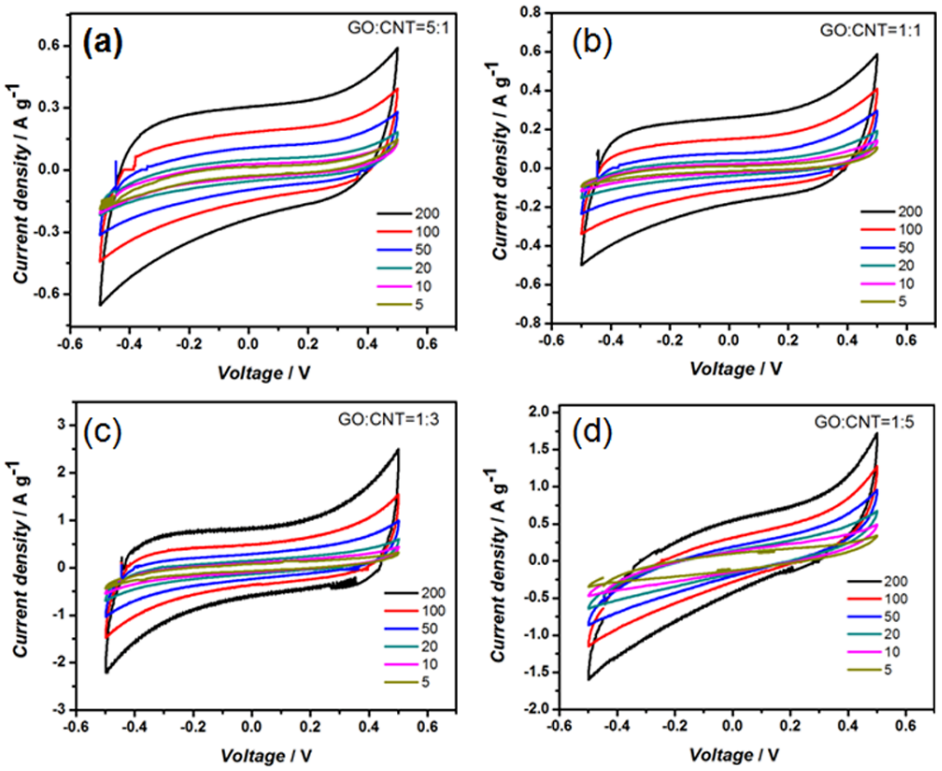

Figure 4.6 Cyclic voltammetry characterization for different ratios of GO/SWCNT at different scan rates. All of the measurements are conducted with 6M KOH electrolyte at room temperature.

The calculated specific capacitance is lower for 1:1 ratio than reported 90 F/g[40] which may attribute to the actual mass of used active material in current measurement. In our process, both sides of woven paper were covered with GO-SWCNT. Although the woven paper has high porosity, ions transport from one side to the other side of the paper would be somehow prevented. Therefore, the actual active material, i.e. material has contribution to capacitance is much less than the total material used for preparation of the electrode. And the calculated value of specific capacitance is thus lower than reported value. Note that each specific capacitance is higher than GO itself (10.9 F/g reported previously).[27] Very recently, a higher value of 417 F/g for functionalized GO has been

achieved at 0.5 A/g.[43] Here, the highest capacitance at 0.5A/g is 295F/g which is comparable with GO-MWCNT 251F/g.[27] Many SWCNT based supercapacitors have demonstrated specific capacitances in the range of 32–142 F/g depending on the functionalization functional groups[23] or types of SWCNT, i.e. metallic or semiconducting tubes.[44-45]

Cycling stability is crucial for supercapacitor devices. We investigated the cycling stability of the material with galvanostatic charge–discharge measurements.

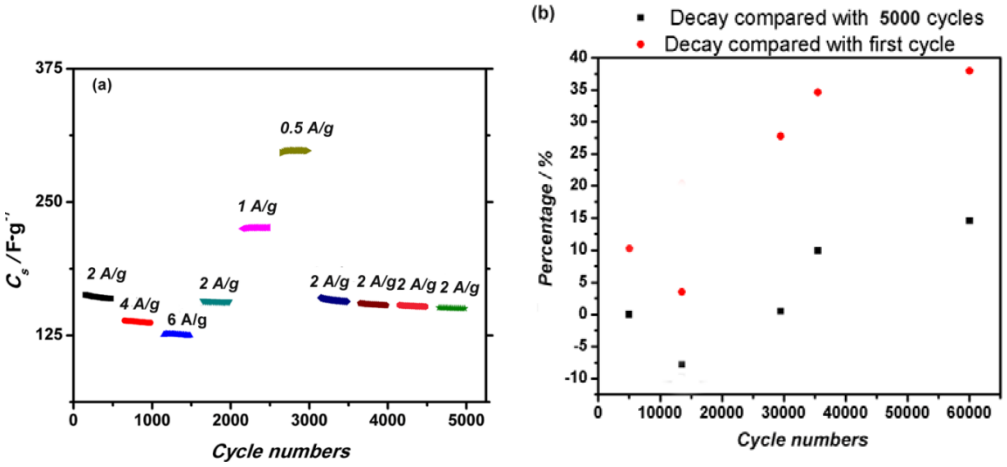

Figure 4.7 Cycling stability characterization. (a) variation of specific capacitance under different current density values (500 cycles for each current density). (b) Comparison of specific capacitance decay with the first cycle and the 5000th cycle. The measurements conducted with a GO/SWCNT ratio of 1:5.

Figure 4.7a presents the cyclic performance measured at different current densities for first 5000 charge-discharge cycles. The specific capacitances at different current densities are calculated through the Eq. (2):

$$C_s = \frac{2i}{m(dV/dt)} \qquad (2)$$

Where *m* is the carbon mass of one electrode, *i* is the discharge current and *dV/dt* is the slope of the discharge curve.

The GO/SWCNT ratio of 1:5 demonstrates the highest specific capacitance, which consistently decreases with an increase in the charge-discharge current density (Figure 6a). We ascribe this phenomenon to reduced access of ions to the active surface, especially for relatively slow faradic reactions.[46] And after 5000 cycles the capacitance decreased 11% which shows the higher stability of the material compared with rGO[30] alone. We continued with charge-discharge cycle at 2A/g for 60000 cycles. Only 64% capacitance retention was observed compared with the first cycle. However, 85% retention was achieved compared with the 5000th cycle (Figure 4.7b). This proves the high stability of composite material for supercapacitor electrode. Interestingly, we observe capacitance increase after 5000 cycles. Active sites for both sides of active material may increase after many cycles and graphene oxide may be partially reduced to graphene or tips of SWCNTs maybe open which increases surface area, therefore the capacitance increased. This phenomenon further assures the stability of the electrode material during long cycling usage.

The energy density (*E*) and power density (*P*) are calculated by using Eq. (3) and (4):

$$E = \frac{1}{2} C_s (\Delta V)^2 \quad (3)$$

and $$P = \frac{E}{t} \quad (4)$$

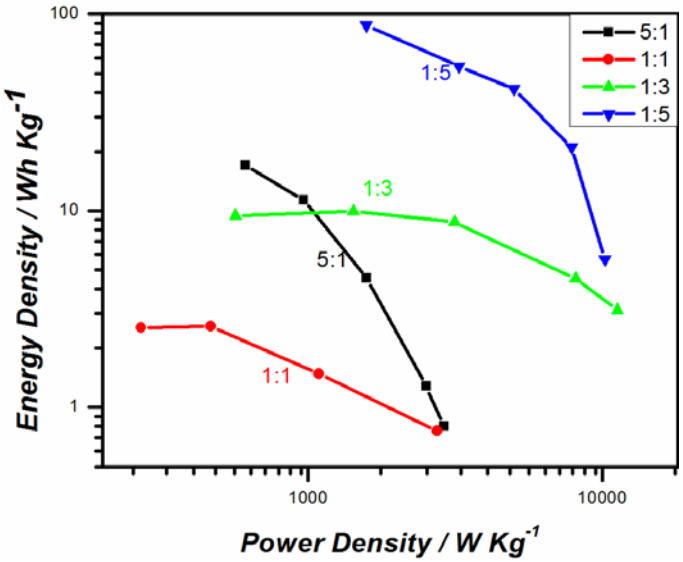

Figure 4.8 Ragone plots for different GO/SWCNT ratios.

where t is the total time of discharge. C_s is the specific capacitance value from charge-discharge, and ΔV is the potential range which is 1.0 V for aqueous normally. Ragone plots were obtained accordingly for different ratio of GO/SWCNT (Figure 4.8). It is clear the composite material has highest power density with the GO/SWCNT ratio of 1:5 which is in accordance with the capacitance measurements. A 1:1 ratio for the ink shows lower performance which is in accordance with CV measurements. Too many bundled CNTs or stacked GO due to the interaction between GO and CNT maybe the reason for such low performance. The power density of the capacitors reaches 10 kW/kg , which is higher than GO based or CNT-based supercapacitors.[30,47-48]

4.1.5 Conclusion

Our studies indicated SWCNTs dispersed using GO material at concentration of 12mg/ml, the highest reported value so far without surfactant assistance. Binder-free

GO/SWCNT composite paper electrodes were prepared via simply dipping paper in aqueous dispersions containing GO and CNTs, followed by 40^{o}C drying in vacuum oven. Without reduction of GO, the composite material displays high relative high gravational specific capacitance of 295 F/g at the charge-discharge current density of 0.5A/g. 85% capacitance retention after 60000 charge-discharge cycles demonstrates its high electrochemical stability as supercapacitor electrodes. These findings pave the way for preparing high performance ink material of energy storage devices.

4.2 Synchronous Chemical Vapor Deposition of Large-Area Hybrid Graphene-Carbon Nanotube Architectures

4.2.1 Introduction

Graphene has recently produced a major scientific sensation due to its promising properties such as high charge carrier mobility, unique band structure, mechanical robustness, high thermal transport, and chemical stability.[49-55] Consequently, there has been a considerable amount of theoretical and experimental research towards potential applications of graphene nanostructures in field-effect transistors, actuators, solar cells, batteries, and sensors.[56-60]

Carbon nanotubes (CNTs), another carbon allotrope, have also been the subject of intensive research over the last two decades because of their exceptional electronic, optical, mechanical and chemical properties.[61-63] Several outstanding features such as peculiar electronic transport, the ability to carry large current densities, high aspect ratio

and fast electron-transfer kinetics, make CNTs appealing for applications in electrochemical sensing, energy storage, field-emission devices and photovoltaics.[63-66]

For realistic utilization of graphene and CNTs, however, there is a need for these carbon allotropes to have engineered architectures with sp^2-hybridized carbon atoms as building blocks. Resulting hybrid structures will combine attractive material properties of both CNTs and graphene with the capability to develop a variety of geometries. [67-74] Therefore, devising a fabrication methodology for spatial distribution of graphene layers and CNTs in hybrid carbon architectures is crucial and rewarding.

The method by which graphene is prepared is critical in functionality of the synthesized carbon hybrid. For example, in hybrids that are constructed from reduction of graphene oxides, there are serious concerns regarding the uniformity and quality of resultant graphene layers.[75] These problems would be pronounced in resulting graphene hybrid structures in form of poor controllability of the nano-architecture and remarkable reduction of surface area, which is a key property of carbon hybrids. Alternatively, when graphene layers are prepared by mechanical exfoliation of graphite or graphite oxide, there are some serious limitations in terms of scalability, reproducibility, and mass fabrication.[50] While the quality of mechanically cleaved graphene in some micron-sized flakes is superior, mechanical exfoliation is size-limited and incapable of volume production of large scale graphene. Another problem of this approach stems from separate synthesis of CNT and graphene in the fabricated carbon hybrid. In this context, Fan *et al* utilized exfoliated graphene oxide layers along with CVD grown CNTs to fabricate CNT/graphene sandwich.[76] While this approach shows a good potential for lab-

scale synthesis of hierarchical nanostructures, its applicability could be enhanced by addressing scalability problems and consistency issues between CNT and graphene that are synthesized with different methods.

It is clear that large-area synthesis of uniform graphene layers is critical for incorporation of graphene-based structures into nano- and opto-electronic devices.[77-78] Among the various approaches for the synthesis of carbon nanotubes and graphene sheets Chemical Vapor Deposition (CVD) shows the highest capacity for large-scale production due to its large throughput, controllability, reproducibility, and capability to deliver in situ growth. While other fabrication approaches, grown nanotubes or graphene should be extracted and transferred, CVD based methodologies can grow directly on the desired substrate. The CVD-grown structures are controllable through careful selection and assembly of the catalyst layers. Repeated reports on CVD grown graphene show that the large-area monolayer graphene film can be grown directly on the nickel and copper surfaces by carbon precipitation or surface-catalyzed mechanism, respectively.[79-82]

The assembly methodology is another important part of the fabrication procedure that substantially affects the quality and applicability of the graphene-CNT hybrids. Within recent years, studies have been aimed towards fabricating hybrid carbon films by surface functionalization, self-organizing of homogeneously mixed solution of dispersed CNTs and reduced graphene oxides. The major advantage of this approach is its scalability and large throughput.[69-70] Nevertheless, the hybrid films prepared by such methods contain considerable amounts of restacked graphene and CNT aggregates, resulting in poor controllability of the hybrid nanostructure and reduction of total active

surface area. Furthermore, generally in all assembly approaches that involve detachment and transfer of CNTs from the growth substrate to another location or structure, the resulting electrical and mechanical contact in the assembled structure would be low.

Another major approach for graphene-CNT assembly was the growth of CNTs on the reduced graphene oxide film, carried out by Lee et al.[67,73-74] In this method, block copolymers has been applied to create uniformly patterned metal catalyst arrays for CNT growth in the carbon hybrid. This creative approach is a technical improvement that produces better electrical contacts and more efficient device integration.

Dong *et al* studied one-step growth of graphene-carbon nanotube hybrids by coating silicon nanoparticles on copper foil and using ethanol vapor as carbon source.[83] The parallel growth of graphene and CNTs increases the potential of this technically attractive approach to improve the quality of contact between CNTs and graphene, as their synthesis is similar in nature. The adopted approach relies on introducing an extra material, Si nanoparticles, for the synthesis of carbon nanotubes. This yields dependence of CNT growth sites on sporadically decorated Si nanoparticles that may influence the uniformity and density of CNTs in the hybrid. Altogether, it seems in almost all synthesis scenarios for graphene-CNT hybrids the vertical CNTs are either transferred from their growth substrate (primarily flat dielectric oxide substrate) or grown by an entirely different fabrication step.

In this section, we aim to depart from serial approaches, where the synthesis of hybrid nanostructures is carried out by sequential addition of different components of the

final composite structure, into a well-designed single-step growth. We demonstrate large-scale synchronous synthesis of graphene and carbon nanotubes into Pillared Graphene Nanostructure (PGN) on the copper foil for the first time (Scheme 1). The initial idea of such 3-D carbon networks was sparked by theoretical studies aiming at introducing novel energy storage assemblies based on tuneable and large surface area nanostructures.[71] While in our first experimental attempts[84] PGN was grown on lithographically patterned, copper evaporated Si/SiO_2 substrate, here for the first time we report large-scale synthesis of this carbon hybrid on plain copper foil. This is a major technological step-up since for all applications in general, and for energy storage devices in particular, the substrate materials for PGN growth needs to be flexible, geometrically adjustable, and conductive. Moreover, in our new synthesis technique the need for lithography pre-patterning of the growth substrate, part of experimental procedure of previous fabrication approach, [84] has been removed. As a result, the fabrication method has upgraded from a "serial" to a large-scale "parallel" technique. Due to the integrated nature of the synthesis method, the resulting hybrid structure shows a superior cohesion and crystalline contact between graphene and CNT building blocks. We also demonstrate the functionality of our fabricated PGN structure by featuring a supercapacitor PGN cell. It is remarkable that the new PGN based supercapacitor was not achievable for graphene-CNT hybrids synthesized on Si/SiO2 substrate as silicon platform is nonconductive and brittle.

4.2.2 Experimental

4.2.2.1 Graphene-CNT Synthesis Procedure

25 μm thick copper foils (from Alfa Aesar, cut into 1cm_2 area) were chosen as the substrate material. An Oxygen plasma treatment (STS Reactive Ion Etcher) was carried out on the copper foil strips surface at 200 W and 100 mTorr for 90 s to create a barrier oxide layer on copper foil. Fe catalyst films with a thickness of 3-5 nm were then deposited on copper oxide using electron beam evaporator (Temescal, BJD-1800). Next, growth foils were loaded into a CVD chamber and heated to 750°C under the flow of 500 sccm of Ar. All flow rates were precisely controlled by using mass flow controllers. To make the velocity profile of gas flow more uniform a total pressure of 650 Torr is maintained in the CVD tube. Once the temperature is stabilized at 750°C, first 100 sccm of H_2 is initiated, and after 5 mins 50 sccm of C_2H_2 is introduced into the tube for 10 to 20 min to begin the synthesis of graphene-CNT hybrid. Upon completion of the CVD growth, C_2H_2 and H_2 gas feeds were stopped, and the furnace was cooled to the room temperature under the protection of Ar gas flow. If needed, graphene-CNT hybrid films were removed from the Cu film by etching in a 1M aqueous FeCl3 solution, followed by cleaning with an aqueous HCl (5%) and D.I. water solution. Subsequently, pillared graphene films were collected from the D.I. water with a substrate of choice.

4.2.2.2 Characterization

Detailed characterization of the synthesized CNT-graphene hybrid films and catalyst surfaces were performed using optical microscopy, Scanning Electron

Microscopy (SEM; Leo, 1550), and Transmission Electron Microscopy (TEM; Philips, CM300) with a LaB_6 cathode operated at 300kV and equipped with an X-ray energy-dispersive spectroscopy (EDS) module. TEM samples were prepared by collecting the etched graphene-CNT films suspended on D.I. water, with a TEM copper grid. Electron diffraction patterns on the graphene-CNT films change from one location to another. The main difference observed is the appearance of other sets of hexagonal spots and the amplification of the ring patterns on the locations with dense CNT growth. Raman spectra were taken with a ThermoFisher Scientific micro-Raman equipped with DXR 532-nm Excitation Laser Set. Most spectra were taken in more than four spots to guarantee the reproducibility of the peak intensities.

4.2.2.3 Preparation of Supercapacitor Test Assembly

To prepare PGN-Supercapacitor Cells the as grown PGN films with copper substrates were cut into equal areas and assembled in split flat cell (MTI EQ-STC). Gamry Reference 600™ was used as electrochemical analyzer for capacitance measurement. Regular filter paper (Whatman 8-um filter paper) were soaked with the electrolyte (2 M Li_2SO_4 solution) was used as separator.

4.2.3 Results and Discussion

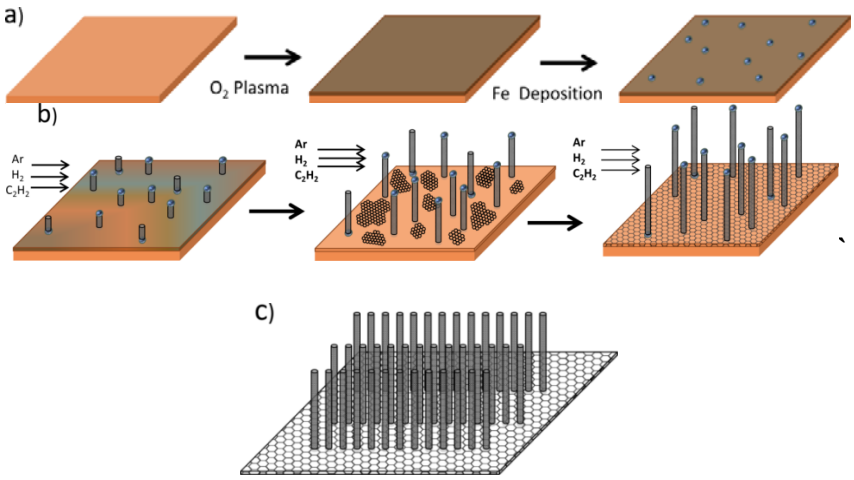

Scheme 4.2 Schematic diagram of (a) preparation of the growth substrate and the catalysts: oxygen plasma treatment of the copper foil followed by iron deposition. (b) Probable mechanism of synchronous growth of CNTs and underlying grapheme. (c) Pillared graphene hybrid structure comprising vertically grown carbon nanotubes as pillars and large-area graphene plane as a floor.

Pillared graphene is a spatial carbon network consisting of CNT pillars grown vertically from large-area graphene planes. This carbon hybrid structure looks like a building under construction, with carbon nanotubes as the pillars and graphene sheets as the floor (Scheme 4.2c). Scheme 4.2a is a schematically illustrating the process used to prepare the growth substrate before the synchronous synthesis. As discussed in the experimental section, Fe particles, "seeds" for CNT growth, were e-beam evaporated on a layer of copper oxide prepared by O_2 plasma treatment of copper foil. We first investigate the CVD growth of CNTs on the processed copper substrate, and then look into the entire perspective on the synchronous synthesis of the cabin hybrid.

As opposed to copper-based CVD growth of graphene, which could be considered experimentally established technique by now [81-82], the synthesis of carbon nanotubes on copper surface is challenging due to the undesired interaction between the metallic

catalysts regularly used for carbon nanotubes (mainly Fe, Co, and Ni) and copper. The main technique used to overcome this obstacle is to deposit an intermediate layer between metallic catalysts and Cu surface to act as a diffusion barrier.[85-88] However, adopting this approach for the CNT-graphene hybrid case introduces extra buffer materials that are hard to remove and tend to stay in the final hybrid structure. This consequently affects the functionality of the carbon hybrid structure, particularly in applications that strongly depend on the composition of the nanostructure used. Such barrier layers would also restrict the exposure of the copper layer to the flow of carbon source gas that is fundamental in our methodology.

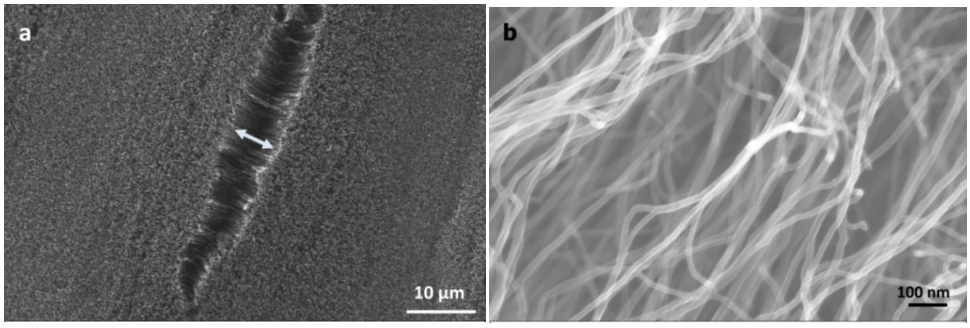

Figure 4.9 (a) Top-veiw SEM micrograph of CNT pillars in CNT-graphene hybrid, grown on pre-oxidized copper foil. The image showing dense and vertically aligned growth of CNT pillars on graphene sheet. (b) Higher magnification SEM micrograph of the CNTs.

Finding a barrier layer, which can be removed or consumed in the course of growth, is necessary. To address this problem we devise a step of oxygen plasma pre-treatment to form a controlled layer of copper oxide on top copper foil, separating it from to-be-deposited CNT catalysts. Copper oxide could be reduced during the growth while hydrogen flow is introduced. Hydrogen reduction of the copper oxide is essentially possible since copper stands below hydrogen in reactivity series. The high temperature

inside the CVD chamber significantly facilitates this reaction. Therefore, as the CNT starts growing from the surface of the copper-copper oxide foil, the oxide layer would be gradually reduced back to zero-valent copper. This finally leads to exposure of the pure copper to acetylene flow, the carbon source gas, and the formation of the graphene layer in parallel with the CNTs' growth. To achieve realistic mass production and reduce the complexity of the fabrication, the need for lithography pre-patterning of the growth substrate, a necessary part of previous fabrication approach, has been removed.[84] Figure 4.9a displays a typical top-view SEM micrograph of a large area CNT-graphene hybrid layer. The gap in the surface, marked with a double arrow, allows us to see the vertical direction of the CNT growth. This figure also shows the uniform morphology of grown CNTs over the large area of the hybrid film. Figure 4.9b is a higher magnification SEM indicating the average diameter of CNTs to be less than 20nm with narrow size distribution. To achieve a better understanding of the role of oxide layer in the synthesis, we conducted a comparative study on two similar copper foils, with and without O_2 plasma treatment.

Figure 4.10a and 4.10b shows SEM micrographs of the surfaces of the copper foil samples unmodified and after O_2 plasma treatment, respectively. Figures 4.11a and 4.11b show the SEM images of (a) unmodified copper, and (b) plasma treated copper surfaces after deposition of 4nm iron followed by CVD process with hydrogen and acetylene. Comparison between figure 4.10a and 4.10b suggests that the oxygen plasma treatment dramatically changes the morphology and size of the surface grains. It appears that through conversion of copper grains to copper oxide grains, oxygen plasma treatment

increases surface roughness and accordingly poses more grains and larger surface area. This produces higher level of surface energy, which consequently results in more active nucleation sites for the CNT growth on the surface. Indeed, according to nucleation and growth theory the higher the energy of the nucleation sites, it is more likely to have higher number of stable embryos on the surface.[89-90] Moreover, considering the total energy of the system for nucleation and growth, more stable nucleation sites results in more unilateral growth.[89,91] Figure 4.11b shows SEM image of the same copper foil (Figure 4.10b) after Fe deposition and CVD process. It is clear that the plasma-treated copper foil substrate gives rise to dense growth of carbon nanotubes with vertical alignment, as opposed to unoxidized copper layer. The oxide layer can also play the role of a barrier, impeding the unfavourable Fe-Cu interaction by separating two catalyst metals. As it can be seen from figure 4.11a, the unoxidized Cu foil would hardly give rise to any carbon nanotubes without any barrier layer. This may be explained by the increasing interaction between Fe and Cu and the possibility of the formation of metal solid solution due to nano-scale sizes of Fe particles and high growth temperature.[86,92] Furthermore, the grown CNTs from this substrate would be much larger in diameter and shorter in length as the sparse nucleation sites allow lateral growth of CNTs.

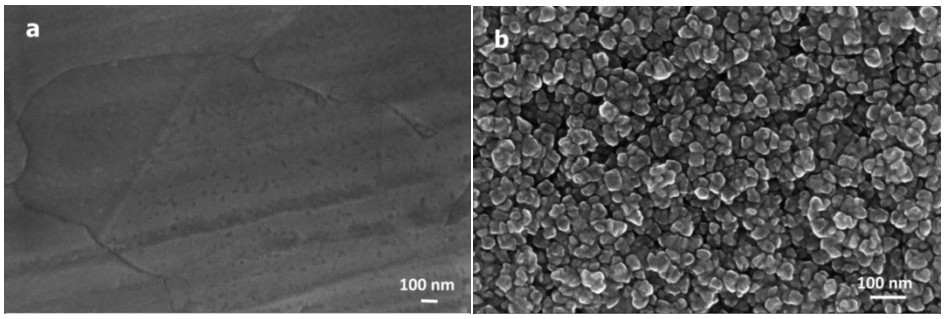

Figure 4.10 SEM micrograph of copper substrate **(a)** before, and **(b)** O_2 plasma.

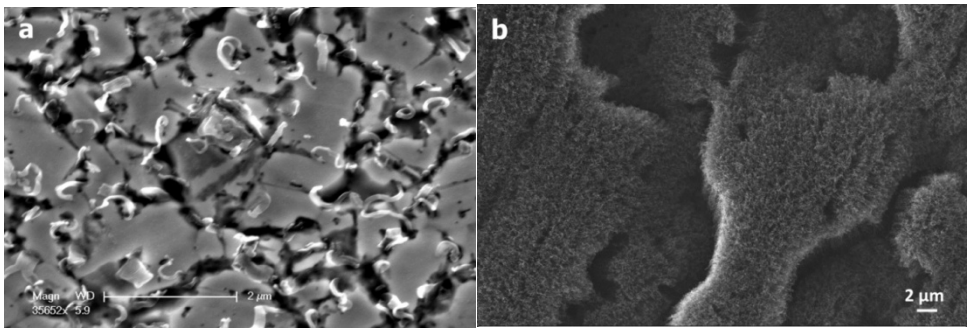

Figure 4.11 SEM image of PGN grown on (a) copper foil exposure to air 12 hours and (b) oxygen plasma treated copper foil, showing dense and aligned growth of CNT pillars on graphene sheet.

The records of our synthesis attempts suggest that an optimized recipe for copper oxidization pre-treatment is critical for the growth of the CNT-graphene hybrid. In fact, even small violations from optimized oxygen plasma specifications could affect the quality of the growth substantially. This could be explained by the significance of the average grain size and the roughness of the growth surface which depends on oxidization conditions. It should be noted that there is very fine balance between the thickness of the oxide layer and the CVD growth conditions, as the hydrogen flow and growth

temperature determine the reduction rate of the oxide layer. This additionally points to the fundamental role of the hydrogen gas flow in CVD growth of pillared graphene. Similar to hydrocarbon catalytic decomposition, hydrogen molecules dissociate in the presence of metallic catalysts and at the growth temperature of around 750K.[93-94] The resulting atomic hydrogen is very reactive and tends to act as an etching agent for carbon, in addition to reducing copper oxide. Therefore, if the selected ratio of acetylene to hydrogen flow is too low, the etching reaction becomes faster than formation sp^2 carbon hybrids. The hydrogen flow contributes to the "growth" part through its role in production of reactive hydrocarbon.[79-82,93]

Scheme 1b illustrates a probable formation process of the pillared graphene hybrid in one-step CVD growth. First, the iron deposited copper foil is exposed to the flow of H_2, C_2H_2, and Ar gasses as described in the experimental section. As CNT nucleation sites form on the copper oxide surface, hydrogen flow starts reducing copper oxide layer as displayed by the change of color on copper oxide layer in the Scheme 4.2b. Next, the oxide layer is completely reduced by hydrogen flow and consequently graphene islands begin to form via surface-catalysis mechanism induced by the exposure of copper to carbon source gas.[81-82] Meanwhile CNTs continue to grow vertically. Finally, the graphene layers cover the substrate and merges with CNTs at their roots on the substrate plane. To gain a deeper insight into the probable synthesis process of pillared graphene hybrids, we consider the CVD growth mechanisms of CNTs and graphene in further detail. In catalytic growth of CNTs by CVD, a metallic catalyst particle, Fe in our case, decomposes the hydrocarbon molecules of a source gas and absorbs carbon atoms to its

structure, until it becomes carbon-saturated. The absorbed carbon atoms diffuse through the bulk body of the catalyst particle and upon saturation, precipitate from the other side to form cylindrically rolled graphene layers.[95] Strong catalyst-substrate interaction results in base-growth mode, where catalysts remain on the substrate; and weak catalyst-substrate interaction yields tip-growth mode, in which catalyst remain on the tip of the growing CNT.[95-96]

The synthesis mechanism for CNT pillars in graphene hybrids is more complicated since it involves the simultaneous growth of graphene and CNTs. In the pillared graphene synthesis, while the CNTs start to grow through the above-mentioned mechanism, copper oxide layer formed by O_2 plasma pre-treatment is gradually reduced by hydrogen flow until copper atoms resurface and are exposed to acetylene flow in the CVD chamber. Subsequently, the graphene films directly grow on the Cu surface by a surface-adsorption mechanism. It is noteworthy that in the copper-based graphene synthesis graphene is growing by a surface-catalyzed mechanism rather than carbon precipitation process that is attributed to grapheme CVD growth by nickel.[79-82]

Considering the overall perspective on the synthesis of pillared graphene, the "floor" graphene grows through carbon nucleation sites. They form by catalytic adsorption of carbon to copper and grow horizontally with the addition of carbon to their boundaries.[81-82] The graphene nucleation sites continue expanding by adsorption of more decomposed carbon atoms to their edges, until graphene domains join and form a graphene sheet.[81] In the meantime, the growing planar graphene islands join cylindrically rolled graphene layers, CNTs, at their interface with the substrate, developing pillared

graphene nanostructure. The copper-based graphene growth also allows a more time-flexible exposure of the metallic catalyst to carbon source gas. This is crucial to our synchronous fabrication, as we require simultaneous growth of graphene and CNTs for pillared graphene hybrid. Using copper catalyst layer also intrinsically yields more uniform graphene with fewer layers.[81-82] As it has been mentioned before, excess hydrogen flow rate could be counter-productive as it removes copper oxide barrier prematurely and thus reduces iron catalysts activity and lifetime through possible Fe-Cu interaction at some CNT nucleation sites. Another probable drawback of surplus hydrogen flow is the overexposure of copper foil to hydrogen that affects the quality of graphene layer in the hybrid.

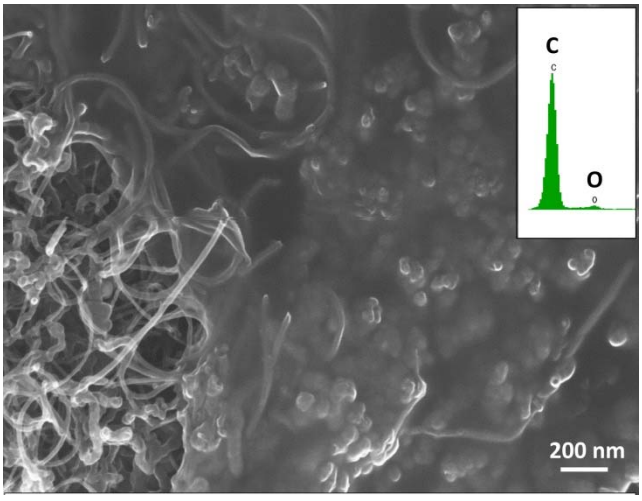

Figure 4.12 Bottom-view SEM micrograph of the backside of the peeled PGN film, showing the graphene film embedding CNT pillars roots.

Further study of the synthesized pillared graphene provides a deeper insight into the growth mechanism of carbon hybrids, and paves the way for their application-oriented fabrication. Figure 4.12 gives an interesting view of the "back side" of a

synthesized graphene-CNT hybrid. To obtain this bottom-view image, the grown hybrid film was peeled using a double sided carbon tape, and then placed onto SEM sample holder. The image displays how CNTs roots are embedded in graphene sheets. This is an important observation which further indicates the cohesion of the hybrid pillared grapheme architecture where CNT "pillars" are connected to graphene "floor". The EDS spectra taken from the backside of the sample verifies carbon as the "floor" material. The SEM image and the fact that carbon tape peeled the whole CNT-graphene hybrid rather than only CNTs, indicates a robust mechanical connection between synchronously synthesized CNTs and graphene. Figure 4.13a displays an optical micrograph of a pillared graphene sample transferred onto SiO_2/Si substrate. To remove the pillared graphene structure from copper foil the underneath Cu attachment was etched using 1M aqueous $FeCl_3$ solution. Subsequently the PGN sample was cleaned by HCl solution/ D.I. water, and then collected by the SiO_2/Si substrate.

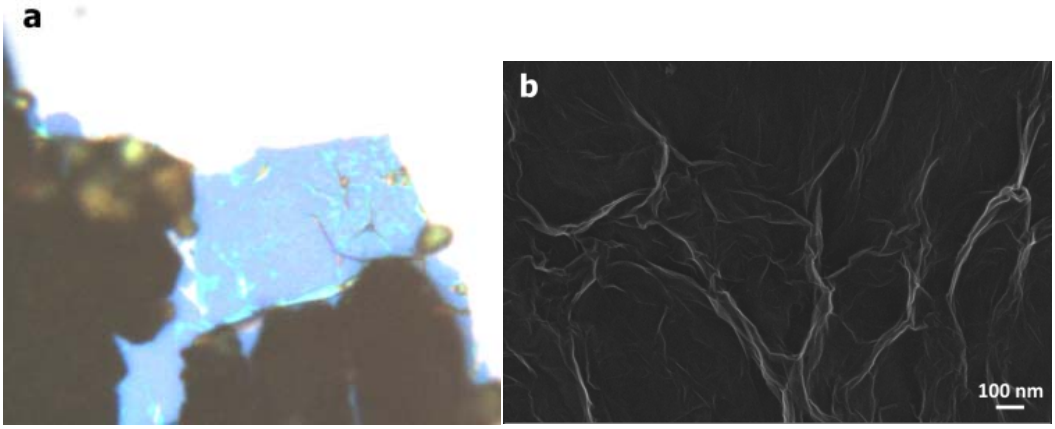

Figure 4.13 (a) Optical micrograph of PGN structure. Partial growth of CNTs reveals graphene underlying film and shows the PGN structure. (b) High magnification SEM micrograph of graphene film in graphene-CNT hybrid.

The optical micrograph was taken of a selected area of PGN that is partially covered by as-grown CNTs (due to scarce to zero presence of Fe catalysts), and thus it reveals the underlying graphene sheet, blue area, under the CNTs. Figure 4.13b shows the SEM image of the graphene layer in the same PGN sample. As it is expected the graphene layer contains wrinkles which are mainly caused by mismatch in the thermal expansion coefficient between copper and graphene.[81]A Typical Raman spectrum taken from CNTs in the pillared graphene is shown in Figure 4.14a. The G band, centered on 1570 cm^{-1}, is the first order Raman mode induced by in-plane vibration of carbon atoms in sp^2 hybridized graphene sheets. As a result, the intensity and sharpness of G band is signifying the presence of crystalline graphitic phase in the synthesized material. The D band at 1335 cm^{-1}, on the other hand, is the defect originated second order Raman band which indicates the level of defects in graphitic sp^2 structures. The nature of this band is related to one-phonon elastic scattering and it is interpreted as a measure of the quantity of sp^3 or dangling sp^2 bonds that are causing structural disorders. Thus, the ratio of D band and G band peak intensities, I_D/I_G, is commonly agreed as a gauge of the quality of CNTs and in general all graphitic materials. The lower values of this ratio show the superior grade of carbon structure and fewer amounts of amorphous carbon disorders and defects. The average value of this ratio taken from our samples is 0.82 which is lower than the values reported from similar studies on the CVD grown CNTs on copper substrates.[85-86,88] The higher quality of PGN structure compared to regular CNTs grown on copper substrate may be explained by the different strategies adopted for the synthesis and in particular the effect of intermediate layers.[85-86] While we oxidized a thin layer of

copper substrate itself to serve as the buffer layer, the general approach is deposit an external intermediate layer as a barrier film on the copper substrate before the CNT growth. This demonstrates the advantage of copper oxide layer in terms of simplicity and final products' quality. The Raman spectra did not show any appreciable radial breathing mode (RBM) peak which indicates that grown CNTs are mostly multiwalled. Figure 6b is a Raman spectrum of graphene sheet in PGN sample. The spectrum, which is taken from areas with no CNT pillars, confirms bi-to few layer graphene as the "floor" material of the hybrid structure.

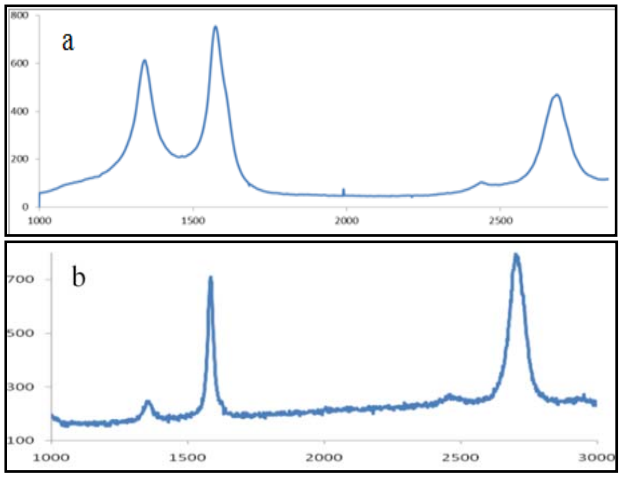

Figure 4.14 (a)Typical Raman Spectra of PGN showing the presence of D, G, and 2D band centered around 1335 cm^{-1}, 1570cm^{-1}, and 2672cm^{-1} respectively (Thermo Fisher DXR micro Raman, λ_{laser} = 532 nm). (b) Raman spectra of the graphene layer in PGN film grown on copper foil.

Figure 4.15 shows a TEM image the of pillared graphene film synthesized from deposited copper layer. To prepare TEM sample, first the graphene-CNT film was etched from copper using Ferric Chloride and Hydrochloric solutions. The suspended hybrid film is then collected from D.I. water by a suitable copper grid. The TEM image shows the

graphene-CNT hybrid through the underlying graphene. This is a very informative image allowing us to look into the interface between CNT pillars and graphene floor of the carbon hybrid. First, the recurring circular hollow patterns in the interface of a CNT and graphene layer, shown with red circle marks, confirm that CNTs' roots are embedded in the graphene sheet. This further indicates the smooth transition between the two carbon allotropes, graphene and CNTs, in the hybrid structure. The Energy Dispersive Spectrum (EDS) taken from the dark spots at the tips of CNTs verifies them as Fe catalyst particles. The presence of the Cu peak in EDS is due to TEM copper grid used for holding the pillared graphene sample. The high number of catalyst particles at the tips of nanotubes suggests the synthesis mechanism of CNTs to be tip-growth, which points to a low level of the interaction between substrate surface and CNTs catalyst particles. The inset selected area diffraction pattern, taken from sparsely grown CNTs area of pillared graphene, shows concentric circles. This is expected because multiwall carbon nanotubes are concentric tubes of cylindrically rolled graphene layers; therefore, we have overlapping sp^2 carbon planes of random orientation with respect to incident electron beam. Furthermore, the typical six-fold symmetry in diffraction spots supports the presence of mono- to few-layer underlying graphene film.[79,97-98]

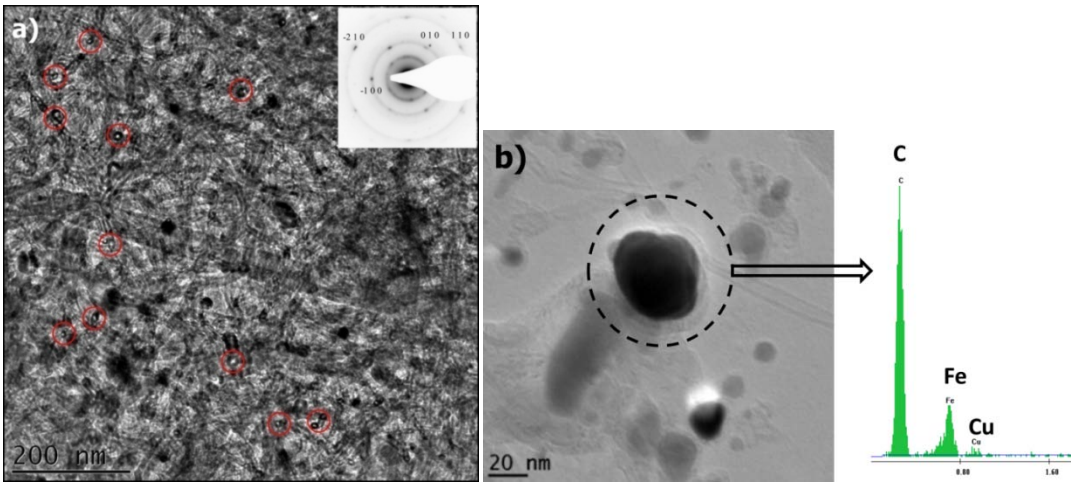

Figure 4.15 (a) TEM micrograph of pillared graphene bottom-view displaying CNTs roots at their interfaces with graphene film, and their tips; inset SAED diffraction pattern taken from pillared graphene. (b) Typical EDS spectrum taken from CNTs tips (dashed area).

4.2.4 Demonstration of PGN Based Supercapacitor Cells

To further prove the potential of the hybrid for energy storage, as-synthesized PGN was utilized as supercapacitor electrode. The supercapacitor cells were prepared from as grown PGN films as described in the experimental section. A two-electrode measurement was then employed for the electrochemical measurement, where the pre-treated two glass slides were assembled split flat cell with the as-soaked polypropylene working as a separator in between. The measurements of cyclic voltammetry (CV) were conducted to show the performance of the supercapacitor. The cyclic voltammetry scans were performed between 0 and 1 V in 6 M KOH aqueous solution (Figure 4.16a, b).

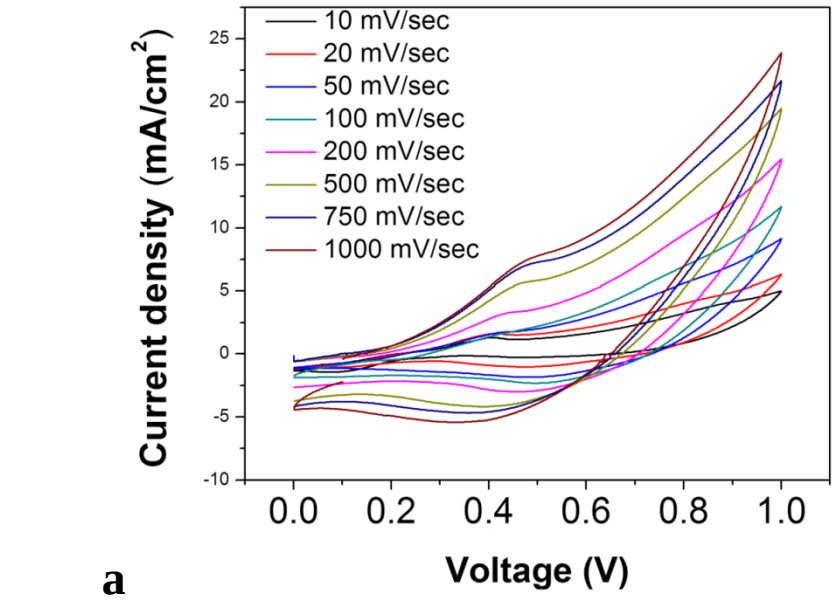

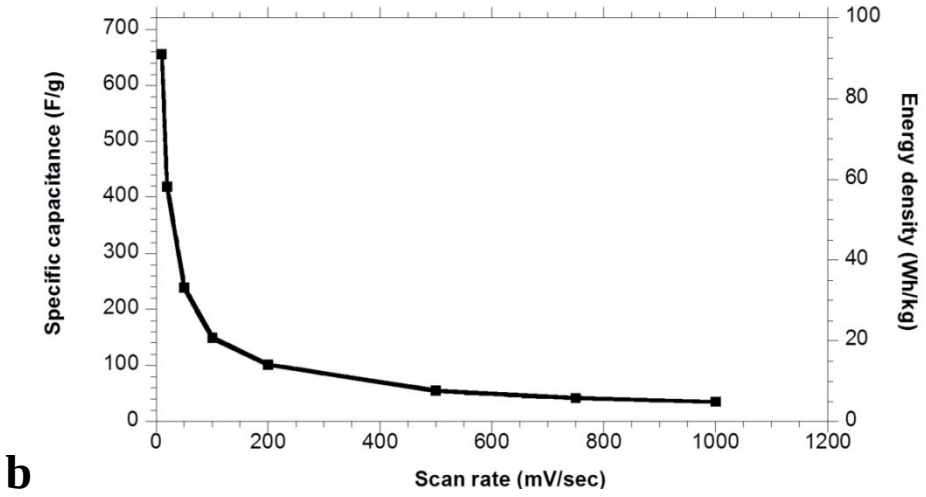

Figure 4.16 (a) CV curves of supercapacitor based on PGN films. The weight of one PGN film is around 200 μg/cm^2. Electrolyte: 6 M KOH aqueous. (b) Specific capacitance and energy density vs. scan rates.

All of the C_s curves show identical behavior. The specific capacitance can be calculated from the curve by using the Equation 1.

$$C_s = \frac{\int IdV}{m \times \Delta V \times S} \qquad (1)$$

Where C_s is the specific capacitance, ∫IdV is the integrated area of the CV curve, m is the mass of the active materials, ΔV is the potential range, and S is the scan rate. The distortion of CV curve from rectangular shape is due to Faradic reactions. The redox peak around 0.4 V indicates the reaction between Fe catalyst and electrolyte. The relatively low specific capacitance compared with the previously reported chemically exfoliated graphene-CNT hybrid and pure graphene is due to the low surface energy of the as synthesized graphene-CNT nanostructure. The relative low capacitance is reasonable due to the surface property of hybrids. The surface of hybrids is hydrophobic which causes low contact surface area between them and electrolyte. Recent research has shown that activated surface of the carbon material will have higher capacitance which provides opportunity to increase the performance of the carbon-based storage devices.[99] We further repeated the measurements with samples after HNO_3 aqueous treatment (HNO_3: D.I. Water=1:4). The specific capacitance of 655 F/g, 420 F/g, 154 F/g, 102 F/g, 55 F/g, 40 F/g were obtained for the sweep rates of 10, 20, 100, 200, 500, and 1000 mV/sec, respectively (Figure8b). Highest specific capacitance of 655 F/g, achieved at a scan rate of 10 mV/sec, suggests the as prepared supercapacitor cell has good performance.[100] The nitric acid treatment can etch Fe catalyst and oxides away, and at the same time enhances the surface wettability of the carbon hybrid. Therefore the surface area increases by means of end-tip opening of carbon nanotubes, which further increases the specific capacitance.

The energy density was calculated by using Equation 2.

$$E = \frac{1}{2} C_s (\Delta V)^2 \tag{2}$$

The energy density increases from 10.05 to 91 Wh/kg (for 10 mV/sec) after acid treatment demonstrating a good performance of the Pillared Graphene Nanostructure supercapcitor comparable to those of carbon based supercapacitors.[101-102]

4.2.5 Conclusion

Large and uniform pillared graphene films were successfully synthesized via simultaneous CVD growth of graphene layers and carbon nanotubes on copper foil. The introduced graphene-CNT hybrid is a remarkable carbon nanostructure with tuneable nano-architectonics, which is central to application-oriented design of hierarchical graphene structures. The unique mechanism of synchronized CVD growth of CNT and graphene contributed significantly to the composure of the final carbon structure. Detailed characterization of synthesized pillared graphene shows the cohesive structure and crystalline contact between the two carbon allotropes in the hybrid. Through its tuneable spatial geometry and attractive material properties, this carbon hybrid shows very promising potential for integration into nanoelectronics, energy storage, and thermal management. These attractive material properties stem from the fact that the synthesized pillared graphene is exclusively built from sp^2 hybridized carbon atoms. The direct growth of PGN on copper foil, a significant technical improvement, opens the door for realistic applications of PGN, in which it is necessary to have a mechanically flexible and

electrically/thermally conductive substrate. As an immediate proof for the functionality of the refined graphene hybrid structure, it has been readily implemented into a supercapacitor cell. The measurement of the supercapacitor cell demonstrates relatively high energy density with good cycling stability that paves the way for developing future higher energy storage devices.

The present work is also innovative for its synchronous approach to synthesis of multi-component hybrids. The introduced fabrication methodology is based on premeditated design of catalysts foundation, analysis of carbon formation mechanisms, and thoughtful timing in the fabrication procedure, as synchronization in the growth process is vital. Accordingly, chemical nature, morphology, and organization of the catalysts, as well as pre-processing of the growth substrate, are the key designing measures of this methodology. The synchronous parallel growth methodology offers a practical high-volume production technique for carbon hybrids. It also does not involve any unconventional laboratory-style step, and is compatible with industrial thin-film fabrication technologies.

4.3 Future Work

I. Printable electrode.

(1) In section 4.1 we presented graphene oxide-carbon nanotube ink material. This material could be dispersed in water which is environmental friendly. Most importantly, the material could be applied on woven paper facilitating the large and cheap production of the material. Actually, the next step would be using the ink to print

electrodes for energy storage devices. In this step, various solvents should be systematically studied to meet with the requirements that after printing the material is effortless to handle, fast drying and durable during cycles. Also, various substrates should be studied to achieve such applications. Interactions between the ink and substrate may vary from van der Waals interaction to hydrogen bonding to covalent bonding.

(2) We have discussed the applicability of GFET for chemical sensor in chapter 3. With the printing technique, GO-CNT material could also be applied for such applications. Several advantages determine the trend using this material: (a) large production (b) easier to handle (c) no further functionalization is needed (d) GO provides sites for further functionalization which could improve the selectivity. Preliminary results have been done on this topic and the as-fabricated sensor shows high sensitivity.

II. Energy storage devices.

(1) Graphene/carbon nanotube hybrid for supercapacitors.

In section 4.2 we presented the synthesis of seamless graphene/carbon nanotube hybrid with one-step CVD method. This work was finished on December 24th, 2010. Right now, many groups have reported the similar results with different approaches. Actually, in this work, different catalyst or substrates could produce better result. For example, by changing copper foil to nickel foam we have obtained 3-D graphene/carbon nanotube foam structure. The obtained material has much better stability and capacitance. The main drawback of copper foil is the weak interaction force between graphene and itself, which resulting low stability of the material for supercapacitor.

(2) Pseudo supercapacitors.

In chapter 1 we discussed the high capacitance and potential of oxide materials for supercapacitors. Also we have obtained GO-CNT ink material. By incorporation of the oxide material with the ink high performance of supercapacitor electrode is expected. For example, I have synthesized MnO_2 nanowires by hydrothermal method. The nanowires have demonstrated high capacitance using Li_2SO_4 as electrolyte. Incorporating this material in to the graphene/carbon nanotube foam has been done and the performance is stunning with specific capacitance of 1100 F/g. Other nanomaterials could also be utilized to improve the specific capacitance, such as NiO, RuO_2 and V_2O_5. The main work should be focused on synthesis of nanomaterials. Studying the interaction between graphene or carbon nanotube and these materials are important to design better electrode systems.

(3) Lithium ion battery anode system.

We have discussed the supercapacitors with the obtained graphene/carbon nanotube hybrid material. These materials definitely could be utilized for lithium ion battery anode system. Several advantages will enable the novel material good candidate for lithium ion battery anode. First, the small CNT diameter (less than 20nm) allows for better accommodation of the large volume changes without the initiation of fracture that can occur in bulk or micron-sized materials. This is consistent with previous studies that have suggested a materials-dependent terminal particle size below which particles do not fracture further. Second, each CNT is electrically connected to the metallic current collector so that all the CNTs contribute to the capacity. Third, the CNTs have direct 1D electronic pathways allowing for efficient charge transport. In electrode microstructures

based on particles, electronic charge carriers must move through small interparticle contact areas. In addition, as every CNT is connected to the current-carrying electrode, the need for binders or conducting additives, which add extra weight, is eliminated. Various substrates and catalysts should be systematically studied for further work.

4.4 References

(1) Z. H. Zhong, D. L. Wang, Y. Cui, M. W. Bockrath, C. M. Lieber,"*Nanowire crossbar arrays as address decoders for integrated nanosystems"* ***Science*** *2003*, *302*, 1377.

(2) J. A. Rogers,"*Electronic materials - Making graphene for macroelectronics"* ***Nature Nanotechnology*** *2008*, *3*, 254.

(3) S. Guo, M. Ghazinejad, X. Qin, H. Sun, W. Wang, F. Zaera, M. Ozkan, C. S. Ozkan,"*Tuning electron transport in graphene-based field-effect devices using block co-polymers"* ***Small*** *2012*, *8*, 1073.

(4) S.-R. Guo, J. Lin, M. Penchev, E. Yengel, M. Ghazinejad, C. S. Ozkan, M. Ozkan,"*Label free DNA detection using large area graphene based field effect transistor biosensors"* ***J. Nanosci. Nanotechnol.*** *2011*, *11*, 5258.

(5) M. K. Shukla, M. Dubey, J. Leszczynski,"*Theoretical investigation of electronic structures and propertiesof C-60-gold nanocontacts"* ***Acs Nano*** *2008*, *2*, 227.

(6) T. O. Wehling, K. S. Novoselov, S. V. Morozov, E. E. Vdovin, M. I. Katsnelson, A. K. Geim, A. I. Lichtenstein,"*Molecular doping of graphene"* ***Nano Letters*** *2008*, *8*, 173.

(7) P. K. Ang, W. Chen, A. T. S. Wee, K. P. Loh,"*Solution-Gated Epitaxial Graphene as pH Sensor"* ***Journal of the American Chemical Society*** *2008*, *130*, 14392.

(8) J. B. Wu, M. Agrawal, H. A. Becerril, Z. N. Bao, Z. F. Liu, Y. S. Chen, P. Peumans,"*Organic Light-Emitting Diodes on Solution-Processed Graphene*

Transparent Electrodes" ***Acs Nano*** *2010*, *4*, 43.

(9) Y. Wang, X. H. Chen, Y. L. Zhong, F. R. Zhu, K. P. Loh,"*Large area, continuous, few-layered graphene as anodes in organic photovoltaic devices"* ***Applied Physics Letters*** *2009*, *95*.

(10) A. P. Alivisatos, I. Gur, N. A. Fromer, C. P. Chen, A. G. Kanaras,"*Hybrid solar cells with prescribed nanoscale morphologies based on hyperbranched semiconductor nanocrystals"* ***Nano Letters*** *2007*, *7*, 409.

(11) Y. W. Zhu, S. Murali, M. D. Stoller, K. J. Ganesh, W. W. Cai, P. J. Ferreira, A. Pirkle, R. M. Wallace, K. A. Cychosz, M. Thommes, D. Su, E. A. Stach, R. S. Ruoff,"*Carbon-Based Supercapacitors Produced by Activation of Graphene"* ***Science*** *2011*, *332*, 1537.

(12) Liming Dai, Dong Wook Chang, Jong-Beom Baek, Wen Lu,"*Carbon Nanomaterials for Advanced Energy Conversion and Storage"* ***Small*** *2012*, *8*, 1130.

(13) Y. P. Zhai, Y. Q. Dou, D. Y. Zhao, P. F. Fulvio, R. T. Mayes, S. Dai,"*Carbon Materials for Chemical Capacitive Energy Storage"* ***Advanced Materials*** *2011*, *23*, 4828.

(14) M. F. El-Kady, V. Strong, S. Dubin, R. B. Kaner,"*Laser Scribing of High-Performance and Flexible Graphene-Based Electrochemical Capacitors"* ***Science*** *2012*, *335*, 1326.

(15) K. J. Ziegler, Z. N. Gu, H. Q. Peng, E. L. Flor, R. H. Hauge, R. E. Smalley,"*Controlled oxidative cutting of single-walled carbon nanotubes"*

Journal of the American Chemical Society *2005*, *127*, 1541.

(16) H. Sato, M. Sano,"*Characteristics of ultrasonic dispersion of carbon nanotubes aided by antifoam"* ***Colloids and Surfaces a-Physicochemical and Engineering Aspects*** *2008*, *322*, 103.

(17) X. H. Peng, S. S. Wong,"*Functional Covalent Chemistry of Carbon Nanotube Surfaces"* ***Advanced Materials*** *2009*, *21*, 625.

(18) G. D. Zhan, X. H. Du, D. M. King, L. F. Hakim, X. H. Liang, J. A. Mccormick, A. W. Weimer,"*Atomic layer deposition on bulk quantities of surfactant-modified single-walled carbon nanotubes"* ***Journal of the American Ceramic Society*** *2008*, *91*, 831.

(19) J. F. Campbell, I. Tessmer, H. H. Thorp, D. A. Erie,"*Atomic force microscopy studies of DNA-wrapped carbon nanotube structure and binding to quantum dots"* ***Journal of the American Chemical Society*** *2008*, *130*, 10648.

(20) Y. Y. Ou, M. H. Huang,"*High-density assembly of gold nanoparticles on multiwalled carbon nanotubes using 1-pyrenemethylamine as interlinker"* ***Journal of Physical Chemistry B*** *2006*, *110*, 2031.

(21) J. Y. Luo, L. J. Cote, V. C. Tung, A. T. L. Tan, P. E. Goins, J. S. Wu, J. X. Huang,"*Graphene Oxide Nanocolloids"* ***Journal of the American Chemical Society*** *2010*, *132*, 17667.

(22) D. S. Yu, L. M. Dai,"*Self-Assembled Graphene/Carbon Nanotube Hybrid Films for Supercapacitors"* ***Journal of Physical Chemistry Letters*** *2010*, *1*, 467.

(23) J. M. Shen, A. D. Liu, Y. Tu, G. S. Foo, C. B. Yeo, M. B. Chan-Park, R. R. Jiang,

Y. Chen,"*How carboxylic groups improve the performance of single-walled carbon nanotube electrochemical capacitors?"* ***Energy & Environmental Science*** *2011*, *4*, 4220.

(24) B. Zhao, P. Liu, Y. Jiang, D. Y. Pan, H. H. Tao, J. S. Song, T. Fang, W. W. Xu,"*Supercapacitor performances of thermally reduced graphene oxide"* ***Journal of Power Sources*** *2012*, *198*, 423.

(25) Y. Chen, X. O. Zhang, D. C. Zhang, P. Yu, Y. W. Ma,"*High performance supercapacitors based on reduced graphene oxide in aqueous and ionic liquid electrolytes"* ***Carbon*** *2011*, *49*, 573.

(26) N. Jha, P. Ramesh, E. Bekyarova, M. E. Itkis, R. C. Haddon,"*High Energy Density Supercapacitor Based on a Hybrid Carbon Nanotube-Reduced Graphite Oxide Architecture"* ***Advanced Energy Materials*** *2012*, *2*, 438.

(27) S. H. Aboutalebi, A. T. Chidembo, M. Salari, K. Konstantinov, D. Wexler, H. K. Liu, S. X. Dou,"*Comparison of GO, GO/MWCNTs composite and MWCNTs as potential electrode materials for supercapacitors"* ***Energy & Environmental Science*** *2011*, *4*, 1855.

(28) J. Jiang, J. Liu, W. Zhou, J. Zhu, X. Huang, X. Qi, H. Zhang, T. Yu,"*CNT/Ni hybrid nanostructured arrays: synthesis and application as high-performance electrode materials for pseudocapacitors"* ***Energy Environ. Sci.*** *2011*.

(29) H. Li, C. Xu, N. Srivastava, K. Banerjee,"*Carbon Nanomaterials for Next-Generation Interconnects and Passives: Physics, Status, and Prospects"* ***Ieee Transactions on Electron Devices*** *2009*, *56*, 1799.

(30) Y. Wang, Z. Q. Shi, Y. Huang, Y. F. Ma, C. Y. Wang, M. M. Chen, Y. S. Chen,"*Supercapacitor Devices Based on Graphene Materials"* ***Journal of Physical Chemistry C*** *2009*, *113*, 13103.

(31) W. Wang, S. Guo, M. Penchev, I. Ruiz, K. N. Bozhilov, D. Yan, M. Ozkan, C. S. Ozkan,"*Three dimensional few layer graphene and carbon nanotube foam architectures for high fidelity supercapacitors"* ***Nano Energy***.

(32) M. Kaempgen, C. K. Chan, J. Ma, Y. Cui, G. Gruner,"*Printable Thin Film Supercapacitors Using Single-Walled Carbon Nanotubes"* ***Nano Letters*** *2009*, *9*, 1872.

(33) L. B. Hu, J. W. Choi, Y. Yang, S. Jeong, F. La Mantia, L. F. Cui, Y. Cui,"*Highly conductive paper for energy-storage devices"* ***Proceedings of the National Academy of Sciences of the United States of America*** *2009*, *106*, 21490.

(34) J. Kim, L. J. Cote, F. Kim, W. Yuan, K. R. Shull, J. X. Huang,"*Graphene Oxide Sheets at Interfaces"* ***Journal of the American Chemical Society*** *2010*, *132*, 8180.

(35) W. S. Hummers Jr, R. E. Offeman,"*Preparation of graphitic oxide"* ***Journal of the American Chemical Society*** *1958*, *80*, 1339.

(36) F. Ali, N. Agarwal, P. K. Nayak, R. Das, N. Periasamy,"*Chemical route to the formation of graphene"* ***Current Science*** *2009*, *97*, 682.

(37) D. C. Marcano, D. V. Kosynkin, J. M. Berlin, A. Sinitskii, Z. Z. Sun, A. Slesarev, L. B. Alemany, W. Lu, J. M. Tour,"*Improved Synthesis of Graphene Oxide"* ***Acs Nano*** *2010*, *4*, 4806.

(38) D. R. Dreyer, S. Park, C. W. Bielawski, R. S. Ruoff,"*The chemistry of graphene oxide"* ***Chemical Society Reviews*** *2010*, *39*, 228.

(39) T. Szabo, O. Berkesi, I. Dekany,"*DRIFT study of deuterium-exchanged graphite oxide"* ***Carbon*** *2005*, *43*, 3186.

(40) L. Qiu, X. W. Yang, X. L. Gou, W. R. Yang, Z. F. Ma, G. G. Wallace, D. Li,"*Dispersing Carbon Nanotubes with Graphene Oxide in Water and Synergistic Effects between Graphene Derivatives"* ***Chemistry-a European Journal*** *2010*, *16*, 10653.

(41) B. Das, R. Voggu, C. S. Rout, C. N. R. Rao,"*Changes in the electronic structure and properties of graphene induced by molecular charge-transfer"* ***Chemical Communications*** *2008*, 5155.

(42) Z. Chen, V. Augustyn, J. Wen, Y. W. Zhang, M. Q. Shen, B. Dunn, Y. F. Lu,"*High-Performance Supercapacitors Based on Intertwined CNT/V2O5 Nanowire Nanocomposites"* ***Advanced Materials*** *2011*, *23*, 791.

(43) F. Yang, B. Luo, Y. Jia, X. Li, B. Wang, Q. Song, F. Kang, L. Zhi,"*Renewing Functionalized Graphene as Electrodes for HighPerformance Supercapacitors"* ***Advanced Materials*** *2012*.

(44) A. Al-Zubaidi, T. Inoue, T. Matsushita, Y. Ishii, T. Hashimoto, S. Kawasaki,"*Cyclic Voltammogram Profile of Single-Walled Carbon Nanotube Electric Double-Layer Capacitor Electrode Reveals Dumbbell Shape"* ***Journal of Physical Chemistry C*** *2012*, *116*, 7681.

(45) Y. Yamada, T. Tanaka, K. Machida, S. Suematsu, K. Tamamitsu, H. Kataura, H.

Hatori,"*Electrochemical behavior of metallic and semiconducting single-wall carbon nanotubes for electric double-layer capacitor"* ***Carbon*** *2012*, *50*, 1422.

(46) "*Carbon coated textiles for flexible energy storage"* ***Energy Environ. Sci.*** *2011*.

(47) C. H. Chen, D. S. Tsai, W. H. Chung, K. Y. Lee, Y. M. Chen, Y. S. Huang,"*Electrochemical capacitors of miniature size with patterned carbon nanotubes and cobalt hydroxide"* ***Journal of Power Sources*** *2012*, *205*, 510.

(48) S. Arepalli, H. Fireman, C. Huffman, P. Moloney, P. Nikolaev, L. Yowell, C. D. Higgins, K. Kim, P. A. Kohl, S. P. Turano, W. J. Ready,"*Carbon-nanotube-based electrochemical double-layer capacitor technologies for spaceflight applications"* ***Jom*** *2005*, *57*, 26.

(49) K. S. Novoselov, A. K. Geim, S. V. Morozov, D. Jiang, M. I. Katsnelson, I. V. Grigorieva, S. V. Dubonos, A. A. Firsov,"*Two-dimensional gas of massless Dirac fermions in graphene"* ***Nature*** *2005*, *438*, 197.

(50) K. S. Novoselov, A. K. Geim, S. V. Morozov, D. Jiang, Y. Zhang, S. V. Dubonos, I. V. Grigorieva, A. A. Firsov,"*Electric Field Effect in Atomically Thin Carbon Films"* ***Science*** *2004*, *306*, 666.

(51) Y. Zhang, Y.-W. Tan, H. L. Stormer, P. Kim,"*Experimental observation of the quantum Hall effect and Berry's phase in graphene"* ***Nature*** *2005*, *438*, 201.

(52) A. K. Geim, K. S. Novoselov,"*The rise of graphene"* ***Nature Materials*** *2007*, *6*, 183.

(53) J.-H. Chen, C. Jang, S. Xiao, M. Ishigami, M. S. Fuhrer,"*Intrinsic and extrinsic performance limits of graphene devices on SiO2"* ***Nat Nano*** *2008*, *3*, 206.

(54) A. A. Balandin, S. Ghosh, W. Bao, I. Calizo, D. Teweldebrhan, F. Miao, C. N. Lau,"*Superior Thermal Conductivity of Single-Layer Graphene"* ***Nano Letters*** *2008*, *8*, 902.

(55) C. Lee, X. Wei, J. W. Kysar, J. Hone,"*Measurement of the Elastic Properties and Intrinsic Strength of Monolayer Graphene"* ***Science*** *2008*, *321*, 385.

(56) F. Schedin, A. K. Geim, S. V. Morozov, E. W. Hill, P. Blake, M. I. Katsnelson, K. S. Novoselov,"*Detection of individual gas molecules adsorbed on graphene"* ***Nature Materials*** *2007*, *6*, 652.

(57) X. Wang, L. Zhi, K. Mullen,"*Transparent, Conductive Graphene Electrodes for Dye-Sensitized Solar Cells"* ***Nano Letters*** *2007*, *8*, 323.

(58) J. Yan, T. Wei, B. Shao, Z. Fan, W. Qian, M. Zhang, F. Wei,"*Preparation of a graphene nanosheet/polyaniline composite with high specific capacitance"* ***Carbon*** *2009*, *48*, 487.

(59) J. Lin, D. Teweldebrhan, K. Ashraf, G. Liu, X. Jing, Z. Yan, R. Li, M. Ozkan, R. K. Lake, A. A. Balandin, C. S. Ozkan,"*Gating of Single-Layer Graphene with Single-Stranded Deoxyribonucleic Acids"* ***Small*** *2010*, *6*, 1150.

(60) E. Yoo, J. Kim, E. Hosono, H.-S. Zhou, T. Kudo, I. Honma,"*Large Reversible Li Storage of Graphene Nanosheet Families for Use in Rechargeable Lithium Ion Batteries"* ***Nano Letters*** *2008*, *8*, 2277.

(61) S. Iijima,"*Helical microtubules of graphitic carbon"* ***Nature*** *1991*, *354*, 56.

(62) M. S. Dresselhaus, G. Dresselhaus, A. Jorio,"*Unusual properties and and structure of carbon nanotubes"* ***Annual Review of Materials*** *2004*, *34*, 247.

(63) Popov, N. Valentin,"*Carbon nanotubes: properties and application"* ***Materials Science and Engineering*** *2004*, *43*, 42.

(64) P. G. Collins, M. S. Arnold, P. Avouris,"*Engineering Carbon Nanotubes and Nanotube Circuits Using Electrical Breakdown"* ***Science*** *2001*, *292*, 706.

(65) A. Javey, J. Guo, Q. Wang, M. Lundstrom, H. Dai,"*Ballistic carbon nanotube field-effect transistors"* ***Nature*** *2003*, *424*, 654.

(66) W. A. De Heer, A. Chatelain, D. Ugarte,"*A Carbon Nanotube Field-Emission Electron Source"* ***Science*** *1995*, *270*, 1179.

(67) D. H. Lee, J. E. Kim, T. H. Han, J. W. Hwang, S. Jeon, S.-Y. Choi, S. H. Hong, W. J. Lee, R. S. Ruoff, S. O. Kim,"*Versatile Carbon Hybrid Films Composed of Vertical Carbon Nanotubes Grown on Mechanically Compliant Graphene Films"* ***Advanced Materials*** *2010*, *22*, 1247.

(68) H. Y. Jeong, D.-S. Lee, H. K. Choi, D. H. Lee, J.-E. Kim, J. Y. Lee, W. J. Lee, S. O. Kim, S.-Y. Choi,"*Flexible room-temperature NO2 gas sensors based on carbon nanotubes/reduced graphene hybrid films"* ***Applied Physics Letters*** *2010*, *96*, 213105.

(69) D. Yu, L. Dai,"*Self-Assembled Graphene/Carbon Nanotube Hybrid Films for Supercapacitors"* ***The Journal of Physical Chemistry Letters*** *2009*, *1*, 467.

(70) V. C. Tung, L.-M. Chen, M. J. Allen, J. K. Wassei, K. Nelson, R. B. Kaner, Y. Yang,"*Low-Temperature Solution Processing of Graphene Carbon Nanotube Hybrid Materials for High-Performance Transparent Conductors"* ***Nano Letters*** *2009*, *9*, 1949.

(71) G. K. Dimitrakakis, E. Tylianakis, G. E. Froudakis,"*Pillared Graphene: A New 3-D Network Nanostructure for Enhanced Hydrogen Storage"* ***Nano Letters*** *2008*, *8*, 3166.

(72) M. D. Stoller, S. Park, Y. Zhu, J. An, R. S. Ruoff,"*Graphene-Based Ultracapacitors"* ***Nano Letters*** *2008*, *8*, 3498.

(73) D. H. Lee, J. A. Lee, W. J. Lee, D. S. Choi, W. J. Lee, S. O. Kim,"*Facile Fabrication and Field Emission of Metal-Particle-Decorated Vertical N-Doped Carbon Nanotube/Graphene Hybrid Films"* ***The Journal of Physical Chemistry C*** *2010*, *114*, 21184.

(74) D. H. Lee, J. A. Lee, W. J. Lee, S. O. Kim,"*Flexible Field Emission of Nitrogen-Doped Carbon Nanotubes/Reduced Graphene Hybrid Films"* ***Small*** *2011*, *7*, 95.

(75) C. Gomez-Navarro, J. C. Meyer, R. S. Sundaram, A. Chuvilin, S. Kurasch, M. Burghard, K. Kern, U. Kaiser,"*Atomic Structure of Reduced Graphene Oxide"* ***Nano Letters*** *2010*, *10*, 1144.

(76) Z. Fan, J. Yan, L. Zhi, Q. Zhang, T. Wei, J. Feng, M. Zhang, W. Qian, F. Wei,"*A Three-Dimensional Carbon Nanotube/Graphene Sandwich and Its Application as Electrode in Supercapacitors"* ***Advanced Materials (Weinheim, Germany)*** *2010*, *22*, 3723.

(77) P. Blake, P. D. Brimicombe, R. R. Nair, T. J. Booth, D. Jiang, F. Schedin, L. A. Ponomarenko, S. V. Morozov, H. F. Gleeson, E. W. Hill, A. K. Geim, K. S. Novoselov,"*Graphene-Based Liquid Crystal Device"* ***Nano Letters*** *2008*, *8*, 1704.

(78) L. A. Ponomarenko, F. Schedin, M. I. Katsnelson, R. Yang, E. W. Hill, K. S.

Novoselov, A. K. Geim,"*Chaotic Dirac Billiard in Graphene Quantum Dots"* ***Science*** *2008*, *320*, 356.

(79) A. Reina, X. Jia, J. Ho, D. Nezich, H. Son, V. Bulovic, M. S. Dresselhaus, J. Kong,"*Large Area, Few-Layer Graphene Films on Arbitrary Substrates by Chemical Vapor Deposition"* ***Nano Letters*** *2008*, *9*, 30.

(80) K. S. Kim, Y. Zhao, H. Jang, S. Y. Lee, J. M. Kim, K. S. Kim, J.-H. Ahn, P. Kim, J.-Y. Choi, B. H. Hong,"*Large-scale pattern growth of graphene films for stretchable transparent electrodes"* ***Nature*** *2009*, *457*, 706.

(81) V. A. Antohe, A. Radu, M. Matefi-Tempfli, A. Attout, S. Yunus, P. Bertrand, C. A. Dutu, A. Vlad, S. Melinte, S. Matefi-Tempfli, L. Piraux,"*Nanowire-templated microelectrodes for high-sensitivity pH detection"* ***Applied Physics Letters*** *2009*, *94*.

(82) M. P. Levendorf, C. S. Ruiz-Vargas, S. Garg, J. Park,"*Transfer-Free Batch Fabrication of Single Layer Graphene Transistors"* ***Nano Letters*** *2009*, *9*, 4479.

(83) X. Dong, B. Li, A. Wei, X. Cao, M. B. Chan-Park, H. Zhang, L.-J. Li, W. Huang, P. Chen,"*One-step growth of grapheneâ€“carbon nanotube hybrid materials by chemical vapor deposition"* ***Carbon*** *2011*, *49*, 2944.

(84) R. K. Paul, M. Ghazinejad, M. Penchev, J. Lin, M. Ozkan, C. S. Ozkan,"*Synthesis of a Pillared Graphene Nanostructure: A Counterpart of Three-Dimensional Carbon Architectures"* ***Small*** *2010*, *6*, 2309.

(85) I. Lahiri, R. Seelaboyina, J. Y. Hwang, R. Banerjee, W. Choi,"*Enhanced field emission from multi-walled carbon nanotubes grown on pure copper substrate"*

Carbon *2010*, *48*, 1531.

(86) H. J. Jiang, C. Du, Z. Q. Zou, X. W. Li, D. L. Akins, H. Yang,"*A biosensing platform based on horseradish peroxidase immobilized onto chitosan-wrapped single-walled carbon nanotubes"* ***Journal of Solid State Electrochemistry*** *2009*, *13*, 791.

(87) H. Wang, J. Feng, X. Hu, K. M. Ng,"*Synthesis of Aligned Carbon Nanotubes on Double-Sided Metallic Substrate by Chemical Vapor Deposition"* ***The Journal of Physical Chemistry C*** *2007*, *111*, 12617.

(88) L. Delzeit, C. V. Nguyen, B. Chen, R. Stevens, A. Cassell, J. Han, M. Meyyappan,"*Multiwalled Carbon Nanotubes by Chemical Vapor Deposition Using Multilayered Metal Catalysts"* ***The Journal of Physical Chemistry B*** *2002*, *106*, 5629.

(89) J. J. De Yoreo, P. G. Vekilov,"*Principles of Crystal Nucleation and Growth"* ***Reviews in Mineralogy & Geochemistry*** *2003*, *54*, 57.

(90) D. R. Askeland, P. P. Phule, *The Science and Engineering Of Materials* 5th ed. ed., Thomson Learning, **2005**.

(91) Z. L. Wang, Y. Liu, Z. Z. Kluwer, *Handbook of Nanophase and Nanostructured Materials*, Academic/Plenum Publishers, **2002**.

(92) C. P. Wang, X. J. Liu, M. Jiang, I. Ohnuma, R. Kainuma, K. Ishida,"*Thermodynamic database of the phase diagrams in copper base alloy systems"* ***Journal of Physics and Chemistry of Solids*** *2005*, *66*, 256.

(93) M. Haluska, M. Hirscher, M. Becher, U. Dettlaff-Weglikowska, X. Chen, S.

Roth,"*Interaction of hydrogen isotopes with carbon nanostructures"* ***Materials Science and Engineering B*** *2004*, *108*, 130.

(94) H. J. Park, J. Meyer, S. Roth, V. Skákalová,"*Growth and properties of few-layer graphene prepared by chemical vapor deposition"* ***Carbon*** *2010*, *48*, 1088.

(95) R. T. K. Baker,"*Catalytic growth of carbon filaments"* ***Carbon*** *1989*, *27*, 315.

(96) A. M. Cassell, J. A. Raymakers, J. Kong, H. Dai,"*Large Scale CVD Synthesis of Single-Walled Carbon Nanotubes"* ***The Journal of Physical Chemistry B*** *1999*, *103*, 6484.

(97) J. C. Meyer, A. K. Geim, M. I. Katsnelson, K. S. Novoselov, T. J. Booth, S. Roth,"*The structure of suspended graphene sheets"* ***Nature*** *2007*, *446*, 60.

(98) J. C. Meyer, A. K. Geim, M. I. Katsnelson, K. S. Novoselov, D. Obergfell, S. Roth, C. Girit, A. Zettl,"*On the roughness of single- and bi-layer graphene membranes"* ***Solid State Communications*** *2007*, *143*, 101.

(99) Y. Zhu, S. Murali, M. D. Stoller, K. J. Ganesh, W. Cai, P. J. Ferreira, A. Pirkle, R. M. Wallace, K. A. Cychosz, M. Thommes, D. Su, E. A. Stach, R. S. Ruoff,"*Carbon-Based Supercapacitors Produced by Activation of Graphene"* ***Science*** *2011*, *332*, 1537.

(100) D. N. Futaba, K. Hata, T. Yamada, T. Hiraoka, Y. Hayamizu, Y. Kakudate, O. Tanaike, H. Hatori, M. Yumura, S. Iijima,"*Shape-engineerable and highly densely packed single-walled carbon nanotubes and their application as super-capacitor electrodes"* ***Nature Materials*** *2006*, *5*, 987.

(101) A. Yu, I. Roes, A. Davies, Z. Chen,"*Ultrathin, transparent, and flexible graphene*

films for supercapacitor application" ***Applied Physics Letters*** *2010*, *96*, 253105.

(102) L. Hu, J. W. Choi, Y. Yang, S. Jeong, F. La Mantia, L.-F. Cui, Y. Cui,"*Highly conductive paper for energy-storage devices"* ***Proceedings of the National Academy of Sciences*** *2009*, *106*, 21490.